Doctoral   **Science**

2014

Low-Toxicity Diacetone Acrylamide-Based Photopolymer For applications in Holography

Dervil Cody
Technological University Dublin, dervil.cody@tudublin.ie

LOW-TOXICITY DIACETONE ACRYLAMIDE-BASED PHOTOPOLYMER FOR APPLICATIONS IN HOLOGRAPHY

Dervil Cody B.Sc.

A thesis submitted for the degree of Doctor of Philosophy to the

Dublin Institute of Technology

Supervisors:

Dr. Emilia Mihaylova, Dr. Izabela Naydenova

Centre for Industrial and Engineering Optics,

School of Physics,

College of Sciences and Health

Dublin Institute of Technology

August 2014

ABSTRACT

Photopolymers are fast becoming one of the most popular holographic recording media due to their suitability for a wide range of holographic applications, such as sensors, diffractive optics and data storage. The majority of the investigated water-soluble holographic photopolymers are Acrylamide (AA) based. However, the toxic and carcinogenic nature of AA is a growing concern. In order for photopolymer recording media to be a viable option for holographic applications, efforts must be made to remove any occupational and environmental hazards involved in large-scale material development and device fabrication.

The main objective of the work presented here is the development and characterisation of an environmentally friendly photopolymer for holographic applications which uses the non-toxic, non-carcinogenic monomer Diacetone Acrylamide (DA) as a substitute for AA in the photopolymer composition. The new DA photopolymer has been shown to achieve diffraction efficiency values of up to 95 % in transmission mode with refractive index modulation values of 3.5×10^{-3}, and diffraction efficiencies of up to 38 % in the reflection regime with the incorporation of a chain transfer agent and after UV post exposure. Parameters such as shrinkage of the photopolymer layer and rate of polymerisation during the recording process have been quantified. The effect of the incorporation of the additives, namely glycerol and zeolite nanoparticles, on the holographic recording properties of the DA-based material has been investigated. A cytotoxicity comparison between the DA and AA photopolymers has also been carried out. The ability of the new photopolymer material to act as a gas sensor has been demonstrated. For the first time, reflection gratings recorded in the photopolymer have been successfully used as pressure-sensing devices, producing a visible and quantifiable colour change under exposure to different pressures.

DECLARATION

I certify that this thesis which I now submit for examination for the award of **Doctor of Philosophy**, is entirely my own work and has not been taken from the work of others, save and to the extent that such work has been cited and acknowledged within the text of my work.

This thesis was prepared according to the regulations for postgraduate study by research of the Dublin Institute of Technology and has not been submitted in whole or in part for another award in any other third level institution. The work reported on in this thesis conforms to the principles and requirements of the DIT's guidelines for ethics in research.

DIT has permission to keep, lend or copy this thesis in whole or in part, on condition that any such use of the material of the thesis be duly acknowledged.

Signature _____ Date _____

 Candidate

ACKNOWLEDGEMENTS

TABLE OF CONTENTS

6. INVESTIGATION OF THE EFFECT OF GLYCEROL ON THE DA PHOTOPOLYMER

LIST OF FIGURES

xviii

LIST OF TABLES

CHAPTER SUMMARY

Chapter 1: describes the basic principles of holographic recording. The different types of recording media available for holography are discussed, as well as outlining some of the main applications of holography which are of interest.

Chapter 2: reviews the development of AA-based holographic photopolymers, recent research in the field of reduced-toxicity holographic photopolymers, and outlines the main motivation for this research. The aims of the PhD research project are presented.

Chapter 3: introduces the Diacetone Acrylamide (DA) photopolymer composition in detail, and describes the steps taken in the optimisation of the DA-based photopolymer.

Chapter 4: deals with the characterisation of the holographic recording ability of the DA photopolymer in transmission mode.

Chapter 5: investigates the extent to which polymerisation-induced shrinkage occurs in the DA photopolymer during holographic recording using interferometric techniques.

Chapter 6: presents the effect which the additive glycerol has on the holographic recording properties of the DA photopolymer in transmission mode.

Chapter 7: deals with the measurement of the polymerisation rate of the DA photopolymer using Raman spectroscopy techniques.

Chapter 8: focuses on the comparative cytotoxicity evaluation carried out of the DA and AA-based photopolymers and their components.

Chapter 9: investigates the effect that the incorporation of BEA-structure zeolite nanoparticles has on the optical and holographic recording properties of the DA photopolymer.

Chapter 10: studies the ability of holographic transmission gratings recorded in the DA-based photopolymer to operate as refractometric gas sensors for hydrocarbon gases.

Chapter 11: deals with the characterisation of the holographic recording ability of the DA photopolymer in reflection mode, as well as the effect of a chain transfer agent on the recording properties.

Chapter 12: investigates the ability of reflection gratings recorded in the DAC photopolymer composition to act as a pressure sensing device.

Chapter 13: summarises the main conclusions from the PhD research, and discusses some potential areas for future work. The outputs resulting from the dissemination of the research are also presented.

1. HOLOGRAPHY

1.1 Introduction

Holography has been in existence since 1947. Dennis Gabor developed the theory of holography while working on the electron microscope [1]. His invention and development of the holographic method earned him the 1971 Nobel Prize in Physics. However, the technique of holography was not practically realised until the advent of the laser in the 1960's, which provided the first truly coherent source of light. In 1962 Emmett Leith and Juris Upatnieks recorded the first 3-D transmission holograms of real objects. Since then, the field of holography has expanded dramatically. It is easy to understand why the field has attracted such interest over the years. By definition, a hologram is a complete record of the phase and amplitude of an object's wavefront [2, 3]. This principle lends itself to a huge variety of applications, from every day items like embossed security holograms on passports and credit cards to holographic data storage (HDS) systems, sensors, 3-D displays, non-destructive interferometric testing methods and advanced scientific tools such as holographic tweezers and electro-optical switching holographic devices. In order to develop such a large range of applications, it is crucial that suitable holographic recording media are readily available. For years silver halide was the medium of choice for holographers. In the past few decades a large variety of alternative media have been developed for holography, such as dichromated gelatin, photoresists, photodicroics, photorefractives, photothermoplastics and photopolymers. Of these, photopolymer materials have been the subject of much study for holographic applications such as HDS, sensors and holographic optical elements (HOEs). Their large dynamic range, high sensitivity, self processing nature, low cost and ease of production make them an attractive candidate.

1.2 Holographic recording methods

The technique of holographic imaging is unique in that it records both the amplitude and phase information of an object. A photosensitive medium is one which responds to incident light via a change in its physical properties. There are some holographic recording materials such as anisotropic recording media which are sensitive to the state of polarisation of the incident light, however most photosensitive materials respond to variations in the intensity of the incident light only. The phase information of an object can be converted to variations in intensity by creating an interference pattern between the light scattered from the object (i.e. the object beam) and a second reference beam which originates from the same coherent light source. The intensity at any point in this interference pattern depends on the phase of the object wave; therefore, the intensity variation recorded in the photosensitive medium (i.e. the hologram) contains both the phase and amplitude information of the object. If the hologram is then illuminated with the same reference beam, the original object wave will be reconstructed and can be viewed by an observer looking through the hologram.

1.2.1 In-line holography

The first holographic recording method, known as In-Line holography, was developed by Gabor in 1948 [1, 2]. In this method, a semi-transparent object is illuminated with a single, collimated, monochromatic, coherent beam perpendicular to the photosensitive medium along the z-axis, as shown in fig. 1.1. Due to the semi-transparent nature of the object, the incident light is then split into two components; the transmitted light which becomes the reference beam and the light scattered from the object, which is the object beam. The complex amplitudes of the reference and object beams can be defined as

$r(x, y)$ and $o(x, y)$. The resultant intensity pattern of the interference of the two beams is described by the sum of the two complex amplitudes, given by:

$$I(x, y) = |r(x, y) + o(x, y)|^2 \qquad (1.1)$$

In the simplest case, the reference beam is a plane wave whose amplitude and phase remain unchanged across the photosensitive medium. Therefore, it can be written as the real constant r [3]:

$$I(x, y) = |r + o(x, y)|^2 \qquad (1.2)$$

$$I(x, y) = r^2 + |o(x, y)|^2 + ro(x, y) + ro^*(x, y) \qquad (1.3)$$

where $o^*(x, y)$ is the complex conjugate of $o(x, y)$.

On exposure to the interference pattern of light, the amplitude transmittance $t(x, y)$ of the photosensitive medium is altered. $t(x, y)$ is related to $I(x, y)$ by:

$$t(x, y) = t_o + \beta T I(x, y) \qquad (1.4)$$

where t_o is the constant background transmittance, β is a parameter determined by the photosensitive medium and processing conditions, and T is the exposure time. Therefore, for the recorded hologram the amplitude transmittance is given by:

$$t(x, y) = t_o + \beta T[r^2 + |o(x, y)|^2 + ro(x, y) + ro^*(x, y)] \qquad (1.5)$$

$$t(x, y) = t_o + \beta T r^2 + \beta T |o(x, y)|^2 + \beta T ro(x, y) + \beta T ro^*(x, y) \qquad (1.6)$$
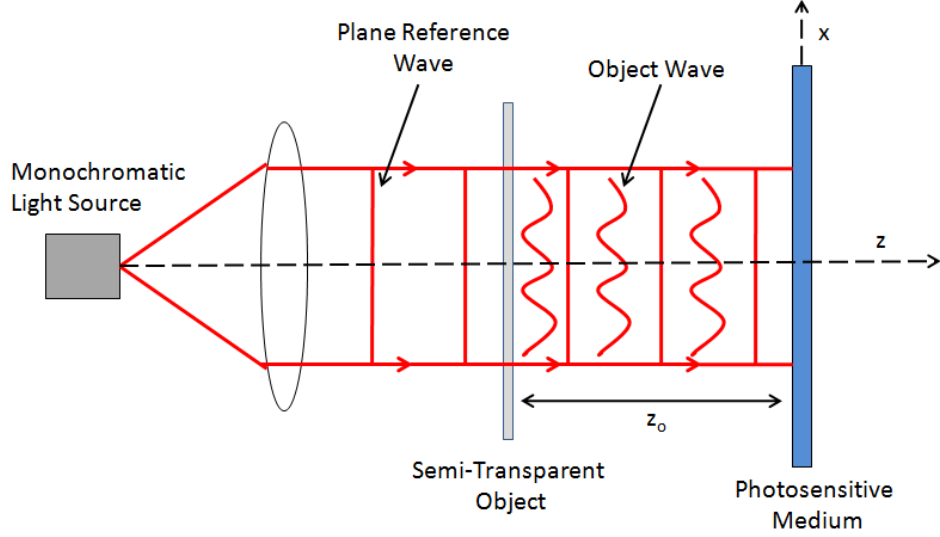
Fig. 1.1. Schematic diagram of in-line holographic recording setup.

In order to reconstruct the hologram, it is illuminated with the same monochromatic, coherent beam of light used to record it as shown in fig. 1.2. Since the complex amplitude at any point in this beam is, apart from a constant factor, the same as that in the original reference beam, the complex amplitude transmitted by the hologram can be written as:

$$u(x,y) = rt(x,y) \qquad (1.7)$$

$$u(x,y) = r[t_o + \beta Tr^2 + \beta T|o(x,y)|^2 + \beta Tro(x,y) + \beta Tro^*(x,y)] \qquad (1.8)$$

$$u(x,y) = r(t_o + \beta Tr^2) + \beta Tr|o(x,y)|^2 + \beta Tr^2 o(x,y) + \beta Tr^2 o^*(x,y) \qquad (1.9)$$

After expansion, the complex transmitted amplitude of the hologram is described by four terms, shown in eqn. 1.9. The first term represents a uniform plane wave which corresponds to the directly transmitted beam. The second term is extremely small in comparison to the other terms and can thus be neglected. The third term is the complex amplitude of the object beam, with some constant factor. It reconstructs the image of the

object in its original position. Since this image is formed behind the hologram, it can be described as a virtual image. The fourth term contains the complex conjugate of the object wave. The image it reconstructs has the opposite curvature to the original object, and is formed in front of the hologram as a real image.
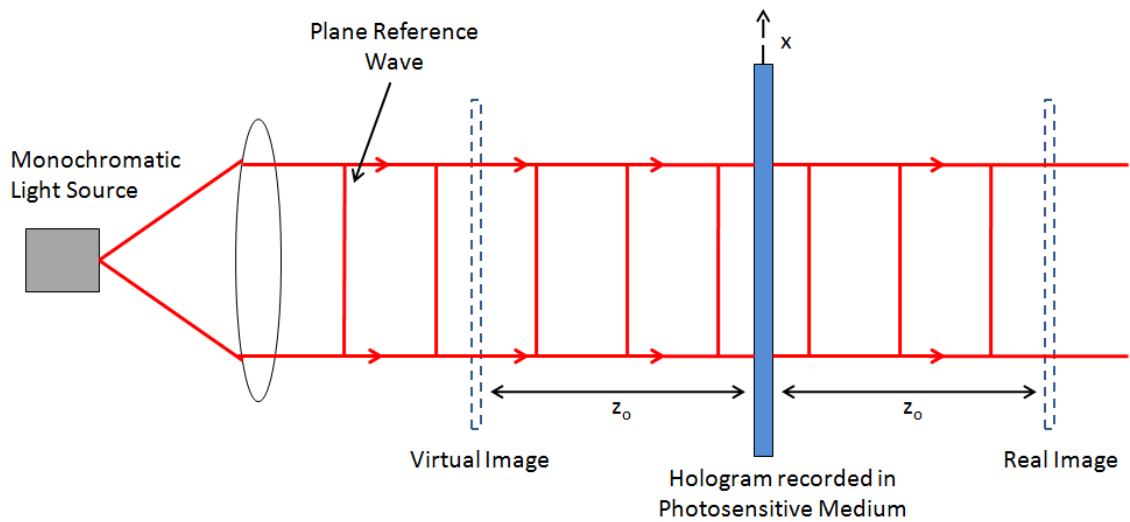
Fig. 1.2. Reconstruction of hologram recorded using in-line holographic method.

While this technique allowed for the first objects to be imaged holographically, the in-line holographic recording method has some problems. The presence of both virtual and real reconstructed images in the same viewing plane (i.e. a twin image) is one of the main-drawbacks of in-line holography, as it degrades the quality of the reconstructed image. Secondly, in order for the second term to be negligible, the object must have a high average transmittance. This limits greatly the range of objects that can be imaged using this holographic technique. Thirdly, holograms recorded in this manner are transmission holograms, as both beams illuminate the photosensitive medium from the same side. In order to reconstruct the hologram, it is therefore necessary to use the same

wavelength as used to record the hologram; thus the in-line holograms cannot be viewed with white light.

1.2.2 Off-axis holography

The twin-image problem was solved in 1962 by Leith and Upatneiks with the development of the off-axis holographic recording method [4, 5]. For this method, a separate reference beam was used for the first time. The object and reference beams were separated at a large enough angle that the resultant images did not overlap. This was a huge step for the field of holography, and together with the production of the first working laser at Hughes Research Laboratories in 1960, allowed the field of holography to expand and diversify.

The recording arrangement used for off-axis recording is shown in fig. 1.3. For simplicity, the assumption has been made that the reference beam is derived from the same light source as the object beam to ensure that the two beams are coherent.
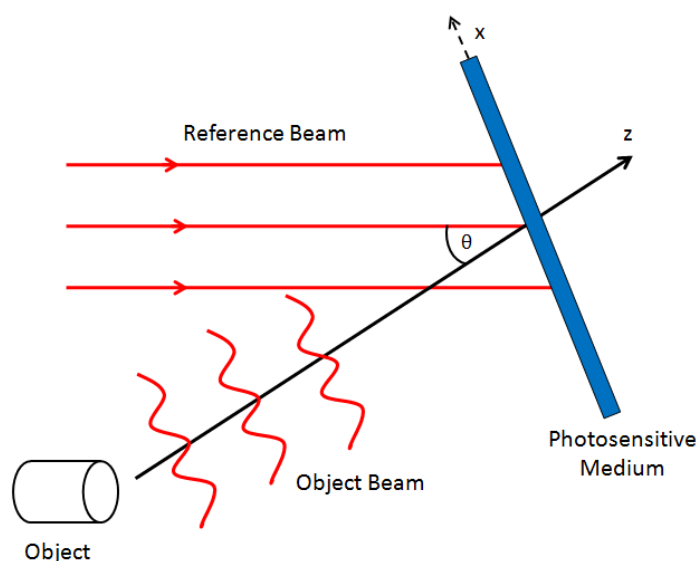
Fig. 1.3. Schematic diagram of off-axis holographic recording setup.

Due to the fact that both the amplitude and phase will vary at each point across the photosensitive medium, the object wave in this scenario is described by :

$$o(x, y) = |o(x, y)|e^{-i\varphi(x,y)} \qquad (1.10)$$

In the case of the plane wave reference beam the amplitude will remain constant. Therefore, the reference wave can be written as:

$$r(x, y) = re^{-i\varphi(x,y)} \qquad (1.11)$$

It is assumed for simplicity that the phase of the reference wave φ will vary in one direction only, x. This gives:

$$\varphi(x) = \boldsymbol{k}.\boldsymbol{r} = |k||r|\cos\theta = \frac{2\pi}{\lambda}x\cos\theta = 2\pi x\frac{\cos\theta}{\lambda} \qquad (1.12)$$

where θ is the angle between the $\boldsymbol{k}$ and $\boldsymbol{r}$ vectors. Therefore, the reference wave is rewritten as:

$$r(x, y) = re^{-i2\pi\varepsilon x} \qquad (1.13)$$

where $\varepsilon = \frac{\cos\theta}{\lambda}$. The resultant intensity of the interference of these two beams is then given by:

$$I(x, y) = |r(x, y) + o(x, y)|^2 \qquad (1.14)$$

$$= |r(x, y)|^2 + |o(x, y)|^2 + r|o(x, y)|e^{-i\varphi(x,y)}e^{-i2\pi\varepsilon x} + r|o(x, y)|e^{i\varphi(x,y)}e^{i2\pi\varepsilon x}$$

$$(1.15)$$

$$= r^2 + |o(x, y)|^2 + 2r|o(x, y)|\cos[2\pi\varepsilon x + \varphi(x, y)] \qquad (1.16)$$

7

The above equation contains the amplitude and phase information of the object wave. This information is then stored as a modulation in amplitude and phase of the photosensitive medium in the form of interference fringes with spatial frequency ε.

The amplitude transmittance of the hologram is then given by:

$$t(x,y) = t_o + \beta TI(x,y)$$

$$= t_o + \beta Tr^2 + \beta T|o(x,y)|^2 + r\beta T|o(x,y)|e^{-i\varphi(x,y)}e^{-e^{i2\pi\varepsilon x}}$$

$$+ r\beta T|o(x,y)|e^{i\varphi(x,y)}e^{e^{i2\pi\varepsilon x}}$$

(1.17)

$$= t_o' + \beta T|o(x,y)|^2 + r\beta T|o(x,y)|e^{-i\varphi(x,y)}e^{-e^{i2\pi\varepsilon x}} + r\beta T|o(x,y)|e^{i\varphi(x,y)}e^{e^{i2\pi\varepsilon x}}$$

(1.18)

where $t_o' = t_o + \beta Tr^2$ is the constant background transmittance.

In order to reconstruct the hologram, the hologram is illuminated with the reference beam used during recording, as shown in fig. 1.4. During reconstruction, the complex amplitude transmittance of the hologram is given by:

$$u(x,y) = r(x,y)t(x,y) \qquad (1.19)$$

$$= t_o'r e^{-i2\pi\varepsilon x} + r\beta T|o(x,y)|^2 e^{-i2\pi\varepsilon x} + \beta Tr^2 o(x,y) + \beta Tr^2 o^*(x,y)e^{-i4\pi\varepsilon x}$$

(1.20)

The first term in eqn. 1.20 corresponds to the transmitted beam intensity. The second term describes a halo surrounding the transmitted beam. The third term contains the object beam with some constant factor, and corresponds to a virtual image of the object

in its original position. The fourth and final term corresponds to the conjugate of the object beam, which produces a real image in front of the photosensitive layer. For this holographic recording configuration, the points on the real and virtual images are located at equal distances from the hologram, but on opposite sides to it. The real image formed is therefore a pseudoscopic image, as the image depth has been inverted. As long as the angle between the recording beams is large enough, the two reconstructed images can be independently viewed.
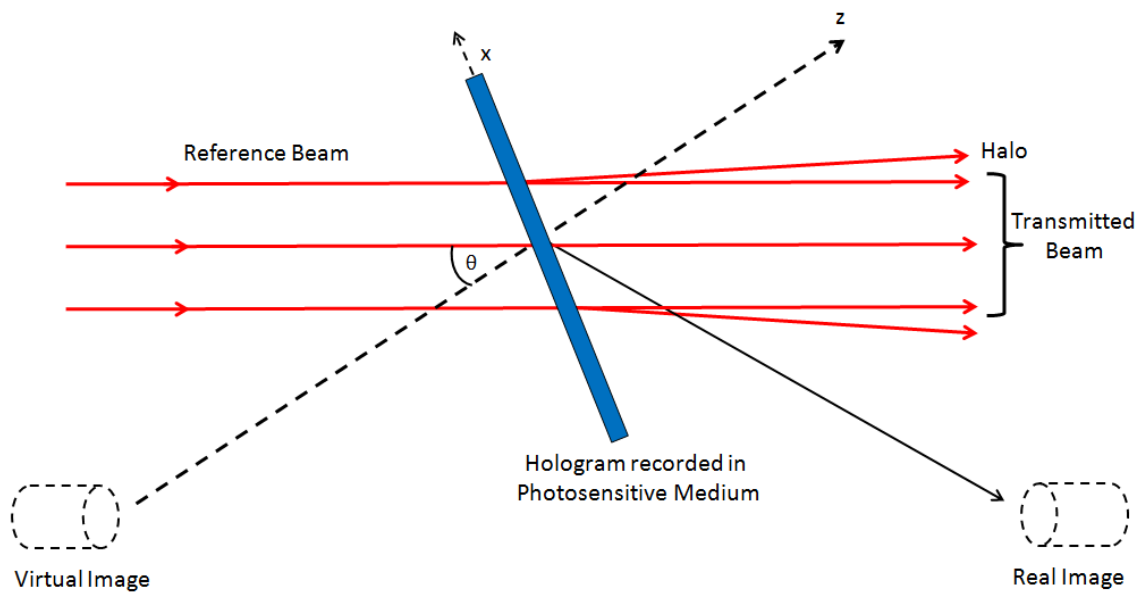
Fig. 1.4. Reconstruction of hologram recorded using off-axis holographic method.

1.3 Classification of holograms

The type of hologram recorded depends on several factors. The recording geometry of the holographic setup will determine whether the hologram is a transmission or reflection hologram. A hologram can be classified as thick or thin depending on the relation between the thickness of the hologram and the average fringe spacing. Whether a hologram is defined as a phase or amplitude hologram will depend on the holographic

9

recording medium used, and therefore the optical characteristic that is modified during holographic recording. In this section these classifications are described in more detail.

1.3.1 Geometry of recording

One of the primary factors used to distinguish between holograms is the geometry used for recording. The two main classifications of holograms distinguishable in this way are transmission and reflection holograms.

1.3.1.1 Transmission holograms

In transmission mode recording, both the reference and object wavefronts are incident on the recording medium from the same side, as shown in fig. 1.5(a). When both the reference and object beams consist of coherent plane waves, this results in the formation of fringes perpendicular to the photosensitive medium surface. These fringes will be spaced equidistantly throughout the photosensitive medium. The spacing of the formed fringes Λ can be calculated using the Bragg equation:

$$m\lambda = 2\Lambda \sin \theta \qquad (1.21)$$

where m is the diffraction order, where λ is the reconstruction wavelength, and θ is half of the total angle between the object and reference waves. The fringe spacing is limited by the angle between the two beams, which must be less than 180°. This restricts the spatial frequency of a hologram recorded in transmission mode to approximately 3000 l/mm for visible wavelengths.

To reconstruct a transmission hologram, the hologram is illuminated with the reference beam used during recording as shown in fig. 1.5(b). The recorded grating will diffract the incoming light to reconstruct the object beam. Embossed holograms found on credit

cards are an example of transmission holograms with a mirrored backing used for security applications.

(a)   **(b)**
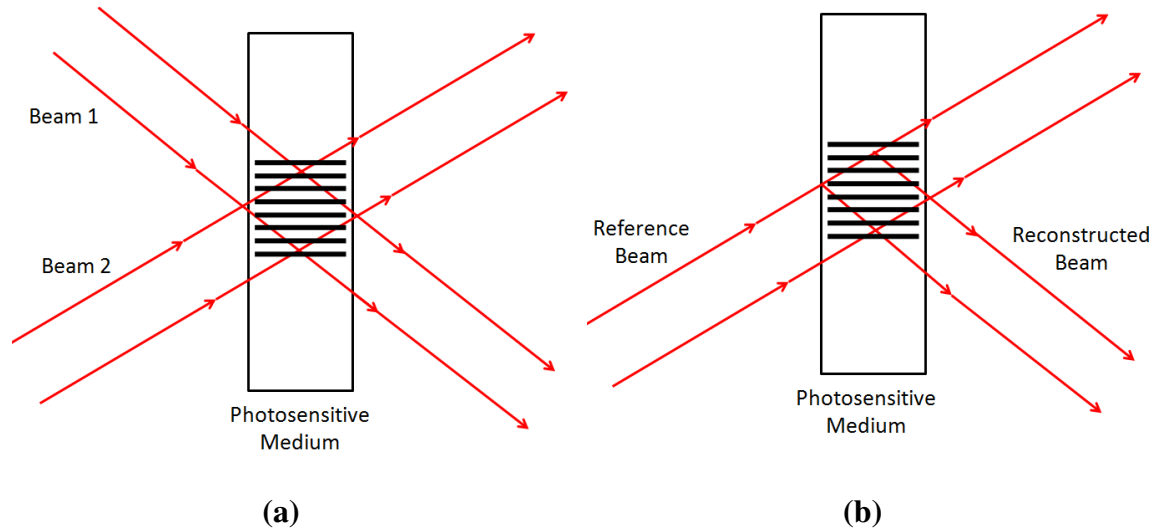
Fig. 1.5. Process for (a) recording and (b) reconstruction of transmission grating.

1.3.1.2 Reflection holograms

In reflection mode recording, the reference and object wavefronts are incident on the recording medium from opposite sides as shown in fig. 1.6(a). When both the reference and object beams consist of coherent plane waves, the fringes are formed parallel to the surface of the photosensitive medium. Reconstruction occurs in a similar fashion as for transmission mode; the reflection grating reflects the reference beam to reconstruct the second recording beam, as shown in fig. 1.6(b). This geometry allows for much higher spatial frequencies to be possible, restricted only by the spatial frequency limitations of the recording medium used. Reflection mode holograms can reconstruct in white light, which is one of the main advantages of this recording geometry.

A popular geometry for reflection mode recording is the Denisyuk type setup [6]. In this method, a single beam first passes through the recording medium. Part of the

transmitted light is then back reflected from the object, as shown in fig. 1.7. The hologram can then be mounted on a reflective backing for viewing by white light.

Table 1.1 outlines some of the main characteristics of both transmission and refection mode holographic recording, as well as listing some potential applications for the two different classifications of hologram.

Table 1.1 Characteristics of transmission and reflection mode holographic recording

	Transmission mode	**Reflection mode**
Recording Geometry	Beams illuminate sample from same side	Beams illuminate sample from opposite sides
Spatial Resolution	Typically max. 3000 l/mm	Typically > 5000 l/mm
Stability Requirements	Less sensitive to stability issues	Requires excellent stability of optical system
Hologram Reconstruction	Reconstruct with monochromatic (laser) light	Reconstruct with white light
Applications	Sensors Holographic Optical Elements Holographic Data Storage Security & Anti-counterfeiting	Display Holography Sensors Holographic Optical Elements Holographic Data Storage Security & Anti-counterfeiting

(a)   (b)
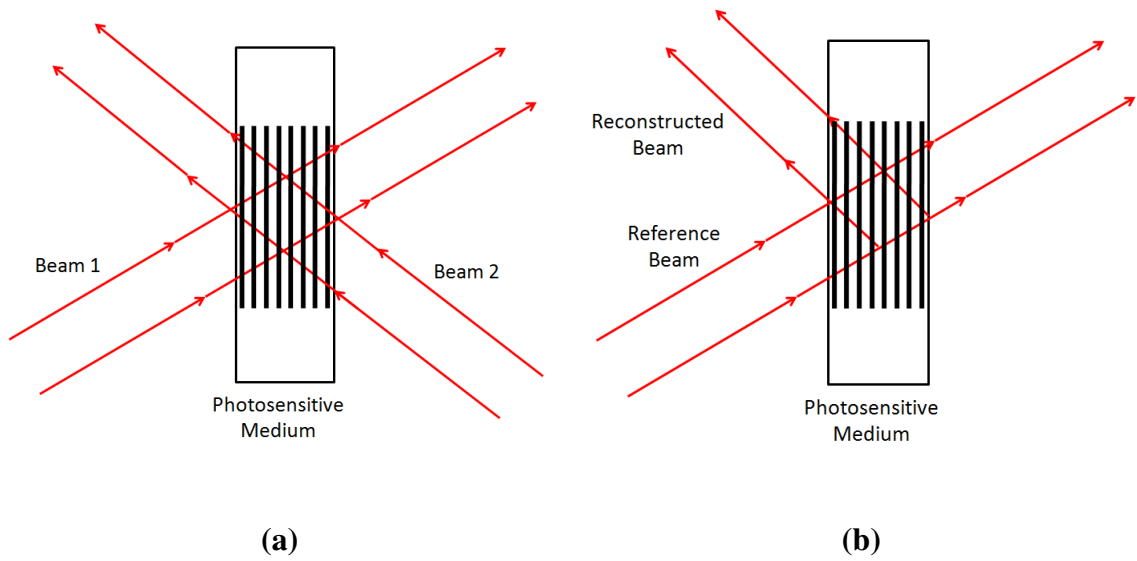
Fig. 1.6. Process for (a) recording and (b) reconstruction of reflection grating.
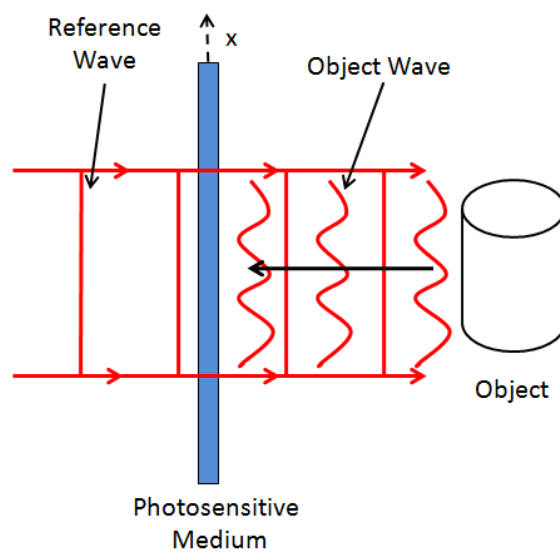
Fig. 1.7. Recording of Denisyuk reflection hologram.

1.3.2 Amplitude and phase holograms

A hologram is classified as either an amplitude or phase hologram depending on which

parameter of the photosensitive medium varies on exposure to light. A hologram is

classified as a phase hologram if the phase of the probe wave is modified on propagation through the medium. This is due to the spatial variation of the thickness or refractive index of the medium which occurs during the recording process. The extent of the variation is proportional to the intensity of the recording light pattern. An amplitude hologram is one in which the absorbance of the photosensitive medium is altered on exposure to light. A common example of an amplitude-type recording medium is a standard photographic emulsion. Both amplitude and phase holograms can be recorded using either transmission or reflection mode geometries.

1.3.3 Thick and thin holograms

A hologram is classified as either thick (volume) or thin depending on the relation between the thickness of the hologram and the average fringe spacing. If the average fringe spacing is small in comparison to the hologram thickness, a hologram will be classified as thick. In order to have a more quantitative method for determining whether a hologram is thick or thin, the Q parameter [7] is used:

$$Q = \frac{2\pi\lambda d}{n\Lambda^2} \tag{1.22}$$

where λ is the recording wavelength, d is the hologram thickness, n is the recording medium refractive index and Λ is the average fringe spacing. Q values > 1 correspond to thick holograms, whereas Q values < 1 are considered thin holograms. In general if Q $\geq$ 10, the hologram is classified as volume.

1.3.3.1 Thin amplitude hologram

For thin holograms, the spatially varying, complex amplitude transmittance can be written as:

$$t(x, y) = |t(x, y)|e^{-\varphi(x,y)} \tag{1.23}$$

For thin amplitude holograms, it is the transmittance $|t(x, y)|$ that varies during hologram reconstruction, and the phase $\varphi(x, y)$ remains approximately constant.

1.3.3.2 Thin phase hologram

For a phase hologram with no losses, the complex amplitude transmittance is given by:

$$t(x) = e^{-\varphi(x)} \tag{1.24}$$

If during holographic recording, the thickness or refractive index change in the recording medium is directly proportional to the intensity of the pattern of light, the complex amplitude transmittance of the hologram can be described using:

$$t(x) = e^{-i\varphi_o}e^{-i\Delta\varphi \cos Kx} \tag{1.25}$$

where φ_o is a constant phase factor, $\Delta\varphi$ is the amplitude of the phase variation, $\boldsymbol{K}$ is the grating vector, and x is the space coordinate. The maximum grating diffraction efficiency is obtained when the Bragg matching condition $\boldsymbol{k_i} + \boldsymbol{K} = \boldsymbol{k_d}$ is met, where $\boldsymbol{k_i}$ and $\boldsymbol{k_d}$ are the incident and diffracted wave vectors.

1.3.3.3 Volume holograms

As mentioned above, the thickness of volume holograms is much larger than the fringe spacing. For volume holograms, the hologram itself is made of layers with periodic variation in transmittance or refractive index.

The grating equation for a volume, phase grating recorded in the transmission regime is given by:

$$m\lambda = 2\Lambda(\sin\theta_1 - \sin\theta_2) \qquad (1.26)$$

where m is the order of diffraction, λ is the reconstruction wavelength, Λ is the fringe spacing, and θ_1 and θ_2 are the angles or incidence and diffraction respectively. Interaction of light with the grating fringes will occur as it travels through the volume grating. There are several factors which determine how much light is diffracted into each order, including grating thickness, fringe contrast, and whether the Bragg condition is met [8]. Maximum diffraction efficiency will be obtained when the reconstruction beam is incident on the grating at a particular angle of incidence θ, called the Bragg angle. The Bragg condition for an unslanted grating is given by:

$$m\lambda = 2\Lambda\sin\theta \qquad , \qquad (1.27)$$

The Bragg condition is satisfied when the wavelength and fringe spacing are such that the angles of incidence and diffraction are equal and opposite with respect to the surface normal. m must also be an integer (e.g. $m = 1$ for first order). Light illuminating the holographic grating at an angle significantly different to the Bragg angle may pass through the grating unaffected. As the light incident angle nears the Bragg angle, light will be efficiently diffracted, reaching a maximum at the Bragg angle exactly.

1.4 Material requirements for holographic recording

There are many requirements that a material must meet in order to be suitable for holographic recording and therefore for holographic applications. An ideal holographic material will have the following properties:

- Large dynamic range to ensure sufficient modulation during exposure

- High spatial resolution for improved quality recording

- Does not suffer from shrinkage during holographic recording

- Low noise i.e. have a fine grain structure to reduce unwanted scatter effects

- Inexpensive to produce

- Sensitive to the available commercial wavelengths

- Straightforward and safe production process

- Unaffected by ambient environmental conditions

There are many different materials available for holographic recording [2, 3]. The recording material chosen will depend largely on the requirements of the holographic application. The main properties of a range of different recording media are outlined below.

1.4.1 Silver halide emulsion

Silver halide is a highly sensitive, low scatter material which can be sensitised for a number of different recording wavelengths. It is the most popular choice for applications such as display holography, where high spatial resolution is required. The development and popularity of silver halide for holographic recording can be attributed mainly to the contributions of several scientists. Prof. Hans Bjelkhagen and Prof.

Nicholas Phillips have published widely on the use of silver halide for the recording of high resolution, full colour holograms [9-14]. They have also been involved in the development of silver-halide sensitized gelatin emulsions which show improved sensitivity in comparison to standard dichromated gelatin media [15-17]. Emulsion grain sizes as small as 5-10 nm can be achieved using the freeze-thaw mechanism developed by Kirillov *et al*. [18, 19]. The hologram is formed by the clustering of dissociated silver atoms within the gelatin, the concentration of which is proportional to the recording intensity. These clusters are then converted to silver during post-processing. The main drawback of this material is that it requires wet processing, and is relatively expensive. Silver halide is one of the few holographic recording media that are available commercially [20]. Commercial producers of silver halide plates include Slavich, Kodak, Agfa and Ilford.

1.4.2 Dichromated gelatin

On exposure to light, the Cr^{+6} ions in the dichromated gelatin are reduced to Cr^{+3}. The Cr^{+3} ions form crosslinks between the gelatin molecules, which causes the gelatin to harden in the illuminated areas. This mechanism can achieve refractive index modulations as large as 0.08 in the dichromated gelatin layers [3]. Dichromated gelatin is very low scattering and can achieve spatial resolutions as high as 5000 l/mm, making it suitable for reflection holography. However, the material is difficult to handle as wet processing is required to obtain the gelatin plates before recording, and then after to obtain the hologram [2]. Also, the photosensitiser used in dichromated gelatin is highly toxic [21]. There are very few commercial producers of dichromated gelatin plates, including Slavich and Kodak.

1.4.3 Photothermoplastics

On exposure to heat, the thermoplastic material is softened. The material can then be deformed via a spatially varying electrostatic field. When it is cooled, the pattern is fixed and a surface modulation is achieved. This can be erased by simply heating the material again. It is reported that commercially available thermoplastics can undergo more than 300 such cycles [3]. Another advantage of this material is that it does not undergo wet-processing. Thermoplastics are highly sensitive materials, however they are expensive to purchase. The only current producer of commercial thermoplastic materials that could be confirmed was the American company Tavex Ltd [2].

1.4.4 Photoresists

Photoresists are thin organic films which produce a hologram on exposure to UV and blue wavelength light. There are two types of photoresist. For negative photoresists, the unexposed areas are dissolved by a developer after exposure. For positive photoresists, the exposed area is dissolved by the developer. A spatial resolution of up to 1500 l/mm is possible [2]. Photoresists have no grain structure and so noise is negligible. These features make them ideal for applications such as the production of blazed holographic diffraction gratings [3]. Sabel *et al* have incorporated epoxy monomers into the SU8 photoresist material to create a diffusing guest-host system which retains the advantages of the robust photoresist [22]. Refractive index modulations of 5×10^{-3} and spatial resolutions of up to 8000 l/mm are reported. Commercial producers of photoresists include Gersteltec and MicroChem.

1.4.5 Photochromic materials

On exposure to light, photochromic materials experience a reversible colour change i.e. the optical density and hence the absorption of the material is modulated. This allows them to record amplitude holograms [2]. Although this effect is reversible, the lifetime of these materials is limited. Photochromics are grain free and can achieve high resolution; however, they are not very sensitive and achieve only low diffraction efficiencies. Recent work published by Ishii *et al* describes the real-time control of holographic images using a photochromic polymer film at a speed equivalent to the time resolution of the human eye [23]. Diffraction efficiencies of 6% for thin amplitude type holograms are reported. Refractive index modulations of 0.85×10^{-3} are reported in 1 μm thick layers of a novel diarylethene-based photochromic material by Zhang *et al* [24]. No current commercial producers of photochromic materials could be identified.

1.4.6 Photodicroic materials

These consist of an alkali halide material (e.g. NaCl, KCl) with an absorption centre. This centre is dicroic i.e. it absorbs light of a specific wavelength and of a defined state of polarisation. While still low, the sensitivity of these materials is higher than for photochromic materials. They can achieve spatial resolutions up to 10,000 l/mm and are rewritable [2].

1.4.7 Photorefractives

Phase holograms are recorded in these materials. Holographic recording occurs as a result of a change in refractive index induced by the opto-electric effect. Trapped electrons are freed on exposure to light, and diffuse into neighbouring unexposed regions, where they are again trapped. The redistribution of electrons with the material

results in the formation of an electric field, and thus a spatially varying refractive index. The type and concentration of dopants in the photorefractive crystal used determines the properties of the hologram recorded [25]. Fe-doped $LiNbO_3$ crystals are popular as they achieve large diffraction efficiencies and have high angular selectivity. Thousands of holograms can be stored in a single $Fe:LiNbO_3$ crystal, which makes them an attractive option for HDS [26]. Such materials are rewritable as a recorded hologram can be erased with uniform illumination, and they require no post-processing. Disadvantages are these photorefractives include strong light-induced scattering, volatility and low response speed.

1.4.8 Holographic polymer-dispersed liquid crystals (H-PDLCs)

Different types of polymers including acrylates [27], epoxy resins [28] and thiol-enes [29] are reported as suitable hosts for liquid crystals, creating a new branch of holographic recording media termed H-PDLC. The hologram is formed as a result of phase separation between the polymer host and the liquid crystals. H-PDLCs combine the advantages of photopolymer media with that of photonic crystals. Holographic patterning of these materials produces switchable devices, an effect which has interesting application for holographic optical elements [30]. H-PDLC materials are reported to achieve diffraction efficiencies greater than 90 % and Δn values of up to 1.8 x 10^{-2} in 23 µm layers [31]. The ability to combine the rewritable nature of H-PDLC media with large Δn, and good response at high spatial frequencies (> 7000 l/mm), makes them a very attractive candidate for HDS applications also [27, 32, 33].

1.4.9 Photopolymers

Holograms are recorded in photopolymers via a radical chain photopolymerisation mechanism. A typical holographic photopolymer [34-40] consists of a main monomer, a cross-linking monomer, an electron donor, a photosensitizing dye, and a polymer binder, which holds all of the components together. These photopolymer components are then spatially redistributed during holographic recording, when photopolymerisation takes place. This reaction involves three steps: initiation, propagation and termination. When illuminated, dye molecules absorb photons of light, and are promoted to excited singlet states.

$$Dye + hv \rightarrow {}^1Dye \bullet \quad \text{(Excited singlet state)} \tag{1.28}$$
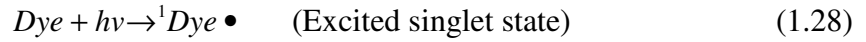
These singlet states can re-emit this energy via fluorescence, or by radiationless energy transfer to another molecule.

$$ {}^1Dye \bullet \rightarrow Dye + hv \quad \text{(Fluorescence)} \tag{1.29}$$

$$ {}^1Dye \bullet + Y \rightarrow Dye + Y \bullet \quad \text{(Fluorescence quenching)} \tag{1.30}$$
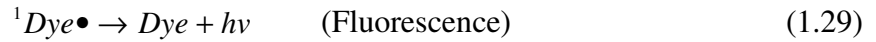
Alternatively, the singlet state can be converted to the more stable and longer lived excited triplet state dye molecule, via intersystem crossing.

$$ {}^1Dye \bullet \rightarrow {}^3Dye \bullet \quad \text{(Intersystem crossing)} \tag{1.31}$$
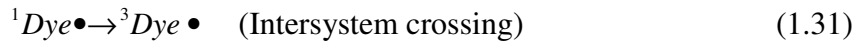
This triplet state dye molecule then reacts with the electron donor to produce a pair of radicals.

$$ {}^3Dye \bullet + ED \rightarrow Dye + ED \bullet \quad \text{(Free radical production)} \tag{1.32}$$

These radicals react with the monomer to produce an initiating species.

$$ED \bullet + M \rightarrow ED - M \bullet \quad \text{(Initiating species)} \tag{1.33}$$
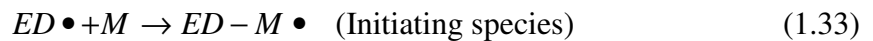
The growing chain continues to add more monomer units via propagation.

$$ED - M \bullet + M \rightarrow ED(M)_2 \bullet \quad \text{(Propagation step)} \tag{1.34}$$

This propagation step will continue until one of two termination reactions occurs, namely combination or disproportionation.

Oxygen quenching is an important process in photopolymer media. It can cause a reduction in the yield of singlet and triplet state dye molecules.

$$^{3}Dye \bullet + ^{3}O_{2} \rightarrow Dye + ^{3}O_{2} \bullet \qquad \text{(Oxygen Quenching)} \qquad (1.35)$$

$$^{1}Dye \bullet + ^{3}O_{2} \rightarrow Dye + ^{1}O_{2} \bullet \qquad \text{(Oxygen Quenching)} \qquad (1.36)$$
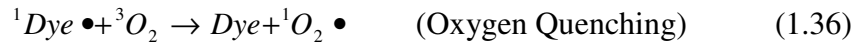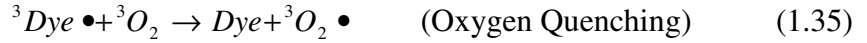
If the concentration of oxygen molecules is large enough, oxygen quenching can also cause an inhibition period at the start of polymerisation, and can lead to a reduction in the bleaching rate. Most of the oxygen in the layer must be used up during holographic exposure before polymerisation can begin [30].

Areas in the material where polymerisation takes place undergo a change in refractive index. The relative difference in refractive index between illuminated and non-illuminated areas of the photopolymer is what constitutes the phase hologram. There is also evidence to show that mass transport of the monomer from the dark to bright fringe regions during polymerisation further increases the refractive index modulation [41].

Photopolymer materials are highly sensitive, with optimum sensitivities of 45 mJ/cm^2 achieved. They are capable of very high spatial resolution. Holograms have been successfully recorded up to 5700 l/mm in an acrylamide (AA)-based photopolymer formulation, making them suitable for reflection mode applications such as colour display holography. Photopolymers are self-developing and require no post-processing, which is an attractive feature for many applications. They are also low cost and are easily prepared. A disadvantage of photopolymers is that they suffer from shrinkage due to holographic recording. This is undesirable for applications such as HDS, as the information stored must be replayed at the exact angle or wavelength used to record it. However, shrinkage has been reduced in photopolymers by the addition of certain

nanoparticles to the composition [42]. Reduction in polymerisation-induced shrinkage has also been observed using the step-growth polymerisation mechanism as described by Hata *et al* [43]. The main advantages and disadvantages of photopolymers for both reflection and transmission mode holographic recording are outlined in table 1.1. Commercial producers of photopolymers for holographic applications include Du Pont, Polygrama and Bayer [2].

1.5 Applications of holography

Holography is an extremely diverse field. The range of holographic applications is vast and ever expanding, from security holograms on banknotes, holographic displays in advertising, to holographic sensors and lenses for solar energy cells. A brief description of a few of the main applications is provided here.

1.5.1 Holographic data storage (HDS)

Limitations on digital data storage are imposed by the fact that the space required to store a single bit of data on an optical disk cannot be reduced below a limit set by the wavelength of the light used. Holography overcomes this by storing a large number of holograms in the same place. GE Global Research announced in 2011 that their micro-HDS system had successfully demonstrated data recording speeds matching those of Blu-Ray technologies [44]. It is expected that HDS technology will soon surpass this. It has the capability of storing 20 times more data than the current leader Blu-Ray on a single disk. This is equivalent to 100 times the data capacity of a standard DVD.

The ideal material for HDS should have several physical properties, including a large dynamic range, high photosensitivity, undergo no dimensional changes and be capable of forming thick layers. Of all holographic recording media, photopolymers and photorefractive materials appear to be the most promising for HDS. Photorefractive materials such as $LiNbO_3$ have many features that making them suitable for HDS; the recorded holograms are rewriteable, they can achieve large refractive index modulation, and the material does not suffer from shrinkage during recording. However, the photosensitivity of photorefractive media is reported to be low [27, 45-47]. Unlike photorefractives, photopolymers demonstrate high photosensitivity. However, photopolymers also face problems such as thickness limitations (approximately 1 mm) and shrinkage. For HDS, a thick, photosensitive material is required. The commercial upper limit on shrinkage for data storage applications is 0.5 % [48]. Research into the suitability of photopolymers and polymer composites for holographic data storage is currently a hot topic, being investigated by many different research groups worldwide [34, 49-55]. In 2008 InPhase Technologies launched their photopolymer-based holographic disk drive, which is considered to be a huge mile stone in the field. Since then commercial companies such as Bayer, DuPont, General Electric and Sony are also becoming more involved in its development.

1.5.2 Holographic display

Holograms are widely used for security and authentication, such as on credit cards and passports. There are two main types: white light-viewable holograms and those which require laser light for reconstruction. Security holograms are extremely difficult to forge, recognisable to the public, and are low cost. Photopolymer materials have been

tipped as "the number one disruptive technology in security printing in the next ten years" by Pira International, a leading market research company who specialise in packaging supply chains [56]. Development of recording media for full colour holography is a growing field. Silver halide materials have to date been the most successful for full colour holography, as they do not suffer from shrinkage, can achieve high sensitivities and demonstrate low scattering. However, silver halide is expensive and requires chemical processing after recording. Meka *et al* have developed a panchromatic AA-based photopolymer which can be used for full colour holography also [57]. Applications in display holographic are highly varied. For example Prof. Hans Bjelkhagen from OpTIC Technium in Wales has been creating holographic images of important historical artefacts, so that they may be put on display in smaller museums across Wales, increasing accessibility for the public [58].

1.5.3 Holographic interferometry

A hologram is a complete record of the wavefront of an object. Therefore, it is a powerful tool, with which it is possible to carry out detailed study of an object. Holographic interferometry is a technique which can be used to study surfaces which are not optically smooth with very high precision and sensitivity. Detailed comparison between the object's wavefront when it is subjected to changes in position, pressure, stress, temperature, vibrations etc. are made by analysing the fringe patterns caused by phase shifting. It is a whole field method and is non-contact, a feature which is desirable for studying delicate materials. Its sensitivity of the wavelength of light allows studying loads much lower than would be applied in practical use. The technique can also be used live [59].

1.5.4 Holographic optical elements (HOEs)

A HOE is a hologram of a light wave converter (lens, prism, mirror etc.) which performs the function of the recorded object with up to 100 % efficiency. They are in general wavelength dependent i.e. they operate best at the wavelength used to record them. It is possible to create HOEs with very large aperture size, and they can be recorded in lightweight materials. This is advantageous as the HOE will be low cost and less bulky than the converter counterpart. A number of HOEs can also be combined into a single layer of photosensitive material to produce a multifunction device.

There are a huge number of applications of HOEs, one of which is use in solar concentrators in order to increase energy output. By surrounding photovoltaic cells with HOE lenses, increased concentrations of light may be focussed on to the cells, hence increasing the energy output of the device. This is a low cost technique which is essential for production on a large scale as would be the case for solar cells. It also removes the need for expensive solar tracking systems. Research into the suitability of an AA-based photopolymer material for recording HOE lenses for solar concentrations is currently being carried out by researchers in the IEO centre [60, 61], and by other research groups world wide [62-65].

Another application of HOEs is in interferometric and shearographic systems for non-destructive testing as discussed in section 1.5.3. Both transmission and reflection mode HOEs have been used to reproduce both reference and diffracted beams, removing the typical complications in interferometric systems associated with alignment of bulky optical components, which can be a time-consuming and difficult process [66-70].

1.5.5 Holographic sensors

Another advancing field is that of holographic sensors. Holograms can be modified to detect and quantify environmental changes, such as changing temperature or humidity, and also the presence of certain substances such as harmful gases and metals. The Cambridge-based company Smart Holograms envisions holographic sensor technologies playing a large role in the medical field; it could allow diabetes patients to accurately monitor their blood-sugar levels, or patients with kidney problems to analyse their adrenaline levels from home [71].

The principle of operation of holographic sensors is straightforward. Dimensional and other changes in the hologram occur in response to some external influence. For example, a change in the refractive index modulation of the hologram due to a physical/chemical interaction between a hologram constituent and some analyte would allow for the detection of the analyte. Alternatively a change in the spacing of a recorded fringe pattern due to shrinkage or swelling of the material results in a change in the angular position of the Bragg peak for transmission holograms, or a change in the spectral position of the Bragg peak in reflection holograms. The IEO has developed humidity and temperature holographic sensors [72, 73] based on this principle using an AA-based photopolymer (see fig. 1.10). Reflection holograms are used as any changes in the hologram are easily observed by eye under white light, such as a change in colour. This is clearly shown in fig. 1.11. For transmission mode sensors, laser light or a photodetector is required to observe any change.

Nanoparticles can be used in conjunction with photopolymer materials to produce some interesting sensing properties. Zeolite nanoparticles have been added to the AA photopolymer to act as analyte traps [74]. The refractive index of the material is then

altered by the presence of the analyte. This principle has been used for a humidity sensor, where the porous zeolite nanoparticles trap water molecules inside. As described previously, this causes the material to swell and the colour of the hologram changes due to a shift in the spectral position of the Bragg peak. Lowe *et al* have developed several sensors in their polymer-based system, designed to detect metal ions [75], monitor glucose levels [76] and quantify the pH of solutions [77].
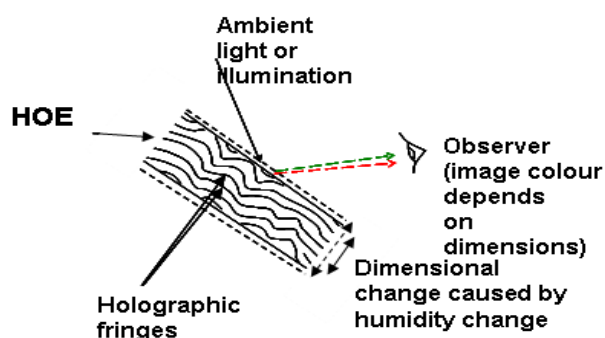
Fig. 1.8. Principle of operation of a holographic humidity sensor developed by IEO which changes colour with changing humidity [72].

Fig. 1.9. Colour change observed in the IEO holographic humidity sensor as the relative humidity is increased from 20-60 % [72].

1.6 Conclusions

In this chapter, a brief overview of the field of holography has been given. The principles behind holographic recording, the different classifications of holograms, numerous holographic recording media and several holographic applications have been described. The mechanism of holographic recording in photopolymers has been outlined in detail.

References:

[1] D. Gabor, "A New Microscopic Principle," Nature 161, 777-778 (1948).

[2] V. Toal, Introduction to Holography, CRC Press, Taylor and Francis Group, 2012.

[3] P. Hariharan, Optical Holography: Principles, Techniques and Applications, Cambridge University Press, 1984.

[4] E. N. Leith, J. Upatnieks, "Reconstructed Wavefronts and Communication Theory", JOSA, 52(10), 1123-1128 (1962).

[5] E. N. Leith, J. Upatnieks, "Wavefront Reconstruction with Continuous-Tone Objects", JOSA, 53(12), 1377-1381 (1963).

[6] H. I. Bjelkhagen, J. Chang, K. Moneke, "High-resolution contact Denisyuk holography", Appl. Opt. 31(8), 1041-1047 (1992).

[7] R. Collier, C. B. Buckart, L. H. Lin, "Optical Holography," Academic Press, New York, (1971).

[8] S. C. Barden, J. A. Arns, W. S. Colburn, "Volume phase holographic gratings and their potential for astronomical applications," SPIE Proc. 3355, 866-876 (1998).

[9] H. I. Bjelkhagen, Silver-halide recording materials for holography and their processing, Springer Science & Business Media, 1995.

[10] H. I. Bjelkhagen, T. H. Jeong, D. Vukičević, "Color Reflection Holograms Recorded in a Panchromatic Ultrahigh-Resolution Single-Layer Silver Halide Emulsion", Journal of Imaging Science and Technology 2, 134-146 (1996).

[11] H. I. Bjelkhagen, D. Vukičević, "Lippmann color holography in a single-layer silver-halide emulsion", Proc. SPIE 2333, Fifth International Symposium on Display Holography (1995).

[12] H. I. Bjelkhagen, T. H. Jeong, "Recording and processing of silver halide color holograms", Proc. SPIE 2405, Holographic Materials (1995).

[13] H. I. Bjelkhagen, D. Vukicevic, "Investigation of silver-halide emulsions for holography", Proc. SPIE 2043, Holographic Imaging and Materials (1994).

[14] N. J. Phillips, "The Role Of Silver Halide Materials In The Formation Of Holographic Images", Proc. SPIE 0532, Holography (1985).

[15] N. J. Phillips, R. D. Rallison, C. A. Barnett, S. R. Schicker, Z. A. Coleman, "Dichromated gelatin--some heretical comments", Proc. SPIE 1914, Practical Holography VII: Imaging and Materials (1993).

[16] J. M. Kim, B. S. Choi, S. I. Kim, J. M. Kim, H. I. Bjelkhagen, N. J. Phillips, "Holographic optical elements recorded in silver halide sensitized gelatin emulsions. Part I. Transmission holographic optical elements," Applied Optics 40, 622-632 (2001).

[17] J. M. Kim, B. S. Choi, Y. S. Choi, J. M. Kim, H. I. Bjelkhagen, N. J. Phillips, "Holographic optical elements recorded in silver halide sensitized gelatin emulsions. Part 2. Reflection holographic optical elements," Applied Optics 41, 1522-1533 (2002).

[18] N. I. Kirillov, N. V. Vasilieva, V. L. Zielikman, "Preparation of concentrated photographic emulsions by means of their successive freezing and thawing," Zh. Nauchn. Prikl. Fotogr. Kinematogr. 15, 441–443 (1970) (in Russian).

[19] H. Bjelkhagen, E. Mirlis, "Colour Holography to produce highly realistic three-dimensional images", Applied Optics 47, 123-133 (2008).

[20] http://www.slavich.com/

[21] W. C. Lin, L. J. Yang, "The Patterning of Glutaraldehyde-Crosslinked Gelatin", Conference Proceedings from 17th IEEE International Conference on Micro Electronic Mechanical Systems, 173-176 (2004).

[22] T. Sabel, S. Orlic, K. Pfeiffer, U. Ostrzinki, Gabi Grutzner, "Free-surface photopolymerizable recording material for volume holography", Optical Materials Express 3(3), 329-338 (2013).

[23] N. Ishii, T. Kato, J. Abe, "A real-time dynamic holographic material using a fast photochromic molecule", Scientific Reports 2(819), doi:10.1038/srep00819 (2012).

[24] Q. Zhang, J. Li, L. Niu, Z. Chen, L. Yang, S. Zhang, L. Cao, F. Zhang, "A rapid response photochromic diarylethene material for rewritable holographic data storage", Chinese Science Bulletin 58(1), 74-78 (2013).

[25] Y. Kong, S. Liu, J. Xu, "Recent Advances in the Photorefraction of Doped Lithium Niobate Crystals", Materials 5, 1954-1971 (2012).

[26] F. H. Mok, "Angle-multiplexed storage of 5000 holograms in lithium niobate", Optics Letters 18(11), 915-917 (1993).

[27] R. Castagna, F. Vita, D. E. Lucchetta, L. Criante, F. Simoni, "Superior-Performance Polymeric Composite Materials for High-Density Optical Data Storage", Advanced Materials 21, 589-592 (2009).

[28] G. Cipparrone, A. Mazzulla, F. Simoni, "Orientational gratings in dye-doped polymer-dispersed liquid crystals induced by the photorefractive effect", Optics Letters 23(19), 1505-1507 (1998).

[29] L. V. Natarajan, D. P. Brown, J. M. Wofford, V. P. Tondiglia, R. L. Sutherland, P. F. Lloyd, T. J. Bunning, "Holographic polymer dispersed liquid crystal reflection gratings formed by visible light initiated thiol-ene photopolymerisation", Polymer 47(12), 4411–4420 (2006).

[30] K. Pavani, "Holographic Liquid Crystal Devices", Doctoral Thesis, Dublin Institute of Technology, 2009 http://arrow.dit.ie/sciendoc/62/.

[31] S. Massenot, J. Kaiser, R. Chevallier, Y. Renotte, "Study of the dynamic formation of transmission gratings recorded in photopolymers and holographic polymer-dispersed liquid crystals", Appl. Opt. 43(29), 5489-97 (2004).

[32] L. Criante, R. Castagna, F. Vita, D. E. Lucchetta, F. Simoni, "Nanocomposite polymeric materials for high density optical storage", J. Opt. A: Pure Appl. Opt. 11, 024011 (2009).

[33] L. Criante, F. Vita, R. Castagna, D. E. Lucchetta, F. Simoni, "Characterization of Blue Sensitive Holographic Polymer Dispersed Liquid Crystal for Microholographic Data Storage", Molecular Crystals and Liquid Crystals 465(1), 203-215 (2007).

[34] R. Jallapuram, I. Naydenova, S.Martin, R. Howard, V. Toal, S. Frohmann, S. Orlic, H. J. Eichler, "Acrylamide-based photopolymer for microholographic data storage", Opt. Mat. 28(12), 1329-33 (2006).

[35] S. Blaya, L. Carretero, R. Mallavia, A. Fimia, R. Madrigal, M. Ulibarrena, D. Levy, "Optimisation of an Acrylamide-based dry film for holographic recording", Applied Optics 37, 7604-7610 (1998).

[36] E. Fernandez, A. Marquez, S. Gallego, R. Fuentes, C. Garcia, I. Pascual, "Hybrid ternary modulation applied to multiplexing holograms in photopolymers for data page storage", Journal of Lightwave Technology 28, 776-783 (2010).

[37] S.Q. Tao, Y.X. Zhao, Y.H. Wan, Q.L Zhai, P.F. Liu, D.Y. Wang, F.P. Wu, "Dual-wavelength sensitized photopolymer for holographic data storage", Japanese Journal of Applied Optics 49, 2010.

[38] F.K. Bruder, F. Deuber, T. Facke, R. Hagen, D. Honel, D. Jurbergs, M. Kogure, T. Rolle, M.S. Weiser, "Full-colour self-processing holographic photopolymers with high sensitivity in red – the first class of instant holographic photopolymers", Journal of photopolymer science and technology 22, 257-260 (2009).

[39] V. Pramitha, K.P. Nimmi, N.V. Subramanyan, R. Joseph, K. Sreekumar, C.S. Kartha, "Silver-doped photopolymer media for holographic recording", Applied Optics 48, 2255-2261 (2009).

[40] S. Liu, J. Sheridan, "Improvement of photopolymer materials for holographic data storage", Journal of Materials Science **44**, 6090-6099 (2009).

[41] I. Naydenova, R. Jallapuram, R. Howard, S. Martin, V. Toal, "Investigation of the diffusion processes in a self-processing acrylamide-based photopolymer system", Applied Optics 43(14), 2900-2905 (2004).

[42] M. Moothanchery, S. Mintova, I. Naydenova, V. Toal, "Nanoparticle doped photopolymer with reduced shrinkage for holographic recording", Photonics 2010: International Conference on Fiber Optics and Photonics, Guwahatti, India, December 11-15, 2010.

[43] E. Hata, Y. Tomita, "Order-of-magnitude polymerisation-shrinkage suppression of volume gratings recorded in nanoparticle-polymer composites", Optics Letters 35(3), 396-398 (2010).

[44]   http://ge.geglobalresearch.com/blog/breakthrough-in-micro-holographic-data-storage/

[45] F. S. Chen, J. T. LaMacchia, D. B. Fraser, "Holographic storage in lithium niobate", Appl. Phys. Lett. 13, 223 (1968).

[46] Y. Song, High Density Data Storage: Principle, Technology, and Materials, World Scientific, 2009.

[47] K. Curtis, L. Dhar, A. Hill, W. Wilson, M. Ayres, Holographic Data Storage: From Theory to Practical Systems, John Wiley & Sons, 2011.

[48] H.J. Coufal, D. Psaltis, G.T. Sincerbox, "Holographic Data Storage", Springer Series in Optical Sciences, Springer-Verlag, Berlin, 2000.

[49] L. Dhar, K. Curtis, M. Tackitt, M. Schilling, S. Campbell, W. Wilson, A. Hill, C. Boyd, N. Levinos, A.Harris, "Holographic storage of multiple high-capacity digital data pages in thick photopolymer systems", Opt. Lett. 23(21), 1710-2 (1998).

[50] S. H. Lin, K. Y. Hsu, W. Z. Chen, W. T. Whang, "Phenanthrenequinone-doped poly(methyl methacrylate) photopolymer bulk for volume holographic data storage", Opt. Lett. 25(7), 451-3 (2000).

[51] H. Sherif, I. Naydenova, S. Martin, C. McGinn, V. Toal, "Characterisation of an acrylamide-based photopolymer for data storage utilizing holographic angular multiplexing", J. Opt. A: Pure Appl. Opt 7, 255-60 (2005).

[52] S. S. Orlov, W. Phillips, E. Bjornson, Y. Takashima, P. Sundaram, L. Hesselink, R. Okas, D. Kwan, R. Snyder, "High-Transfer-Rate High-Capacity Holographic Disk Data-Storage System", Appl. Opt. 43(25), 4902-14 (2004).

[53] E. Fernández, M. Ortuño, S. Gallego, C. García, A. Beléndez, I. Pascual, "Comparison of peristrophic multiplexing and a combination of angular and peristrophic holographic multiplexing in a thick PVA/acrylamide photopolymer for data storage", Appl. Opt. 46(22), 5368-73 (2007).

[54] J. T. Sheridan, M. R. Gleeson, C. E. Close, J. V. Kelly, "Optical Response of Photopolymer Materials for Holographic Data Storage Applications", Amer. Sci. Pub. 7(1), 232-242 (2007).

[55] L. Criante, F. Vita, R. Castagna, D. E. Lucchetta, F. Simoni, "Characterization of Blue Sensitive Holographic Polymer Dispersed Liquid Crystal for Microholographic Data Storage", Molecular Crystals and Liquid Crystals 465(1), 203-215 (2007).

[56] http://www.smitherspira.com/most-disruptive-technologies-in-security-printing-revealed-by-pira-international.aspx

[57] C. Meka, R. Jallapuram, I. Naydenova, S. Martin, V. Toal, "Development of a panchromatic acrylamide based photopolymer for multicolour reflection holography" Applied Optics 49, 1400-05 (2010).

[58] H. I. Bjelkhagen, A. Osanlou, "Color holography for museums: bringing the artifacts back to the people", Proc. SPIE 7957, Practical Holography XXV: Materials and Applications, 79570B (February 07, 2011).

[59] M. Moothanchery, I. Naydenova, V. Bavigadda, S. Martin, V. Toal, "Real-time shrinkage studies in photopolymer films using holographic interferometry" Proc. SPIE 8437, Real-Time Image and Video Processing, 84370I (June 1, 2012).

[60] I. Naydenova, H. Akbari, C. Dalton, M. Y. M. Ilyas, C. P. T. Wei, V. Toal, S. Martin, "Photopolymer Holographic Optical Elements for Application in Solar Energy Concentrators", Holography – Basic Principles and Contemporary Applications, InTech, 2013.

[61] H. Akbari, I. Naydenova, S. Martin, "Using acrylamide-based photopolymers for fabrication of holographic optical elements in solar energy applications," Applied Optics 53, 1343-1353 (2014).

[62] C. G. Stojanoff, R. Kubitzek, S. Tropartz, K. Froehlich, O. Brasseur, "Design, fabrication, and integration of holographic dispersive solar concentrator for terrestrial applications", Proc. SPIE 1536, Optical Materials Technology for Energy Efficiency and Solar Energy Conversion (1991).

[63] Y. W. Zhang, C. S. I. Ih, H. F. Yan, M. J. Chang, "Photovoltaic concentrator using a holographic optical element", Applied. Optics 27, 3556-3560 (1988).

[64] X. Ren, S. Liu, X. Zhang, X. Chen, "Fabrication of holographic Fresnel lens used as solar concentrator", Proc. SPIE 6832, Holography and Diffractive Optics III (2007).

[65] S. Shaji, V. Vadivelan, K. P. T. Ajith, "A multi-beam holographic light concentrator for solar applications", SPIE Proc. 6832, Holography and Diffractive Optics III (2007).

[66] E. Mihaylova, I. Naydenova, S. Martin, V. Toal, "Electronic speckle pattern shearing interferometer with a photopolymer holographic grating", Applied Optics 43(12), 2439 – 2442 (2004).

[67] E. Mihaylova, I. Naydenova, Barry Duignan S. Martin, V. Toal, "Photopolymer diffractive optical elements in Electronic speckle pattern shearing interferometry", Optics and Lasers in Engineering 44, 965-974 (2006).

[68] V. Bavigadda, R. Jallapuram, E. Mihaylova, V. Toal, "Electronic speckle-pattern interferometer using holographic optical elements for vibration measurements", Optics Letters 35(19), 3273-3275 (2010).

[69] V. Bavigadda, R. Jallapuram, V. Toal, E. Mihaylova, " Vibration phase measurements using holographic optical elements", Optics Letters 35(19) 3273-3275 (2010).

[70] R. Jallapuram, C. Healy, E. Mihaylova, V. Toal, "In-plane sensitive electronic speckle pattern interferometer using a diffractive holographic optical element", American Journal of Physics 79, 389-391 (2011).

[71] http://www.sciencedaily.com/releases/2008/02/080204085305.htm

[72] I. Naydenova, R. Jallapuram, V. Toal, S. Martin, "A Visual Indication of Environmental Humidity Using a Colour Changing Hologram Recorded in a Self-Developing Photopolymer", Applied Physics Letters 92, 031109 (2008).

[73] I. Naydenova, J. Raghavendra, V.Toal, S. Martin, "Characterisation of the humidity and temperature responses of a reflection hologram recorded in acrylamide-based photopolymer", Sensors and Actuators B: Chemical 139, 35-38 (2009).

[74] E. Leite, I. Naydenova, N. Pandey, T. Babeva, G. Majano, S. Mintova, "Investigation of the light induced redistribution of zeolite beta nanoparticles in an acrylamide-based photopolymer" J. Opt. A 11(2), 024016 (2009).

[75] B. M. González, G. Christie, C. A.B. Davidson, J. Blyth, C. R. Lowe, "Divalent metal ion-sensitive holographic sensors", Analytica Chimica Acta 528(2), 219–228 (2005).

[76] S. Kabilan, J. Blyth, M. C. Lee, A. J. Marshall, A. Hussain, X.-P. Yang, C. R. Lowe, "Glucose-sensitive holographic sensors", Journal of Molecular Recognition 17(3), 162-166 (2004).

[77] A. J. Marshall, J. Blyth, C. A. B. Davidson, C. R. Lowe, "pH-Sensitive Holographic Sensors", Anal. Chem. 75 (17), 4423–4431 (2003).

2. LOW-TOXICITY PHOTOPOLYMER MEDIA FOR HOLOGRAPHIC APPLICATIONS

2.1 Introduction

As discussed in chapter 1, there is a large range of media available for holographic recording, each with their own inherent advantages and disadvantages. Of these, photopolymer materials have been the subject of much study for holographic applications such as HDS, sensors, HOEs and security devices. Their large dynamic range, high sensitivity and self processing nature make them an attractive candidate. AA-based photopolymers in particular have been very popular among the research community. This is easy to understand, as they are water soluble, easy to prepare, low cost and readily record bright, efficient holograms. In recent years however, as holographic applications are becoming more and more of a reality, there has been a move in the research community towards photopolymer materials that not only perform well holographically, but that are low-toxicity and environmentally compatible.

In this chapter, a review of the development of AA-based holographic photopolymers is presented, in order to familiarise the reader with the current state-of-the-art. The recent research in the field of reduced-toxicity photopolymer formulations for holographic applications is discussed, as well as outlining the main motivation for this research. Finally, the aims of the PhD research project are presented.

2.2 Overview of the development of AA-based holographic photopolymers

The first description of the dye-sensitized polymerisation of AA was outlined by Oster *et al* in 1957 [1], in which the polymerisation of AA in solution was induced by visible

light in the presence of the sensitizer riboflavin. In 1965 Chen combined the electron donor Triethanolamine (TEA) with the photosensitive dye Methylene Blue, creating a photoinitiating system that was used to induce polymerisation in an aqueous AA-based solution [2]. In 1969 Close *et al* successfully recorded the first holograms in a liquid state photopolymer system with diffraction efficiencies of up to 45 % [3]. In 1970 Jenney recorded phase holograms with resolution up to 3000 l/mm in AA-based photopolymer materials that were self-developing, but required post exposure fixing with UV-light [4]. In 1975 Sadlej *et al* proposed an AA and Methylene Blue photopolymer system with a new component, the binder polyvinyl alcohol (PVA), which allowed for the production of solid photopolymer layers for the first time [5]. Sugawara *et al* demonstrated the suitability of TEA over other photoinitiators when combined with Methylene Blue dye [6], and diffraction efficiencies of up to 65 % were observed to last for 80 days in the AA-based photopolymer layers.

In 1987, a photopolymer system was developed by Calixto which contained AA as the monomer, PVA as the binder, TEA as the photoinitiator, and Methylene Blue as the photosensitive dye [7]. He demonstrated the feasibility of this material for holographic recording applications, as well as its ease of production and self-processing nature. Diffraction efficiencies of approximately 10 % were obtained using an exposure energy of 94 mJ/cm^2. In 1994 a further step was made by Martin *et al*, with the addition of a cross-linking monomer N,N'-methylenebisacrylamide (BA) to a photopolymer composition similar to the one described by Calixto, using Erythrosin B as the photosensitizer. This was proven to improve the stability and lifetime of the recorded gratings [8]. The effect and role of the different components of the composition was investigated, as was the suitability of five different xanthene dyes as potential photosensitisers. Erythrosin B was selected as a suitable photosensitive dye due to its

effect on the sensitivity of the photopolymer system, which was shown to increase by a factor of five in comparison to the non-xanthene dye Fluorescein. Since then, this photopolymer system has been used by holographic research groups worldwide [9-14], due to its ease of preparation, self-processing nature, and suitability for a large variety of holographic applications. A significant step in the development of AA-based photopolymer layers is its optimisation for recording in reflection mode by suppressing the short polymer chains diffusion by selecting a binder matrix with low permeability. This enables the recording of reflection mode, full-colour holograms and colour-changing holographic sensors in this material [14-17]. An extensive description on the early photopolymer systems and commercial photopolymers has been given by Pramitha [18].

2.3 Motivation for the development of low-toxicity holographic photopolymers

There is a currently a huge movement in industry worldwide towards "Green" production i.e. products and processes that reduce or eliminate the use or generation of hazardous and toxic substances. Government directives and legislation have been introduced in both Europe and the United States to this effect [19, 20].

The development of PVA/AA photopolymer materials for holographic applications has been a hot research topic since the late 1950s. However, the toxic nature of these photopolymer materials is a growing concern. This toxicity can be largely attributed to the carcinogenic nature of the monomer AA [21-24]. AA is a main component of the standard photopolymer composition, and is both carcinogenic and toxic in its monomer form. It is classified as a carcinogen by both the World Health Organisation (WHO) and the International Agency for Research on Cancer (IARC) [24, 41]. The toxicity of AA

has been extensively investigated, using both in vivo and in vitro cytotoxicity methods [25-31]. An extensive study into the chemical and biochemical safety of AA carried out by Friedman [32] found that AA is involved in reactions with proteins such as haemoglobin, enzymes, and DNA.

As holographic technologies are advanced, there is going to be a need for recording media which can be produced in bulk with little risk to workers or the environment. In order for photopolymer recording media to be a viable option for holographic applications, efforts must be made to reduce the potential occupational and environmental hazards involved in future large-scale material development and device fabrication. The relevance of this is further highlighted by a report published by the European Commission on Environmental Policy for 2010, in which a large emphasis is placed on the risk assessment of chemicals used in manufacturing [33].

Several low-toxicity materials have been proposed as alternatives for holographic applications to the standard AA-based photopolymer. Ortuno *et al* have developed a low-toxicity material called "Biophotopol", which uses the low toxicity material Sodium Acrylate (NaAO) as the substitute monomer for AA [34-36]. A maximum diffraction efficiency of 77 % at the Bragg angle is reported for 900 μm thick NaAO photopolymer layers. These samples were tested at a spatial frequency of 1125 l/mm, with a recording intensity of 5 mW/cm^2. A refractive index modulation of approximately 2.24×10^{-4} is reported for the NaAO photopolymer. This is a factor of a magnitude lower than the refractive index modulation achieved with the standard PVA/AA composition. This could be partly due to the difference in the refractive index of the AA and NaAO based materials [35]. Although the ability to produce thick layers is advantageous, the shrinkage of the NaAO photopolymer has been measured at approximately 3 %, making it unsuitable for certain applications including HDS.

A low-toxicity material using PVA photosensitized with dihydrated copper chloride ($CuCl_2(2H_2O)$)) has been developed by Olivares-Perez et al [37]. An attractive feature of this material is its ability to conduct electricity, making it a candidate for opto-electric applications. The $CuCl_2(2H_2O)$ sensitizer was chosen as it can be mixed with aqueous solutions and has low toxicity, which makes it attractive for production of diffractive optical elements. Preliminary results show a maximum diffraction efficiency of 3.9 % for transmission gratings recorded in 200 μm thick layers. The recording of such low diffraction efficiency gratings in this material requires relatively high exposure energy of 4 J/cm^2. However, it is acknowledged that this is due to the large thickness of the layers which is known to present difficulties for holographic recording, both in terms of increased scattered and absorption, and also increased optical thickness [38].

A second low-toxicity material has been developed by Olivares-Pérez et al which uses the Nopal Cactus as a component of the holographic recording material [39]. Mg^{+2} ions which are a part of the chlorophyll core of the cactus are substituted with Fe^{+2} ions on exposure to light, forming a photosensitive substance. The Fe^{+2} solution obtained from the fermented cactus is used as a photosensitizer. Combined with a PVA matrix, the substance can be used as a recording medium. Preliminary results show that the low-toxic and self-developing material is capable of recording diffraction gratings with diffraction efficiencies of up to 32 % at a spatial frequency of approximately 650 l/mm. However, as the spatial frequency is increased above this, there is a significant decrease in the achievable diffraction efficiency. Another disadvantage of this material is the lengthy production process; the Fe^{+2} extract requires 10-18 days for optimum fermentation, after which it can be stored for 30-60 days only at 5-10°C. This is a considerably longer and more complicated production procedure than for a standard photopolymer material.

The replacement of AA with lower toxicity monomers is not only limited to materials developed for holographic applications; this same process has been carried out in order to reduce the toxicity of polymer gel dosimeter recipes also [40].

It is evident that there is need for a photopolymer material that is both holographically sensitive enough to meet the requirements of a wide range of holographic applications, and low-toxic in order to reduce the occupational and environmental hazards involved in production on a large scale.

2.4 Aims of the PhD Research

- To develop and optimise a novel, low-toxicity photopolymer material which uses the monomer Diacetone Acrylamide (DA) instead of AA. DA is a low-toxic material and it is classified as a non-carcinogen by the IARC [41, 42].

- To characterise the holographic recording ability of the DA photopolymer in both the transmission and reflection regimes of recording. By characterising the photopolymer in this way, its suitability for a wide range of holographic applications such as holographic sensors and HOE development is investigated.

- To characterise the rate of different processes occurring in the DA-photopolymer during holographic recording, namely the rate of polymerisation of the DA monomer, and the rate of polymerisation-induced shrinkage.

- To conduct an independent cytotoxicity evaluation of the DA-based and AA-based photopolymers, in order to justify the monomer replacement.

- To investigate the effect of different additives, namely Glycerol and Zeolite Nanoparticles, on the holographic recording properties of the DA-based photopolymer.

- To show that the DA photopolymer can be used to develop holographic gas sensors which are capable of detecting hydrocarbon gases at different concentrations.

- To prove that pressure sensors can be developed using reflection holograms recorded in the DA-photopolymer.

2.5 Conclusions

In this chapter, the history of the development of AA-based photopolymer materials has been summarised. Following this, a review of the developments made to date in non-toxic photopolymer research has been given. This was done in order to introduce the research presented here, which is the development and characterisation of a novel, low-toxicity photopolymer system using DA as the replacement for AA. The motivation behind this, namely the push towards reduced toxicity and occupational hazards in the large scale production of holographic photopolymer devices, has been explained in detail.

References:

[1] G. K. Oster, G. Oster, G. Prati, "Dye-sensitized Photopolymerization of Acrylamide", J. Am. Chem. Soc. 79(3), 595-8 (1957).

[2] C. Chen, "Dye-sensitized photopolymerization. I. Polymerization of acrylamide in aqueous solution sensitized by methylene blue–triethanolamine system", J. Pol. Sci. A 3(3), 1107-25 (1965).

[3] D. H. Close, A. D. Jacobson, J. D. Margerum, R. G. Brault, F. J. McClung, "Hologram recording on photopolymer materials", Appl. Phys. Lett. 14, 159 (1969).

[4] J. A. Jenney, "Holographic recording with photopolymers", JOSA 60(9), 1155-61 (1970).

[5] N. Sadlej, B. Smolinska, "Stable photo-sensitive polymer layers for holography", Optics and Laser Technology 7(4), 175-9 (1975).

[6] S. Sugawara, K. Murase, T. Kitayama, "Holographic recording by dye-sensitized photopolymerization of acrylamide", Appl. Opt. 14(2), 378-82 (1975).

[7] S. Calixto, "Dry polymer for holographic recording", Appl. Opt. 26(18), 3904-3910 (1987).

[8] S. Martin, P. Leclere, Y. Renotte, V. Toal, Y. F. Lion, "Characterization of an acrylamide-based dry photopolymer holographic recording material", Opt. Eng. 33, 3942 (1994).

[9] S. Blaya, L. Carretero, R. Mallavia, A. Fimia, R. Madrigal, M. Ulibarrena, D. Levy, "Optimisation of an Acrylamide-based dry film for holographic recording", Applied Optics 37, 7604-7610 (1998).

[10] C. Neipp, S. Gallego, M. Ortuño, A. Márquez, A. Beléndez, I. Pascual, "Characterization of a PVA/acrylamide photopolymer. Influence of a cross-linking monomer in the final characteristics of the hologram", Opt. Comm. 224(1-2), 27-34 (2003).

[11] H. Yao, M. Huang, Z. Chen, L. Hou, F. Gan, "Optimisation of two-monomer-based photopolymer used for holographic recording", Mat. Lett. 56(1-2), 3-8 (2002).

[12] J. Zhu, G. Wang, Y. Hao, B. Xie, A. Y. S. Cheng, "Highly sensitive and spatially resolved polyvinyl alcohol/acrylamide photopolymer for real-time holographic applications", Opt. Express 18(17), 18106-12 (2010).

[13] F. T. O'Neill, J. R. Lawrence, J. T. Sheridan, "Thickness variation of self-processing acrylamide-based photopolymer and reflection holography", Opt. Eng. 40(4), 533-9 (2001),

[14] I. Naydenova, R. Jallapuram, R. Howard, S. Martin, V. Toal, "Investigation of the Diffusion Processes in a Self-Processing Acrylamide-Based Photopolymer System", Appl. Opt. 43(14), 2900-05 (2004).

[15] R. Jallapuram, "Optimization of an acrylamides-based photopolymer for reflection holographic recording", Doctoral Thesis, Dublin Institute of Technology, 2005.

[16] C. Meka, R. Jallapuram, I. Naydenova, S. Martin, V. Toal, "Development of a panchromatic acrylamide based photopolymer for multicolour reflection holography" Applied Optics 49, 1400-05 (2010).

[17] I. Naydenova, J. Raghavendra, V.Toal, S. Martin, "Characterisation of the humidity and temperature responses of a reflection hologram recorded in acrylamide-

based photopolymer", Sensors and Actuators B: Chemical 139, 35-38 (2009).

[18] V. Pramitha, "A new metal ion doped panchromatic photopolymer for holographic applications", Doctoral Thesis, Cochin University of Science and Technology, November 2010.

[19] Directive 2011/65/EU of the European Parliament and the Council of 8 June 2011 on the restriction of the use of certain hazardous substances in electrical and electronic equipment [2011] OJ L174/88.

[20] 108th Congress S.2967 To provide for the implementation of a Green Chemistry Research and Development Program, and for other purposes. [2004] S 2967 IS.

[21] D. D. McCollister, F. Oyen, V. K. Rowe, "Toxicology of Acrylamide", Toxicology and Applied Pharmacology 6, 172-181 (1964).

[22] A. G. Lawrence, R. Gentry, T. McDonald, H. Bartow, J. Bounds, N. Macdonald, H. Clewell, B. Allen, C. Van Landingham, "Acrylamide: Review of Toxicity Data and Dose-Response Analyses for Cancer and Noncancer Effects", Critical Reviews in Toxicology 36, 481-608 (2006).

[23] D. J. King, R. R. Noss, "Toxicity of polyacrylamide and acrylamide monomer", Rev. Environ. Health 8, 3-16 (1989).

[24] Health implications of acrylamide in food: report of a joint FAO/WHO consultation, WHO Headquarters, Geneva, Switzerland, 25-27 June, 2002.

[25] X. X. Ma, G. D. Yao, H. Cheng, Q. L. Zeng, Q. Chen, "Effects of acrylamide on DNA damage in human keratinocytes", Anal. Chem. 76(5), 1518-1523 (2004).

[26] J. E. Klaunig, L. M. Kamendulis, "Mechanisms of acrylamide induced rodent carcinogenesis", Adv. Exp. Med. Biol. 561, 49-62 (2005).

[27] J. Park, L. M. Kamendulis, M. A. Friedman, J. E. Klaunig, "Acrylamide-induced Cellular Transformation", Toxicol. Sci. 65(2), 177-183 (2001).

[28] A. G. Lawrence, R. Gentry, T. McDonald, H. Bartow, J. Bounds, N. Macdonald, H. Clewell, B. Allen, C. Van Landingham, "Acrylamide: Review of Toxicity Data and Dose-Response Analyses for Cancer and Noncancer Effects," Crit. Rev. Toxicol. 36(6-7), 481-608 (2006).

[29] H. Tsuda, C. S. Shimizu, M. K. Taketomi, M. M. Hasegawa, A. Hamada, K. M. Kawata, N. Inui, "Acrylamide; induction of DNA damage, chromosomal aberrations and cell transformation without gene mutations", Mutagenesis 8(1), 23-29 (1993).

[30] K. A. Johnson, S. J. Gorzinski, K. M. Bodner, R. A. Campbell, C. H. Wolf, M. A. Friedman, R. W. Mast, "Chronic toxicity and oncogenicity study on acrylamide incorporated in the drinking water of Fischer 344 rats", Toxicol. Appl. Pharmacol. 85(2), 154-168 (1986).

[31] T. Takahashi, M. Yoshii, T. Kawano, T. Kosaka, H. Hosoya, "A new approach for the assessment of acrylamide toxicity using a green paramecium", Toxicol. In Vitro 19(1), 99-105 (2005).

[32] M. Friedman, "Chemistry, Biochemistry and Safety of Acrylamide. A Review", J. Agric. Food Chem. 51(16), 4504-4526 (2003).

[33] European Commission on Environmental Policy, FP7 Cooperative Work Program 2010: Environment, p. 50, 29/07/2009.

[34] M. Ortuno, E. Fernandez, S. Gallego, A. Belendez, I. Pascual, "New photopolymer holographic recording material with sustainable design," Optics Express 15, 12426-12435 (2007).

[35] S. Gallego, A. Marquez, M. Ortuno, S. Marini, J. Frances, "High environmental compatibility photopolymers compared to PVA/AA based materials at zero spatial frequency limit," Optical Materials 33, 531-537 (2011).

[36] M. Ortuno, S. Gallego, A. Marquez, C. Neipp, I. Pascual, A. Belendez, "Biophotopol: a sustainable photopolymer for holographic data storage applications", Materials 5, 772-783 (2012).

[37] A. Olivares-Perez, M.P. Hernandez-Garnay, I. Fuentes-Tapia, J.C. Ibarra-Torres, "Holograms in polyvinyl alcohol photosensitized with $CuCl_2(H_2O)$", Optical Engineering 50, 0658011-0658016 (2011).

[38] M. Mahmud, I. Naydenova, N. Pandey, T. Babeva, R. Jallapuram, S. Martin, V. Toal, "Holographic recording in acrylamide photopolymers: Thickness limitations", Applied Optics, 48(14), 2642-2648 (2009).

[39] A. Olivares-Pérez, S.Toxqui-López, A. L. Padilla-Velasco, "Nopal Cactus (Opuntia Ficus-Indica) as a Holographic Material", Materials 5, 2383-2402 (2012).

[40] R. J. Senden, P. De Jean, K. B. McAuley, L. J. Schreiner, "Polymer gel dosimeters with reduced toxicity: a preliminary investigation of the NMR and optical dose-response using different monomers", Physics in Medicine and Biology 51(14), 3301-3314 (2006).

[41] J. Siemiatycki, L. Richardson, K. Straif, B. Latreille, R. Lakhani, S. Campbell, M Rousseau, P. Boffetta, "Listing Occupational Carcinogens", Environ. Health Perspect. 112, 1447–1459 (2004).

[42] *Diacetone Acrylamide*; Sigma-Aldrich;

http://www.sigmaaldrich.com/catalog/DisplayMSDSContent.do (accessed 30/6/11).

3. OPTIMISATION OF THE DA PHOTOPOLYMER FOR TRANSMISSION MODE RECORDING

3.1 Introduction

The aim of this chapter is to introduce the Diacetone Acrylamide (DA)-based photopolymer composition in detail, and to describe the steps taken in the optimisation of the DA-based formulation. A brief description of each of the individual photopolymer components is given in order to better understand their role in the photopolymer composition. The optimisation of the holographic photopolymer formulation for the monomer DA for transmission mode recording is presented.

3.2 Description of the photopolymer components

3.2.1 Diacetone Acrylamide

N-(1,1-Dimethyl-3-oxobutyl) Acrylamide, or Diacetone Acrylamide (DA) as it is commonly known, is a vinyl functional monomer which has the appearance of a white, crystalline solid. The synthesis of DA from acetone, acrylonitrile and sulphuric acid is outlined in [1]. It is described to contain only 0.1 wt.% Acrylamide (AA) as synthesised by Sigma Aldrich [2, 3]. The chemical structures of DA and AA are shown in fig. 3.1.

DA was chosen as the primary monomer for this photopolymer composition due to its low-toxicity nature. It is listed as a category four material in terms of its acute toxicity, as opposed to AA which is a high-risk category three material [3, 4]. DA is classified as a non-carcinogen by the International Agency for Research on Cancer [2]. Aside from its low toxicity, DA is a highly hydrophilic, water-soluble material, which is essential to ensure its compatibility with the rest of the photopolymer composition. It readily

polymerises with a variety of co-monomers [5] which is of importance in holographic formulations as the inclusion of a crosslinking monomer is very beneficial for the stability of the recorded gratings.

The properties of the main monomer used in the photopolymer composition is of utmost importance; parameters such as the rates of diffusion and polymerisation of the monomer molecules during holographic recording depend greatly on the physical properties such as size and shape of the monomer molecules. The size of the DA monomer molecule is estimated to be 10×4 Å; this makes the DA monomer molecule twice as large as the AA molecule, which have dimensions of 5×4 Å. It is expected that this will have an effect on the holographic recording properties of the DA-based material.

The Raman spectrum of DA measured at 660 nm is shown in fig. 3.2. The peaks at 1625 cm^{-1} and 1284 cm^{-1} correspond to the C=C double bond and C-H vinyl bond of the DA monomer.

The monomer AA was also used for comparison purposes. The Raman spectrum of AA is shown in fig. 3.3. The peaks at 1633 and 1284 cm^{-1} correspond to the C=C double bond and the C-H vinyl bond respectively [6].
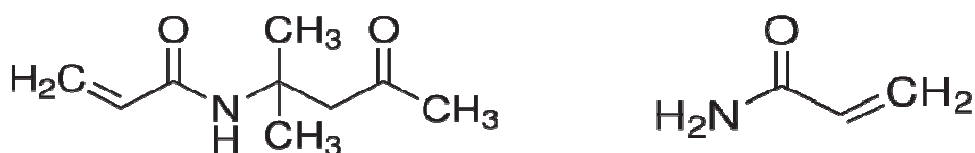
Fig. 3.1. Chemical structures of DA (left) and AA (right).

54
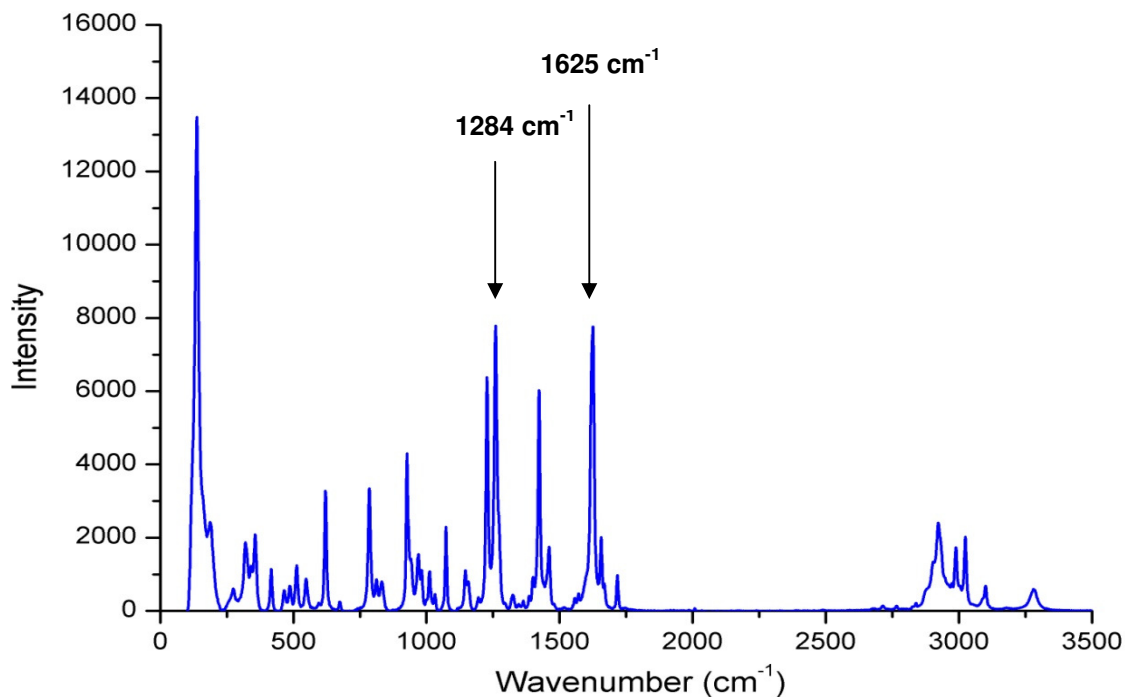
Fig. 3.2. Raman spectrum of the DA monomer taken at 660 nm using a ×100 objective and an 1800 l/mm grating. A Jobin Yvon LabRam 1B Spectrometer was used for all Raman measurements.
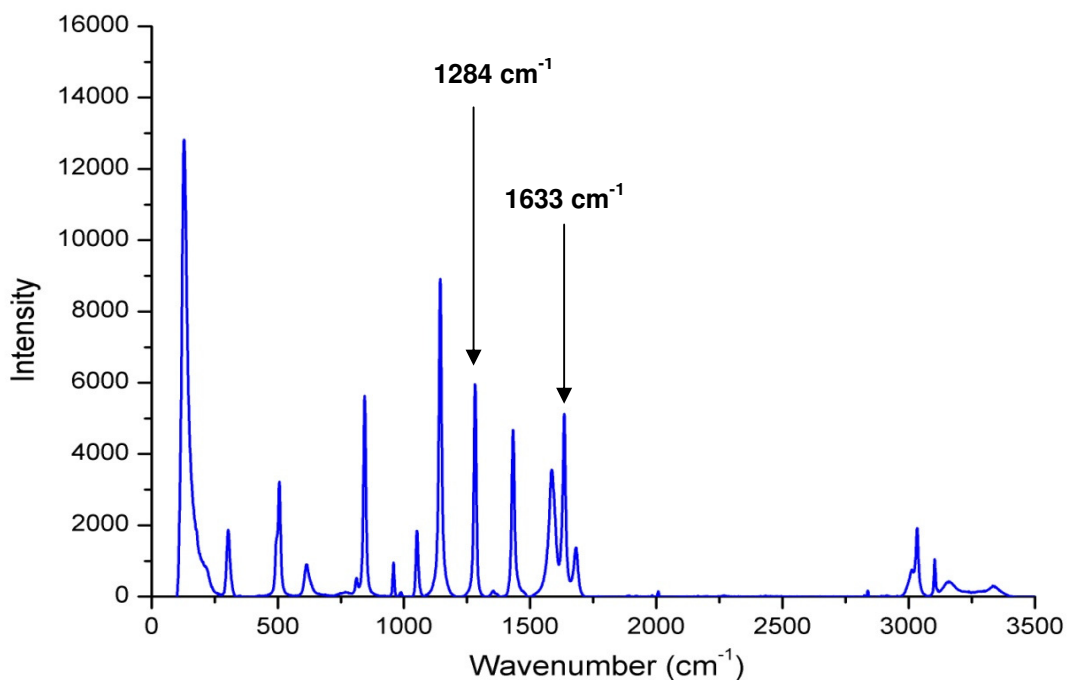
Fig. 3.3. Raman spectrum of the AA monomer taken at 660 nm using a ×100 objective and an 1800 l/mm grating.

55

3.2.2 N, N-methylene-bisacrylamide

N, N-methylene-bisacrylamide (BA) was chosen as the crosslinking monomer for the DA photopolymer formulation. BA is a well-known crosslinker for AA; a polyacrylamide gel formed from the combination of AA and BA is commonly used in the biological industry as an electrophoresis matrix for the separation of proteins and nucleic acids [7]. The chemical structure for BA is shown in fig. 3.4, and the mechanism for the crosslinking of AA polymer chains by BA is shown in fig. 3.5. The use of BA as a crosslinker in AA-based holographic formulations is well established [8-10], and its role within the photopolymer during holographic recording is well understood [11-14]. The function of the crosslinker in the photopolymer composition is to bind the polymer chains together during the photoinduced polymerisation reaction. This restricts diffusion of the polymer chains out of the illuminated regions, thus maximising the refractive index modulation of the recorded hologram. The presence of the crosslinker also prohibits post-recording decay of holograms recorded in the photopolymer. It is expected that BA will function in the same fashion as a crosslinker for DA as for the AA monomer. The Raman spectrum for BA is shown in fig. 3.6. The peak at 1629 cm^{-1} corresponds to the C=C double bond of BA.
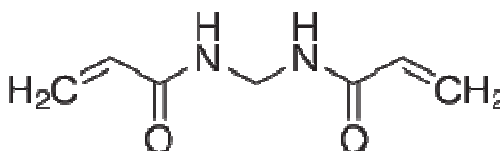
Fig. 3.4. Chemical structure of BA.
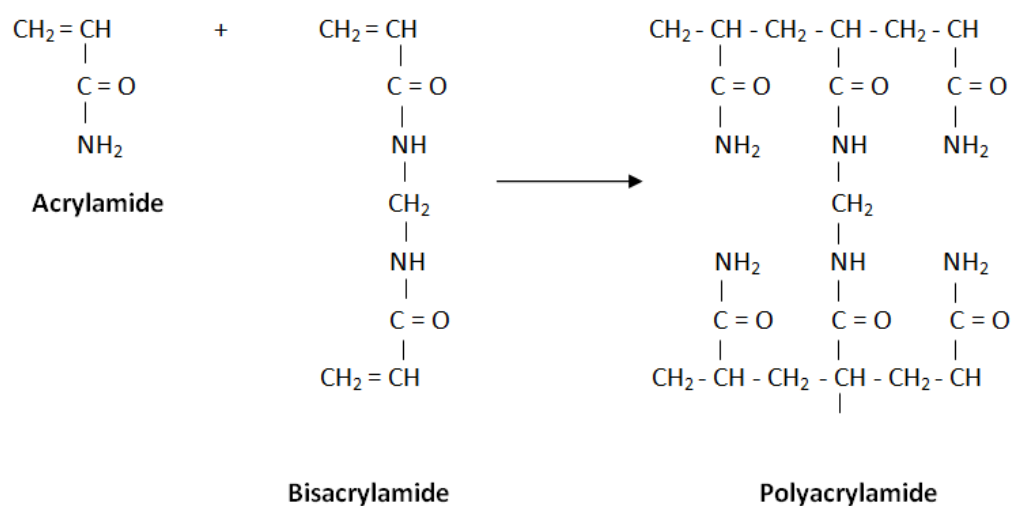
Fig. 3.5 Crosslinking reaction between AA and BA to produce crosslinked polyacrylamide.
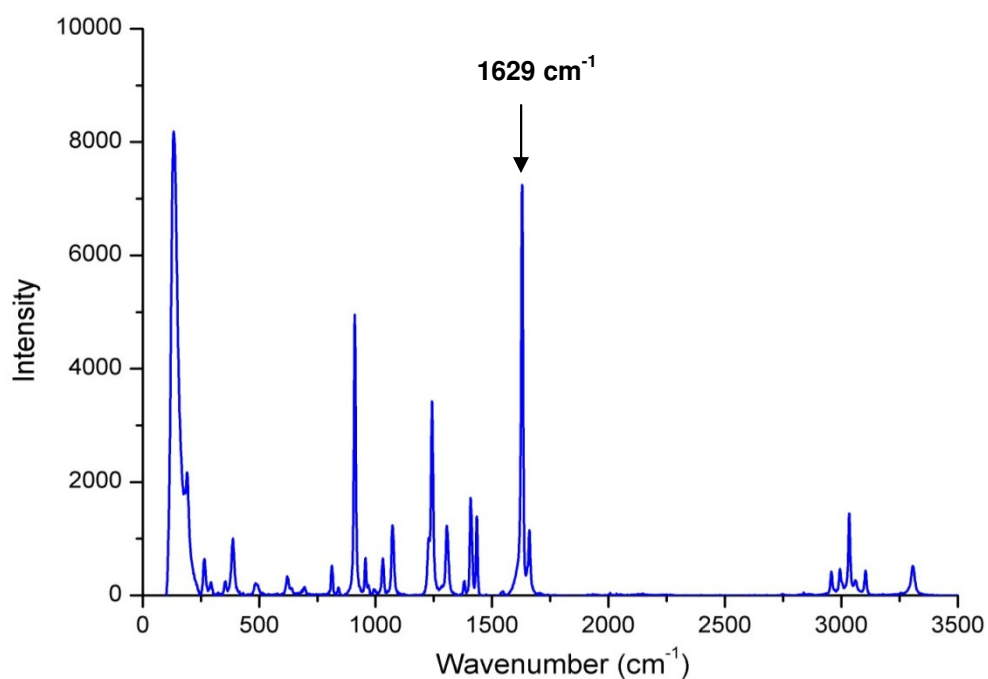
Fig. 3.6. Raman spectrum of the BA crosslinking monomer taken at 660 nm using a ×100 objective and an 1800 l/mm grating.

57

3.2.3 Triethanolamine

Triethanolamine (TEA) is used as an electron donor in the photopolymer composition. Its function is to create free radicals upon illumination in order to facilitate the photopolymerisation reaction. TEA also acts as a plasticizer; it improves layer stability by preventing crystallisation of the solid components out of the photopolymer layers.

A study has been carried out by Lu *et al* into the ability of different amine compounds to act as electron donors in acrylate photopolymer formulations, namely TEA, Diethanolamine (DEA), Ethanolamine (EA), Triethylamine (TETN) and Diethy-lamine (DETN) [15]. The holographic capability of the different electron donors was measured in terms of their ability to record high diffraction efficiency gratings, the photo-bleaching coefficient, and the quantum yield. In all cases TEA obtained the optimum values.

The molecular structure of TEA is shown in fig. 3.7.
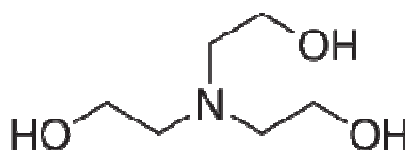
Fig. 3.7. Chemical structure of TEA.

3.2.4 Polyvinyl Alcohol

The function of the binder matrix is to hold all of the photopolymer components together in the composition and to facilitate the formation of a solid layer. A 10 %

wt/vol Polyvinyl Alcohol (PVA) solution was used for all experiments related to the optimisation of the composition. The chemical structure of PVA is shown in fig. 3.8. 80 % hydrolysed PVA was used. Different percentages of hydrolysation of PVA in the standard AA-based formulation have previously been investigated by researchers in the Centre for Industrial and Engineering Optics [16]. A hydrolysation percentage of PVA of 80 % was shown to be optimum, in particular for reflection mode recording, as the rate of diffusion was observed to be slowest at this percentage. Slow diffusion is advantageous to prevent polymer chain diffusion out of illuminated areas within a grating, which leads to a reduction in grating diffraction efficiency.
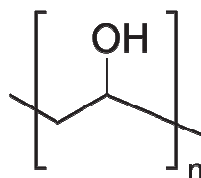
Fig. 3.8. Chemical structure of PVA.

3.2.5 Photosensitive Dye

When selecting a photosensitive dye for a photopolymer system, it is important that the dye meets certain criteria. Strong absorption of the dye at the illumination wavelength is required for more effective excitation of the dye molecules. It is important that the quantum yield of triplet state excited dye molecules is high, as this is the state required for successful interaction with the electron donor, as discussed in chapter 1. Finally it is important that the photosensitising system i.e. the dye and the electron donor, is efficient in producing free radicals. Based on the above described criteria, two photosensitive dyes were chosen: Erythrosin B and Methylene Blue.

3.2.5.1 Erythrosin B

The ability of different dyes as to act as sensitisers in a photopolymer system at a recording wavelength of 514 nm was investigated by Martin [16]. The dyes investigated were Flourescein, Eosin Y, Phloxine B, Erythrosin B and Rose Bengal. The five dyes were compared in terms of their quantum yield of bleaching and quantum yield of initiation of polymerisation at an excitation wavelength of 514 nm. In both cases, Erythrosin B was determined to be the most efficient dye.

Erythrosin B was used in the work presented here as the sensitising dye for all experiments carried out using a recording wavelength of 532 nm. Erythrosin B is a fluorescent, xanthene dye, and its chemical structure is shown in fig. 3.9(a). It is sensitive to wavelengths of light between 400 and 550 nm as shown in its absorption spectrum in fig. 3.9(b). This makes it suitable for holographic recording at 532 nm.

(a)   (b)
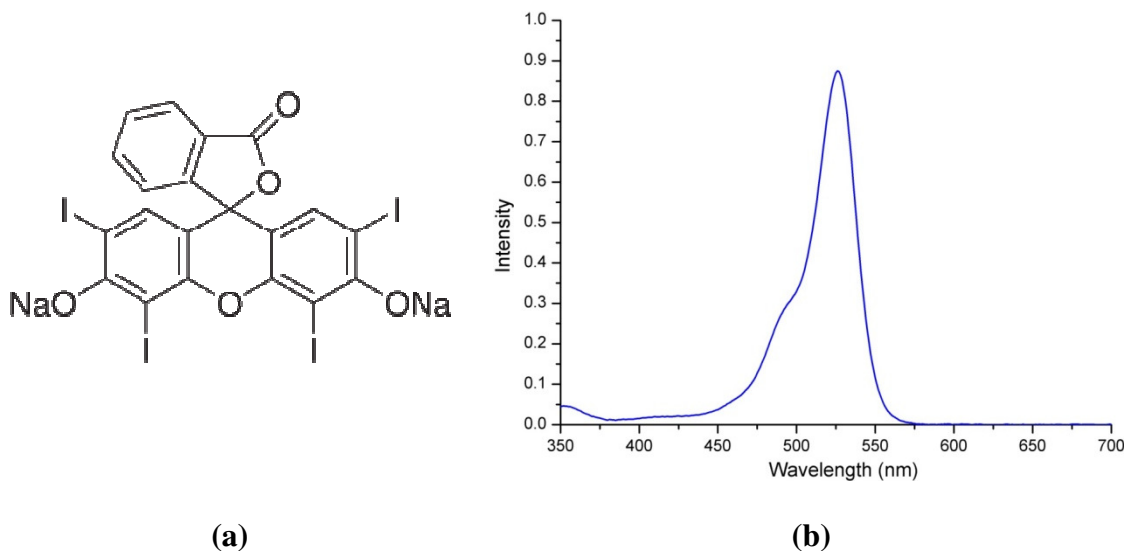
Fig. 3.9. (a) Chemical structure of Erythrosin B; (b) absorption spectrum of Erythrosin B dye measured with a UV-Vis spectrometer.

3.2.5.2 Methylene Blue

Methylene Blue was used as the sensitising dye in all experiments carried out at a recording wavelength of 633 nm. Methylene Blue is a thiazine dye, indicating that it contains a ring of four carbon atoms, one nitrogen atom and one sulphur atom, which can be seen in its chemical structure in fig. 3.10(a). It is sensitive to wavelengths of light between 500 and 700 nm as shown in its absorption spectrum in fig. 3.10(b).

(a)   (b)
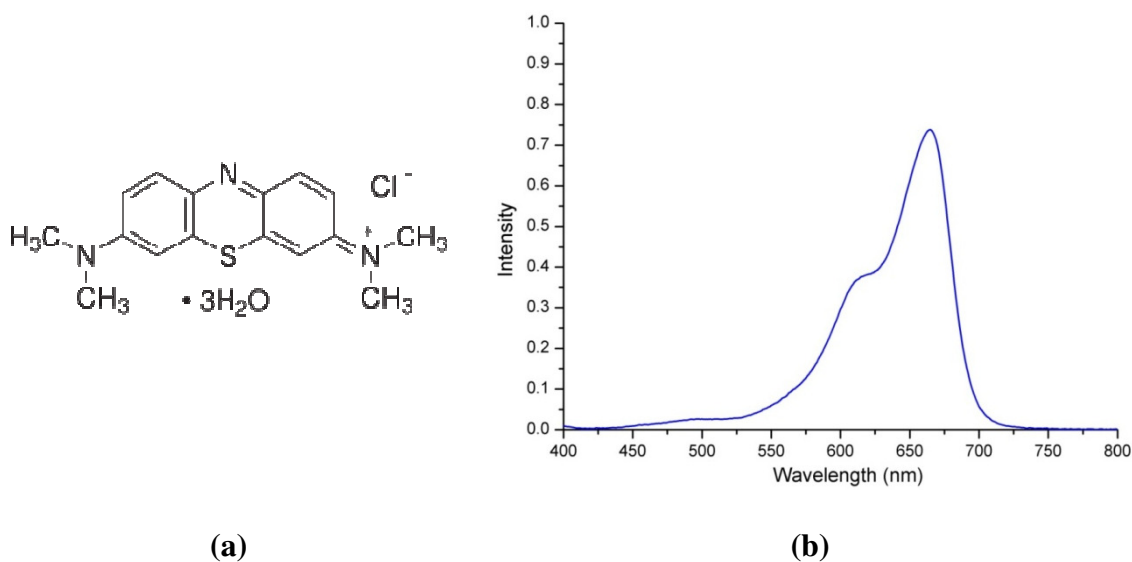
Fig. 3.10. (a) Chemical structure of Methylene Blue; (b) absorption spectrum of Methylene Blue dye measured with a UV-Vis Spectrometer.

All chemicals were purchased from Sigma Aldrich and used without further purification.

3.3 DA-based composition optimisation

In order to characterise the holographic recording capability of the DA photopolymer material, the photopolymer composition first had to be optimised for the new component. This allowed for the limits of the new monomer in relation to the photopolymer composition to be investigated, such as its solubility in solution. It is essential that all components are fully dissolved in order for high optical quality layers to be obtained.

A simple systematic method was introduced in order to effectively optimise the composition. The standard AA-based photopolymer formulation was used as the initial guideline for the new material formulation, as this composition was rigorously optimised previously by Martin [17]. Therefore, the volumes of the binder, electron donor and photosensitiser remained the same. The first step was to determine the optimum concentration of the main monomer DA in the photopolymer composition. This step is described below in section 3.3.2. The recording ability of the different compositions was tested by recording transmission gratings at a spatial frequency of 1000 l/mm. Once the optimum concentration had been determined using this method, the crosslinking monomer BA was added to the formulation and its concentration was optimised in the same way as described in section 3.3.3.

3.3.1 Experimental setup

Un-slanted holographic transmission gratings were recorded using a 532 nm Nd:YVO$_4$ laser as shown in fig. 3.11. The vertically polarised beam was split in two via a beamsplitter. The inter-beam angle was set at 30° in order to produce gratings with a

spatial frequency of 1000 ± 30 l/mm. The absorption of the photopolymer at 633 nm is negligible, therefore a 633 nm He-Ne laser was used as a probe beam at the Bragg angle to enable the diffracted beam intensity to be monitored in real time. An optical power meter (Newport 1830-C) recorded the intensity of the diffracted beam and the data was transferred to a computer via a data acquisition unit. The diffraction efficiency, η, of the recorded grating is defined here as the ratio of the intensity of the first diffraction order and the incident intensity of the probe beam.
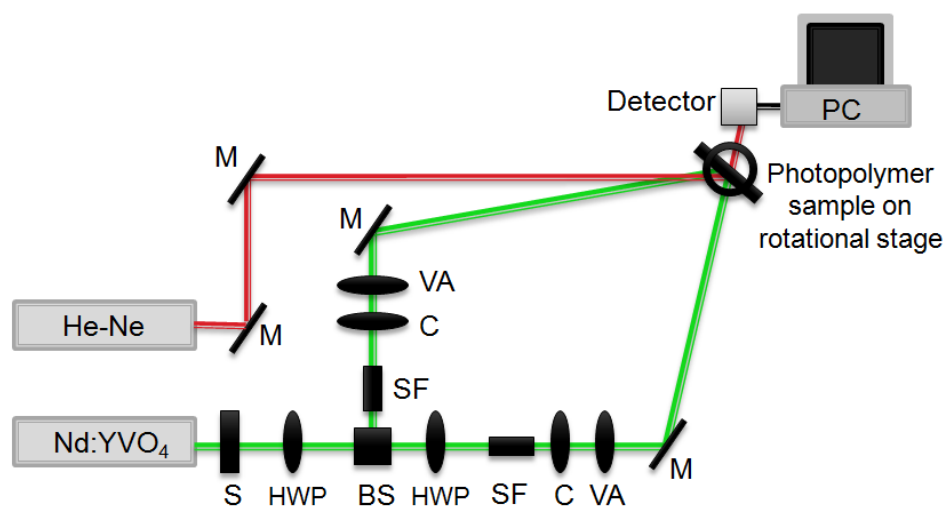
Fig. 3.11. Experimental setup: S: shutter, HWP: half wave plate, BS: polarising beam splitter, SF: spatial filter, C: collimator, VA: variable aperture, M: mirror.

3.3.2 DA concentration optimisation results

The optimum concentration of DA was investigated by preparing photopolymer solutions with DA concentrations ranging from 10.52 to 26.08 wt. % of the total solid material in the photopolymer layer. The concentrations of the rest of the photopolymer components were kept constant and no crosslinker was added. Table 3.1 shows the

compositions prepared. Above a concentration of 22.72 wt. %, the optical quality of the layers deteriorated as the solubility threshold for the DA monomer in solution had been reached. Transmission gratings were then recorded as described in section 3.3.1 using the prepared layers in order to determine the concentration of DA which would yield the highest value for η. These values were then plotted against the wt. % concentration of DA, and the results of this are shown in fig. 3.12. A maximum η of 42 % was obtained in layers with thickness of 50 ± 5 µm for a DA concentration of 22.72 wt. %. As this concentration is exceeded, η decreases due to deterioration in the optical quality of the layers from solid material precipitating out of the layers. Therefore, the concentration of 22.72 wt. % was chosen as the optimum concentration of solid DA monomer in the photopolymer composition.

Table 3.1 Compositions for DA concentration optimisation

Composition	PVA (ml)	TEA (ml)	EB dye (ml)	DA (g)	wt. % of DA in the solid layer
1	20	2	4	0.5	10.52
2	20	2	4	0.75	14.99
3	20	2	4	1.0	19.04
4	20	2	4	1.25	22.72
5	20	2	4	1.5	26.08
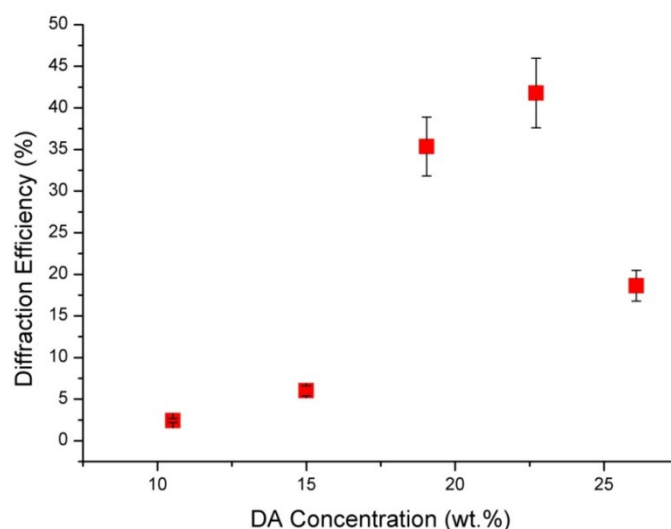
Fig. 3.12. η (%) of transmission gratings vs. DA concentration (wt. %).

3.3.3 BA concentration optimisation

Once the optimum concentration of DA per 20 ml of 10 % wt/vol PVA had been found, this total amount of monomer was then divided between the main monomer DA and the crosslinking monomer Bisacrylamide (BA) in different ratios. The total amount of monomer had to be kept constant as a further increase would have exceeded the limit of solubility. This would cause monomer to precipitate out of the binder, reducing the optical quality of the layers. It is important that the optimum ratio of main monomer to crosslinker is found in order to ensure that the maximum rate of stable, crosslinked polymer chain growth possible is achieved, thus maximising the recording capability of the new material.

Table 3.2 shows the compositions prepared with different ratios of DA to BA while keeping the total solid monomer concentration constant at 22.72 wt. %. Photopolymer layers prepared with composition B were observed to be the most stable. Layers prepared from the other solutions were of poor optical quality, due to BA precipitation

65

out of the layers while drying overnight. This effect was observed 24 hours after holographic recording in layers prepared from composition B. Therefore, to prevent this and improve the shelf-life of samples recorded with the photopolymer, the amount of BA was reduced in composition B by 20 %. The details of the final composition are shown in table 3.2.

Fig. 3.13 shows real-time η growth curves of transmission gratings recorded in the 50 ± 5 µm thick DA photopolymer layers prepared with and without the crosslinking monomer BA. This highlights the important role of BA in the photopolymer. Diffusion of polymer chains from illuminated to non-illuminated regions during holographic recording results in deterioration of grating quality, and significantly reduces η. Therefore, the optimum concentrations of DA and BA for holographic recording were concluded to be 18.36 wt. % and 3.67 wt. % respectively. This composition recorded diffraction gratings with the highest value of η, while ensuring layers were of high optical quality and longer shelf-life.

Table 3.2 Compositions for BA concentration optimisation

Composition	PVA (ml)	TEA (ml)	EB dye (ml)	DA (g)	BA (g)
A	20	2	4	1.125	0.125
B	20	2	4	1.0	0.25
C	20	2	4	0.875	0.375
D	20	2	4	0.75	0.5
E	20	2	4	0.625	0.625
F	20	2	4	0.5	0.5
Final	20	2	4	1.0	0.2
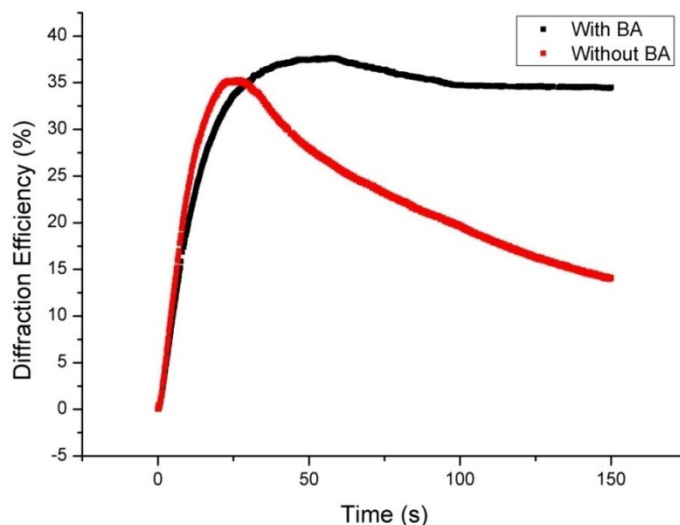
Fig. 3.13. Real-time η growth curves for 50 ± 5 µm thick DA photopolymers with BA (blue) and without BA (red).

3.4 Conclusions

A description of the different components of the photopolymer composition and their individual role has been given. It was shown that DA can successfully substitute AA as main monomer in a photopolymer composition. Thus a new low-toxicity monomer suitable for holographic recording was identified.

The photopolymer composition has been optimised for the new monomer DA. A concentration of 18.36 wt. % was observed to be optimum for the DA monomer, recording gratings with the highest η of 42 % in 50 ± 5 µm thick layers. A concentration of 3.67 wt. % was observed to be optimum for the BA crosslinker. The ability of the crosslinking monomer to prevent deterioration of the holographic grating due to restriction of diffusion of polymer chains was demonstrated.

These results are promising for future development of DA-based photopolymer media aiming to achieve holograms with high η, while reducing the toxicity of the overall photopolymer composition.

References:

[1] N. V. Tale, R. N. Jagtap, "Synthesis of diacetone acrylamide monomer and the film properties of Its copolymers", Iranian Polymer Journal 19(10), 801-810 (2010).

[2] J. Siemiatycki, L. Richardson, K. Straif, B. Latreille, R. Lakhani, S. Campbell, M Rousseau and P. Boffetta, "Listing Occupational Carcinogens", Environ. Health Perspect. 112, 1447–1459 (2004).

[3] *Diacetone Acrylamide*; Sigma-Aldrich; http://www.sigmaaldrich.com/catalog/DisplayMSDSContent.do (accessed 30/6/11).

[4] *Acrylamide*; Sigma-Aldrich; http://www.sigmaaldrich.com/catalog/DisplayMSDSContent.do (accessed 30/6/11).

[5] L. E. Coleman, J. F. Bork, D. P. Wyman and D. I. Hoke, "Synthesis and polymerization of *N*[2-(2-methyl-4-oxopentyl)]-acrylamide–A new reactive vinyl monomer", Journal of Polymer Science 3, 1601-1608 (1965).

[6] S. Singh, S. K. Srivastava, D. K. Singh, "Hydrogen bonding patterns in different acrylamide–water clusters: microsolvation probed by micro Raman spectroscopy and DFT calculations", RSC Adv. 4, 1761-1774 (2014).

[7] I. M. Rosenberg, "Protein Analysis and Purification - Benchtop Techniques", 2nd Edition, Birkhauser, Boston, 1996.

[8] S. Martin, P.E. Leclere, Y. L. M. Renotte, V. Toal, Y. F. Lion, "Characterization of an acrylamide-based dry photopolymer holographic recording material", Opt. Eng. 33(12), 3942-3946 (1994).

[9] M. Ortuño, S. Gallego, C. García, I. Pascual, C. Neipp, A. Beléndez, "Holographic Characteristics of an Acrylamide/Bisacrylamide Photopolymer in 40–1000 µm Thick Layers", Phys. Scr. 118, 66-68 (2005).

[10] S. Blaya, L. Carretero, R. F. Madrigal, A. Fimia, "Study of Effect of Bifunctional Crosslinking Agent in Polyvinylalcohol-Based Photopolymerizable Holographic Recording Material Using Angular Responses", Jpn. J. Appl. Phys. 4(1) 3730 (2002).

[11] C. Neipp, S. Gallego, M. Ortuño, A. Márquez, A. Beléndez, I. Pascual, "Characterization of a PVA/acrylamide photopolymer. Influence of a cross-linking monomer in the final characteristics of the hologram", Optics Communications 224(1-3), 27-34 (2003).

[12] M. Ortuño, E. Fernandez, A. Márquez, S. Gallego, C. Neipp, A. Beléndez, I. Pascual, "Effect of the incorporation of N,N′-methylene-bis-acrylamide on the multiplexing of holograms in a hydrophilic acrylamide photopolymer", Optics Communications 268(1), 133-137 (2006).

[13] R. Jallapuram, I. Naydenova , V. Toal, S. Martin, R. Howard, "Spatial frequency response of acrylamide holographic photopolymer", Proceedings of International Conference on Laser Applications and Optical Metrology, New Delhi, 275-279, 2003.

[14] S. Gallego. M. Ortuno, C. Garcia, C. Neipp, A. Belendez, I. Pascual, "High-efficiency volume holograms recording on acrylamide and N,N′methylene-bis-

acrylamide photopolymer with pulsed laser, Journal of Modern Optics 52(11), 1575-1584 (2005).

[15] H. Lu, R. P. Li, C. X. Sun, Y. Xiao, D. G. Tang, M. J. Huang, "Holographic property of photopolymers with different amine photoinitiators", Chin. Phys. B 19(2), 0242121-0242127 (2010).

[16] R. Jallapuram, I. Naydenova, V. Toal, R. Howard, "Spatial frequency response of acrylamide holographic photopolymer", Proceedings of International Conference on Laser Applications and Optical Metrology, Anamaya Publishers, New Delhi, 275-279 (2003).

[17] S. Martin, "A new photopolymer recording material for holographic applications: photochemical and holographic studies towards an optimized system", Doctoral Thesis, Dublin Institute of Technology, 1995.

4. CHARACTERISATION OF THE HOLOGRAPHIC RECORDING ABILTY OF THE DA PHOTOPOLYMER IN TRANSMISSION MODE

4.1 Introduction

As discussed in chapter 1, there are many holographic applications for which the transmission regime of recording is suitable, including holographic sensors, transmission mode HOEs, and HDS. Although the spatial resolution is not as high as for reflection mode (up to 5700 l/mm for AA-based photopolymer media [1]), transmission mode gratings with spatial resolutions of up to 3000 l/mm are still achievable. In general the holographic recording ability of different recording media is compared in transmission mode, as unlike in reflection mode, holograms with high diffraction efficiency are readily recordable. In reflection mode the maximum achievable diffraction efficiency is limited by the resolution of the recording media. The stability requirements of a transmission-mode system are also significantly less than in reflection mode, which is an important factor when considering practical restrictions of the holographic recording setup.

The holographic recording ability of the DA photopolymer was investigated in the transmission mode of recording for a range of different recording parameters, including recording intensity and exposure energy, spatial frequency of recording, and sample thickness. Full characterisation of the holographic recording ability of the DA material allows an insight into which holographic applications it will be best suited for.

By characterising the recording exposure energy and intensity dependence of the DA photopolymer, the holographic sensitivity of the material is determined. Recording intensities ranging from 1 to 10 mW/cm^2 were investigated, for exposure energies of 20 to 100 mJ/cm^2. The exposure energy dependence study was carried out at two different

spatial frequencies: 1000 and 3000 l/mm. For large-scale holographic device fabrication fast production is obviously favourable, so it is important that the material can successfully record holograms when exposed to high recording intensities allowing for shorter exposure times and therefore a higher rate of production.

The spatial frequency dependence of the photopolymer was investigated for a range of spatial frequencies in transmission mode: 100, 300, 1000 and 3000 l/mm. Holographic applications such as display holography and full-colour holograms require that the recording medium has high spatial resolution, so it is important that the new material's response at higher spatial frequencies is investigated. For most applications such as holographic sensors, 1000 l/mm is an acceptable spatial frequency. For other applications such as HOE lenses for solar collectors, lower spatial frequencies are favourable in order to maximise the angle of collection of light and improve solar cell efficiencies.

In order to characterise the response of the DA photopolymer at different sample thicknesses, gratings were recorded in layers ranging in thickness from 20 to 110 µm. This allowed for the optimum thickness of the material to be determined, while also characterising the performance of the photopolymer over a range of thicknesses. HDS requires thick layers, as holograms must be multiplexed in order to increase the volume of data that can be stored. For other applications such as HOEs, thinner layers may be desirable depending on the requirements of the device. Table 4.1 below outlines a few of the application-specific parameters for different holographic applications.

For each recording parameter characterisation, comparison is made between the performance of the DA and AA-based photopolymers. The holographic recording ability of the AA photopolymer has been extensively characterised elsewhere [2-6].

The ability of the DA photopolymer to record transmission mode, micro-patterned surface structures was also investigated. These structures can have interesting applications in sensing and HOE devices

Table 4.1 Parameters for transmission mode holographic applications

Application	Spatial Frequency	Diffraction Efficiency (η)	Thickness	Other
HDS	High as possible (3000 l/mm) to maximise data storage density	Large number of gratings with low η	High as possible to maximum volume of stored holograms	Low Shrinkage Large Dynamic Range
HOE Lenses for Solar Applications	Low, to maximise collection angle (100-300 l/mm)	High as possible (> 90%) to maximise diffraction	Thinner layers may be favourable for most HOEs (low cost, lightweight). Also must be thin to increase acceptable angle width	-
Sensors (Gases, humidity, temperature etc.)	-	For visual device: high as possible so hologram is visible to user	Thinner layers will be favourable (low cost, lightweight)	Material must be functionalised for desired analyte
Holograms for Security and Anti-Counterfeit Applications	-	For overt feature: high as possible so hologram is visible to user	Thinner layers will be favourable to reduce costs, depends on specific product	Large viewing angle

4.2 Experimental

4.2.1 Materials

The DA and AA photopolymer compositions were prepared as described in fig. 4.1. For the DA photopolymer solution, 1.0 g DA, 0.2 g N, N-methylene-bisacrylamide (BA), 2 ml triethanolamine (TEA) and 4 ml Erythrosin B 0.11 % wt/vol dye solution were

added to 20 ml of 10 % wt/vol polyvinyl alcohol (PVA). For the AA photopolymer solution, 0.6 g AA, 0.2g BA, 2 ml TEA and 4 ml Erythrosin B were added to 17.5 ml of 10 % wt/vol PVA. The photopolymer solution was then deposited on to glass slides (75 × 25 mm) and allowed to dry for 12-24 hours in darkness under normal laboratory conditions (20-25 °C, 40-60 % RH). Layer thickness was measured using a white-light surface profiler (Micro XAM S/N 8038), and was found to be 60 ± 5 µm. This was the standard photopolymer layer thickness used for all measurements, excluding the thickness dependence study.
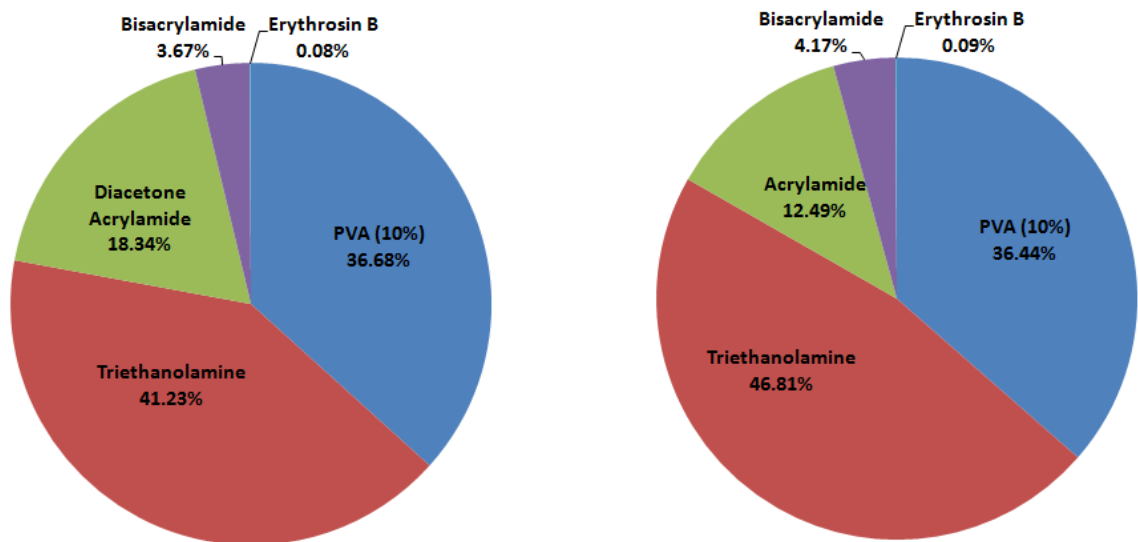
Fig. 4.1. Pie chart representations of the wt. % composition of the DA and AA photopolymers.

4.2.2 Methods

A two-beam holographic optical setup as shown in fig. 4.2 was used to record un-slanted transmission gratings using a 532 nm vertically-polarised Nd:YVO$_4$ laser. The spatial frequency of the recorded grating was controlled by varying the angle between the two recording beams according to the Bragg equation, as described in section

74

1.3.1.1 of chapter 1. The intensity of the recording beams was controlled using a neutral density filter. The absorption of the photopolymer sensitized with Erythrosin B dye is negligible at 633 nm, so a 633 nm He-Ne laser was used as the probe beam at the Bragg angle. As the recorded gratings are isotropic in nature, their diffraction efficiency is not dependent on the polarisation of the probe beam. An optical power meter (Newport 1830-C) was used to record the intensity of the diffracted beam, and LabVIEW software was used to plot the data in real-time. In order to measure the diffracted intensity dependence on the incident angle of the probe beam, the grating was placed on a rotational stage (Newport ESP 300). The accuracy of this measurement was 1×10^{-3} deg.

The spatial frequency of recording and the layer thickness used allow for application of Kogelnik's coupled-wave theory for volume, thick gratings [7], which is used here to determine the refractive index modulation, Δn, of the recorded gratings:

$$\Delta n = \frac{\lambda \cos\theta \, \sin^{-1}(\sqrt{\eta})}{\pi d} \tag{4.1}$$

where θ, λ are the reconstruction beam incident angle and wavelength, and d is the thickness of the photopolymer layer. η is the diffraction efficiency of the recorded grating at the Bragg angle, defined here as the ratio of the intensity of the first diffraction order I_d and the incident intensity I_{in} of the probe beam:

$$\eta = \frac{I_d}{I_{in}} \times 100 \tag{4.2}$$
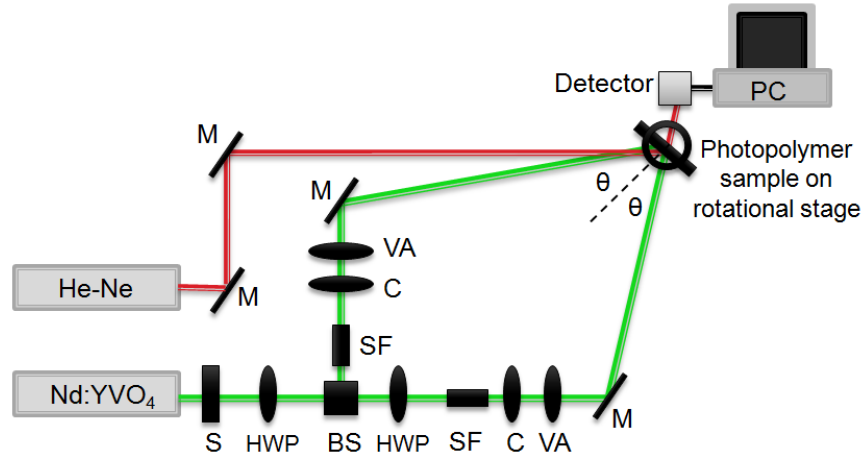
Fig. 4.2. Experimental setup for recording un-slanted transmission gratings: S: shutter, HWP: half wave plate, BS: polarising beam splitter, SF: spatial filter, C: collimator, VA: variable aperture, M: mirror.

4.3 Results and Discussion

4.3.1 Investigation of the dependence of Δn on recording intensity and exposure energy

4.3.1.1 Dependence of Δn on recording intensity for the DA and AA photopolymers at 1000 l/mm

The intensity and exposure energy dependence of the DA and AA photopolymers was investigated by recording transmission gratings in 60 ± 5 µm thick layers using the holographic setup outlined in section 4.2.2 at a spatial frequency of 1000 l/mm. The total recording intensity was varied from 1-5 mW/cm^2, and the exposure energy was kept constant at 100 mJ/cm^2. The results for the Δn of gratings recorded at each recording intensity in the DA and AA photopolymer layers is shown in fig. 4.3.

The DA photopolymer achieves a maximum Δn of 3.3×10^{-3} at a recording intensity of 2 mW/cm^2. There is limited intensity dependence for the DA photopolymer, which has

a stable Δn of between 2.25×10^{-3} and 3.3×10^{-3} over the range of intensities tested. This is a desirable feature for production on a large scale in industry, as short recording times at high intensities are required in order to optimise production efficiencies. Uniform intensity dependence also reduces the need for a perfectly stable laser system, as the material is less sensitive to small changes in intensity. The AA photopolymer reaches its maximum Δn of 4.1×10^{-3} for a total intensity of 4 mW/cm^2. Therefore, Δn for the DA photopolymer is 80 % of that achieved with the AA photopolymer.
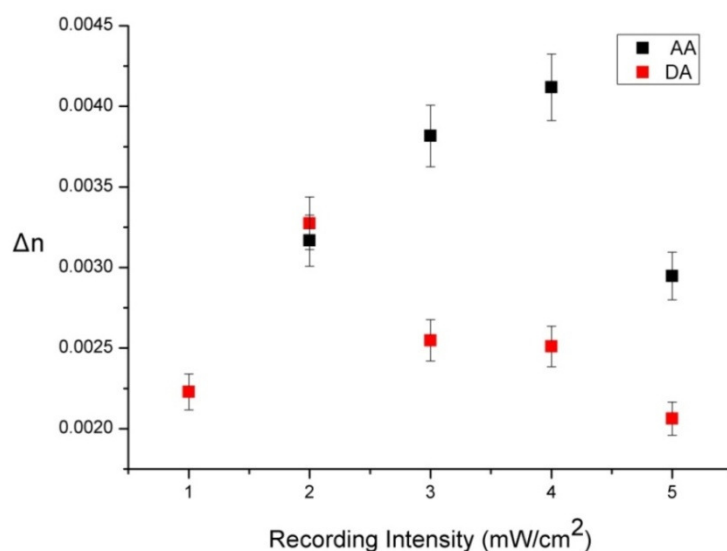
Fig. 4.3. Δn vs. recording intensity (mW/cm^2) for the DA and AA photopolymers at 1000 l/mm. Total exposure energy is 100 mJ/cm^2.

The optimum recording intensity for the AA photopolymer was observed to be twice as high as that required for the DA photopolymer. In order to explain this, the basic mechanism behind grating formation in photopolymers must be described. The two

main processes which govern hologram formation are polymerisation and diffusion. The ratio of the polymerisation rate to the diffusion rate is an important factor [8]. The rate of polymerisation is proportional to the recording intensity used, as this controls the number of photons available to produce free radicals which initiate the polymerisation reaction. If the polymerisation rate is very fast, as is the case at higher recording intensities, the diffusion rate must be fast also in order to facilitate the movement of the monomer molecules within the illuminated regions, so that they can react with a free radical and be polymerised. If this is not the case and monomer diffusion does not occur at a fast enough rate, then the proportion of monomer molecules that are polymerised in the illuminated regions will be lower, and therefore Δn of the recorded grating will be reduced as a result.

The DA monomer molecules are large in size (approximate size of 10×4 Å) in comparison to the AA monomer molecules (approximate size of 5×4 Å) and so they diffuse at a slower rate. Therefore, for the DA monomer lower recording intensities will be optimum, as polymerisation must proceed at a slower rate in order to be in balance with the slower diffusion. The AA molecules are restricted less due to their smaller size, and so can diffuse quickly enough to be polymerised at the higher recording intensities.

As can be seen in fig. 4.4, the DA photopolymer maintains the same trend in Δn vs. recording intensity over a range of exposure energies. As expected Δn increases with increasing exposure energy, as the duration of exposure is extended and so the material is polymerised for longer time periods.
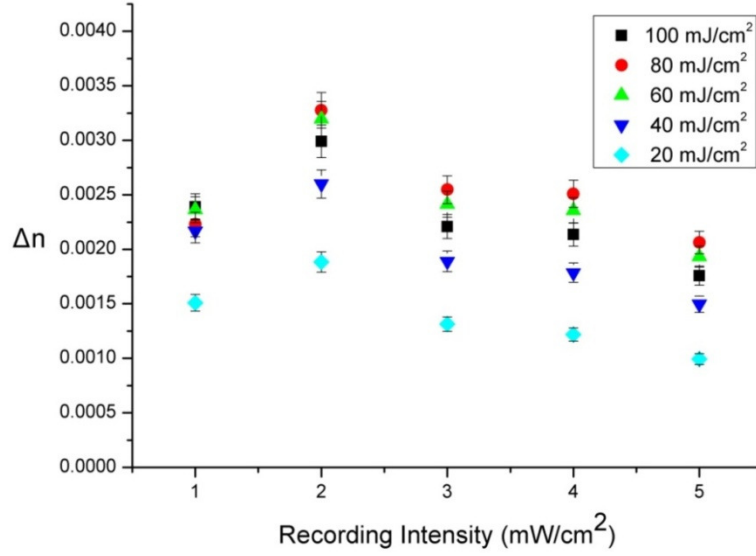
Fig. 4.4. Δn vs. recording intensity (mW/cm^2) for the DA photopolymer. The exposure energy is varied from 20-100 mJ/cm^2.

4.3.1.2 Response of the DA photopolymer to a recording intensity of 10 mW/cm^2 at 1000 l/mm

The ability of the DA photopolymer to record at the highest available recording intensity of 10 mW/cm^2 was investigated. As is shown in fig. 4.5, the DA-based material achieves a maximum Δn of 2.25×10^{-3} for an exposure energy of 100 mJ/cm^2. This is a reduction of 30 % on the Δn value obtained for the optimum recording intensity of 2 mW/cm^2. As mentioned previously the rate of polymerisation increases with increasing recording intensity due to the higher volume of free radicals produced. This also results in an increase in the rate of termination due to the increased volume of free radicals available for recombination. This most likely explains the observed drop in Δn as the recording intensity is increased to 10 mW/cm^2. However, this is still an acceptable Δn value for most holographic applications. As mentioned previously, the

use of high recording intensities allows for much faster recording, which is necessary for hologram production on a large scale.
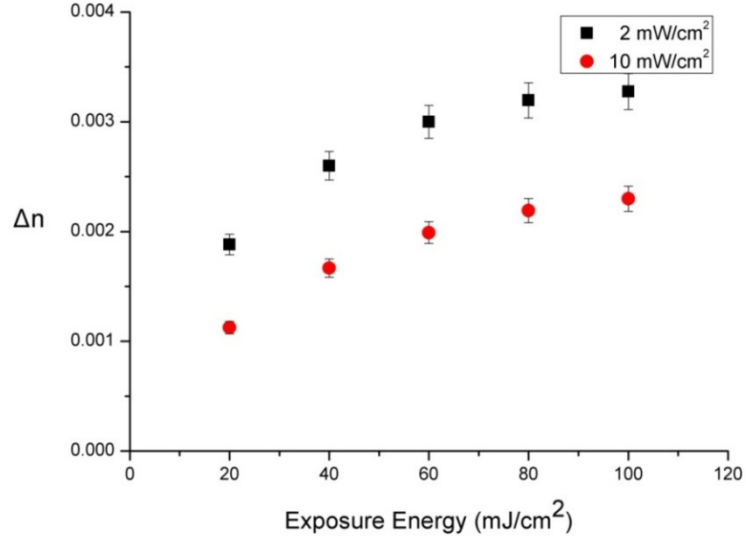
Fig 4.5. Δn vs. recording intensity (mW/cm^2) for the DA photopolymer for recording intensities of 2 and 10 mW/cm^2. The exposure energy is varied from 20-100 mJ/cm^2.

4.3.1.3 Dependence of Δn on recording intensity for the DA photopolymer at 3000 l/mm

As can be seen from fig. 4.6, there is a significant decrease in the maximum Δn achieved at the higher spatial frequency of 3000 l/mm compared to the response at 1000 l/mm. The maximum Δn at 3000 l/mm for the DA photopolymer is 4.6×10^{-4} recorded with a total intensity of 4 mW/cm^2 for 25 seconds. Similarly to the 1000 l/mm results, Δn increases with exposure energy due to the increased time available for polymerisation. The AA-based photopolymer has been reported to obtain Δn values of 8.5×10^{-4} for an 8 second exposure to a recording intensity of 7 mW/cm^2 at this spatial frequency. As was observed, a significant reduction in Δn is to be expected as spatial frequency is increased. This is due to the decreased fringe spacing or period. At very

low fringe spacing as is the case at 3000 l/mm (0.33 µm), it is thought that two main factors contribute to the observed decrease in Δn: growth of long polymer chains out of the illuminated fringe regions, and diffusion of short polymer chains out of the illuminated regions [9, 10]. This decrease in Δn of transmission gratings recorded at higher spatial frequencies has previously been modeled [8].

As observed in fig. 4.6, the results indicate that higher recording intensities are favourable at higher spatial frequencies. By increasing the intensity, the rate of polymerisation of the monomer molecules in the material is increased. If the polymerisation occurs at a sufficiently fast rate, the formation of short polymer chains is promoted due to the increased volume of free radicals produced. This restricts the growth of long polymer chains out of illuminated fringe regions. Also, diffusion of short polymer chains from illuminated regions becomes less likely, as the density and solidity of the photopolymer layer is increased. Optimisation of the DA photopolymer composition will need to be done to further improve its suitability for high spatial frequency recording in the transmission regime. One option is to incorporate a chain transfer agent, which would prevent the diffusion of short polymer chains by decreasing the permeability of the photopolymer matrix, as well as restricting the overall length to which the polymer chains can grow [11].
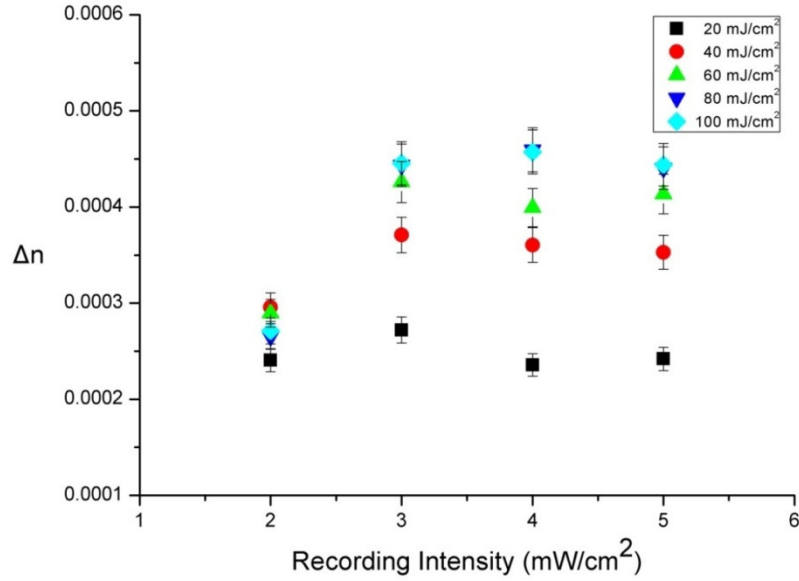
Fig. 4.6. Δn vs. recording intensity (mW/cm^2) for the DA photopolymer at 3000 l/mm. The exposure energy is varied from 20-100 mJ/cm^2.

4.3.2 Investigation of the dependence of Δn on spatial frequency

The spatial frequency dependence of the DA photopolymer was investigated by recording transmission gratings in DA layers at four different spatial frequencies: 100, 300, 1000 and 3000 l/mm. While the quantity of spatial frequencies investigated is limited due to time restrictions, the range of spatial frequencies tested is broad, including spatial frequencies near the maximum and minimum limits for transmission mode recording. A total recording intensity of 2 mW/cm^2 was used with total exposure energy of 200 mJ/cm^2. The results of this study are shown in fig. 4.7. Δn is observed to increase with increasing spatial frequency up to 3.3×10^{-3} at 1000 l/mm. As the spatial frequency is further increased to 3000 l/mm, Δn is significantly reduced to 2.7×10^{-4}.

An explanation for the observed trend in spatial frequency can be obtained by considering the relationship between the fringe spacing and the rate of monomer

diffusion. It is known the monomer diffusion is a large factor in the formation of high Δn gratings [8]. At the lowest spatial frequency tested, 100 l/mm, the fringe spacing is 10 µm. This corresponds to the maximum distance that the DA monomer molecules must diffuse either within the bright fringe region, or from the dark to bright fringe regions, in order to be polymerised. This is a very large distance for the DA monomer molecules to traverse. Therefore, the percentage of the total monomer molecules that can successfully diffuse from dark regions into illuminated regions and be polymerised will be relatively low. This corresponds to a low value of Δn. As the spatial frequency is increased up to 1000 l/mm, the fringe spacing is significantly reduced from 10 µm to 1 µm. Therefore, the percentage of monomer molecules that can diffuse from dark to bright regions and be polymerised is increased. Accordingly, the Δn value at 1000 l/mm is significantly higher than at 100 l/mm, increasing by approximately 40 %. However, as the spatial frequency is increased further to 3000 l/mm, Δn is again observed to decrease significantly. As discussed in section 4.3.1.3, the fringe spacing at 3000 l/mm is very low (0.33 µm), and it is likely that this decrease in Δn can be attributed to diffusion of polymer chains from bright to dark fringe regions, as well as growth of longer polymer chains out of the illuminated areas.
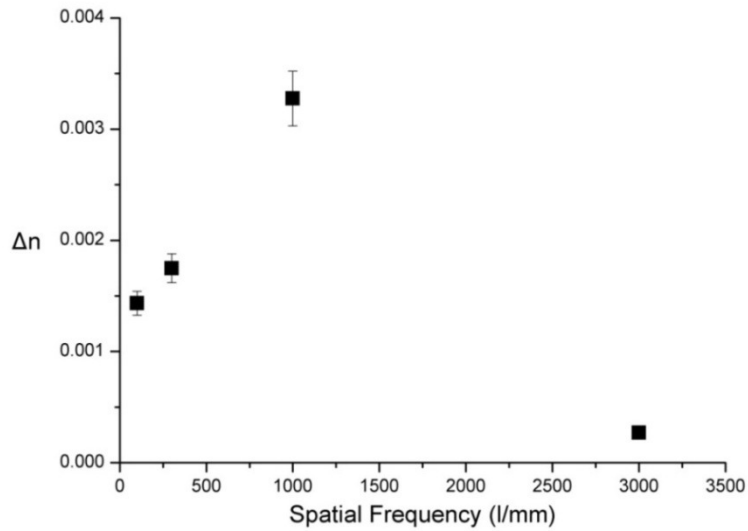
Fig. 4.7. Δn vs. spatial frequency (l/mm) for the DA photopolymer. Gratings were recorded using a total intensity of 2 mW/cm^2 and an exposure time of 100 seconds, for spatial frequencies of 100, 300, 1000 and 3000 l/mm.

4.3.3 Investigation of the dependence of Δn on sample thickness

4.3.3.1 Dependence of Δn on sample thickness for the DA and AA photopolymers

The dependence of Δn on sample layer thickness was determined by recording transmission gratings in DA photopolymer layers with thicknesses ranging from 20-110 µm. This was carried out at a spatial frequency of 1000 l/mm, and a total recording intensity of 2 mW/cm^2 was used. AA photopolymer layers were tested also for comparison purposes. The results of this study are shown in fig. 4.8.

Both the DA and AA compositions follow the same trend of decreasing Δn with increasing sample thickness. This trend can be explained by considering that the absorption of light by the photopolymer layers increases with increasing optical density. Consider a photopolymer sample to be made up of a large number of thinner layers

stacked on top of each other. When illuminated, a proportion of the light is absorbed by the initial layers. By the time the light reaches layers further within the sample, there are less photons available to initiate polymerisation, and so Δn growth is restricted. As the overall sample thickness is increased, this process becomes more pronounced as more photons are absorbed initially, and so Δn is reduced due to the lower number of initiating species available to initiate polymerisation. This effect is less significant in thinner layers. These results are in agreement with those observed by Mahmud *et al*, who observed that by increasing the thickness of the AA photopolymer layers to 250 µm and above, η of the recorded gratings is reduced [12]. In the case of such thick layers, both scattering and absorption will result in losses in η. A solution to this issue was found in the attenuation of the optical density of the AA photopolymer layers by reduction of the dye concentration. In order to investigate the dependence of Δn on thickness further, the real-time growth curves of the holographic gratings recorded in different DA sample thicknesses were obtained.
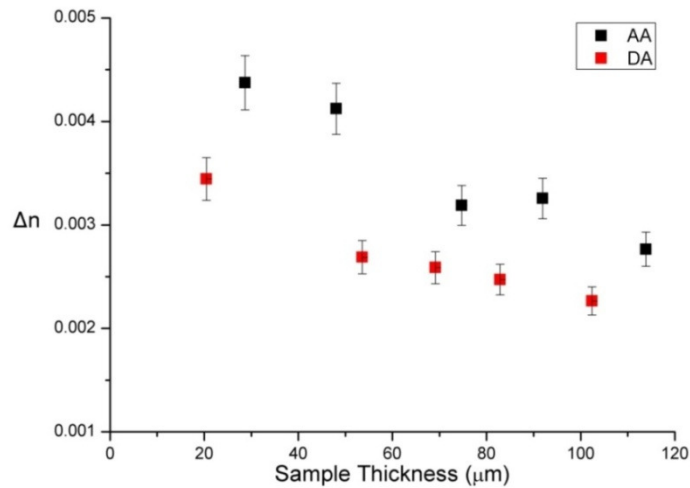
Fig 4.8. Δn vs. sample thickness (µm) for the DA and AA photopolymer compositions. Gratings were recorded using a total intensity of 2 mW/cm^2 and an exposure time of 100 seconds, for a spatial frequency of 1000 l/mm.

4.3.3.2. Real-time Δn growth curves for the DA photopolymer

Real-time Δn growth curves were obtained for the DA photopolymer for sample thicknesses of 20, 50, 70, 80 and 100 ± 5 µm. A recording intensity of 2 mW/cm^2 and an exposure time of 150 seconds were used for all measurements. The results of this study are shown in fig. 4.9. A clear trend is observed. As before, as sample thickness is reduced, the maximum Δn achieved is increased. A second trend was also observed; the rate of polymerisation is faster in the thinner layers. This is most likely due to the higher number of initiating species per unit volume of photopolymer in thinner layers available to initiate polymerisation. In thicker layers, the number of initiating species per unit volume of photopolymer will be relatively lower, and so polymerisation will proceed at a slower rate as a result. This is in agreement with the results observed for the DA photopolymer in section 4.3.3.1. Thickness characterisation is important for consideration of applications where high holographic performance in thicker layers is required, such as HDS.
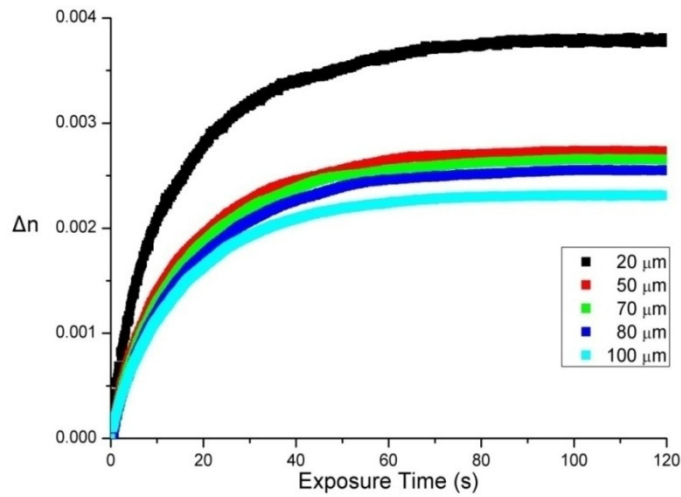
Fig. 4.9. Real-time Δn growth curves for DA photopolymer layers exposed to a 2 mW/cm^2 beam for 150 seconds. Sample thicknesses of 20, 50, 70, 80 and 100 ± 5 µm were used.

4.3.4 Micropatterning study for the DA photopolymer

4.3.4.1 Theory

The holographic micropatterning of dry photopolymer surfaces via transmission mode, photoinduced inscription is of interest for various applications such as diffractive optical elements and sensing [13, 14]. Important characteristics of a material in relation to micropatterning are its spatial resolution, the amplitude of photoinduced surface relief, the required recording time for achievement of maximum surface modulation and its long-term stability. Photopolymer materials are an attractive option for this application as patterns can be induced by light alone, and no post-processing is required.

The ability of the AA-based photopolymer to record surface relief modulations has previously been investigated by Naydenova *et al* [15]. It was shown that the recording of volume phase gratings in AA photopolymer layers is accompanied by periodic surface modulations with amplitudes of up to 3 µm at spatial frequencies of less than 10 l/mm. As the spatial frequency of recording is increased above 25 l/mm, the surface modulation amplitude is reduced to below 0.5 µm. This implies a strong dependence of the surface relief modulation on spatial frequency. For the AA-based photopolymer it was observed that the surface relief peaks coincide with the illuminated or bright fringe regions. There was also observed to strong dependence of the peak amplitudes on the recording intensity and exposure energy used. These two facts together suggest that the mechanism of peak formation is strongly related to the diffusion of monomer into the illuminated regions during holographic recording. For other photopolymer media such as the single-monomer system described by Boiko *et al*, the surface peaks were observed to coincide with the unilluminated areas of the sample, suggesting that

photopolymerisation-induced shrinkage plays a larger role in these systems than monomer diffusion [14].

A brief study into the ability of the DA photopolymer to record periodic surface microstructures has been carried out. First, simple transmission gratings were recorded as described in section 4.2.2 at a spatial frequency of 130 l/mm. The amplitude of the surface modulation of the recorded gratings was measured using a white-light surface profiler (Micro XAM S/N 8038). The effect of different recording intensities and exposure energies on the surface modulation amplitude of the gratings was investigated. The next step was to investigate the abiilty of the DA photopolymer to record a simple cross-grating pattern as shown in fig. 4.10. To do this, a transmission grating was first recorded in the photopolymer layer. The sample was then rotated by 90° and a second grating was then recorded in the same layer. This produces a symmetrical cross-grating pattern. If an asymmetrical pattern is required, the spatial frequency of the recording setup can be changed between recordings.
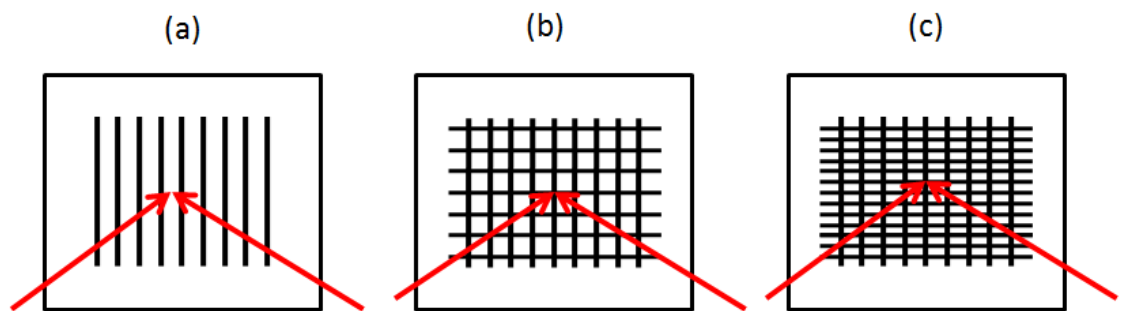
Fig. 4.10. Pattern recording in photopolymer layer. After recording of the first grating (a), the sample is rotated at 90º and a second grating is recorded (b). (c) shows the recording of an assymetrical pattern.

4.3.4.2 Results and Discussion

i) Patterning of simple diffraction gratings

The effect of the recording intensity and exposure energy on the surface modulation of the DA photopolymer was investigated at a spatial frequency of 130 l/mm. Gratings were recorded with recording intensities of 0.5, 1 and 2 mW/cm^2. Exposure energies of 50, 100 and 150 mJ/cm^2 were used. The surface of the gratings was then studied using a white-light surface profiler (Micro XAM S/N 8038), to quantify the amplitude of the surface modulation. The surface relief amplitude was measured as the difference in height between the middle of the bright fringe and the middle of the dark fringe. A typical surface profile of a transmission grating is shown in fig. 4.11. The results for the intensity and exposure energy dependence study are shown in fig. 4.12.
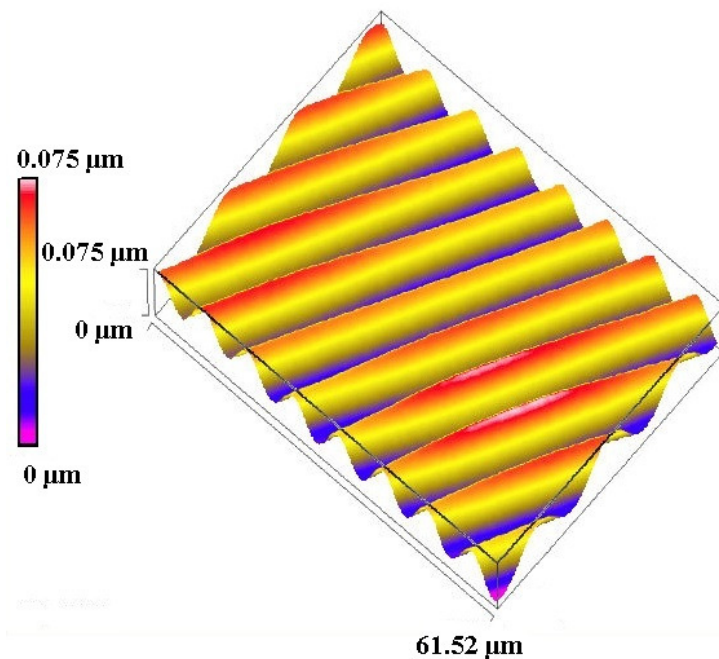
Fig. 4.11. Surface modulation profile of a grating recorded in the DA photopolymer with a recording intensity of 2 mW/cm^2 and an exposure energy of 50 mJ/cm^2, imaged with the white-light surface profiler (Micro XAM S/N 8038).
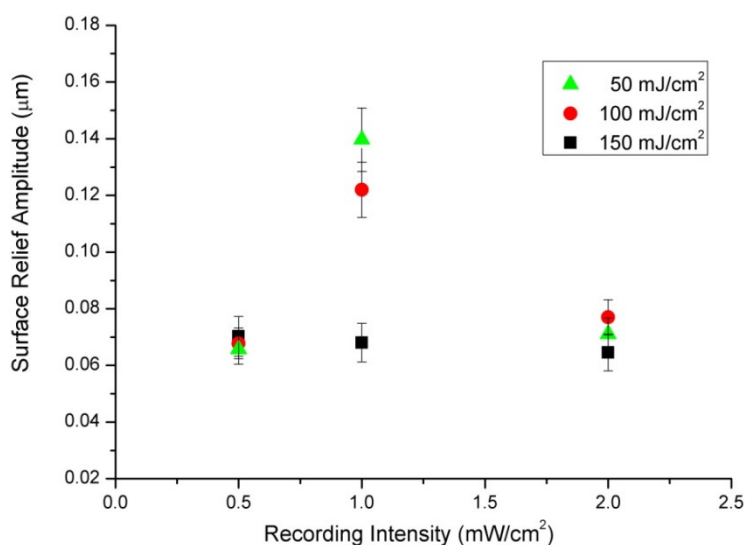
Fig. 4.12. Surface relief amplitude (µm) vs. recording intensity (mW/cm^2) for transmission gratings recorded in the DA photopolymer with exposure energies of 50, 100 and 150 mJ/cm^2.

There is a clear optimum recording intensity of 1mW/cm^2 for the DA photopolymer, which gives the largest surface relief amplitude of 0.14 µm for an exposure energy of 50 mJ/cm^2. As the intensity is increased to 2 mW/cm^2, the amplitude decreases significantly by nearly 50 %. This could be explained by the fact that at lower recording intensities the individual polymer chains are expected to grow longer due to the lower concentration of free radicals. This will also result in a lower rate of termination, aiding the growth of longer polymer chains. Therefore, more monomer molecules will be consumed per photon via the process of polymerisation, and so the final gradient in monomer concentration will be higher. This will lead to more monomer molecules diffusing from bright to dark fringe areas, thus increasing the surface relief amplitude of the grating. At the higher recording intensity of 2 mW/cm^2, polymerisation will occur at a faster rate due to the increased concentration of photons. This will result in shorter

chain formation and stiffening of the polymer material, reducing the net surface relief amplitude. At recording intensities below 1 mW/cm^2, the rate of polymerisation may be too slow for the optimum ratio of the rate of polymerisation to the rate of diffusion in the photopolymer layer to be realised, hence lower surface modulation amplitudes are observed.

A clear dependence of surface relief amplitude on exposure energy is observed at 1 mW/cm^2, with lower exposure energies producing the largest surface relief amplitudes. The decrease in surface relief amplitude observed at higher exposure energies may be caused by excessively long exposure times, allowing for the diffusion and growth of polymer chains out of the illuminated area. As the recording intensity is increased to 2 mW/cm^2, there is no visible trend in exposure energy. This is most likely due to faster polymerisation resulting in the polymer material stiffening, which would prevent diffusion of the polymer chains.

An optimum surface relief modulation of 0.14 µm was obtained for the DA photopolymer at 130 l/mm. This compares favourably with the AA photopolymer, for which a maximum modulation of 0.035 µm was obtained at a spatial frequency of 100 l/mm [15]. This may be explained by the fact that the DA photopolymer has a higher concentration of monomer, 18.34 wt. %, in comparison to that of the AA photopolymer, 12.49 wt. %. It is likely that the extent of surface relief modulation is directly related to the concentration of monomer in the photopolymer layer. Due to the results observed with the AA photopolymer in [15], it is expected that by reducing the spatial frequency of recording the surface relief amplitude of the DA photopolymer can be further increased.

It appears that the amplitude of the relief pattern in fig. 4.11 is not fully uniform across the imaged area. This lack of homogeneity is most likely due to variations in the intensity of the light pattern used to record the surface microstructures. This would result in variations in the extent of local polymerisation. However it is worth noting that although there is a variation in the height of the peaks, this is accompanied by a change in the depth of the troughs, which is not clearly visible here. Therefore, the overall modulation amplitude remains approximately uniform, within the error bars that are shown in fig. 4.12.

ii) Cross-grating patterning

The ability of the DA photopolymer to record cross-gratings (as shown in fig. 4.10) was investigated. In order to successfully make two sequential recordings, the material used must have a large dynamic range. It is also important that only some of the monomer is consumed during the first recording, in order for the second recording to be successful.

A recording intensity of 1 mW/cm^2 was used to record the cross-gratings in the DA photopolymer as this was the optimum recording intensity observed in section i). Different combinations of recording times for the two exposures were tested; the most successful of these combinations were (a) 50 sec + 100 sec, and (b) 75 sec + 150 sec. It was necessary for the second exposure time to be longer than the first, as a proportion of the monomer had already been polymerised in the initial exposure, and therefore the permeability of the material was decreased as a result. Images of the surface relief amplitudes for the two different exposure time combinations are shown in fig. 4.13. The pattern shown in fig. 4.13(b) is more well-defined with peaks of approximately uniform height, in comparison to fig 4.13(a) in which there appears to be a less well-defined

structure. This suggests that longer exposures are important for the successful recording of uniform patterns. The surface relief amplitude is also higher in the case of the longer exposures, with a total modulation of 0.086 µm in comparison to 0.075 µm for the shorter exposure combination.

The advantage of this technique of recording is that large area optical elements with a variety of patterns can be obtained with no need to produce a specially designed mask for every single pattern. Patterns with differently shaped unit cells can be inscribed by simply rotating the photopolymer plate by different angles, and by changing the spatial frequency of recording.

(a)   **(b)**
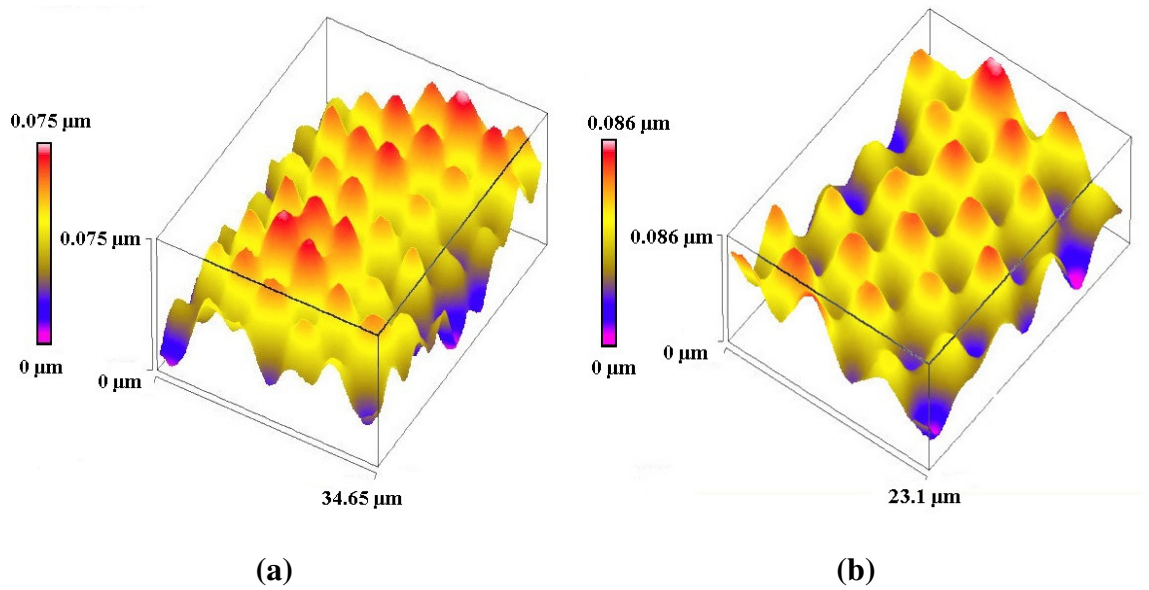
Fig. 4.13. Surface modulation of a cross-grating recorded in the DA photopolymer with a recording intensity of 1 mW/cm^2 for exposure times of (a) 50 and 100 seconds, and (b) 75 and 150 seconds, imaged with the white-light surface profiler.

4.4 Conclusions

The holographic recording ability of the DA photopolymer in transmission mode has been extensively characterised. The new material achieves Δn values of 3.3×10^{-3} for a recording intensity of 2 mW/cm^2 in 60 µm layers. This is 80 % of the Δn achieved with the standard AA photopolymer composition. At a spatial frequency of 1000 l/mm, gratings with η values of up to 80 % have been achieved in 60 µm thick layers.

Intensity dependence characterisation studies show that the material has a relatively uniform response to a large range of intensities, from 1-10 mW/cm^2. This is favourable for large scale industrial device fabrication, as it eliminates the need for absolute laser output stability. It also allows for exposure times to be significantly reduced via the use of high recording intensities, which would result in reduced production times.

An investigation into the DA material's response over a range of spatial frequencies has shown maximum Δn at a spatial frequency of 1000 l/mm. This is a suitable spatial frequency for a large range of holographic applications such as sensors and HOEs. The material responds well at the lower spatial frequencies of 100 to 300 l/mm also. This is advantageous for applications such as holographic lenses in solar collectors, for which as large a collection angle as possible is required. At the higher spatial frequency of 3000 l/mm there is limited recording ability. However, such high spatial frequencies are usually only required for holographic display applications, where resolution is crucial. In general, reflection mode recording is preferential for this type of application, due to the increased resolution which this geometry allows, as well as viewing in white light.

The holographic recording ability for a range of DA sample thicknesses has been investigated. This study shows that optimum Δn values are achieved in thin, 20 µm layers. This is promising for applications or devices which require a lightweight

holographic element. There is a reduction of up to 40 % in Δn as the sample thickness is increased from 20 to 100 µm. While this is a significant decrease, the Δn values obtained at higher thicknesses are still within the range acceptable for holographic applications. A possible solution to this issue could be the attenuation of the optical density of the photopolymer layers by reduction of the dye concentration.

The suitability of the DA photopolymer for the recording for transmission mode, periodic surface microstructures has been investigated. The amplitude of the surface relief was shown to depend on both the recording intensity and exposure energy used. An optimum surface relief modulation of 0.14 µm was obtained for gratings recorded in the DA photopolymer at a spatial frequency of 130 l/mm. This compares favourably with the AA photopolymer results for which a maximum modulation of 0.035 µm was reported at a spatial frequency of 100 l/mm. The DA photopolymer also demonstrated its ability to successfully record more complex, cross-grating structures.

References:

[1] C. Meka, R. Jallapuram, I. Naydenova, S. Martin, V. Toal, "Development of a panchromatic acrylamide-based photopolymer for multicolor reflection holography", Appl. Opt. 49(8), 1400-1405 (2010).

[2] S. Martin, C. A. Feely, V. Toal, "Holographic characteristics of an acrylamide based recording material", Applied Optics 36, 5757-5769 (1997).

[3] S. Martin, P. Leclere, Y. Renotte, V. Toal, Y. Lion, "Characterisation of an acrylamide-based dry photopolymer holographic recording material" Optical Engineering 33, 3942-3946 (1995).

[4] H. Sherif, I. Naydenova, S. Martin, C. McGinn, V. Toal "Characterisation of an acrylamide-based photopolymer for data storage utilizing holographic angular multiplexing", J. Opt. A: Pure Appl. Opt 7, 255-260 (2005).

[5] R. Jallapuram, I. Naydenova, S. Martin, R. Howard, V. Toal, Sven Frohmann, Susanna Orlic, Hans J Eichler, "Acrylamide based photopolymer for micro-holographic data storage", Optical Materials 28, 329-1333 (2006).

[6] R. Jallapuram, I. Naydenova, S. Martin, R. Howard, V. Toal, "Raman spectroscopy for the characterization of polymerization rate in an acrylamide-based photopolymer", Applied Optics 47, 206-212 (2008).

[7] H. Kogelnik, "Coupled wave theory for thick hologram gratings", Bell Syst. Tech. J. 48(9), 2909-2947 (1969).

[8] I. Naydenova, R. Jallapuram, R. Howard, S. Martin, V. Toal, "Investigation of the diffusion processes in a self-processing acrylamide-based photopolymer system", Applied Optics 43, 2900-2905 (2004).

[9] D. Mackey, T. Babeva, I. Naydenova, V. Toal, "A diffusion mode for spatial dependent photopolymerisation", Mathematics in Industry 15(2), 253-258 (2010).

[10] J. T. Sheridan, J. R. Lawrence, "Nonlocal-response diffusion model of holographic recording in photopolymer", Journal of the Optical Society of America A 17(6), 1108-1114 (2000).

[11] T. Babeva, I. Naydenova, D. Mackey, S. Martin, V. Toal, "Two-way diffusion model for short-exposure holographic grating formation in Acrylamide-based photopolymer", Journal of Optical Society of America B 27, 197-203 (2010).

[12] M. S. Mahmud, I. Naydenova, N. Pandey, T. Babeva, R. Jallapuram, S. Martin, V. Toal, "Holographic recording in acrylamide photopolymers: thickness limitations", Applied Optics 48(14), 2642-2648 (2009).

[13] C. Croutxe-Barghorn, D. Lougnot, "Use of self-processing dry photopolymers for the generation of relief optical elements: a photochemical study", Pure Appl. Opt. 5, 811-825 (1996).

[14] Y. Boiko, V. Slovjev, S. Calixto, D. Lougnot, "Dry photopolymer films for computer-generated infrared radiation focusing elements," Appl. Opt. 33, 787-793 (1994).

[15] I. Naydenova, E. Mihaylova, S. Martin, V. Toal, "Holographic patterning of acrylamide–based photopolymer surface", Opt. Express, 13(13), 4878-4889 (2005).

5. STUDY OF SHRINKAGE IN THE DA PHOTOPOLYMER USING HOLOGRAPHIC INTERFEROMETRY

5.1. Introduction

Polymerisation-induced shrinkage is a well-documented effect [1-5]. As polymer chains form in the illuminated regions of a holographic grating during exposure, the density of the region is increased. The individual monomer molecules polymerise and become tightly packed together in a chain formation, resulting in shrinkage of the photopolymer layer. This shrinkage alters the diffraction properties of the grating as it is recorded. Shrinkage is a major disadvantage of photopolymer materials, as it restricts their suitability for certain holographic applications. This is particularly true for HDS. Unlike conventional optical and magnetic data storage techniques, HDS utilises the fact that holograms have high angular selectivity. Therefore, if the dynamic range of the medium permits, multiple holograms can be stored in the same area by shifting the angle of recording. This is known as hologram angular multiplexing. However, if the recording medium suffers from shrinkage due to recording, then the exact angle of recording and therefore the angle of reconstruction are shifted, and so read-out of these holograms is not possible without additional compensation for this shift.

Currently the upper limit for shrinkage in commercial HDS materials is 0.5 % [6]. Different methods have been employed to measure the shrinkage of the IEO's AA photopolymer. One method involves monitoring the shift in the position of the Bragg curve of the recorded grating due to shrinkage of the photopolymer layer during exposure [7, 8]. This method gives a maximum relative shrinkage value of 1.3 % for the AA photopolymer in 60 ± 5 µm layers for a recording intensity of 5 mW/cm^2.

A second method has been developed by Moothanchery *et al* [9, 10] which allows for the monitoring of the shrinkage of the photopolymer layer in real-time using holographic interferometric techniques. This method measures the maximum relative shrinkage of the undoped AA photopolymer to be 4.3 % for 70 ± 5 µm layers exposed to a recording intensity of 5 mW/cm^2. This real-time technique is advantageous over the Bragg curve method for measuring shrinkage, as it allows for the dimensional changes in the material to be monitored as they occur, and therefore provides more information about the dynamics of the shrinkage process, rather than just a single measurement made after recording has finished. This method also produces a more accurate value of shrinkage than the Bragg shift method. The holographic interferometric shrinkage results for the AA photopolymer compare well with those obtained by Moothanchery *et al* using a third method to measure the shrinkage of the same photopolymer material. This third method uses electron speckle pattern interferometric techniques with a double beam exposure, and gives a maximum relative shrinkage value of 3.7 % for the 160 µm thick AA photopolymer layers exposed to a total intensity of 5 mW/cm^2 [10].

Here, the real-time holographic interferometry technique developed by Moothanchery *et al* is used to measure the shrinkage occurring in the DA photopolymer composition during holographic recording in real-time. The influence of recording intensity, exposure energy and sample thickness on the amount of shrinkage was investigated. This allows for extensive comparison with the AA photopolymer material, and investigation of the DA photopolymer's suitability for HDS applications for a wide range of parameters.

5.2 Theory

5.2.1 Investigation of shrinkage in photopolymer systems

Extensive experimental work has been carried out in order to quantify and reduce the amount of shrinkage occurring in different photopolymer systems. Zhao *et al* calculated shrinkage in the Du Pont photopolymer to be 5.25 % using the Bragg curve shift method [11]. In this widely-used method, the fractional change Δd in the sample thickness d is calculated from monitoring the shift between the initial $\emptyset_0$ and final $\emptyset_1$ slant angles:

$$\frac{\Delta d}{d} = \frac{\tan \emptyset_1}{\tan \emptyset_0} - 1 \tag{5.1}$$

$\emptyset_0$ and $\emptyset_1$, as shown in fig. 5.1, are determined from the position of the Bragg peak maximum before and after shrinkage occurs due to exposure. As already discussed, this method was used to measure the shrinkage of the IEO's AA-based photopolymer, which was found to be 1.32 %, significantly lower than that of the Du Pont photopolymer [7].
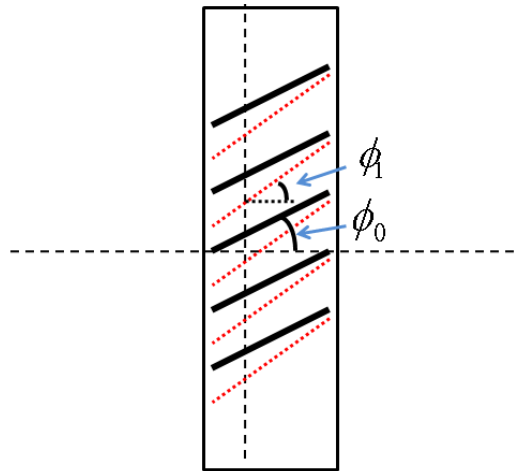
Fig. 5.1. Schematic diagram showing re-orientation of fringes in a transmission grating as a result of shrinkage. $\emptyset_0$ and $\emptyset_1$ are the initial and final slant angles.

A major development has been the incorporation of different additives in the photopolymer material in order to suppress the polymerisation-induced shrinkage. The idea of incorporating nanoparticles was introduced by Vaia *et al* [12]. The nanoparticles are redistributed within the photopolymer layer during holographic recording due to concentration gradients caused by diffusion of the monomer. As shown in fig. 5.2, the nanoparticles diffuse into the unilluminated fringe regions, therefore reducing the amount of shrinkage that can occur. Suzuki [13] and Sanchez [14] tested this experimentally by including TiO_2 nanoparticles in their acrylate photopolymers. In both studies it was shown that the amount of shrinkage, measured using the Bragg curve shift method, decreases due to the addition of the nanoparticles. The Δn of the recorded holograms was also improved. Moothanchery *et al* reported significant reduction in the shrinkage of their AA photopolymer with the incorporation of silica MFI-type zeolites (silicalite-1). Using the Bragg curve shift method, shrinkage of the zeolite doped AA photopolymer has been shown to decrease from 1.32 to 0.57 %, just above the commercial limit on shrinkage for HDS [8].

The effect of other additives aside from nanoparticles on the shrinkage of photopolymer systems has also been investigated. Trentler *et al* found that shrinkage values as low as 0.67 % could be achieved with the inclusion of cross-linking epoxy resin materials [15]. Cheah found that the addition of short glass fibres to an acrylate photopolymer resulted in reduced amounts of volume shrinkage [16]. Lee [17] and Chen [18] investigated the effect of organic-inorganic hybrid matrices on the level of shrinkage in photopolymers. Using this technique shrinkage values as low as 0.1 % have been observed, which is well below the commercial limit of shrinkage for data storage of 0.5 %.

Interference Pattern

Photopolymer layer without light exposure

When light is incident on photopolymer layer

● Monomer ● Nanoparticle 🟢 Polymer chain
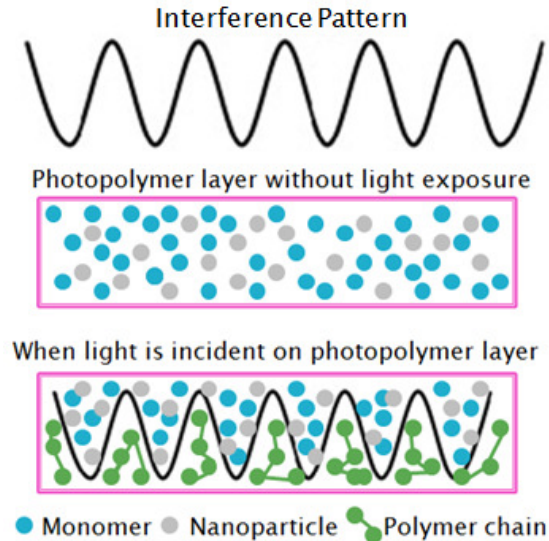
Fig. 5.2. Schematic diagram of grating formation in a photopolymer material doped with nanoparticles.

Gallego *et al* have developed a novel method of measuring shrinkage in an acrylate formulation using a reflection interferometer setup [19]. Shrinkage values of up to 3 % were measured, and it was observed that volume shrinkage decreases with increasing the spatial frequency of recording.

Several models have been put forward in order to describe the effect of shrinkage in holographic photopolymers: the fringe plane rotation model [20, 21], the average refractive index change model [22], the fringe plane rotation and average refractive index change model [23, 24], and the fringe bending model [25]. For all of these methods, lateral shrinkage is considered to be less prevalent than transverse shrinkage (i.e. changes in the sample thickness) due to strong adhesion of the photopolymer material to the glass substrate. A comprehensive review of the different models has been carried out by Moothanchery *et al* [10].

5.2.2 Interferometry

The term interferometry refers to a group of techniques which involve superimposing waves in order to extract information about the waves themselves, or some object in their path [26]. When two waves of identical frequency are combined, the resulting pattern is determined by the phase difference between the two waves; waves that are in phase will undergo constructive interference while waves that are out of phase will undergo destructive interference. Interferometers are widely used for the measurement of small displacements, surface irregularities or refractive index changes, with accuracy to the order of the wavelength of the light used. The most widely known type of interferometer is the Michelson interferometer, shown in fig. 5.3.
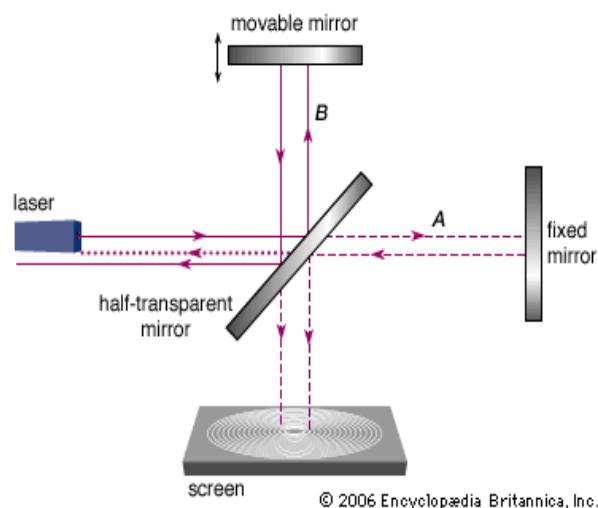
Fig. 5.3. Michelson interferometer setup.

5.2.3 Holographic interferometry

Holographic interferometry is a non-contact technique which can be used to study surfaces which are not optically smooth with very high precision and sensitivity. Its discovery is accredited to Leith and Upatnieks in 1963 [27], but it was not until the

103

work of Powel and Stetson in 1965 that the observed phenomenon was explained [22]. They observed that any change in the position of optical components in a holographic recording setup will result in the production of bright and dark fringes on the image of the reconstructed hologram. These fringes result from a phase shift due to the interference of the wavefronts from the displaced surfaces. By studying these fringes, detailed comparison between an object's wavefront when it is subjected to changes in position, pressure, stress, temperature, vibrations etc. and the unperturbed wavefront can be made.

Several different methods can be employed to carry out holographic interferometric measurements. Double exposure interferometry involves the recording of two separate holograms on the same photosensitive plate [24]. In the first hologram the object is unperturbed, while in the second hologram the object is displaced. Both holograms are reconstructed and interference fringes result from their superimposition. A second method commonly used is the live fringe technique [24]. In this method, a hologram is recorded on a photosensitive plate, developed, and repositioned exactly as before. The plate is then illuminated with both the object and reference beam. By displacing the object, the path length of the object beam is changed, resulting in the observation of interference fringes. An advantage of this method is that the formation of the fringe pattern can be observed in real-time. A disadvantage is the difficulty arising from replacing the holographic plate in the exact same position after development. Photopolymer materials offer an advantage over other holographic recording media for this live interferometric method, as they do not require any post-processing once recording has been completed and so do not have to be removed or replaced.

5.2.4 Determination of photopolymer shrinkage by holographic interferometry

The technique used to measure the shrinkage of the DA photopolymer material in real-time has been developed by Moothanchery *et al* [9, 10]. In this method, a hologram of the object is recorded at 633 nm; in this case the object is a DA photopolymer layer with negligible absorbance at this wavelength. A simple grating is then recorded in the object itself at a wavelength of 532 nm. This causes the object to shrink, changing the optical path length L of the 633 nm object beam. This object beam, which is changing in real-time, is interfered with the reconstructed beam of the unperturbed object. This produces interference fringes on the reconstructed image of the object hologram, which are captured in real-time using a CMOS camera. Fig. 5.4 shows an example of images of a hologram of the AA photopolymer layer surface before exposure and again after exposure in which the interference fringes are visible [9]. From these captured interferograms, it is possible to calculate the change in the optical path length *L* of the object beam from the number of fringes *n* via eqn. 5.2:

$$L = n\lambda \tag{5.2}$$

where λ is the wavelength used. Eqn. 5.3 relates the optical path length to the absolute shrinkage in microns Δd of the photopolymer layer:

$$L = \Delta d(\cos\theta_1 + \cos\theta_2) \tag{5.3}$$

Where θ_1 is the angle of illumination, and θ_2 is the angle of reconstruction (fig. 5.5). By combining eqns. 5.2 and 5.3, the absolute shrinkage can be directly calculated from the number of fringes *n*:

$$n\lambda = \Delta d(\cos\theta_1 + \cos\theta_2) \tag{5.4}$$

$$\Delta d = \frac{n\lambda}{(\cos\theta_1 + \cos\theta_2)} \tag{5.5}$$

Using this technique the shrinkage as a percentage of the DA photopolymer sample thickness d was determined for each interference fringe at the time it was observed. Therefore, the evolution of shrinkage in the DA photopolymer layers in real-time was determined for different sample thicknesses, exposure energies and recording intensities.

(a)   (b)
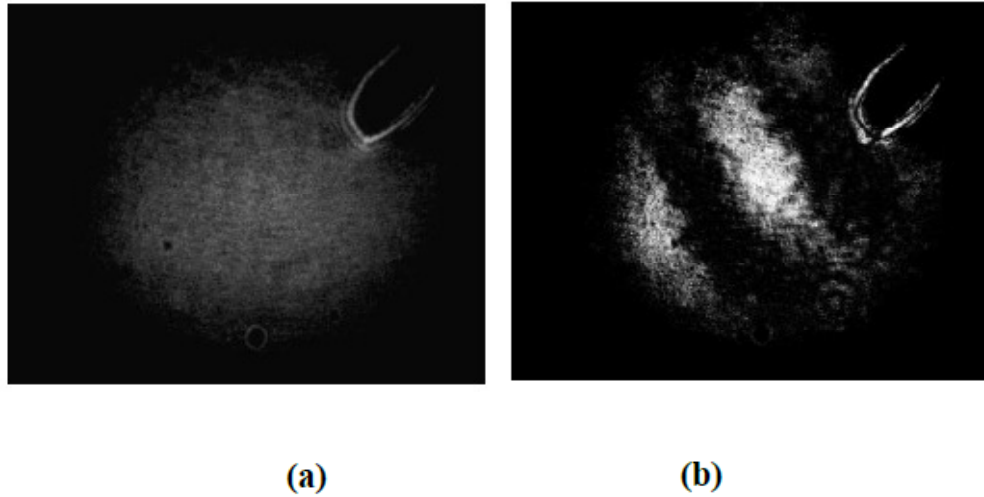
Fig. 5.4. (a) Reconstructed hologram of the AA photopolymer layer surface before exposure; (b) Reconstructed hologram of the AA photopolymer layer surface during exposure with visible shrinkage fringes [9].
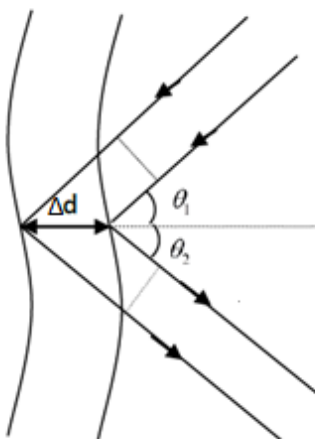
Fig. 5.5. Diagram of the optical path difference Δd between two wavefronts [10].

5.3 Experimental

5.3.1 Materials

It was necessary to prepare two different types of photopolymer samples for these experiments, as two different laser wavelengths were used. A green-sensitised photopolymer solution was prepared for recording at 532 nm, and a red-sensitised photopolymer solution for recording at 633 nm. For the 532 nm recordings, the standard DA photopolymer solution was prepared. For the 633 nm measurements which produce the interferograms of the DA photopolymer layers, an AA-based photopolymer solution was used. This was done to allow for accurate comparison with the AA photopolymer shrinkage measurements carried out by Moothanchery *et al*, by using the same recording conditions and recording material to produce a hologram of the unexposed DA photopolymer surface. The two photopolymer compositions used are described in table 5.1. The DA photopolymer layers were prepared by depositing 0.5, 0.8 and 1.4 ml of solution onto 75 × 25 mm glass microscope slides to produce dry sample thicknesses

of 45, 90 and 120 ± 5 µm. The AA photopolymer layers were prepared by depositing 0.6 ml of photopolymer solution onto the same glass slides, producing a dry sample thickness of 60 ± 5 µm. The layers were dried for approximately 24 hours before recording at room temperature.

Table 5.1 DA and AA photopolymer solutions for shrinkage measurements

	Green-sensitised DA photopolymer	Red-sensitised AA photopolymer
10 % wt/vol PVA (ml)	20	17.5
TEA (ml)	2	2
DA (g)	1	-
AA (g)	-	0.6
BA (g)	0.2	0.2
0.11 % wt/vol Erythrosin B dye s.s. (ml)	4	-
0.11% wt/vol Methylene Blue dye s.s. (ml)	-	4

5.3.2 Methods

The interferometer setup used is shown in fig. 5.6. The 532 and 633 nm beams were spatially filtered, collimated and then split in two using beam splitters. The two 633 nm beams were used in an interferometric arrangement to monitor the changes due to shrinkage in the Erythrosin B sample during exposure. To do this, one of the 633 nm beams was reflected from the surface of the Erythrosin B sample (object beam). The other 633 nm beam, the reference beam, was partially reflected from a glass plate and directed so that it interfered with the object beam on the red-sensitive Methylene Blue sample, thus recording a hologram of the surface of the Erythrosin B sample. An exposure time of 140 seconds and an intensity of 0.5 mW/cm^2 were used for this

recording. Using the 532 nm interferometer, a grating was then recorded in the Erythrosin B sample, causing it to shrink. The real-time 633 nm object beam from the shrinking DA photopolymer layer was then interfered with the reconstructed object beam from the unexposed DA photopolymer layer on a screen. This allowed the resulting interferograms to be video recorded in real-time using a CMOS camera. The angles of illumination and observation of the 633 nm object beam were 26.2° and 33.7° respectively. An image subtraction method was used in order to overcome the limited visibility of the fringes. A reference frame of the hologram recorded in the Methylene Blue sample (before the 532 nm exposure began) was subtracted using LabVIEW software from the other live frames to achieve this. A comprehensive description of the LabVIEW program used can be found elsewhere [10]. The intensity of the 532 nm laser was controlled using a neutral density filter.
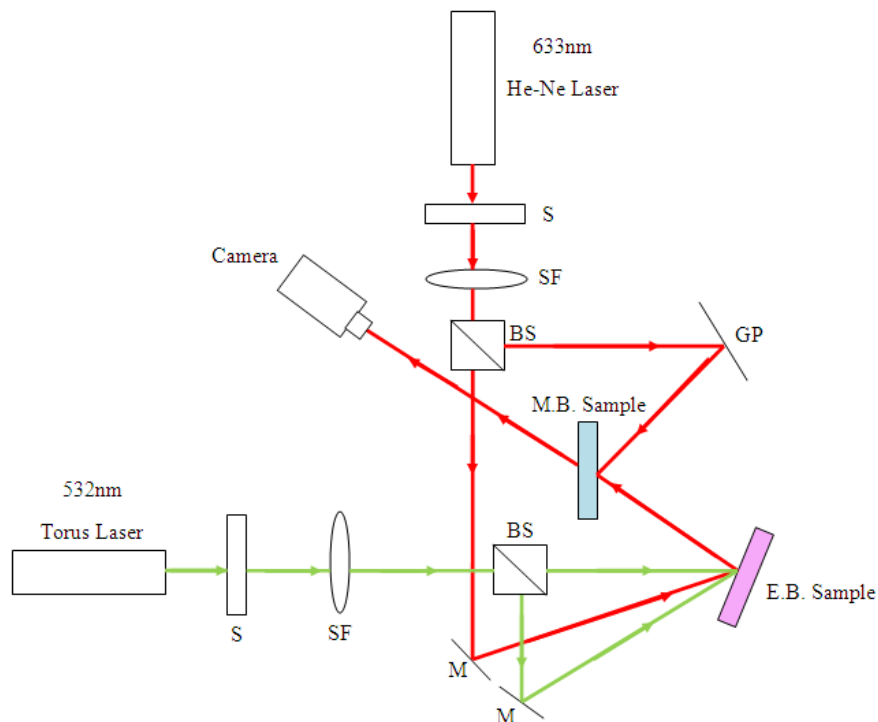
Fig. 5.6. Holographic interferometry setup; S: Shutter, SF: Spatial Filter, BS: Beam Splitter, GP: Glass Plate, M: Mirror.

5.4 Results and Discussion

5.4.1 Dependence of shrinkage on sample thickness

The influence of the sample thickness on the amount of shrinkage which occurs during holographic recording was investigated in real-time for three sample thicknesses: 45, 90 and 120 µm. For comparison purposes, two different definitions of shrinkage are used here; relative shrinkage, measured as a percentage of the overall sample thickness, and absolute shrinkage, the actual change in sample thickness measured in microns. The trends in both relative and absolute shrinkage for the DA photopolymer for a recording intensity of 1 mW/cm^2 are shown in fig. 5.7. In both cases, shrinkage is observed to increase with increasing sample thickness for the DA layers. This is expected as in thicker layers more monomer is available to be polymerised during recording. Therefore, the thicker layers will shrink to a greater degree due to the increased density of the polymer chains upon formation. The same trend of increasing shrinkage with sample thickness was observed for the higher recording intensities of 5 and 10 mW/cm^2 (see fig. 5.8). This is the opposite of the trend observed for the AA photopolymer.
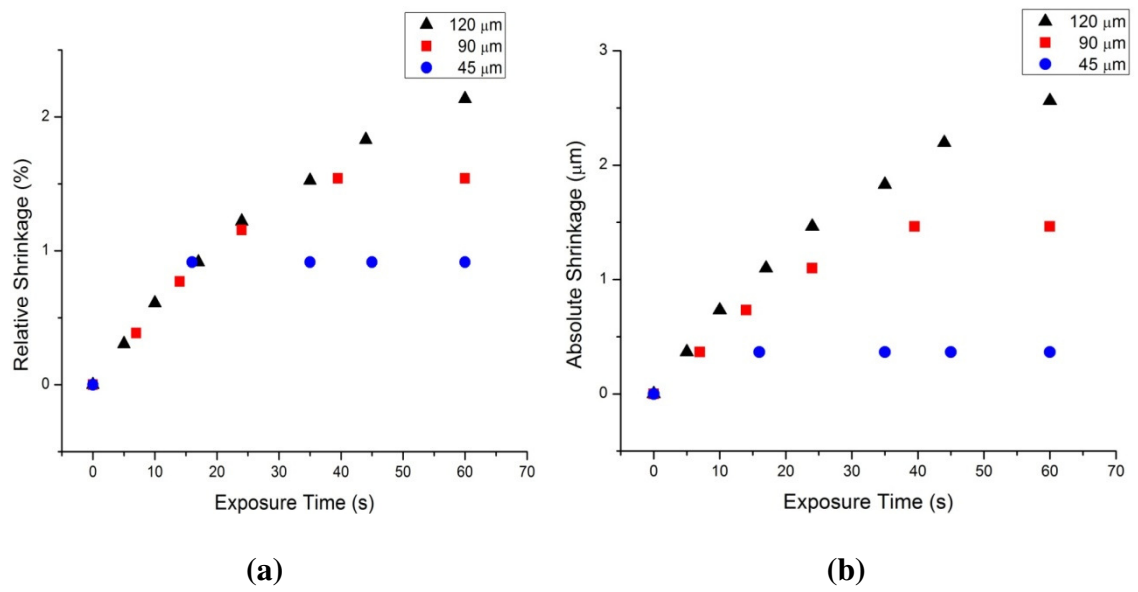
Fig. 5.7. (a) Relative shrinkage (%) vs. exposure time (s); (b) Absolute shrinkage (µm) vs. exposure time (s). DA photopolymer layers with thickness of 45, 90 and 120 µm DA were tested for a recording intensity of 1 mW/cm^2.
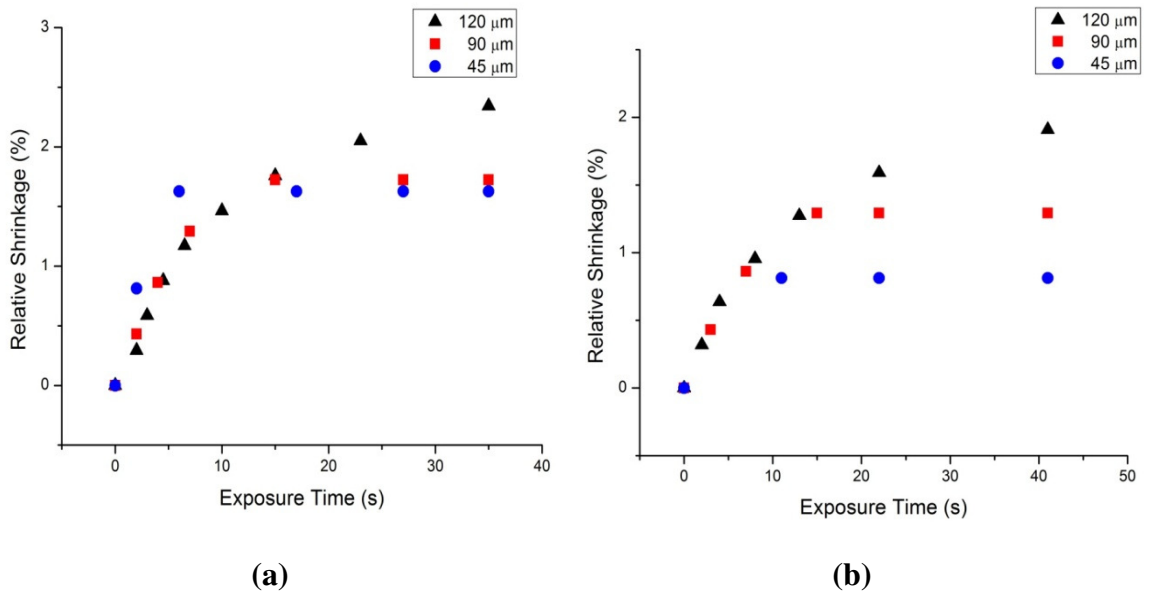
Fig. 5.8. Relative shrinkage (%) vs. exposure time (s) for 45, 90 and 120 µm DA photopolymer layers for a recording intensity of (a) 5 mW/cm^2 and (b) 10 mW/cm^2.

5.4.2 Dependence of shrinkage on recording intensity

The influence of recording intensity on the amount of shrinkage occurring during holographic recording was investigated for three different recording intensities: 1, 5 and 10 mW/cm^2. The experiments were carried out for three different sample thicknesses: 45, 90 and 120 µm. The real-time data for the three different thicknesses are shown in fig. 5.9. No clear dependence of relative shrinkage on recording intensity was observed for any of the sample thicknesses tested; the same approximate shrinkage value is achieved for all intensities once saturation is reached. It has been observed previously that the DA monomer molecule shows limited intensity dependence during holographic recording [28, 29]. This is likely attributed to the DA monomer molecule's large size, which reduces the rate at which the monomer molecules can diffuse. As the recording intensity is increased, the amount of shrinkage is not affected as the large DA monomer molecules cannot diffuse quickly enough to be polymerised at this faster rate.

In fig. 5.10, the relative shrinkage is shown in real-time as a function of exposure energy for the three tested recording intensities for 120 µm thick layers. It is observed that the rate of shrinkage as a function of exposure energy is faster at lower recording intensities. The same trend is observed for 45 and 90 µm thick layers also. This can be explained by the fact that at lower intensity, the concentration of free radicals is reduced, and so long polymer chain growth is promoted. There is a lower volume of free radicals resulting in a lower rate of termination. Thus for the same exposure energy absorbed by the layer, the shrinkage at lower intensity is effectively larger than the one caused by illumination with higher intensity. This is the same as the trend observed for the AA photopolymer by Moothancherry *et al* [10]. There is a much larger difference observed in the rate of shrinkage between 1 and 5 mW/cm^2 than between 5 and 10 mW/cm^2. This indicates that there exists a critical recording intensity beyond which

further increase of the intensity will have a limited effect on the rate of shrinkage as a function of exposure energy.

(a)

(b)

(c)
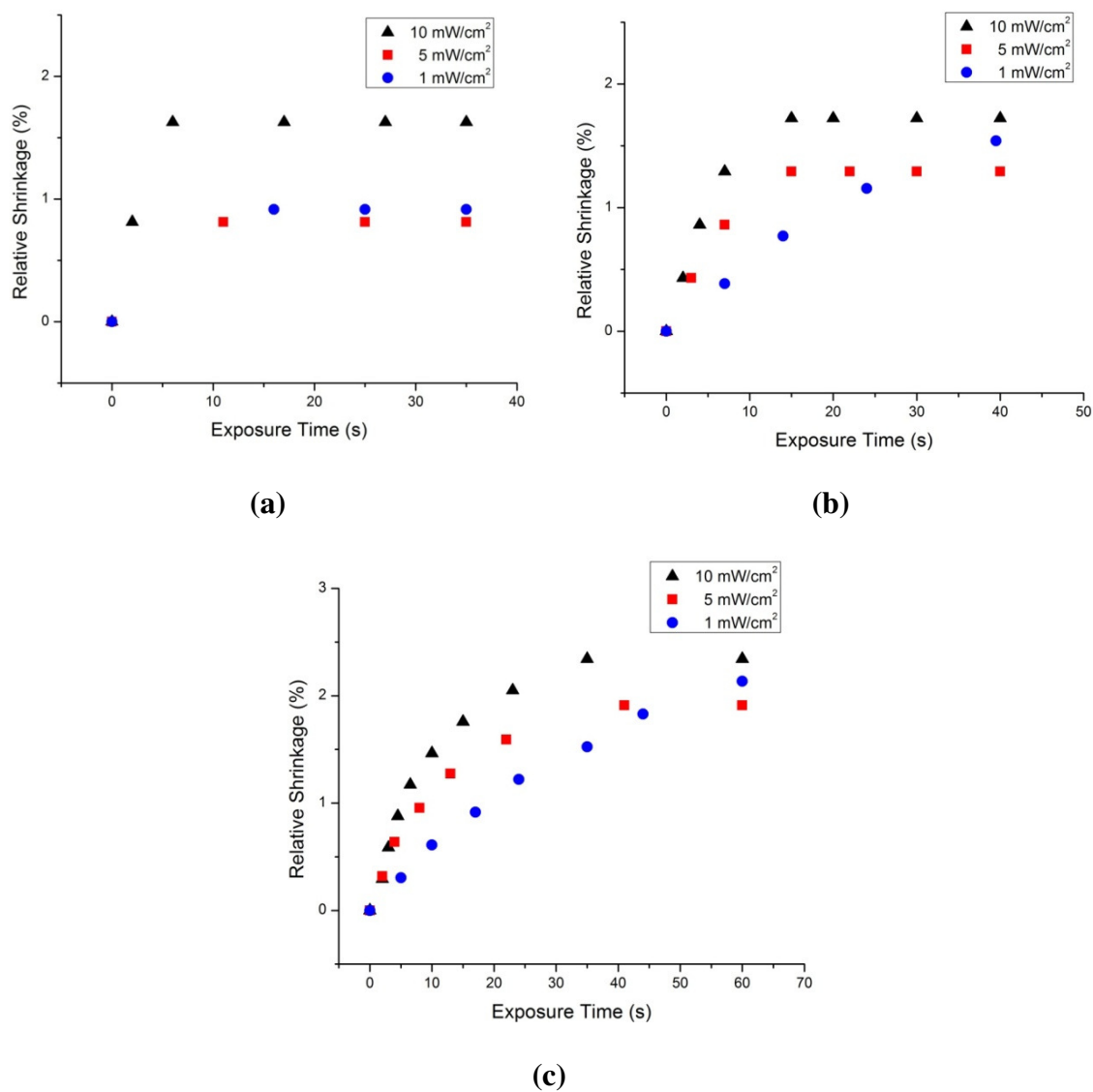
Fig. 5.9. Relative shrinkage (%) vs. exposure time (s) for DA photopolymer layers of thickness (a) 45 µm (b) 90 µm and (c) 120 µm exposed to 1, 5 and 10 mW/cm^2.
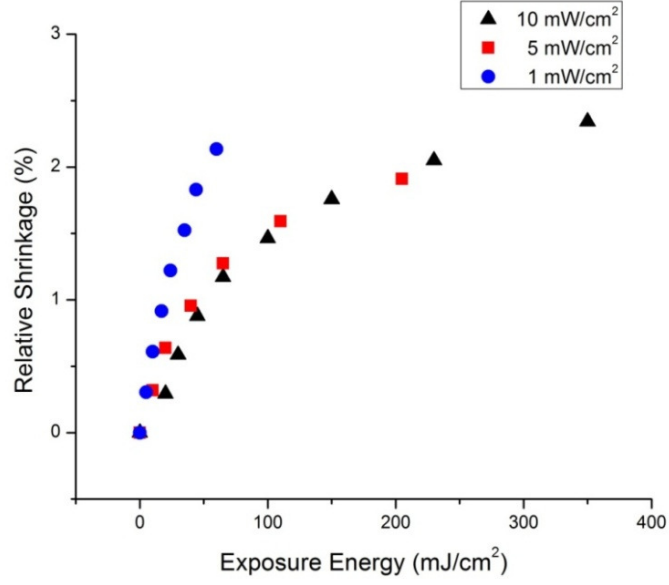
Fig. 5.10. Relative shrinkage (%) vs. exposure energy (mJ/cm^2) for 120 µm DA photopolymer layers exposed to 1, 5 and 10 mW/cm^2.

5.4.3 Fitting of experimental data

In the work by Moothanchery *et al* [10], the relative shrinkage vs. exposure time data for the AA photopolymer was fitted with a double exponential function of the form

$$y = y_o + A_1 e^{\left(\frac{x}{t_1}\right)} + A_2 e^{\left(\frac{x}{t_2}\right)} \tag{5.6}$$

where y_o is the final shrinkage value, A_1, A_2 are the amplitudes of the first and second processes, and t_1, t_2 are the time constants for the first and second processes. Initially a single exponent function was fitted, however this was not observed to be a good fit due to high errors. It was observed that there are two processes taking place that determine the dynamics of the photopolymer shrinkage, in particular for higher recording intensities. The first process is characterised by a time constant of few seconds while the second process is characterised by a time constant in the order of tens of seconds.

114

Moothanchery *et al* postulate that the slower second process, characterised by the longer time constant, is related to the rate of polymerisation of monomer molecules. As the recording intensity is increased, the value for the second time constant decreases as expected with faster polymerisation. The faster process which is observed at higher recording intensities is thought to be governed by the rate of crosslinking of the AA photopolymer composition [10].

Here, a double exponential function has been fitted to the relative shrinkage vs. exposure time data for the DA photopolymer in order to compare the values extracted for the final shrinkage, the time constants for the two processes and their amplitudes with that of the AA photopolymer. This was done for the 120 µm thick DA photopolymer layers to allow for comparison with the 110 µm thick AA photopolymer layers, for recording intensities of 1, 5 and 10 mW/cm^2. The fitted curves are shown in fig. 5.11 and the extracted values are given in table 5.2.
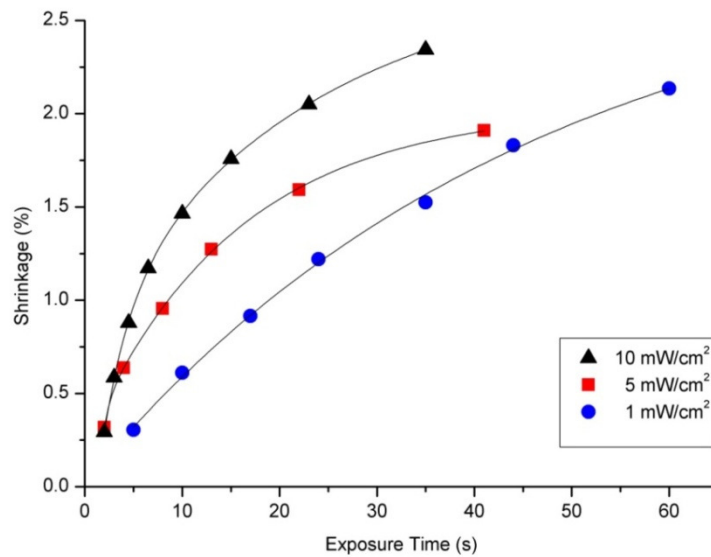
Fig. 5.11. Shrinkage (%) vs. exposure time (s) curve for 120 µm for DA photopolymer for recording intensities of 1, 5 and 10 mW/cm^2, fitted with a double exponential function.

Table 5.2. Data from double exponential fit of relative shrinkage vs. exposure time

	Intensity (mW/cm^2)	y_o (%)	A_1	t_1 (s)	A_2	t_2 (s)
	1	2.92±0.17	NA	NA	2.89±0.14	45.79±5.04
DA	5	2.20±0.78	0.77±1.43	4.87±8.36	1.47±0.84	25.00±48.89
	10	2.75±0.09	1.40±0.07	2.78±0.32	1.94±0.04	22.47±3.29
	1	3.3±0.03	NA	NA	3.4±0.03	62.5±0.0004
AA	5	3.3±0.05	0.86±0.08	9.6±0.014	2.44±0.05	71.4±0.001
	10	2.8±0.10	1.28±0.25	3.02±0.15	1.83±0.15	34.4±0.006

From the results for the DA photopolymer it is shown that as was the case for AA, the process characterised by the shorter time constant was not evident at the lowest recording intensity tested of 1 mW/cm^2. For a lower recording intensity, the rate at which the free radicals are generated will be lower and hence the crosslinking process will be slower. For this reason a single exponential fit is sufficient to fit the dynamics of the shrinkage process at such low intensity of recording.

As the recording intensity is increased to 5 mW/cm^2, there does appear to be two processes in operation. As the recording intensity is increased, the rate of free radicals generation is faster and the density of free radicals in unit volume will be higher, resulting in faster and greater extent of crosslinking of polymer chains. This is reflected in the faster process observed in the shrinkage dynamics. However, it is not possible to draw any more conclusions regarding a trend in the crosslinking rate due to the large error on both the time constant and amplitude values for the 5 mW/cm^2 data. This large error is most likely due to the fact that there are very few data points available for a double exponential fit.

As the recording intensity is increased again to 10 mW/cm^2, the faster crosslinking process becomes more prevalent, however its significance is still small relative to the second process, which is associated with the rate of polymerisation of the DA monomer molecules.

By comparing the final shrinkage values for the DA and AA photopolymers at all intensities, it is shown that this final shrinkage is slightly higher for the AA photopolymer than the DA photopolymer at all three recording intensities. This is most likely attributed to the ability of the smaller AA monomer molecules to diffuse at a faster rate, thereby promoting the growth of longer polymer chains, resulting in increased shrinkage in comparison to the DA photopolymer.

5.5 Conclusions

The polymerisation-induced shrinkage due to holographic recording in the DA photopolymer material has been measured using real-time holographic interferometry techniques.

The effect of sample thickness on the level of shrinkage has been investigated for 45, 90 and 120 µm thick layers. It was observed that the amount of shrinkage as a percentage of sample thickness is increased as sample thickness is increased, irrespective of the recording intensity used. For thicker layers, more monomer molecules are available for polymerisation, therefore the density of the polymerised chains will be higher as a result, and more shrinkage will occur.

The effect of recording intensity on the amount of shrinkage was investigated for three recording intensities; 1, 5 and 10 mW/cm^2. It was observed that for lower recording

intensities, larger shrinkage is observed in comparison to higher recording intensities at constant exposure energy. This may be explained by the fact that at lower recording intensities, the concentration of free radicals is reduced, and so long polymer chain growth is promoted. This results in increased shrinkage. This effect becomes less pronounced as the intensity is increased above 5 mW/cm^2.

The real-time shrinkage vs. exposure time data for the 120 µm thick DA photopolymer layers was fitted with a double exponential function. It was observed that the rate of shrinkage as a function of time is increased as the recording intensity is increased. From comparison with the results of Moothanchery *et al*, it was observed that the DA photopolymer on average demonstrates approximately 10-15 % less shrinkage as a percent of sample thickness than the AA photopolymer. This is most likely due to the difference in the monomer molecule sizes and their respective diffusion rates, both of which govern the ability of the photopolymer media to produce long polymer chains. It was shown that there are two processes at work in the DA photopolymer which govern the rate of shrinkage; the main, slower process is related to the rate of polymerisation of the monomer molecules, while the faster, secondary process is related to the rate of crosslinking of polymer chains. This secondary process becomes more prevalent as the recording intensity is increased.

It is clear from the data that the shrinkage levels of the undoped DA photopolymer are too high for it to be considered suitable for certain holographic applications like HDS. However, the addition of nanoparticles to the composition in the future is likely to significantly reduce the amount of DA photopolymer shrinkage. This expectation is based on the fact that MFI-type zeolites were previously shown to reduce the shrinkage of the AA-based photopolymer [8].

References:

[1] L. Shou-Jun, L. Guo-Dong, H. Qing–Sheng, W. Min- Xian, "Holographic formation in dry photopolymer film with shrinkage", Chinese Phys. 13, 1428-31 (2004).

[2] J. Boyd, T. Trentler, R. Wahi, Y. Vega-Cantu, V. Colvin, "Effect of film thickness on the performance of photopolymers as holographic recording materials", Appl. Opt 39, 2353-8 (2000).

[3] M. Atai, D. Watts, "A new kinetic model for the photopolymerization shrinkage-strain of dental composites and resin-monomers", Dental Materials 22, 785-91 (2006).

[4] L. Seungwoo , J. Yong-Cheol , H. Yongjoon, K. Sun-Il, C. Yoon-Sun, P. Jung-Ki, "Holographic photopolymers of organic/inorganic hybrid interpenetrating networks for reduced volume shrinkage", J. Mater. Chem. 19, 1105-14 (2009).

[5] J. T. Gallo, C. M. Verber, "Model for the effects of material shrinkage on volume holograms", Appl. Opt. 33, 6797-804 (1994).

[6] H. J. Coufal, D. Psaltis, G. T. Sincerbox, Holographic Data Storage, Springer Series in Optical Sciences, Springer-Verlag, Berlin, 2000.

[7] M. Moothanchery, I. Naydenova, V. Toal, "Studies of shrinkage as a result of holographic recording in acrylamide-based photopolymer film", Appl. Phys. A 104, 899-902 (2011).

[8] M. Moothanchery, I. Naydenova, S. Mintova, V. Toal, "Nanozeolite doped photopolymer layers with reduced shrinkage", Opt. Express 19, 25786-91 (2011).

[9] M. Moothanchery, V. Bavigadda, V. Toal, I. Naydenova, "Shrinkage during holographic recording in photopolymer films determined by holographic interferometry", Appl. Optics 52(35), 8519-8527 (2013).

[10] M. Moothanchery, "Studies of shrinkage in photopolymerisable materials for holographic applications", Doctoral Thesis, Dublin Institute of Technology, 2013.

[11] C. Zhao, J. Liu, Z. Fu, R. T. Chen, "Shrinkage correction of volume phase holograms for optical interconnects", Proc. SPIE. 3005 (1997).

[12] R. Vaia, C. Dennis, L. Natarajian, V. Tondiglia, D. Tomlin, T. Bunning, "One-step, micrometer-scale organization of nano and mesoparticles using holographic photopolymerization: A generic technique", Adv. Mater.13, 1570-1574 (2001).

[13] N. Suzuki, Y. Tomita, T. Kojima, "Holographic recording in TiO2 nanoparticle-dispersed methacrylate photopolymer films", Appl. Phys. Lett 81, 4121-4123 (2002).

[14] C. Sanchez, M. Escuti, C. van Heesch, C. Bastiaansen, D. Broer, J. Loos, R. Nussbaumer, "TiO2 nanoparticle-photopolymer holographic recording", Adv. Func. Mater. 15, 1623-1629 (2005).

[15] T. J. Trentler, J. E. Boyd, V. L. Colvin, "Epoxy resin-photopolymer composites for volume holography", Chem. Mater. 12, 1431- 1438 (2000).

[16] C. M. Cheah, J. Y. H. Fuh, A. Y. C. Nee, L. Lu, "Mechanical characteristics of fiber-filled photo-polymer used in stereolithography," Rapid Prototyping Journal 5, 112-119 (1999).

[17] S. Lee, Y. C. Jeong, Y. Heo, S. Kim, Y. S. Choi, J. K. Park, "Holographic photopolymers of organic/inorganic hybrid interpenetrating networks for reduced volume shrinkage", J. Mater. Chem. 19, 1105–1114 (2009).

[18] J. H. Chen, C. T. Yang, C. H. Huang, M. F. Hsu, T. R. Jeng, "Study of Optical Properties of Glass-Like Polymer Material for Blue Laser Holographic Optic Data Storage Recording," IEEE Transactions on Magnetics 45 , 2256-2259 (2009).

[19] S. Gallego, A. Marquez, D. Mendez, "Analysis of PVA/AA based photopolymers at the zero spatial frequency limit using interferometric methods", Appl. Optics. 47, 2557–2563 (2008).

[20] J. R. Meyer-Arendt, Introduction to classical and modern optics, 4th edition, Prentice-Hall Inc., New Jersey (1995).

[21] R. K. Erf, Holographic non-destructive testing, Academic Press. Inc, London (1974).

[22] Powell, Stetson, "Interferometric vibration analysis by wavefront reconstruction", JOSA 55, 1593-1598 (1965).

[23] R. Jones, C. Wykes, Holographic and Speckle interferometry, Cambridge University Press, Cambridge (1983).

[24] P. K. Rastogi, Optical measurement technique and applications, Artech House Inc, Norwood, USA (1997).

[25] R. C. Samson, "Holographic interferometry applications in experimental mechanics", Exp. Mech. 10, 312-320 (1970).

[26] P. Hariharan, Basics of Interferometry, Academic Press, 2010.

[27] E. N. Leith, J. Upatnieks, "Wavefront reconstruction with continuous-tone objects", JOSA 53(12), 1377-1381 (1963).

[28] D. Cody, I. Naydenova, E. Mihaylova, "New non-toxic holographic photopolymer material", J. Opt. 14(1), 015601 (2012).

[29] D. Cody, I. Naydenova, E. Mihaylova, "Effect of glycerol on a diacetone acrylamide-based holographic photopolymer material", Appl. Opt. 52(3), 489-494 (2013).

6. INVESTIGATION OF THE EFFECT OF GLYCEROL ON THE DA PHOTOPOLYMER

6.1 Introduction

Glycerol is a transparent, viscous liquid that is reported to have low toxicity [1]. It is widely used in the food and pharmaceutical industries as a solvent and lubricant. Its chemical structure consists of three hydroxyl groups attached to carbon atoms, as shown in fig. 6.1. Glycerol has been extensively documented to have some very interesting effects on the properties of different chemical and polymer systems.
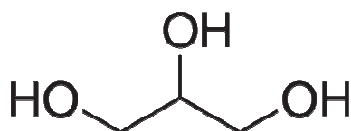
Fig. 6.1. Chemical structure of glycerol.

One of glycerol's most common uses in industry and research is as a plasticiser. It has been used as such in the development of non-toxic biodegradable polymers [2-5]. The benefits of increased plasticisation of photopolymer layers are numerous, such as increased capacity of monomer dissolution without crystallisation, and improved optical quality of layers. However, the main benefit is the potential for increased diffusion of photopolymer components during exposure. This was the initial reason for the inclusion of glycerol in the DA photopolymer composition. Faster diffusion within the photopolymer layer increases the probability for the formation of free radicals and therefore the initiation of polymer chains. Faster monomer diffusion also promotes long chain growth. Glycerol was added to the DA photopolymer composition in order to investigate if a plasticiser such as glycerol would have the above effects on the photopolymer system during holographic recording.

Here, the effect of glycerol on the holographic recording properties of the DA-based photopolymer has been investigated. Comparison is made between the DA photopolymer both with and without glycerol for a range of parameters including the dependence of the Δn on recording intensity, exposure energy, sample thickness and spatial frequency. The influence of glycerol on the photoinitiating system has been investigated also by studying its effect on parameters such as the duration of the inhibition period, the rate of photobleaching, and the absorbance of the different dyes Erythrosin B, Methylene Blue and Eosin Y.

6.2 Theory

The effects of glycerol on the different components of polymer-based systems have been documented extensively in the literature. A brief review of some such effects is given here.

Glycerol is reportedly involved in the spontaneous polymerisation of monomeric AA in water-glycerol solutions [6-8]. Bol'shakov *et al* suggest that the polymerisation proceeds during the dissolution of AA in glycerol and leads to formation of gel globules within which the polymer chain growth takes place [6]. It was discovered by Osmanov *et al* that on addition of glycerol to water, the molecular mass of the polyacrylamide formed drops sharply [8]. This is attributed to increased viscosity of the mixture with the addition of glycerol.

Glycerol is documented to interact with crosslinking monomers such as bisacrylamide also. Raman studies by Jiserak *et al* showed that the addition of glycerol to their two-monomer system causes the percentage of polymerised bisacrylamide to increase [9].

The percentage of polymerised bisacrylamide was shown to increase with the concentration of glycerol added. The glycerol was not shown to affect the rate of polymerisation of the main monomer in the composition, only that of the crosslinking monomer. A paper by Yuan *et al* documents the accelerating effect that plasticisers have on the crosslinking reaction between acrylonitrile-butadiene rubber and copper sulfate [10]. In certain cases, glycerol has been documented to act itself as a crosslinker in different polymerisation reactions [11, 12].

As a highly viscous liquid, glycerol naturally affects the viscosity of any medium it is added to. Oster *et al* used glycerol to vary the viscosity of an AA-riboflavin photopolymer system [13]. They observed that the molecular weight of the polymers formed increased with increasing viscosity. Meyer *et al* [14] and Galassi [15] noted that the addition of glycerol to two very different photosensitive systems caused up to an order of magnitude drop in the photobleaching rate, which they attribute to increasing viscosity. Another possible explanation in the drop in photobleaching rate may be glycerol's inhibition effects. As described in section 1.4.9 of chapter 1, the polymerisation reaction is inhibited by any element or compound that acts as a free radical trap. Oxygen is one such inhibitor. Oxygen dissolved in the photopolymer layer will inhibit and, at high enough concentrations, even prevent AA polymerisation [16]. The product of the reaction between oxygen and dye molecules is inert, that can therefore not initiate a free radical and be involved in polymerisation [17]. This principle has been used for the development of oxygen sensors [18, 19]. Ren *et al* found that at low concentrations (< 60 % v/v), glycerol stimulated the rate of oxygen uptake in PSI particles [20]. This implies glycerol can act as a reducing agent and increase oxygen levels in photosensitive systems, creating inhibition effects. Kishore *et al* have shown

that the reaction of OH radicals from glycerol with triethanolamine molecules also yields oxidising species, further exacerbating this effect [21].

Glycerol's nature as a reducing agent has been reported to affect the sensitivity of certain photosensitive dyes also. Von Hubl observed a marked increase in the sensitivity of Methylene Blue dye to light with the addition of glycerol [22]. Methylene Blue can bleach by reduction or oxidation. Von Hubl noted that when this reaction proceeds via reduction, the dye's colour returns when it is exposed to air.

From reviewing the literature it is clear that glycerol has a pronounced effect on the physical and chemical properties of nearly all of the different individual photopolymer components, namely the main monomer, crosslinking monomer, electron donor and photosensitizing dye. It is of interest therefore to investigate the effect of glycerol on the DA photopolymer system as a whole, and as a result on the holographic recording ability of the DA material.

6.3 Experimental

6.3.1 Preparation of glycerol-doped DA photopolymer layers

The effect of different concentrations of glycerol as a % of total solid weight (wt. %) on the optical quality of the DA photopolymer layers was investigated. Dry layers which contained 0.0, 10.3, 18.8, 25.7 and 31.6 wt. % glycerol were prepared. The 18.8 wt. % layers were of the best optical quality. This concentration of glycerol resulted in improved uniformity and evenness of the layers. It also significantly reduced the formation of small air bubbles within the DA photopolymer layer during the drying process. This is important for minimising scattering effects during recording, which

restict the ability to record high diffraction efficiency gratings. Concentrations of glycerol higher than 18.8 wt. % were not favourable as by increasing the concentration of glycerol in the photopolymer layers, the overall concentration of DA monomer and therefore the maximum achievable diffraction efficiency is reduced. Fig. 6.2 clearly demonstrates the improvement that glycerol has on sample optical quality. This is most likely due to its function as a plasticiser. Table 6.1 shows the formulation of the DA0 (without glycerol) and DAG (with glycerol) compositions that were used throughout this study.
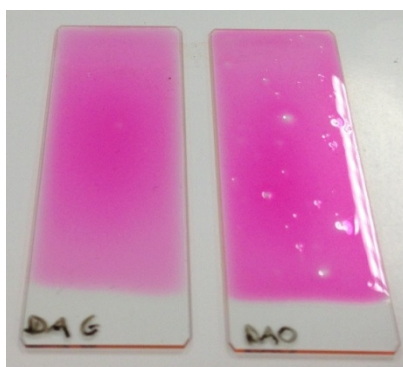
Fig. 6.2. Photo taken of DAG (left) and DA0 (right) samples, to illustrate the effect of glycerol on the DA sample optical quality.

Table 6.1 Composition of the DA0 and DAG photopolymers

	DA0	DAG
10 % wt/vol PVA (ml)	20	20
TEA (ml)	2	2
DA (g)	1	1
BA (g)	0.2	0.2
0.11 % wt/vol Erythrosin B stock solution (ml)	4	4
Glycerol (ml)	1	-

6.3.2 Methods

The same holographic recording setup as described in chapter 4 was used for all characterisation of the DAG photopolymer. Briefly, a two-beam holographic optical setup was used to record un-slanted transmission gratings using a 532 nm vertically-polarised Nd:YVO$_4$ laser. The spatial frequency of the recorded grating was controlled by varying the angle between the two recording beams. The intensity of the recording beams was controlled using a neutral density filter. A 633 nm He-Ne laser was used as the probe beam at the Bragg angle. An optical power meter (Newport 1830-C) was used to record the intensity of the diffracted beam, and LabVIEW software was used to plot the data in real-time. The grating was placed on a rotational stage (Newport ESP 300) in order to measure the diffracted intensity dependence on the incident angle of the probe beam after recording. The accuracy of this measurement was 1×10^{-3} deg. The refractive index modulation, Δn, and the diffraction efficiency, η, were calculated as previously described in section 4.2.2 of chapter 4.

6.4 Results and Discussion

6.4.1 Transmission mode holographic recording characterisation of the DAG photopolymer

6.4.1.1 Dependence of Δn on recording intensity for the DAG photopolymer at 1000 l/mm

Holographic transmission gratings were recorded in the DAG photopolymer at a spatial frequency of 1000 l/mm. The recording intensity was varied from 1-5 mW/cm^2, with

constant exposure energy of 100 mJ/cm^2. The results for Δn for both the DA0 and DAG compositions are shown in fig. 6.3.
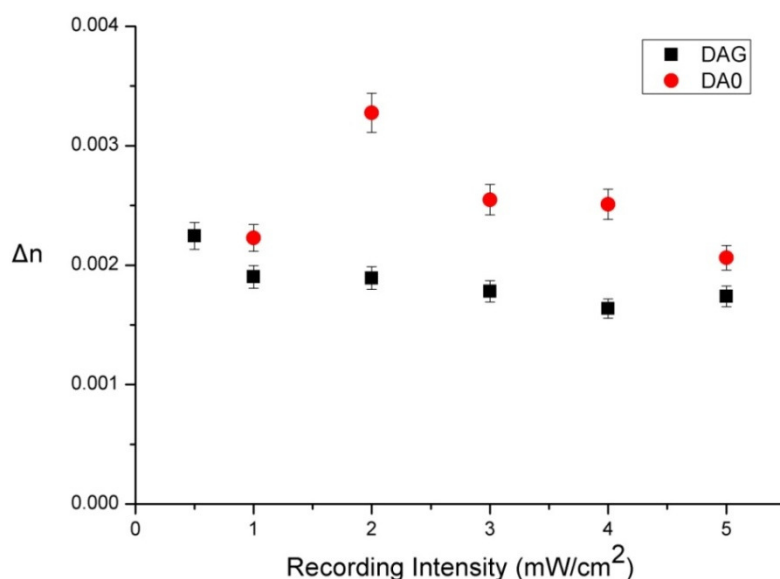
Fig. 6.3. Δn vs. recording intensity for the DA0 (no glycerol) and DAG (with glycerol) compositions at 1000 l/mm for an exposure energy of 100 mJ/cm^2.

The intensity dependence for DAG is observed to be approximately uniform over the range of intensities tested. In general, increasing the recording intensity increases the concentration of free radicals produced, and therefore increases the probability of a free radial reacting with a monomer to initiate a polymer chain. However, the probability of this reaction occurring is already increased due to the inclusion of glycerol. Glycerol acts as a plasticiser, which allows the unreacted monomer to diffuse more quickly both into and within the illuminated regions of the photopolymer layer. This increases the probability of the monomer reacting with a free racial to initiate a polymer chain, or alternatively attaching itself to an existing polymer chain. For DA0, an optimum intensity of 2 mW/cm^2 is observed. In this case the diffusion of monomer molecules without glycerol will be slower. Therefore, there exists an optimum ratio between the rate of diffusion and the rate of polymerisation (controlled by the recording intensity)

for which the Δn will be optimum due to the growth of long polymer chains [23]. Increasing the recording intensity beyond 2 mW/cm^2 does not result in increased Δn, as higher recording intensities promote the growth of short polymer chains. In general, longer polymer chains are preferential for the formation of high Δn gratings at this relatively low spatial frequency.

It is observed that the Δn for DA0 is higher than that for DAG at all intensities. This can be explained by considering that DAG has a slightly lower wt. % of DA monomer than DA0, due to the addition of glycerol. DA0 contains 3.8 wt. % more monomer than DAG, which may explain the difference in Δn. When the concentration of DA monomer in the DAG composition was increased beyond its current value, the optical quality of the photopolymer layers was reduced, hence this concentration was chosen.

Higher recording intensities of 10 and 20 mW/cm^2 were then investigated, and the results of this are shown in fig. 6.4. It is observed that there is little difference in the Δn achieved using recording intensities of 2, 10 or 20 mW/cm^2 over a range of exposure energies. As discussed above, this uniform intensity dependence is due to glycerol's nature as a plasticiser, allowing for increasing diffusion of the monomer molecules within the DAG photopolymer layer during holographic recording. The uniform intensity response of the DAG material is a desirable feature for holographic applications, as the use of high recording intensities allows for much faster recording, which is necessary for hologram production on a large scale.
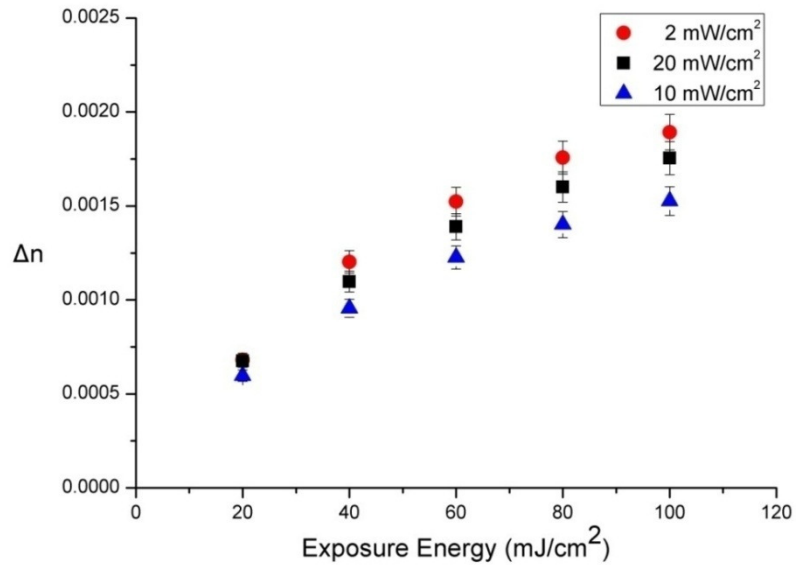
Fig. 6.4. Δn vs. exposure energy (mJ/cm^2) for DAG samples tested at low (2 mW/cm^2) and high (10 and 20 mW/cm^2) recording intensities.

6.4.1.2 Dependence of Δn on recording intensity for the DAG photopolymer at 3000 l/mm

The maximum Δn for different recording intensities was investigated for the DAG photopolymer at the higher spatial frequency of 3000 l/mm. The result of this study is shown in fig. 6.5. As the spatial frequency is increased, the maximum Δn for DAG decreased, as was also observed for DA0. This is due to the reduction in fringe spacing of the grating, which results in diffusion and growth of polymer chains out of the illuminated fringe regions, thereby reducing Δn. DAG achieves a maximum Δn of 3.5×10^{-4}, which is slightly lower than that achieved with the DA0 composition. However, there appears to be very little if any intensity dependence at the range of recording intensities tested for the DAG photopolymer.
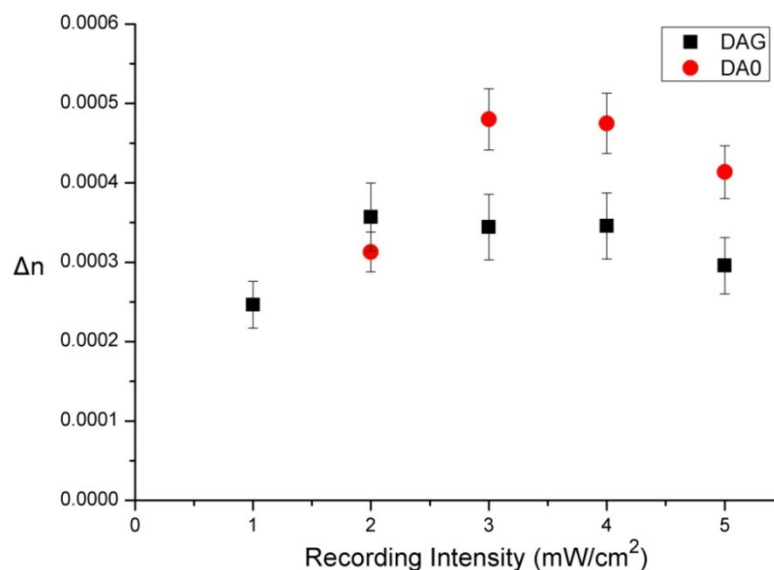
Fig. 6.5. Δn vs. recording intensity for DA0 and DAG at 3000 l/mm for an exposure energy of 100 mJ/cm^2.

6.4.1.3 Dependence of Δn on spatial frequency of recording for the DAG photopolymer

The spatial frequency response of the DAG material was investigated by recording transmission gratings at spatial frequencies of 100, 300, 1000 and 3000 l/mm. The gratings were recorded using a total intensity of 2 mW/cm^2 and an exposure energy of 100 mJ/cm^2. The results of this study for the DAG composition are shown in fig. 6.6. The results for the DA0 composition are included for comparison.

At 100 l/mm, the lowest spatial frequency tested, the same relatively low Δn value (1.3×10^{-3}) is achieved for both the DA0 and DAG compositions. At such a low spatial frequency, the fringe spacing is very large at 10 µm and so the addition of a plasticiser such as glycerol cannot sufficiently increase diffusion in order to overcome these large distances.

As the spatial frequency is increased to 300 l/mm, the fringe spacing is significantly reduced to 3.33 µm. The Δn of the DAG composition at this spatial frequency is increased to 4.5×10^{-3}, significantly larger than the Δn for DA0 of 1.8×10^{-3}. The large improvement in Δn may be explained by increased diffusion of monomer molecules both within and into the illuminated regions which are considerably smaller at 300 l/mm than for the lower spatial frequency of 100 l/mm, where the inclusion of glycerol was shown to have no effect. The increased diffusion results in improved mobility of the monomer molecules, which will facilitate the mass transport and the density change between the dark and the bright regions, resulting in increased Δn.

However, as the spatial frequency is increased further to 1000 l/mm, the Δn measured for DA0 overtakes that of DAG. It is possible that at 1000 l/mm, faster diffusion is now less critical than it was at 300 l/mm, as the distance over which the monomer molecules must travel is reduced as fringe spacing is 1 µm, and so the effect of glycerol is relatively reduced.

As the spatial frequency is again increased to 3000 l/mm, the Δn achieved with both compositions is very low. At such low fringe spacings (0.33 µm), diffusion of mobile polymer chains and growth of polymer chains out of the illuminated areas is likely, which contributes to the observed decrease in the recording ability of both materials.
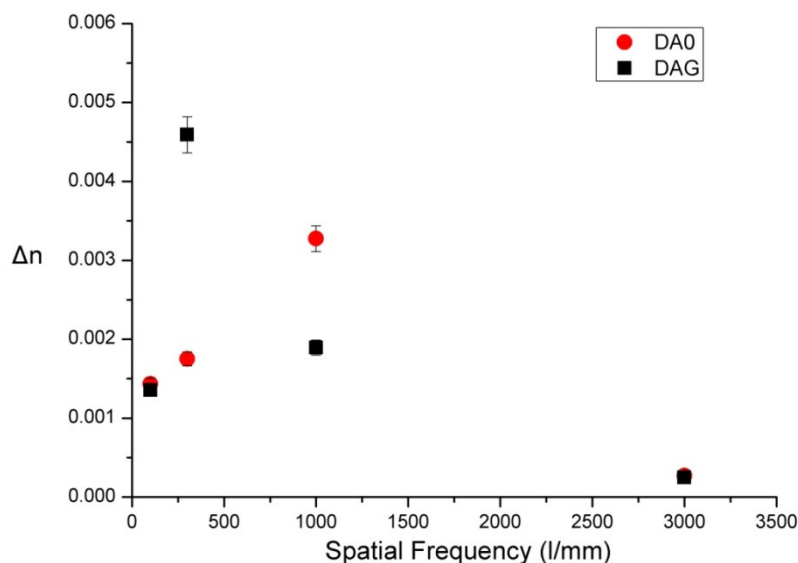
Fig. 6.6. Δn vs. spatial frequency for the DA0 and DAG compositions.

6.4.2 Effect of glycerol on the photoinitiating system

6.4.2.1 Investigation of inhibition effects due to glycerol

An inhibition period was observed at the start of recording for some of the photopolymer layers containing glycerol. This delay is caused by oxygen-quenching in the layer, a process outlined in section 1.4.8. The relationship between the duration of the inhibition period and the recording intensity used for DAG is shown in fig. 6.7. As the recording intensity is increased, the inhibition period becomes shorter. This trend is expected, as by increasing the number of photons reaching the layer, any oxygen present in the layer is consumed faster. Once the threshold concentration of oxygen above which inhibition occurs is reached (the "inhibition threshold" [17]), polymerisation can continue as normal.

This trend in inhibition period may contribute to the trend in Δn at different recording intensities for the DAG composition as inhibition periods have a significant effect on

the effective recording intensity. As shown in fig. 6.7, the inhibition periods are of longer duration at lower recording intensities. This will result in reduced effective recording intensities. Due to the inhibition period, a smaller number of free radicals may be created initially, and thus the polymerisation occurs at a slower rate. This effect is more pronounced at the lower recording intensities. Since the effective recording intensity is reduced, the rate of polymerisation will initially be lower; this may result in the ratio of the diffusion and polymerisation rates being favourable for long polymer chain growth, as the reduced rate of polymerisation is favourable for the larger DA molecules which move slowly. This effect may ultimately contribute to higher Δn, as observed at 0.5 mW/cm^2 in fig. 6.3. As the recording intensity is increased, the inhibition period is reduced, and so the rate of polymerisation is no longer restricted in this manner.
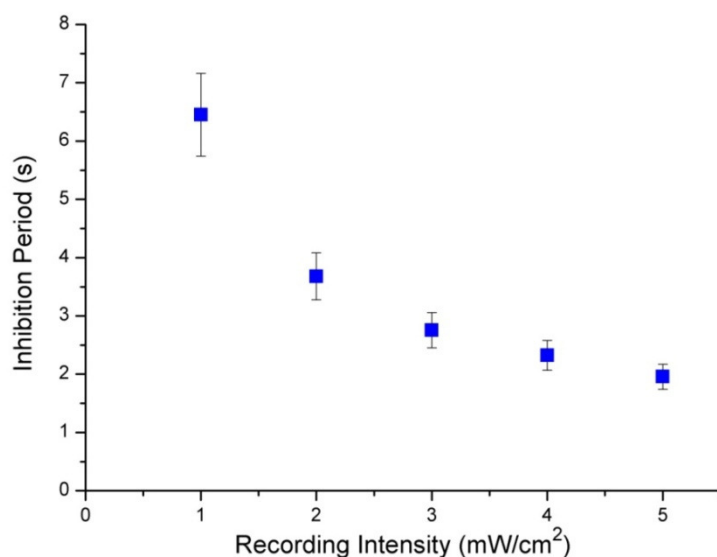
Fig. 6.7. Inhibition period observed at start of exposure (s) vs. recording intensity (mW/cm^2) for DAG samples.

6.4.2.2 Effect of glycerol on the rate of photobleaching of the DA photopolymer

Studies on the bleaching rates of the DA0 and DAG compositions were carried out, in order to determine if the drop observed by Meyer *et al* [14] and Galassi [15] in the bleaching rate due to the presence of glycerol occurred too in the DA photopolymer system. In order to determine the bleaching rate, photopolymer samples were illuminated with a single 2 mW/cm^2 532 nm beam. The intensity of the transmitted beam was plotted in real-time. The slope of this curve was then plotted against layer thickness, in order to obtain a picture of the dependence of the rate of bleaching on layer thickness. This was done for the DA0, DAG and standard AA compositions and the results of this study are shown in fig. 6.8.

It is observed that the rate of photobleaching is faster for DA0 than for DAG at all sample thicknesses. This implies that the addition of glycerol decreases the rate of photobleaching of the DA-based composition. As described in section 6.2, glycerol is a reducing agent and has been shown to stimulate the level of oxygenation in different materials. During holographic exposure, most of the oxygen in the layer must be first used up before polymerisation can begin. Increased levels of oxygen in the DAG samples due to the presence of glycerol would inhibit the bleaching of the material via the oxygen-quenching reaction described in section 1.4.8, which may explain the drop in bleaching rate. The AA-based photopolymer has a lower rate of photobleaching than either of the DA compositions, however, this composition contains a different monomer and so the bleaching mechanisms are not directly comparable. Lower photobleaching is a desirable feature for holographic photopolymers. Slower bleaching means that more dye molecules are available to absorb a photon and initiate polymerisation, allowing for higher Δn values to be reached.
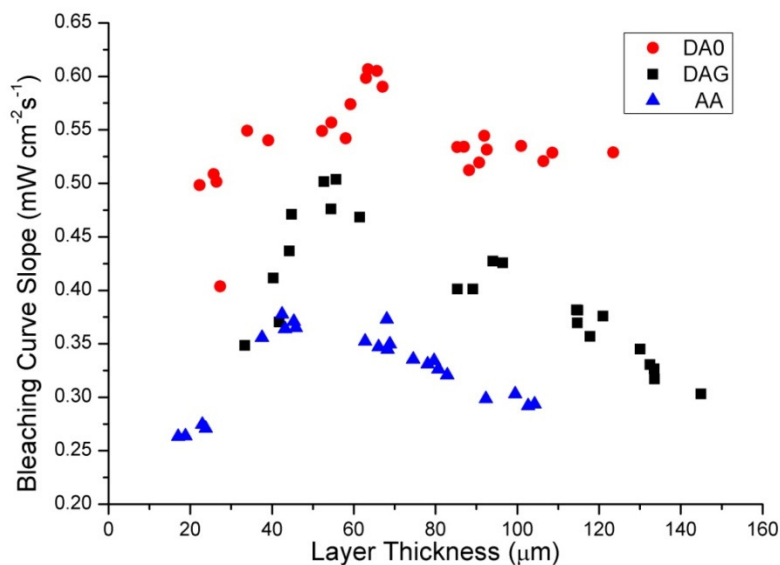
Fig. 6.8. Bleaching curve slope (mW/cm^{-2}s^{-1}) vs. layer thickness (µm) for the DA0, DAG and AA compositions.

Another possible explanation is that glycerol slows the rate of bleaching due to the increased viscosity of the DAG composition. Meyer *et al* and Galassi have attributed glycerol's effect on the rate of photobleaching of different materials to its effect on solution viscosity. To investigate this, the viscosity of the DA0, DAG and AA compositions was determined in order to see if as solution viscosity is increased, the rate of photobleaching decreases, as predicted by Meyer and Galassi's work. The viscosity of the solutions was measured using a tuning fork vibrational digital viscometer, and the results are shown in Table 6.2.

As expected, the viscosity of the DA photopolymer is increased with the addition of glycerol. However, the trend in viscosity does not match that of the trend in photobleaching. The rate of photobleaching of the AA composition is slower than both that of DA0 and DAG, but the viscosity of the AA solution is lower than that of both DA compositions also. Therefore, it is not possible to conclude that viscosity alone determines the rate of photobleaching of the photopolymer compositions.

136

Table 6.2 Viscosity of DA0, DAG and AA compositions

Composition	Viscosity (mPa/s)
DA0	9.84 ± 0.47
DAG	10.60 ± 0.43
AA	8.64 ± 0.30

6.4.3 Study of the effect of glycerol on the absorbance of different photosensitive dyes

Absorbance is a quantitative measurement expressed as a logarithmic ratio between the radiation falling upon a material, I_o, and the radiation transmitted through a material, I_t:

$$A_\lambda = \log_{10} \frac{I_o}{I_t} \qquad (6.1)$$

Von Hubl observed that the addition of glycerol to the photosensitive dyes Methylene Blue, Phenosafranine and Scarlet resulted in a marked increase in sensitivity to light, up to a thousand fold [22]. Here, the effect of glycerol on the absorbance of three different dyes used widely as photosensitisers in holographic photopolymers, namely Erythrosin B, Methylene Blue and Eosin Y has been investigated in order to determine if a similar improvement in sensitivity would be observed. The normalised absorbance spectra for the three dyes tested are shown in fig. 6.9.

A Perkin Elmer Lambda 900 UV/VIS/NIR Spectrometer was used for all measurements in the wavelength region of 350 - 850 nm. The concentration of the dye molecules in solution was kept constant, in order for accurate comparison of the different spectra to be carried out. The concentration of each dye in aqueous solution was kept constant at 2×10^{-5} Mol/L. The number of glycerol molecules added to the solution was then varied

from one tenth that of the dye molecules ($\times \frac{1}{10}$), to one thousand times the number of

dye molecules ($\times 1000$) in order to investigate the effect of glycerol concentration on

each dye's absorbance.
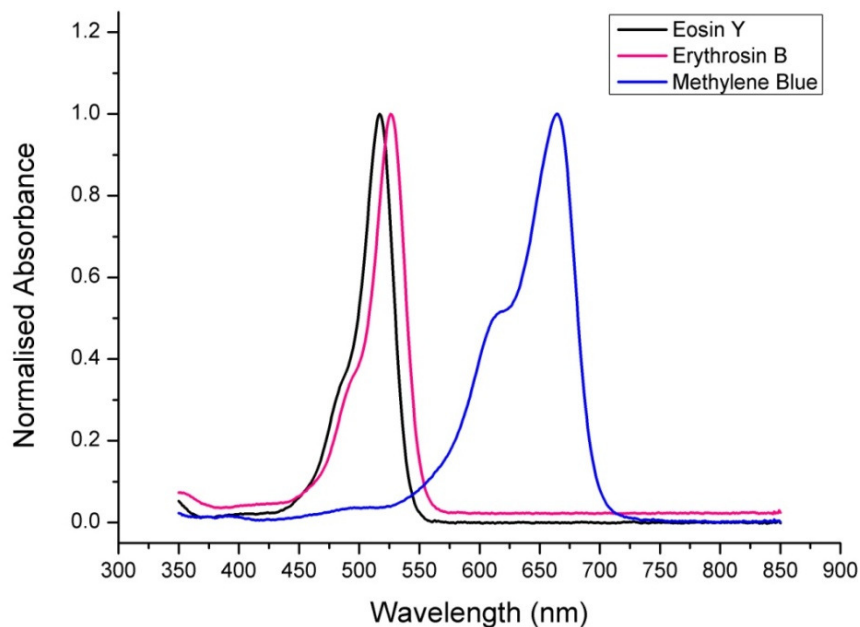
Fig. 6.9. Normalised absorbance vs. wavelength spectra for the Eosin Y, Erythrosin B

and Methylene Blue dyes.

6.4.3.1 Erythrosin B

i) Dye preparation calculations

The molar mass of Erythrosin B is 879.87 g/mol. A 2×10^{-5} mol/L solution was

prepared by adding 0.01760 g of Erythrosin B dye to 100 ml of deionised water.

ii) Glycerol concentration calculations

The molar mass of glycerol is 92.09 g/mol. The prepared 2×10^{-5} mol/L Erythrosin B dye solution contained 1.2044×10^{19} molecules. Therefore, the concentration of glycerol solution in water required to have 1.2044×10^{19} molecules is:

$(2 \times 10^{-5}$ mol/L$) \times (92.09$ g /mol$) = 1.8418 \times 10^{-3}$ g/L

The density of glycerol is 1.25 g/ml, therefore the concentration of glycerol in ml/L required in order to have the same number of glycerol molecules as dye molecules is:

$(1.8418 \times 10^{-3}$ g/L$) \div (1.25$ g/ml$) = 1.473 \times 10^{-3}$ ml/L

In order to have ten times as many glycerol molecules as dye molecules ($\times 10$), the desired concentration of glycerol is:

$(2 \times 10^{-4}$ mol/L$) \times (92.09$ g /mol$) = 1.84 \times 10^{-2}$ g/L $= 1.473 \times 10^{-2}$ ml/L

In order to have one tenth the number of glycerol molecules as dye molecules ($\times \frac{1}{10}$), the desired concentration of glycerol is:

$(2 \times 10^{-6}$ mol/L$) \times (92.09$ g /mol$) = 1.84 \times 10^{-4}$ g/L $= 1.473 \times 10^{-4}$ ml/L

The same procedure was used for the $\times 100$ and $\times 1000$ as many glycerol molecules as dye molecules calculations. The dye and glycerol solutions were then combined in equal parts, and stirred magnetically for 1 hour before use.

iii) Erythrosin B and Glycerol: Absorbance results

As can be seen in fig. 6.10, there is an increasing trend in absorbance as the number of glycerol molecules is increased from zero up to ×1000 number of Erythrosin B dye molecules. At 100:1 the largest increase is observed, the absorbance is increased from 0.986 to 1.026, an increase of 4.06 % compared to the pure dye solution. These results suggest that glycerol has some influence on the absorbance of the Erythrosin B dye over the range of wavelengths investigated, as for all ratios tested there is an increase in absorbance compared to that of the dye solution only. The Glycerol-Erythrosin B compositions all reach maximum absorbance at a wavelength of 527 nm.
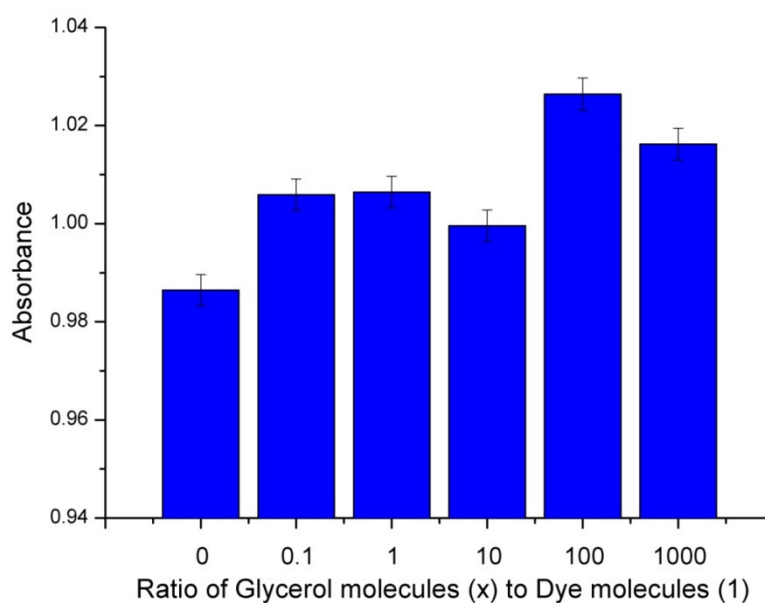
Fig. 6.10. Absorbance vs. the ratio of glycerol molecules to Erythrosin B dye molecules (x:1).

6.4.3.2 Methylene Blue

i) Dye preparation calculations

The molar mass of Methylene Blue is 319.85 g/mol. A 2×10^{-5} mol/L solution was prepared by adding 0.00640 g of Methylene Blue dye to 100 ml of deionised water.

ii) Glycerol concentration calculations

See section 6.4.3.1 ii)

iii) Methylene blue and Glycerol: Absorbance results

Similarly to Erythrosin B, the results shown in fig. 6.11 indicate a small change in the absorbance of the Methylene Blue dye due to glycerol. The largest increase in absorbance is observed for the 1:1 composition, with an increase in absorbance of 0.92 %. After this point the absorbance begins to decrease. As stated earlier, glycerol is a reducing agent and can lead to the bleaching of dye molecules via oxygenation. This is a possible explanation for why at higher levels of glycerol, the absorbance decreases due to preliminary bleaching of the dye molecules. The Glycerol-Methylene B compositions reach a maximum absorbance at a wavelength of 664-665 nm.
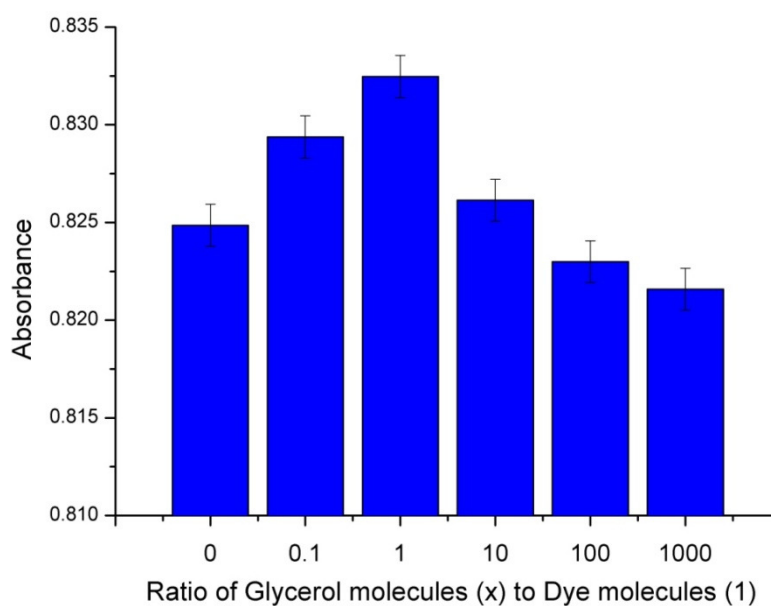
Fig. 6.11. Absorbance vs. the ratio of glycerol molecules to Methylene Blue molecules (x:1).

6.4.3.3 Eosin Y

i) Dye preparation calculations

The molar mass of Eosin Y is 691.85 g/mol. A 2×10^{-5} mol/L solution was prepared by adding 0.01384 g of Eosin Y dye to 100 ml of deionised water.

ii) Glycerol concentration Calculations

See section 6.4.3.1 ii)

iii) Eosin Y and Glycerol: Absorbance results

The addition of glycerol to the Eosin Y dye produces a clear trend in absorbance over the range of wavelengths tested, as shown in fig. 6.12. The absorbance increases with increasing numbers of glycerol molecules, and reaches a maximum when the number of

142

glycerol molecules equals the number of dye molecules. A maximum increase in absorbance of 2.22 % is observed for this ratio. After this point absorbance gradually decreases, most likely due to preliminary bleaching. However, the absorbance remains higher than is observed for the pure dye solution. The Eosin Y-Glycerol compositions all reach maximum absorbance at a wavelength of 517 nm.
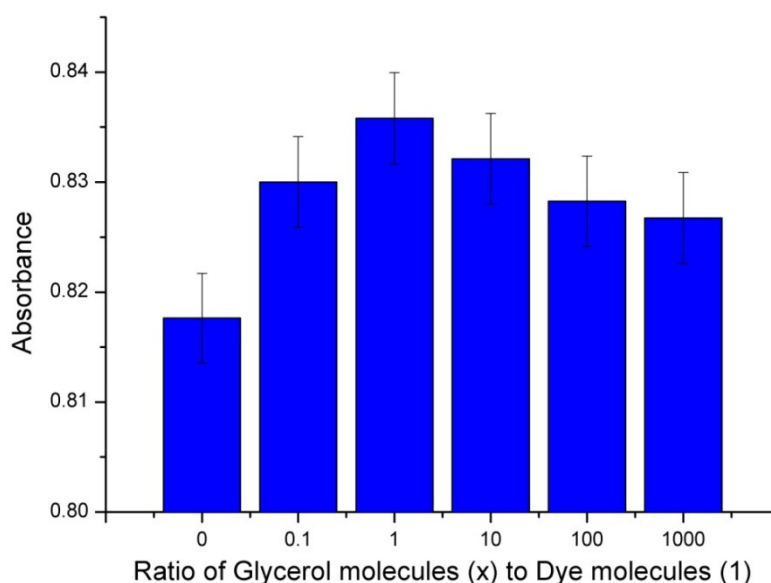
Fig. 6.12. Absorbance vs. the ratio of glycerol molecules to Eosin Y dye molecules (x:1).

6.4.3.4 Discussion of absorbance study results

The effect of glycerol on the absorbance of three different photosensitive dyes has been investigated. In the case of all three dyes, the addition of glycerol results in small increases in the absorbance of the dye molecules, as shown in fig. 6.13. There also appears to be some critical glycerol molecule concentration above which the absorbance of the dye molecules is no longer increased. This effect may be due to increased

viscosity of the solution due to the presence of glycerol, which was observed by Galssi and Meyer *et al* to reduce photobleaching rates [14, 15].

While the results do not provide an answer for why Von Hubl observed such a marked increase in sensitivity with the addition of glycerol, they do imply that there are certain conditions for which the addition of glycerol will result in increased absorbance of light by the photosensitive dyes tested here. Further optimisation of holographic photopolymers with the addition of glycerol, in particular with the Erythrosin B photosensitiser for which the maximum increase was observed, may yield improved holographic sensitivities in the future.
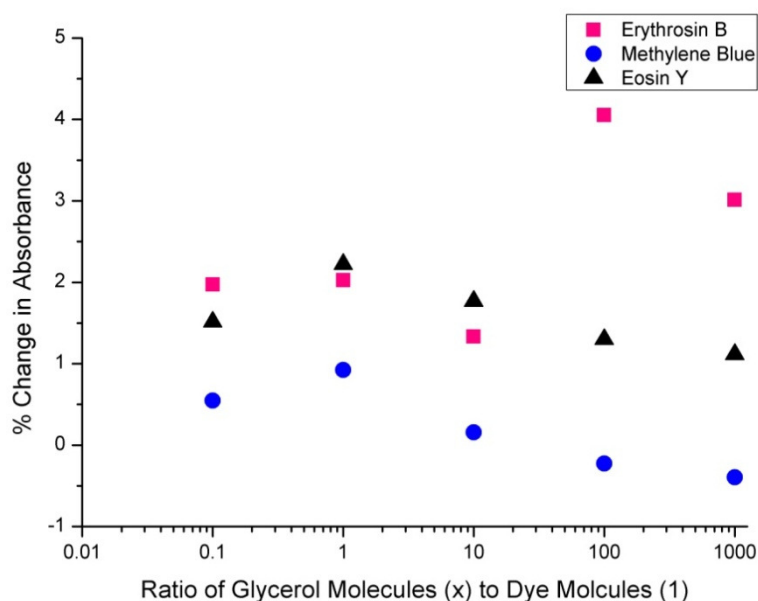
Fig. 6.13. % change in absorbance vs. ratio of glycerol molecules (x) to dye molecules (1) for Erythrosin B, Methylene Blue and Eosin Y.

6.5 Conclusions

A review of the literature on glycerol's influence on different polymer and photosensitive systems has been presented.

It has been demonstrated that glycerol significantly improves the optical quality, uniformity and reproducibility of the DA photopolymer layers. This is very important for any future device fabrication.

The effect of glycerol on the holographic recording ability of the DA photopolymer in the transmission mode of recording has been investigated. The addition of glycerol results in a 30 % decrease in the maximum achievable Δn of the DA-based photopolymer in the transmission mode of recording at 1000 l/mm; however, a more uniform response to recording intensity is observed and Δn values of up to 2.25×10^{-3} are still obtained. The increased uniformity of the response to recording intensity is most likely caused by glycerol's nature as a plasticiser, resulting in increased diffusion of monomer molecules, and is a desirable feature for large scale production.

The response of the DAG photopolymer over a range of spatial frequencies has been characterised. The inclusion of glycerol has shown to significantly increase the Δn achievable for transmission gratings at a spatial frequency of 300 l/mm up to 4.5×10^{-3} in comparison to 1.75×10^{-3} for the DA0 composition, an improvement of nearly 160 %. This result is implies that the DAG photopolymer is suitable for applications which require low spatial frequencies transmission gratings.

The effect of glycerol on the photoinitiating system of the DA photopolymer has been investigated. The addition of glycerol is shown to induce an inhibition effect at the start of recording, most likely due to increased oxygenation of the photopolymer layers. This

effect is diminished as recording intensity is increased. The addition of glycerol was also shown to reduce the rate of photobleaching of the DA photopolymer layer. Slower bleaching is beneficial for photopolymer systems as it means that more dye molecules are available to absorb a photon and initiate polymerisation, allowing for higher Δn values to be reached. The effect of different concentrations of glycerol on the absorbance of three different photosensitive dyes was also investigated. Small increases in absorbance only were observed, with maximum increases of 4.06, 2.22 and 0.92 % measured for the Erythrosin B, Eosin Y and Methylene Blue dyes respectively. These results suggest that there is little to no interaction between glycerol and the dye molecules.

References:

[1] D. M. Sanderson, "A note on glycerol formal as a solvent in toxicity testing", J. Pharm. Pharmacol. 11, 150-156 (1959).

[2] M. Belgacem, A. Gandini, "Monomers, Polymers and Composites from Renewable Resources", Elsevier, 2011.

[3] S. Sun, Y. Song, Q. Zheng, "Morphologies and properties of thermo-molded biodegradable plastics based on glycerol-plasticized wheat gluten", Food Hydrocolloids 21(7), 1005–1013 (2007).

[4] P. Hernández-Muñoz, R. Villalobos, A. Chiralt, "Effect of cross-linking using aldehydes on properties of glutenin-rich films", Food Hydrocolloids 18(3), 403-411 (2004).

[5] F. Chen, L. Zhang, "New Evidences of Glass Transitions and Microstructures of Soy Protein Plasticized with Glycerol", Macromol. Biosci. 5(3), 237-245 (2005).

[6] A. I. Bol'shakov, D. P. Kiryukhin, "Spontaneous polymerisation of acrylamide in glycerol", Polymer Science Series A 49(9), 975-980 (2007).

[7] R. A. Barry, R. F. Shepherd, J. N. Hanson, R. G. Nuzzo, P. Wiltzius, J. A. Lewis, "Direct-write assembly of 3D hyrogel scaffolds for guided cell growth", Advanced Materials 21, 1-4 (2009).

[8] T. O. Osmanov, N. V. Kozlova, V. Y. Markov, "Polymerisation of acrylamide in water-glycerol mixtures", Polymer Science U.S.S.R. 32(4), 650-654 (1990).

[9] A. Jirasek, M. Hilts, A. Berman, K. B. McAuley, "Effects of glycerol co-solvent on the rate and form of polymer gel dose response", Phys Med Biol. 54(4), 907-918 (2009).

[10] X. Yuan, F. Shen, G. Wu, C.Wu, "Effects of small molecule plasticiser on the coordination crosslinking reaction between acrylonitrile-butadiene rubber and copper sulfate", Polymer Composites 29(3), 302-306 (2008).

[11] A. Lee, G. Ordoñez, S. Chakraborty, "Novel glycerol-crosslinked poly(acrylic acid) hydrogel for encapsulation and release of benzocaine", Philippine Science Letters 4(20), 82-87 (2011).

[12] C. C. Byoung, H. C. Mi, C. Yong-Chan, "Effect of glycerol cross-linking and hard segment content on the shape memory property of polyurethane block copolymer", Journal of Materials Science 42(16), 6524-6531 (2007).

[13] G. K. Oster, G. Oster, G. Prati, "Dye-sensitized photopolymerisation of acrylamide", J. Am. Chem. Soc. 79(3), 595-598 (1957).

[14] T. Meyer, G. Tollin, J. Hazzard, M. Cusanovich, "Photoactive yellow protein from the purple phototropic bacterium", Biophysics Journal 56, 559-564 (1989).

[15] L. Galassi, "Wavelength dependence of the tie course of fluorescence enhancement and photobleaching during irradiation of ethidium bromide-stained nuclei", European Journal of Histochemistry 44, 419-432 (2000).

[16] P. Menter, "Acrylamide polymerisation – a practical approach", Bio-Rad Laboratories, Alfred Nobel Drive, Hercules, CA 94547 USA, 1156 (2000).

[17] A. V. Galstyan, R. S. Hakobyan, "Study of the inhibition period prior to the holographic grating formation in liquid crystal photopolymerizable materials", Electronic-Liquid Crystal Communications, http://www.e-lc.org/docs/2004_05_05_11_13_17, (2004).

[18] M. A. Chan, J. L. Lawless, S. K. Lam, D. Lo, "Fiber optic oxygen sensor based on phosphorescence quenching of erythrosin B trapped in silica-gel glasses", Analytica Chimica Acta 408(1-2), 33-37 (2000).

[19] S. K. Lam, E. Namdas, D. Lo, "Effects of oxygen and temperature on phosphorescence and delayed fluorescence of erythrosin B trapped in sol-gel silica", Journal of Photochemistry and Photobiology A: Chemistry 118(1), 25-30 (1998).

[20] X. Ren, Z. Yang, T. Kuang, "Solvent-induced changes in photochemical activity and conformation of photosystem I particles by glycerol", Biol. Chem. 387(1), 23-29 (2006).

[21] K. Kishore, G. R. Dey, T. Mukherjee, "OH radical reactions with ethanolamines: formation of reducing as well as oxidizing radicals", Res. Chem. Intermed. 30(9), 837-845 (2004).

[22] C. W. Bennett, "Glycerol as sensitizer", Journal of Physical Chemistry 16, 614-615 (1912).

[23] I. Naydenova, R. Jallapuram, R. Howard, S. Martin, V. Toal, "Investigation of the diffusion processes in a self-processing acrylamide-based photopolymer system," Appl. Opt. 43, 2900-2905 (2004).

7. DETERMINATION OF THE POLYMERISATION RATE OF THE DA0 AND DAG PHOTOPOLYMERS

7.1 Introduction

The polymerisation rate of a material is the rate at which the individual monomer molecules are polymerised, forming polymer chains. One of the key factors that affects the dynamics of holographic recording in photopolymer materials is the ratio of the rate of polymerisation to the rate of diffusion in the material. This is a high interest area in the study of photopolymers, and various theories have been proposed to explain the relationship [1-13].

The Two-Way Diffusion model was first proposed by Naydenova *et al* to explain the observed relationship between the polymerisation and diffusion rates in AA-based photopolymer formulations [1, 2]. It was then fully developed as a mathematical model by Babeva *et al* [3]. During holographic recording, the monomer molecules diffuse into and within the illuminated regions, encounter a free radical, and become polymerised. If the polymerisation reaction occurs at too fast a rate, a proportion of the monomer molecules will not diffuse quickly enough before the permeability of the bright fringe region decreases significantly and hence cannot be polymerised in this region, and so Δn of the recorded hologram will be reduced accordingly. The length of the polymer chains formed is also dependent on the recording intensity used. At high recording intensities short polymer chains are formed due to the increased concentration of initiating species, which may diffuse out of the illuminated regions, thus degrading Δn of the recorded grating.

The dependence of the rate of polymerisation on recording intensity has previously been investigated. Some early models [14-16] predict a linear dependence on intensity. Kwon

et al postulated that the polymerisation rate depends on the square root of the recording intensity [17] and define the relationship between polymerisation rate and recording intensity as:

$$\frac{1}{t} = kI^{0.5} \qquad (7.1)$$

where *t* is the polymerisation time constant, *k* is the polymerisation rate, and *I* is the recording intensity. However, these models assume that the rate of initiation is equal to the rate of termination, and that the free radical concentration is constant throughout polymerisation. Jallapuram *et al* [4] adapted the above equation for the more general form:

$$\frac{1}{t} = kI^{\gamma} \qquad (7.2)$$

where γ is the polymerisation rate dependence parameter, which determines the dependence on recording intensity.

The polymerisation rate of the AA-based photopolymer material developed by the Centre for Industrial and Engineering Optics has previously been measured by Jallapuram *et al* experimentally using Raman spectroscopy techniques [4]. In a Raman spectrometer, laser light of a defined wavelength is incident on a material which excites the molecules to produce molecular vibrations, phonons or other excitations in the system. This excitation results in the energy of the laser photons being shifted up or down, which provides information about the vibrational modes in the system. Vibrational information is specific to the chemical bonds and symmetry of molecules [18]. The polymerisation rate of the AA photopolymer was determined by measuring the real-time change in the intensity of the Raman peaks at 1607 and 1629 cm^{-1}, which correspond to the C=C double bonds of the AA and BA monomers, for the

photopolymer as it was polymerised for different exposure times. The experiments were carried out for uniform illumination, which ensures that the polymerisation rate does not depend on an assumed diffusion time. The polymerisation rates for the AA and BA monomers were measured to be 0.100 s^{-1} and 0.114 s^{-1} respectively. The polymerisation rate dependence parameter γ was found to be 0.27 and 0.32 for the AA and BA monomers. This differs from the value for γ assumed by Kwon *et al* of 0.5, and implies that the relationship between the polymerisation rate and recording intensity is weaker for the AA photopolymer system than expected.

A similar method has been employed here to determine the polymerisation rate of the DA0 and DAG photopolymers by monitoring the change in intensity of the 1628 cm^{-1} peak as the material is polymerised. This peak is in fact the superposition of two separate peaks at 1624.7 and 1629.9 cm^{1} which correspond to the C=C double bonds of the DA and BA monomers respectively (see fig. 7.1). Photopolymer samples were exposed to a single homogeneous 532 nm beam for different intensities and exposure times. On exposure to light, photoinduced-polymerisation occurs within the sample and the C=C double bonds of the monomer are converted to C-C single bonds. The intensity of the 1628 cm^{-1} peak in these samples was monitored with respect to a reference double peak at 1450 cm^{-1}, the intensity of which remained constant during polymerisation. An example of the Raman spectra obtained for DA0 samples exposed to a recording intensity of 4 mW/cm^{2} for different durations is shown in fig. 7.2.

Due to the restrictions imposed by the resolution of the Raman spectrometer, it was not possible to resolve the C=C peaks of the DA and BA monomer molecules separately, therefore the polymerisation rates of the DA and BA monomers could not be individually calculated for the DA-based photopolymer composition. However, by monitoring the change in the intensity of the superimposed peak, the polymerisation rate

of the overall composition can be determined. This method allows for comparison of the polymerisation rates of the DA0 and DAG compositions, as well as the polymerisation rate dependence parameters, as the same peak has been monitored in both materials. Further information about the effect of glycerol on the holographic recording mechanisms of the DA photopolymer system can be obtained. However, it does not allow for direct comparison of the DA-based photopolymers with the standard AA photopolymer, for as discussed above, the C=C double bond peaks for the AA and BA monomers were resolvable in this instance.
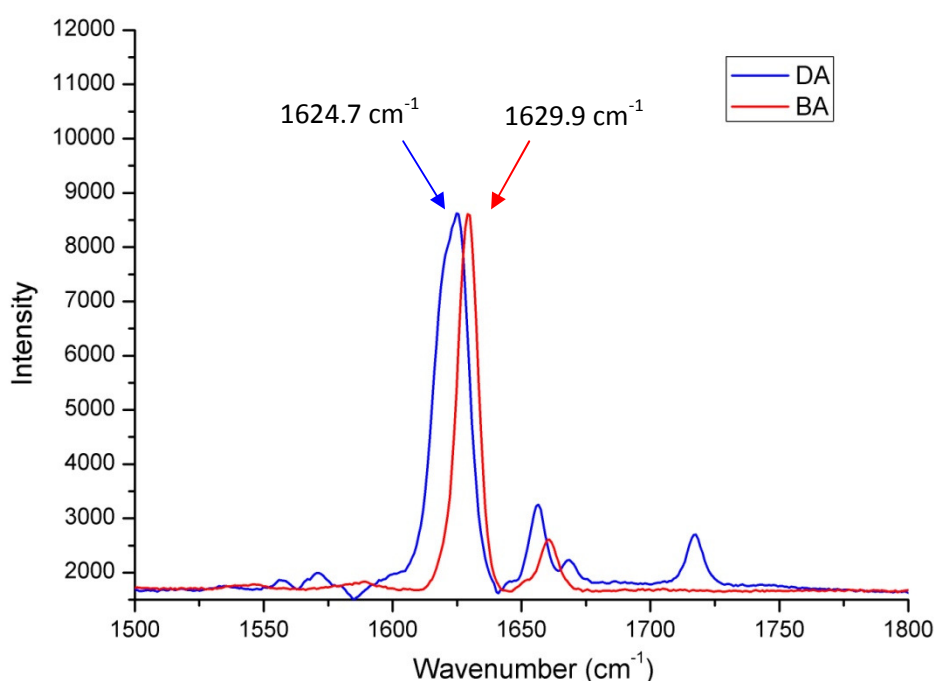
Fig. 7.1. Raman spectra taken at an excitation wavelength of 659.27 nm of the DA and BA monomers. The peaks at 1624.7 cm^{-1} (blue) and 1629.9 cm^{1} (red) correspond to the C=C double bonds of DA and BA respectively.
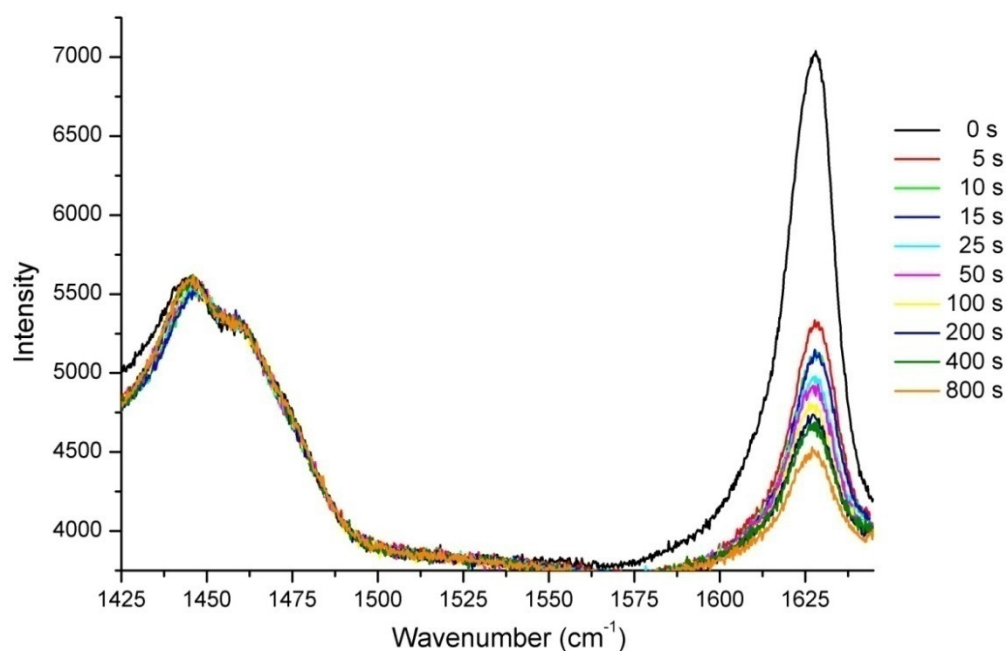
Fig. 7.2. Raman spectra taken at an excitation wavelength of 659.27 nm of DA0 photopolymer samples exposed to a beam intensity of 4 mW/cm^2 for durations of 0, 5, 10, 15, 25, 50, 100, 200, 400 and 800 seconds. The intensity of the peak at 1628 cm^{-1} corresponding the superimposed C=C double bond of the DA and BA monomers decreases as the exposure duration is increased, while the reference double peak at 1450 cm^{-1} remains constant.

7.2 Experimental

7.2.1 Materials

The DA0 and DAG photopolymer compositions were prepared as described in table 6.1 of section 6.2.1. Samples were prepared by depositing 0.5 ml of photopolymer solution on to 75 × 25 mm glass microscope slides, and allowed to dry for 12-24 hours in darkness under normal laboratory conditions (20-25 °C, 40-60 % RH). Layer thickness

was measured using a white-light surface profiler (Micro XAM S/N 8038), and was found to be 60 ± 5 µm.

7.2.2 Methods

7.2.2.1 Sample polymerisation method

The experimental setup used for exposing the DA0 and DAG samples is shown in fig. 7.3. DA0 and DAG photopolymer layers were exposed to a single homogeneous 532 nm vertically polarized beam at intensities of 0.5, 2 and 4 mW/cm^2. Exposure times of 5, 10, 15, 25, 50, 100, 200, 400 and 800 seconds were used. Unsensitised layers of the same thickness were prepared also for reference, as no polymerisation would take place in these layers. A 10 mW/cm^2 659.27 nm laser was used to obtain the vibrational Raman spectra of the exposed area of each sample, as the Erythrosin B-sensitised samples show minimum absorbance at this wavelength. An 1800 l/mm grating and a ×100 objective were used. Ten 100 second exposures were accumulated and averaged for each sample.

Each spectrum of the exposed samples were normalised to the 1450 cm^{-1} double peak of the unexposed reference sample (without Erythrosin B dye), as this sample was observed to remain unchanged during polymerisation. The intensity of the 1628 cm^{-1} peak was then recorded for each exposure time.
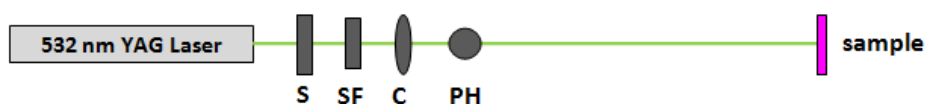
Fig. 7.3. Experimental setup for exposing the Erythrosin B-sensitised DA0 and DAG samples. S: shutter, SF: spatial filter, C: collimator, PH: pinhole.

7.2.2.2 Data analysis method

A single exponential decay function was used by Jallapuram *et al* to fit the intensity vs. exposure time data for the AA-based photopolymer as discussed in [4]. Different exponential decay functions including single, double and triple exponential decays, were fitted to the intensity vs. exposure time data for both the DA0 and DAG data. However, none of these functions gave a good fit to the data obtained. The function best observed to fit the data was the Kohlrausch stretched exponential function of the form:

$$y(x) = e^{\left(-\frac{x}{t}\right)^{\beta}} \tag{7.3}$$

where β is some perturbation of the system for which $0 < \beta < 1$, and t is the time constant for the reaction [19, 20].

The Krohlrausch function, or stretched exponential function as it is now more commonly known, was first described by Rudolph Krohlrausch in 1854 [19, 21]. Krohlrausch found that this function accurately describes the time evolution of the discharge of a capacitor, for which standard exponential functions did not provide a good fit. It has since been observed that the stretched exponential function is often more appropriate for modelling relaxation processes in different materials, including polymers, than standard exponentials [20]. This is partly due to the fact that a relaxation process depends on the entire spectrum of relaxation times, so its structure will be non-linear and not purely exponential.

De Gennes uses the stretched exponential function to model large-scale chain dynamics of polydispersive systems [22]. He defines β as an exponent that is sensitive to the presence or absence of entanglement of the polymer chains, and that it should also vary depending on the length of the polymer chains formed. It has already been discussed

156

that the length of the polymer chains formed is directly dependent on the intensity of the recording beam. Chen postulates that β may be related to the distribution of chain lengths, or disorder of the system [23]. As the value for β goes to 1, a normal exponential is obtained which produces a single time constant for the reaction. Alternatively, as the value for β goes to 0, multiple time constants are necessary, implying more disorder in the system.

7.3 Results and Discussion

7.3.1 Polymerisation rate calculation for DA0 photopolymer

The data for the intensity of the 1628 cm^{-1} peak vs. exposure time for the DA0 photopolymer layers exposed to recording intensities of 0.5, 2 and 4 mW/cm^2 is shown in fig. 7.4. The data was fitted with the stretched exponential decay function given by eqn. 7.3 using Origin v. 8.5 software. The values for the time constant t were extracted, and the results are shown in table 7.1. The R^2 values for each set of data show good agreement between the stretched exponential fit and the experimental data. The values of γ and k were determined using eqn. 7.2 by first plotting the logarithm of the polymerisation time constant t against the logarithm of the exposure intensity, and then fitting the data using a linear function as shown in fig. 7.5. The slope of the linear fit equals -γ, and the intercept of the linear fit is equal to -log(k). This gives a value for k of 0.020 s^{-1} and a value for γ of 1.07 for the DA0 photopolymer.

Table 7.1. Data from stretched exponential function fit of intensity vs. exposure time for DA0

Intensity (mW/cm^2)	t (s)	R^2 value
0.5	100.05	0.98
2	25.28	0.99
4	10.40	0.99
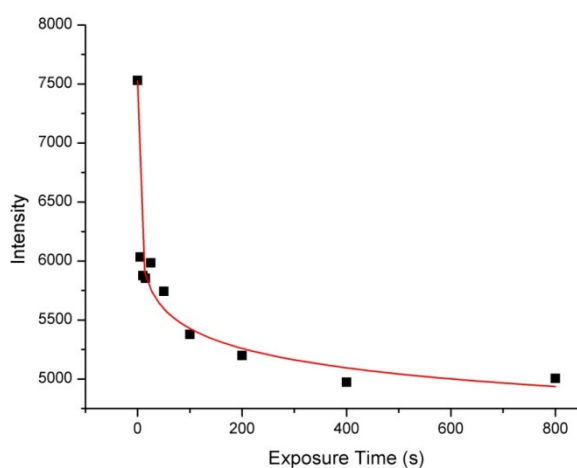
(a)
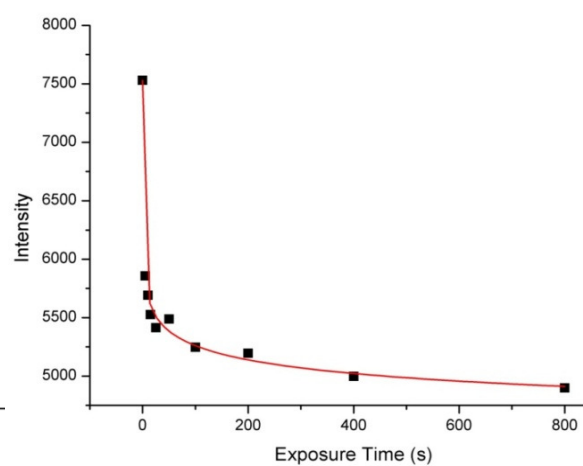
(b)
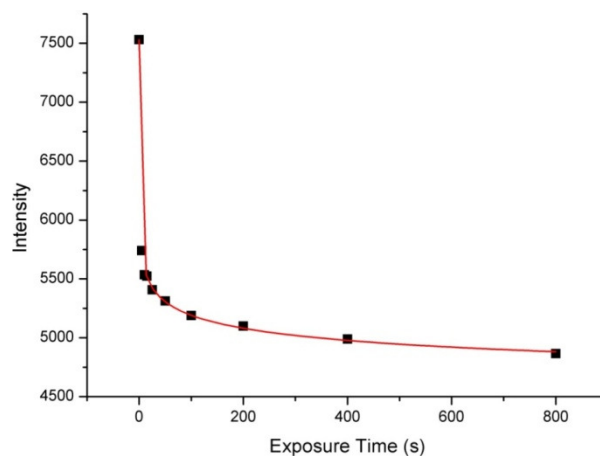
(c)

Fig. 7.4. Graph of 1628 cm^{-1} peak intensity vs. exposure time (s) for DA0 photopolymer samples exposed to a recording intensity of (a) 0.5 mW/cm^2, (b) 2 mW/cm^2, and (c) 4 mW/cm^2. The data has been fitted with a stretched exponential decay function.
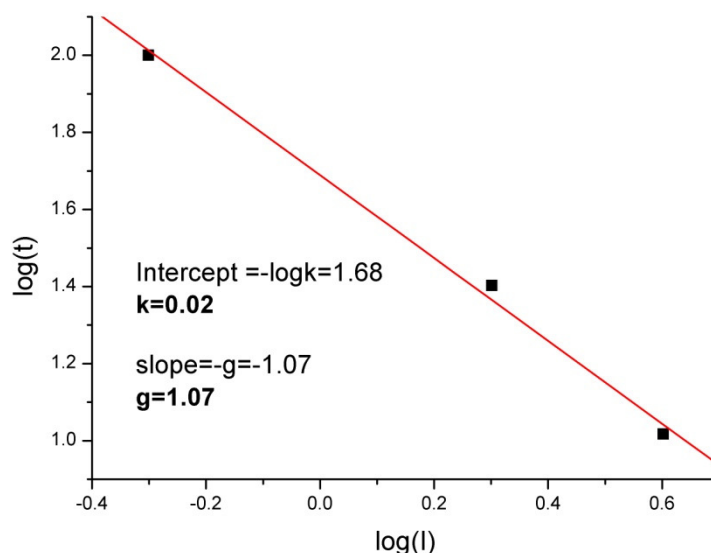
Fig. 7.5. log(t) vs. log(I) for the DA0 photopolymer samples. The solid red line corresponds to a linear fit of the data points.

7.3.2 Polymerisation rate calculation for DAG photopolymer

The data of the intensity of the 1628 cm^{-1} peak vs. exposure time for the DAG photopolymer layers exposed to recording intensities of 0.5, 2 and 4 mW/cm^2 is shown in fig. 7.6. As in the case of DA0, the data was fitted with the stretched exponential decay function given by eqn. 7.3. The values for the time constant t were extracted, and the results are shown in table 7.2. R^2 values of 0.99 were obtained for all three sets of data, showing good agreement between the stretched exponential fit and the experimental data. As previously, the values of γ and k were determined using eqn. 7.2 by first plotting the logarithm of the polymerisation time constant t against the logarithm of the exposure intensity, and then fitting the DAG data using a linear function as shown in fig. 7.7. The slope of the linear fit equals -γ, and the intercept of the linear fit is equal to -log(k). This gives a value for k of 0.032 s^{-1}, and a value for γ of 0.68 for the DAG photopolymer.

159

Table 7.2. Data from stretched exponential function fit of intensity vs. exposure time for DAG

Intensity (mW/cm^2)	t (s)	R^2 value
0.5	53.41	0.99
2	16.57	0.99
4	13.77	0.99

(a)

(b)

(c)
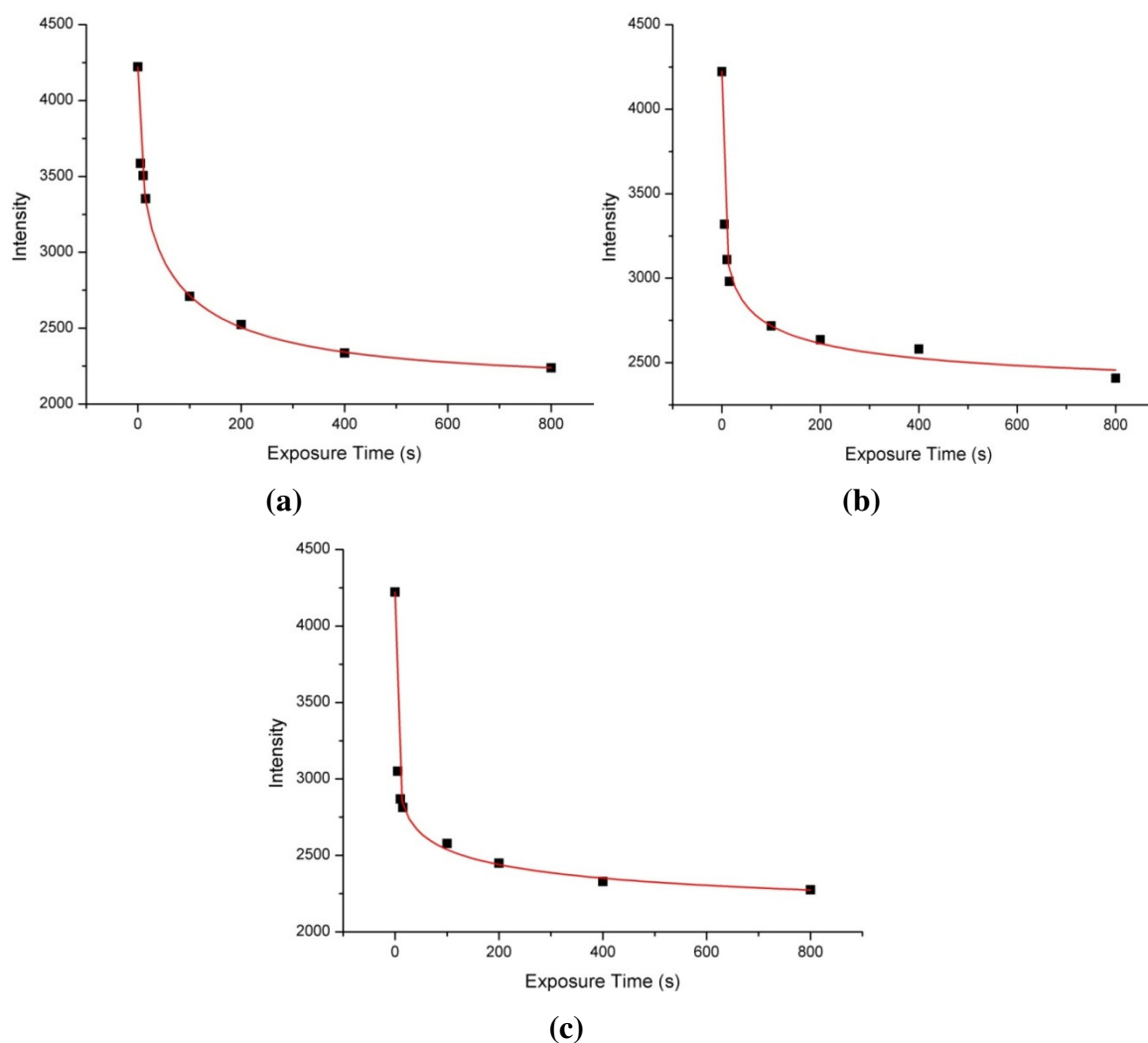
Fig. 7.6. Graph of 1628 cm^{-1} peak intensity vs. exposure time (s) for DAG photopolymer samples exposed to a recording intensity of (a) 0.5 mW/cm^2, (b) 2 mW/cm^2, and (c) 4 mW/cm^2. The data has been fitted with a stretched exponential decay function.
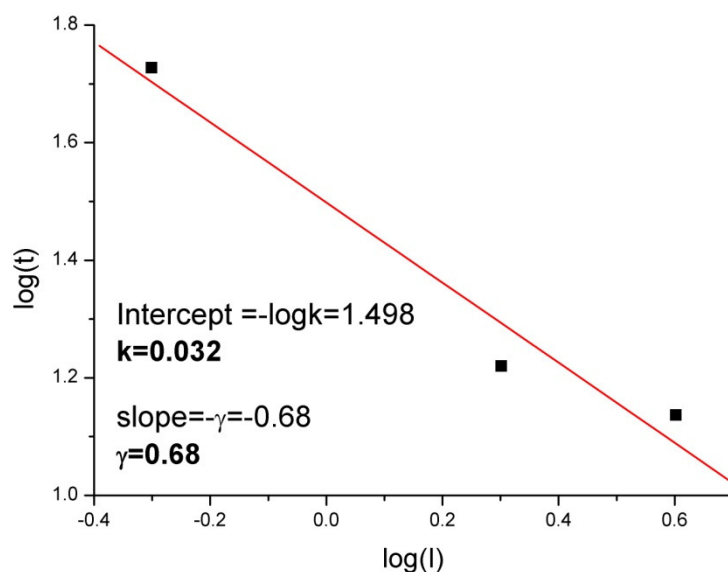
Fig. 7.7. log(t) vs. log(I) for the DAG photopolymer samples. The solid red line corresponds to a linear fit of the data points.

7.3.3 Comparison of the DA0 and DAG polymerisation rate results

The rates of polymerisation for the DA0 and DAG photopolymer were found to be 0.020 s^{-1} and 0.032 s^{-1} respectively. This implies that the inclusion of glycerol significantly increases the rate of polymerisation of the DA photopolymer by as much as 60 %. As discussed previously, glycerol is a plasticiser. Therefore, its inclusion improves the ability of the unreacted DA monomer molecules, and also the free radicals, to diffuse within the photopolymer layer during illumination. This increases the probability of an interaction which will result in the initiation of polymer chains or growth of existing chains, thus increasing the rate of polymerisation of the DA photopolymer.

The rate of polymerisation of the AA-based photopolymer was calculated by Jallapuram *et al* to be 0.100 s^{-1} [4]. As mentioned previously, direct comparison cannot be made

between the DA-based and AA-based material due to the inability to resolve the separate C=C bonds of the DA and BA monomers within the photopolymer. However, it is likely that the polymerisation rate of the AA-based formulation is faster than for the DA-based compositions due to the smaller size of the AA monomer molecules, allowing for fast diffusion of the monomer molecules within the photopolymer layer. This is reflected in the values for the polymerisation rates obtained for DA0 and DAG.

The polymerisation rate dependence parameter γ was found to be 1.07 and 0.68 for the DA0 and DAG photopolymers respectively. γ is a direct measure of the dependence of the polymerisation rate on the recording intensity used. The value for γ for DAG is 36 % lower than for DA0. Therefore, the DAG photopolymer is less dependent on recording intensity than the DA0 photopolymer. This agrees with the results observed in section 6.3.1 of chapter 6, which showed that the Δn of transmission gratings recorded in the DAG photopolymer had limited intensity dependence in comparison to that of the DA0 photopolymer. In general, increasing the recording intensity increases the concentration of free radicals produced, and therefore increases the probability of a free radial reacting with a monomer molecule to initiate a polymer chain. However, the probability of this reaction occurring is already increased due to the inclusion of glycerol, as discussed above. Therefore, the dependence of polymerisation rate on recording intensity is limited for DAG.

Values for β were extracted from the stretched exponential fits for both the DA0 and DAG photopolymer. As discussed earlier, it has been postulated by De Gennes that β is sensitive to the presence or absence of entanglement of the polymer chains, and that it should also vary depending on the length of the polymer chains formed i.e. it will change depending on the recording intensity used [22]. The values for β for both the DA0 and DAG compositions are presented in table 7.3. It is shown that as the recording

intensity increases, the value for β decreases. This is expected, as by increasing the recording intensity, the number of free radicals generated is increased, thereby reducing the length of polymer chains and also the extent of chain entanglement. At all recording intensities, the value for β is higher for the DAG composition than for DA0. This implies that the inclusion of glycerol in the DA photopolymer composition increases the length and also the extent of entanglement of the growing polymer chains. The difference in β between DA0 and DAG is more significant at lower recording intensities. Glycerol is a plasticiser and therefore may be promoting increased diffusion of monomer molecules as well as the growing polymer chains, resulting in increased chain length and possibly increased chain entanglement. This may also result in increased homogeneity of the chain lengths, and therefore less disorder in the system as postulated by Chen [23]. As the recording intensity is increased, this effect becomes less pronounced due to the increased concentration of free radicals.

Table 7.3. β values for the DA0 and DAG photopolymers from stretched exponential fit

Intensity (mW/cm^2)	β values for DA0	β values for DAG
0.5	0.199 ± 0.023	0.449 ± 0.026
2	0.155 ± 0.013	0.214 ± 0.016
4	0.153 ± 0.026	0.201 ± 0.037

7.4 Conclusions

The polymerisation rates of the DA0 and DAG photopolymer have been measured using Raman spectroscopy methods. A stretched exponential decay function has been applied to the data to extract polymerisation rate values of 0.020 s^{-1} and 0.032 s^{-1} for

DA0 and DAG respectively. This implies that the inclusion of glycerol increases the rate of polymerisation of the DA photopolymer by up to 60 %. The faster polymerisation rate observed for DAG due to the inclusion of the plasticiser glycerol, allowing for increased diffusion of the monomer molecules and initiating species thereby increasing the rate at which the polymerisation reaction can occur.

The polymerisation rate dependence parameter γ was found to be 1.07 and 0.68 for the DA0 and DAG photopolymers respectively. The lower γ value for DAG reflects the lesser dependence of the polymerisation rate on the recording intensity used for the glycerol-doped material.

By studying the values for the parameter β extracted from the stretched exponential fit for the DA0 and DAG compositions, new information has been provided about the role of glycerol in the DA photopolymer. The results indicate that glycerol increases the length of the DA polymer chains and the degree of chain entanglement. It has also been observed that the inclusion of glycerol in the DA photopolymer is beneficial for holographic recording in reflection mode. This will be discussed further in chapter 11.

References:

[1] I. Naydenova, R. Jallapuram, S. Martin, R. Howard, V. Toal, "Investigations of the diffusion processes in self-processing acrylamide-based photopolymer system", Applied Optics, 43(14), 2900 (2004).

[2] S. Martin, I. Naydenova, V. Toal, R. Jallapuram, R. Howard, "Two way diffusion model for the recording mechanism in a self developing dry acrylamide photopolymer",

SPIE proceedings of the International Conference on Holography, Optical Recording and Processing of Information 6252, 37-44, (2006).

[3] T. Babeva, I. Naydenova, D. Mackey, S. Martin, V. Toal, "Two way diffusion model for short-exposure holographic grating formation in acrylamide-based photopolymer", J. Opt. Soc. Am. B 27(2), 197-203 (2010).

[4] R. Jallapuram, I. Naydenova, H. Byrne, S. Martin, R. Howard, V. Toal, "Raman spectroscopy for the characterization of the polymerisation rate in an acrylamide-based photopolymer", Appl. Opt. 47(2), 206-212 (2008).

[5] D. Cody, I. Naydenova, E. Mihaylova, "Effect of glycerol on a diacetone-acrylamide based holographic photopolymer", Appl. Opt. 52(3) 489-494 (2013).

[6] M. X. Tang, A. Redler, D. Topgaard, C. Schmidt, H. S. Kitzerow, "Kinetics of the grating formation in holographic polymer-dispersed liquid crystals: NMR measurement of diffusion coefficients", Colloid Polym. Sci. 290(8), 751-755 (2012).

[7] S. Gallego, A. Marquez, M. Ortuno, S. Marini, I. Pascual, A. Belendez, "Monomer diffusion in sustainable photopolymers for diffractive optics applications", Opt. Mat. 33(11), 1626-1629 (2011).

[8] D. Yu, H. Liu, Y. Jiang, X. D. Sun, "Mutual diffusion dynamics with nonlocal response in SiO2 nanoparticles dispersed in PQ-PMMA bulk photopolymer", Opt. Express 19(15), 13787-13792, (2011).

[9] O. Martinez-Matos, M. L. Calvo, J. A. Rodrigo, P. Cheben, F. del Monte, "Diffusion study in tailored gratings recorded in photopolymer glass with high refractive index species", Appl. Phys. Lett. 91(14), 141115, DOI: 10.1063/1.2794792 (2007).

[10] M. Toishi, T. Tanaka, K. Watanabe, K. Betsuyaku, "Analysis of photopolymer media of holographic data storage using non-local polymerisation driven diffusion model", Jpn. J. Appl. Phys. 1 46(6A), 3438-3447 (2007).

[11] V. Moreau, Y. Renotte, Y. Lion, "Characterization of DuPont photopolymer: determination of kinetic parameters in a diffusion model", Appl. Opt. 41(17), 3427-3435 (2002).

[12] G. H. Zhao, P. Mouroulis, "Diffusion model of hologram formation in dry photopolymer materials", J. Mod. Optic. 41(10), 1929-1939 (1994) .

[13] J. Sheridan, M. Downey, F. T. O'Neill, "Diffusion-based model of holographic grating formation in photopolymers: generalized non-local material responses", J. Opt. A-Pure Appl. Op. 3(6), 477-488 (2001).

[14] I. Aubrecht, M. Miler, I. Koudela, "Recording of holographic diffraction gratings in photopolymers: theoretical modeling and real-time monitoring of grating growth," J. Mod. Opt. 45, 1465–1477 (1998).

[15] W. S. Colburn, K. A. Haines, "Volume hologram formation in photopolymer materials," Appl. Opt. 10, 1636–1641 (1971).

[16] V. L. Colvin, R. G. Larson, A. L. Harris, and M. L. Shilling, "Quantitative model of volume hologram formation in photopolymers," J. Appl. Phys. 81, 5913–5923 (1997).

[17] J. H. Kwon, H. C. Hwang, and K. C. Woo, "Analysis of temporal behavior of beams diffracted by volume gratings formed in photopolymers," J. Opt. Soc. Am. B 16, 1651–1657 (1999).

[18] D. J. Gardiner and P. R. Graves, Practical Raman Spectroscopy, 1st edition, Springer-Verlag, 1989.

[19] R. Kohlrausch, "Theorie des Elektrischen R¨uckstandes in der Leidener Flasche" Pogg. Ann. Phys. Chem. 91, 179–214 (1854).

[20] R. S. Anderssen, S. A. Husain, R. J. Loy, "The Kohlrausch function: properties and applications", Anziam J. 45, 800-816 (2004).

[21] M. Berberan-Santos, E. N. Bodunov, B. Valeur, "History of the Kohlrausch (stretched exponential) function: Focus on uncited pioneering work in luminescence", Annalen der Physik 17(7), 460-461 (2008).

[22] P. G. de Gennes, "Relaxation anomalies in linear polymer melts", Macromolecules 35, 3785-3786 (2002).

[23] R. Chen, "Apparent stretched-exponential luminescence decay in crystalline solids", Journal of Luminescence 102-103, 510-518 (2003).

8. CYTOTOXICITY EVALUATION OF THE DA PHOTOPOLYMER AND ITS COMPONENTS

8.1 Introduction

As discussed in chapter 2, AA, a main component of the standard photopolymer composition, is both carcinogenic and toxic in its monomer form. This toxicity has been extensively investigated, using both in vivo and in vitro methods [1–12]. An extensive study into the chemical and biochemical safety of AA carried out by Friedman [13] found that AA is involved in reactions with proteins such as haemoglobin, enzymes, and DNA. Aside from its high toxicity, the carcinogenic nature of AA certainly justifies why it has been substituted with the non-toxic monomer DA in the holographic photopolymer composition.

With this, a comparative study into the in vitro cytotoxicity of the two monomers DA and AA has been carried out [14]. To the best of the authors' knowledge this was the first time an evaluation has been carried out of the cytotoxicity of the DA monomer. The cytotoxicity of the three different photopolymers discussed in this thesis (DA0, DAG and AA) was also investigated, in order to evaluate the toxicity of the final product developed for holographic applications. The toxicities of the individual components which comprise each of the photopolymers were evaluated also, in order to have a more thorough understanding of any risks involved in the production process due to toxicities of the raw materials.

Cytotoxicity is defined as the quality of being toxic (a result in cellular viability or normal function) to cells. This can vary depending on the type of cells, or cell line, used. Two immortalised noncarcinogenic human cell lines were employed for the evaluation, namely, HaCaT, a normal dermal keratinocyte (fig. 8.1), and BEAS-2B, a

normal bronchial epithelial cell line (fig. 8.2). These cell lines were chosen as they reflect inhalation and dermal exposure routes, thought to be the most likely routes of exposure, in particular for photopolymer material and device production on a large scale. For cytotoxic evaluation the 3-(4,5-dimethylthiazol-2-yl)-2,5-diphenyltetrazolium bromide (MTT) assay (Sigma Aldrich) was used [15, 16].
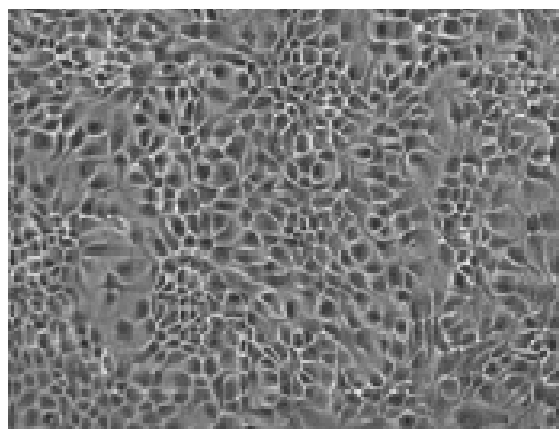
Fig.8.1. Confocal microscope image of confluent HaCaT cells.
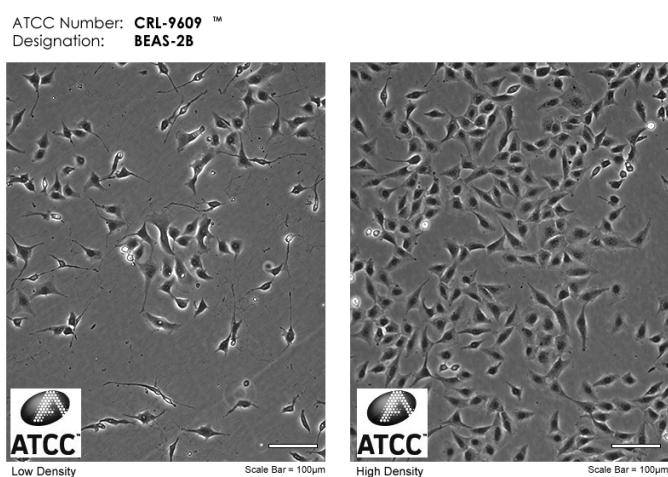
Fig. 8.2. Image of BEAS-2B cells at two different confluence levels. Image source: ATCC-LGC (No: CRL-9609).

8.2 Experimental

8.2.1 Cell culture

Cell culture refers to the complex process whereby cells are removed from an animal or plant and grown under controlled conditions. The HaCaT cells were cultured in a DMEM-F12 medium supplemented with 10 % foetal bovine serum (FBS). The BEAS-2B cells were cultured in a 10 % FBS-supplemented RPMI-1640 medium. Both media were supplemented with 2 mM L-glutamine, which serves as an energy source for the cells, and also 45 IU/ml penicillin and 45 IU/ml Streptomycin, two antibiotics which aid in the prevention of contamination of the cells by bacteria. The cells were stored in flasks at 37 °C in a humidified incubator with a 5 % CO_2 gas mixture.

Both the HaCaT and BEAS-2B cell lines are adherent lines, and therefore once a high enough confluency (70-80 %) had been reached, the cells needed to be harvested from the flasks in order to be used for cytotoxic evaluation. This is a standard procedure, carried out using a 1:1 mixture of EDTA : 0.25 % Trypsin. The flasks are rinsed with phosphate buffer solution (PBS) and then trypsinised, i.e. the trypsin solution is added to the flask to aid cell detachment. Depending on the cell line used, a period of time is allowed for the cells to detach. The cell-trypsin solution is then added to media (5 ml media per 1 ml cell-trypsin), which neutralises the trypsin. A small amount of this solution can then be used to seed a new flask for further culture.

A Coulter Counter was used to obtain a cell count for the cell suspensions. For testing, the 96-well plates were seeded at a density of 1×10^5 cells/ml for 24 hour exposures, 5×10^4 cells/ml for 48 hour exposures and 4×10^4 for 72 hour exposures, with at least three independent replicates. Cells were allowed to attach for 24 hours before being exposed to the compound under evaluation.

8.2.2 MTT assay evaluation

MTT assays are colorimetric assays which measure the viability of cells (i.e. if the cell is alive and able to proliferate) based on the reduction of the soluble, yellow tetrazolium salt (MTT) into an insoluble, purple formazan precipitate as shown in fig. 8.3, which can be solubilised by the addition of an organic solvent and quantified spectroscopically. This reduction can only occur in mitochondrially active cells, and since for most cell populations the total mitochondrial activity is related to the number of viable cells, it can therefore be used as a measure of the cell viability.
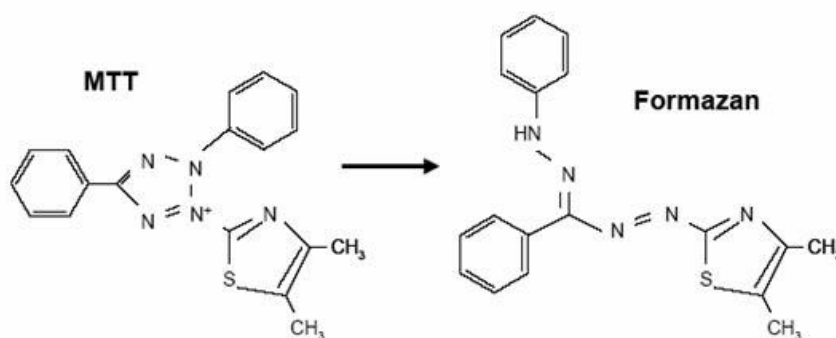
Fig. 8.3. Reduction of the yellow MTT to purple formazan.

After the seeded plates had been exposed to the test compound for the desired time, the test compound was removed and the cells were rinsed with PBS. 100 µL of freshly prepared MTT dye/media solution (0.25 mg/L) was then added to each well. The plates were then incubated for three hours. Following this, the plates were rinsed again with PBS and 100 µL of the organic solvent DMSO was added to each well. The plates were then shaken at 240 rpm for 15 minutes. The absorbance and hence the cell viability was then measured at 540 nm using a microplate reader. Fig. 8.4 shows a 96-well HaCaT plate dosed with AA after the MTT dye reduction has taken place.

171
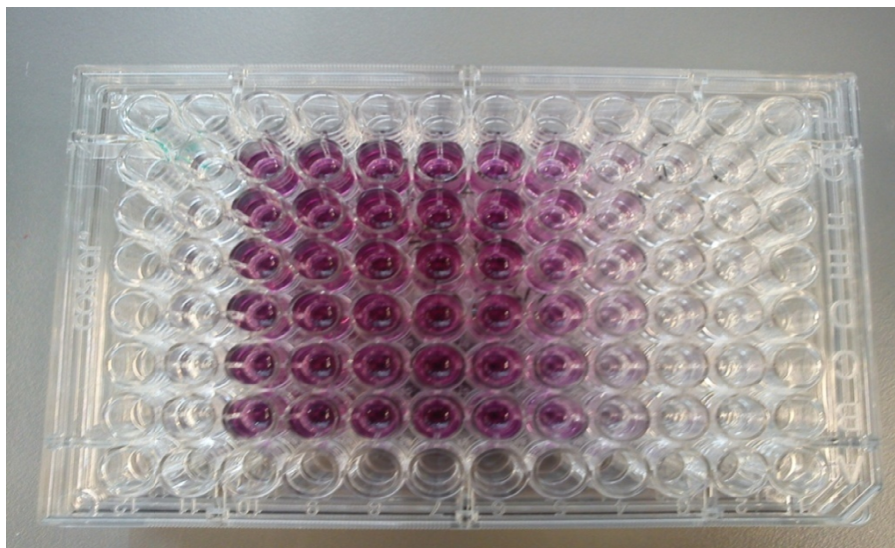
Fig. 8.4. A 96-well HaCaT plate dosed with AA and exposed for 72 hours, after addition of MTT assay.

8.2.3 Statistics and LD$_{50}$ calculation

The LD$_{50}$ value, or lethal dose value, is the dose concentration at which the cellular viability is reduced by 50 % [17]. Differences between compounds and the control were evaluated using the statistical analysis package SPSS 14.0. Statistically significant differences were set at $p < 0.01$. Normality of data was confirmed with Q-Q percentile plots and Kolmogorov-Smirnov tests. Equality of variances was evaluated using Levène's tests. One-way analysis of variances (ANOVA) followed by Dunnett's multiple comparison tests was carried out for normally distributed samples with homogeneous variances. Cytotoxicity data was fitted to a sigmoidal curve and a four-parameter nonlinear logistic model was used to calculate the lethal dose of the test compound that caused a 50 % inhibition in comparison to untreated controls (LD$_{50}$) (see fig. 8.5 for example). All LD$_{50}$ values were calculated using the average cytotoxicity data of the three independent experimental results and their associated errors. LD$_{50}$

values are reported with ± 95 % confidence intervals (± 95 % CI). LD_{50} values were estimated using Xlfit3, a curve fitting add-on for Microsoft_Excel (ID Business Solutions, UK).
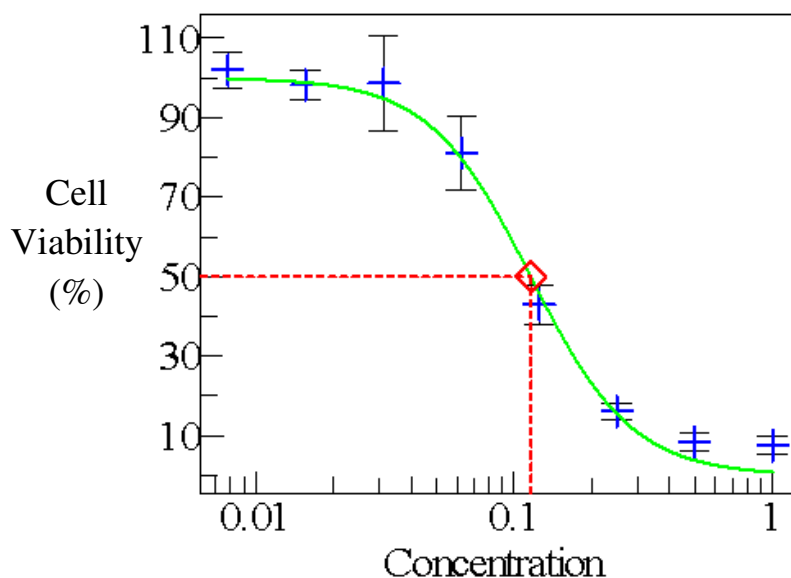
Fig. 8.5. Example of cytotoxicity data fitted with a sigmoidal curve using Xlfit3 software, used to extract the LD_{50} value for a test compound.

8.2.4 Compound Preparation

Solutions of each of the test compounds were prepared as described in table 8.1 in media aseptically. The DA0, DAG and AA photopolymers were prepared as described in chapter 6. The solutions were sonicated for 10 minutes to ensure complete dispersion, and then sterile filtered, except in the case of Erythrosin B. When sterile filtered, it is probable that the concentrations of the different solutions were reduced; the concentration of Erythrosin B dye in solution was visibly reduced.

Table 8.1 Preparation of test compounds for cytotoxicity study

Test Compound	% Concentration of Compound	Comments
Diacetone Acrylamide	10 % wt/vol	-
Bisacrylamide	10 % wt/vol	-
Acrylamide	10 % wt/vol	-
Erythrosin B	10 % wt/vol	Not sterile filtered
Triethanolamine	10 %vol/vol	-
Polyvinyl Alcohol	10 % wt/vol	-
Glycerol	5 % vol/vol	-
DA0 photopolymer	10 % vol/vol	Prepared in dark
DAG photopolymer	10 % vol/vol	Prepared in dark
AA photopolymer	10 % vol/vol	Prepared in dark

8.3 Results and Discussion

8.3.1 Monomer cytotoxicity results

The comparative cytotoxicity results for the DA and AA monomers are shown below for the HaCaT and BEAS-2B cell lines. The cell viability data is expressed as an average of three independent experiments ± standard deviation for each independent experiment. "*" denotes a statistically significant ($p<0.01$) difference from the unexposed control. In all viability experiments a positive (kill) control of a 10% DMSO solution made up in media was employed for assay verification.

8.3.1.1 DA monomer cellular viability results

The cellular viability as a percentage of the control for each dose of the DA monomer tested is shown for the HaCaT and BEAS-2B cell lines in figs. 8.6 and 8.7 respectively. In the DA0 photopolymer solution, the concentration of the DA monomer is 0.038 mg/ml. At this concentration, the HaCaT cell viability is observed to decrease by a maximum of 20 % for all three exposure times. For the BEAS-2B cell line, a maximum decrease in cell viability of 10 % is observed at this concentration. As the concentration of DA is increased to the maximum value of 1 mg/ml, cell viability is observed to decrease by up to 40 % for the HaCaT cell line, and 20 % for the BEAS-2B cell line. This indicates that the dermal cell line is more sensitive to the DA monomer than the bronchial cell line.
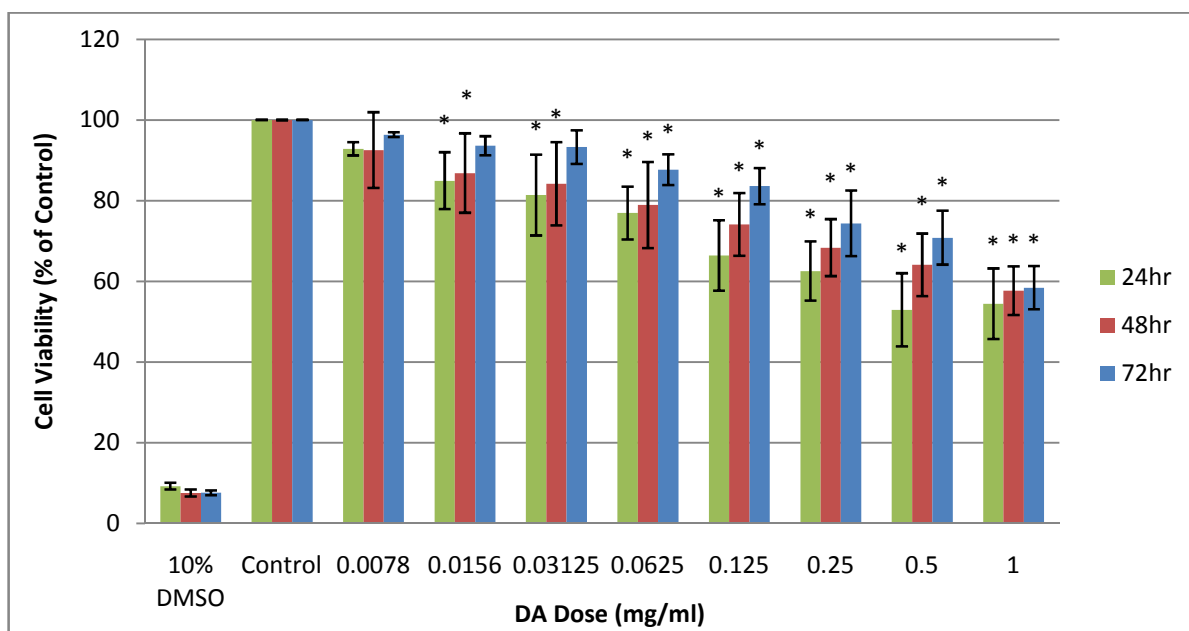
Fig. 8.6. Cellular viability vs. DA monomer dose for the HaCaT cells for 24, 48 and 72 hr exposures.
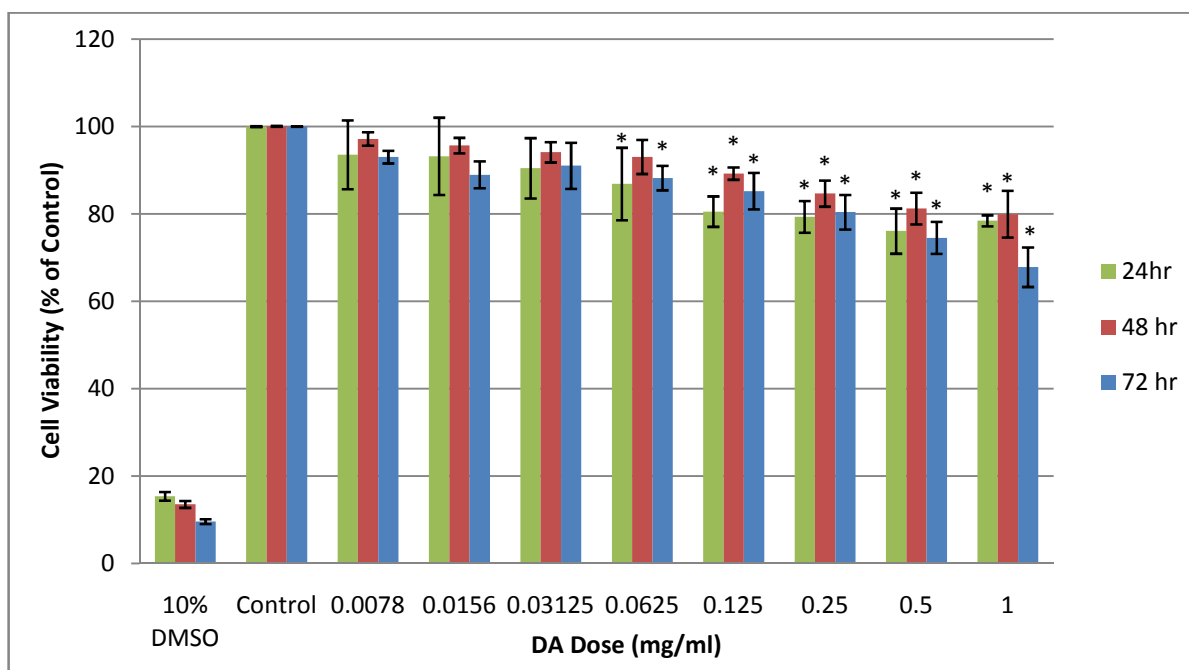
Fig. 8.7. Cellular viability vs. DA monomer dose for the BEAS-2B cells for 24, 48 and 72 hr exposures.

8.3.1.2 AA monomer cellular viability results

The cellular viability as a percentage of the control for each dose of the AA monomer tested is shown for the HaCaT and BEAS-2B cell lines in figs. 8.8 and 8.9 respectively. In the case of both cell lines there is a clear dependence of cell viability on exposure time, with significantly less cell death occurring for the 24 hr exposure then for the 48 and 72 hr exposures in the dose range of 0.0625 - 0.25 mg/ml. The concentration of AA monomer in the AA photopolymer solution is 0.026 mg/ml. At this concentration no significant cell death is observed for either cell line. However, in both cases as the dose is increased to 1 mg/ml, the cell viability is significantly decreased by up to 80%. This decrease is twice as large as the decrease observed for the DA monomer at the same

concentration for the HaCaT cell line, and four times as large as for the BEAS-2B cell line.
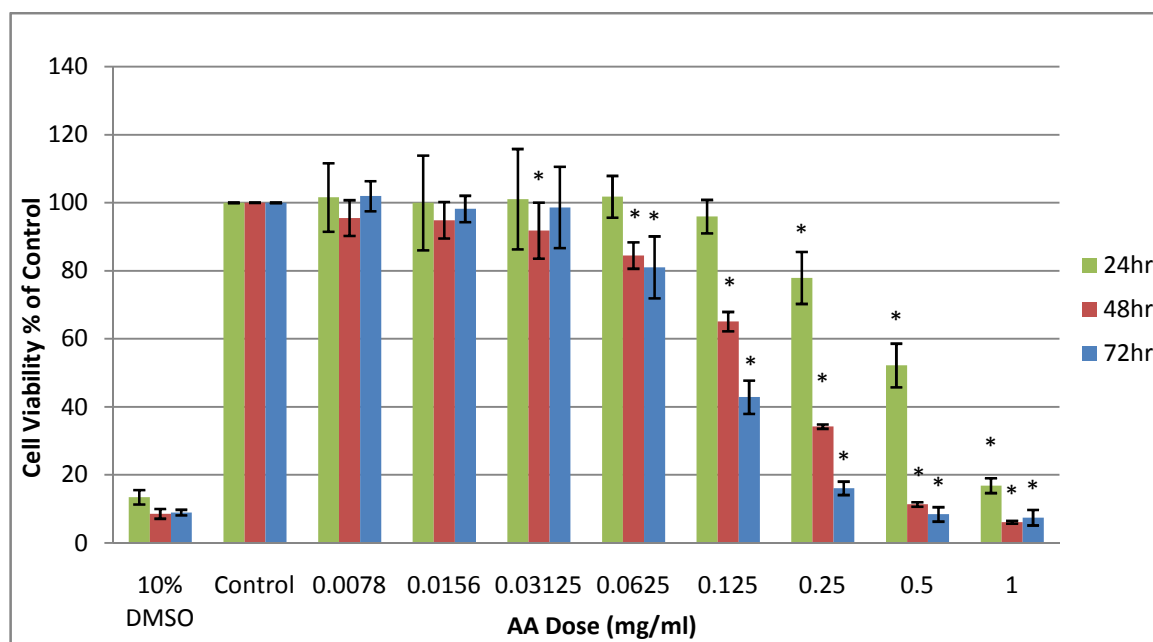
Fig. 8.8. Cellular viability vs. AA monomer dose for the HaCaT cells for 24, 48 and 72 hr exposures.
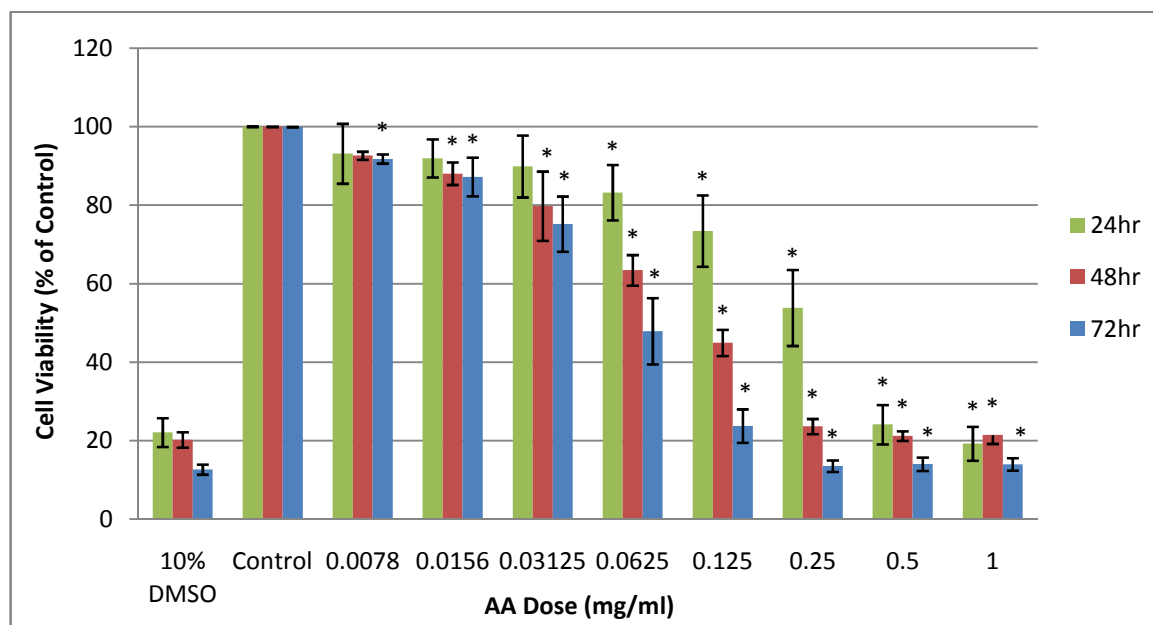
Fig. 8.9. Cellular viability vs. AA monomer dose for the BEAS-2B cells for 24, 48 and 72 hr exposures.

8.3.1.3 LD$_{50}$ results for monomer cytotoxicity study

The LD$_{50}$ values for the DA and AA monomers are shown in table 8.2 for all three exposure times and both cell lines tested. For the HaCaT cell line, there is an order of magnitude difference in the LD$_{50}$ values between the AA and DA monomers for all exposures. For the BEAS-2B line, the difference is even more considerable; the LD$_{50}$ values for the DA monomer are two orders of magnitude larger than those for AA. These results show that the DA monomer exhibits a significantly lower toxicity profile than AA for both the dermal and bronchial cell lines, and justifies the replacement of AA with DA with the view to reducing the occupational hazards for large scale production of photopolymer-based devices and products.

Table 8.2 LD$_{50}$ values for DA and AA monomers

		LD$_{50}$ 24HR (mg/ml)	LD$_{50}$ 48HR (mg/ml)	LD$_{50}$ 72HR (mg/ml)
HaCaT	DA monomer	4.78	3.92	3.55
	AA monomer	0.50	0.17	0.12
BEAS-2B	DA monomer	38.49	21.48	7.25
	AA monomer	0.26	0.11	0.06

The significant difference in LD$_{50}$ values between the two cell lines for both the DA and AA monomers may be attributed to the fact that the dermal skin line is by nature more robust than the bronchial cell line. However, in both cases there is a clear difference between the LD$_{50}$ values for DA and AA. There are several factors which may contribute to the difference in toxicity, the first of which is the size of the monomer molecules. As shown in fig. 8.10, the AA molecules are smaller in size than the DA molecules. Therefore, the AA molecules may more easily permeate the cell membrane by passive diffusion or through aqueous pores [18]. In addition to that, previous studies

suggest that hydrogen-bonding interactions between the $CONH_2$ part of the AA molecule and cell membrane components may enhance the monomers ability to alter cell membrane structures and accelerate its diffusion and penetration [13]. When comparing the cytotoxic effect of the two monomers at the same concentration, a high number of smaller molecules as in the case of AA is favourable for interaction with cells as it results in an increase in the overall surface area. This makes an interaction more likely to occur [19]. Also, the reactive site may be blocked by another part of the molecule, such as the large group in the case of the DA molecule. Using the molecular weights of the two monomers, the ratio of the number of AA molecules to DA molecules is calculated to be 2.4 : 1. This means that a higher number of AA molecules are available to cause cell death.
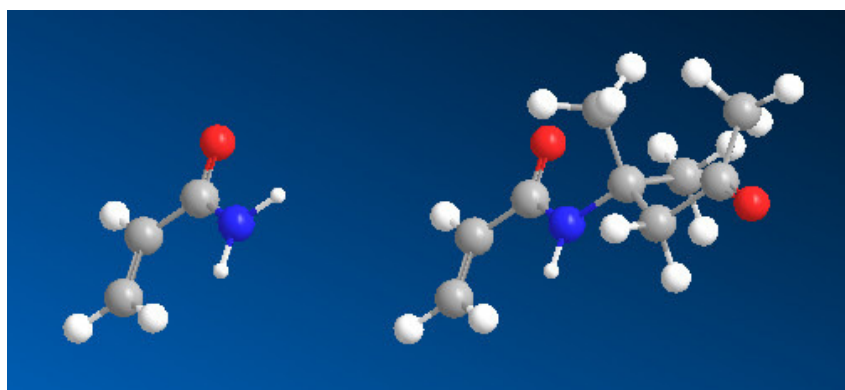
Fig. 8.10. 3D representation of the molecular structure of the AA (CH_2=$CHCONH_2$) and DA ($CHCONHC(CH_3)_2CH_2COCH_3$) molecules.

8.3.2 Photopolymer cytotoxicity study

A comparative study of the cytotoxicity of the three photopolymer compositions DA0, DAG and AA has been carried out using the HaCaT and BEAS-2B cell lines. This allows for a fuller picture of the cytotoxicity of the overall photopolymer compositions,

not just the monomer used. The data for cell viability vs. photopolymer dose is presented for each photopolymer composition, followed by a comparison of the LD_{50} values of the three compositions.

8.3.2.1 DA0 photopolymer cellular viability results

The data for cell viability vs. DA0 photopolymer dose for the HaCaT and BEAS-2B cell lines is shown in figs. 8.11 and 8.12 respectively. For the highest concentration tested, 1 mg/ml, cell viability drops by 85-95 % in both cases, for all three exposure times.
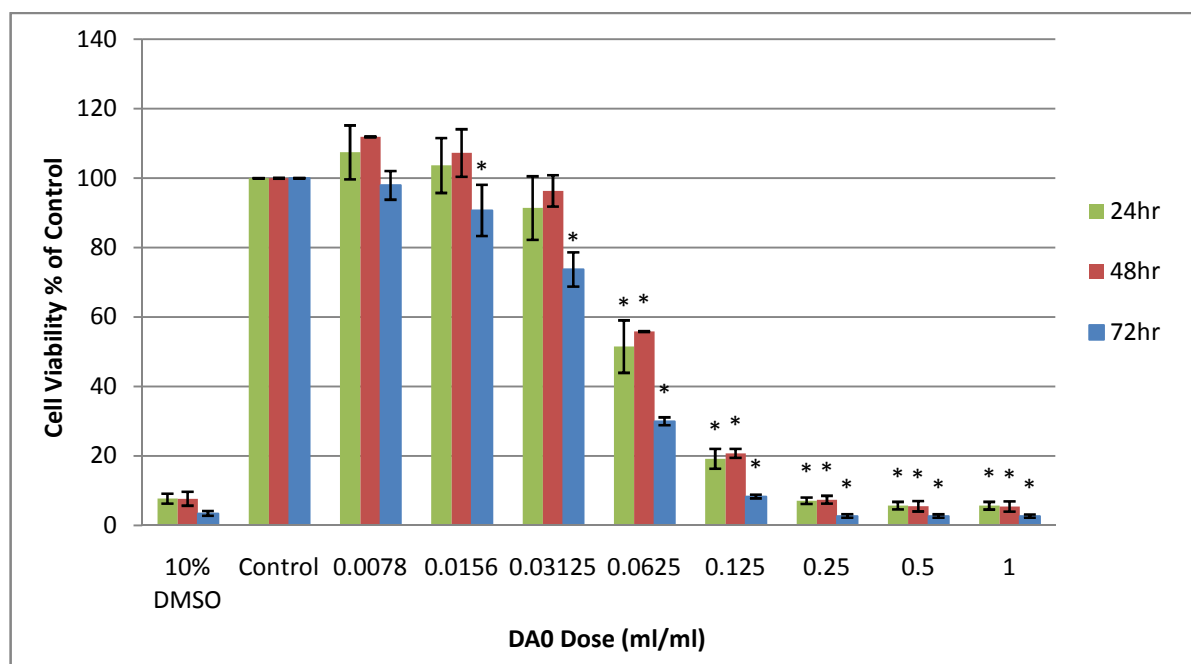
Fig. 8.11. Cellular viability vs. DA0 photopolymer dose for the HaCaT cells for 24, 48 and 72 hr exposures.
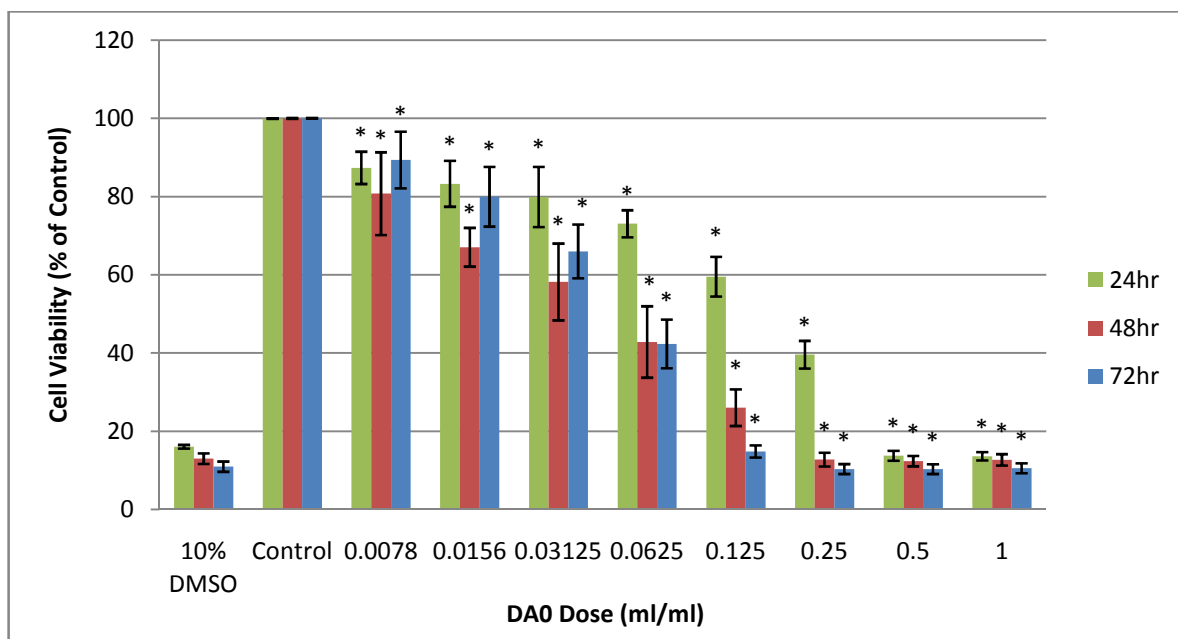
Fig. 8.12. Cellular viability vs. DA0 photopolymer dose for the BEAS-2B cells for 24, 48 and 72 hr exposures.

8.3.2.2 DAG photopolymer cellular viability results

The data for cell viability vs. DAG photopolymer dose for the HaCaT and BEAS-2B cell lines is shown in figs. 8.13 and 8.14 respectively. The lowest amount of cell death is observed to occur for the 24 hour exposure; no significant difference is observed between the 48 and 72 hour exposures. Once again, cell viability is observed to drop by up to 95 % as the concentration of photopolymer is increased to 1 mg/ml.
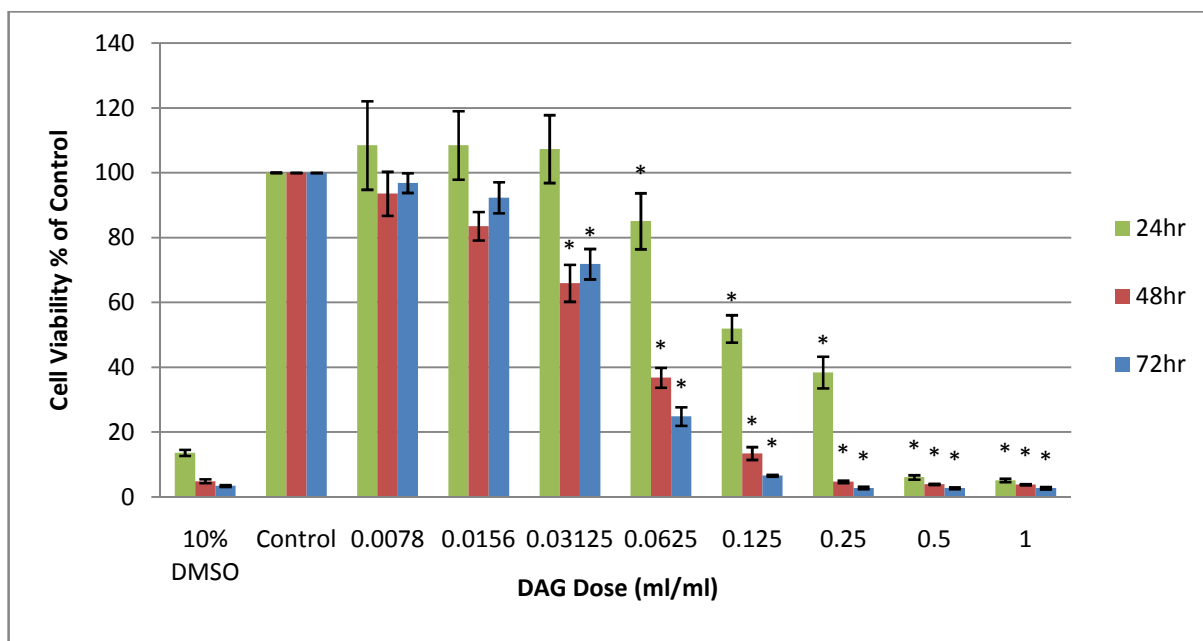
Fig. 8.13. Cellular viability vs. DAG photopolymer dose for the HaCaT cells for 24, 48 and 72 hr exposures.
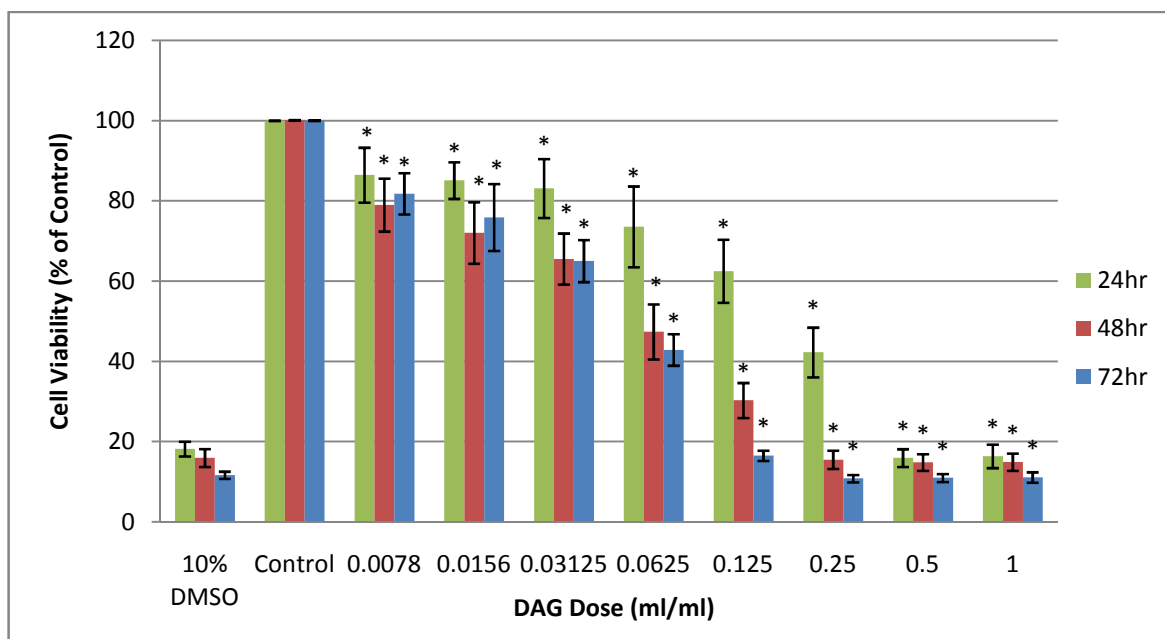
Fig. 8.14. Cellular viability vs. DAG photopolymer dose for the BEAS-2B cells for 24, 48 and 72 hr exposures.

8.3.2.3 AA photopolymer cellular viability results

The data for cell viability vs. AA photopolymer dose for the HaCaT and BEAS-2B cell lines is shown in figs. 8.15 and 8.16 respectively. A clear dependence on exposure time is observed for both cell lines, with the least cell death occurring for the 24 hour exposure. As was the case for the DA-based photopolymers, cell viability is observed to drop by up to 95 % as the concentration of photopolymer is increased to the maximum dose tested of 1 mg/ml.
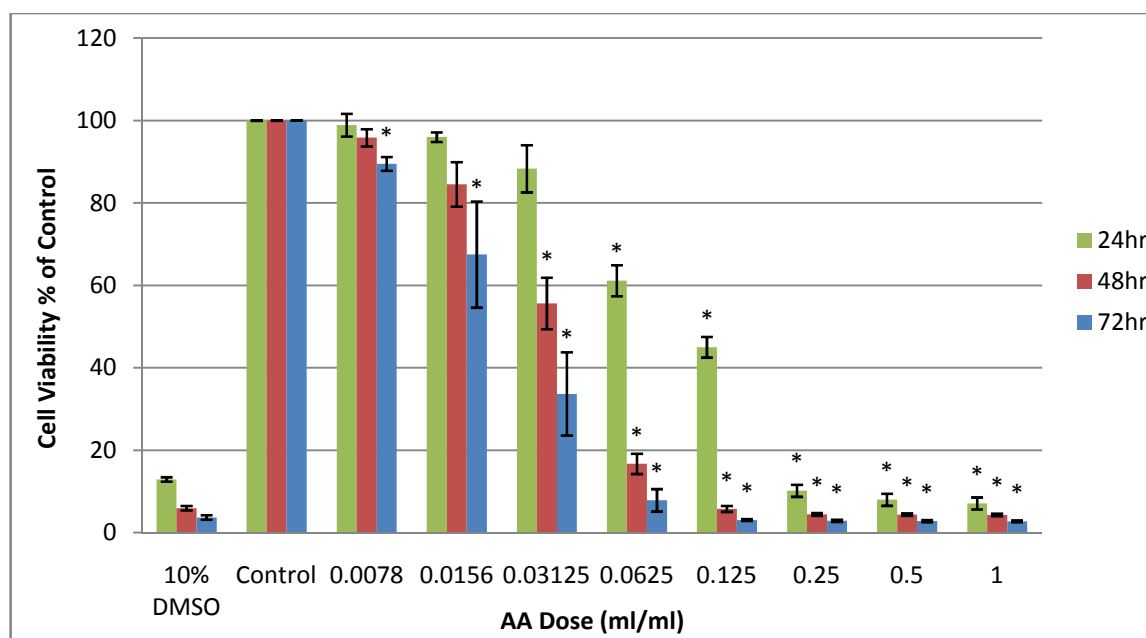
Fig. 8.15. Cellular viability vs. AA photopolymer dose for the HaCaT cells for 24, 48 and 72 hr exposures.
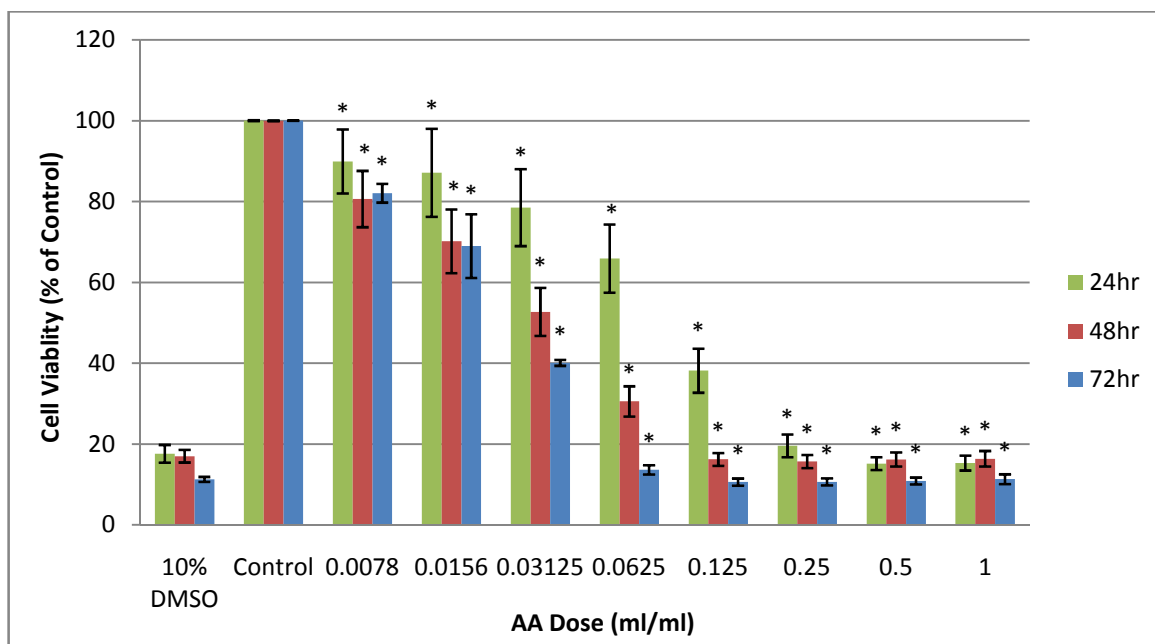
Fig. 8.16. Cellular viability vs. AA photopolymer dose for the BEAS-2B cells for 24, 48 and 72 hr exposures.

8.3.2.4 LD_{50} results for photopolymer cellular viability study

The LD_{50} values for the DA0, DAG and AA photopolymers are shown in table 8.3. In the case of both cell lines, the LD_{50} values for the DA0 and DAG photopolymers are twice that of the AA photopolymer. However, in all cases the LD_{50} value is very low, and so this difference is not considered significant. These results suggest that another common component of the photopolymer composition is contributing to the overall cytotoxicity of the DA photopolymer compositions.

It was determined that the crosslinking monomer N, N' Methylenebisacrylamide (BA) was most likely to be the contributing cytotoxic component. While BA is not a recognised carcinogen as in the case of AA, it is classified as a category 4 toxin [20].

An evaluation of the cytotoxicity of the BA crosslinker was carried out in order to investigate its influence on the overall toxicity of the final photopolymer material.

Table 8.3 LD_{50} values for DA0, DAG and AA photopolymers

		LD_{50} 24HR (ml/ml)	LD_{50} 48HR (ml/ml)	LD_{50} 72HR (ml/ml)
HaCaT	DA0	0.07	0.07	0.05
	DAG	0.16	0.04	0.04
	AA	0.09	0.03	0.02
BEAS-2B	DA0	0.15	0.04	0.05
	DAG	0.16	0.05	0.04
	AA	0.09	0.03	0.02

8.3.2.5 BA crosslinking monomer cellular viability and LD_{50} results

The data for cellular viability vs. BA dose for the HaCaT and BEAS-2B cell lines is shown in figs. 8.17 and 8.18 respectively. The concentration of BA in the DA0 photopolymer solution is 0.0077 mg/ml. At this concentration, very little cell death is observed for the BA monomer. As the dose is increased to the maximum dose of 1 mg/ml however, cell viability decreases by approximately 90 % for the HaCaT cell line, and 80 % for the BEAS-2B cell line. This is approximately the same amount of cell death as a percentage of the control as occurs for the AA monomer.
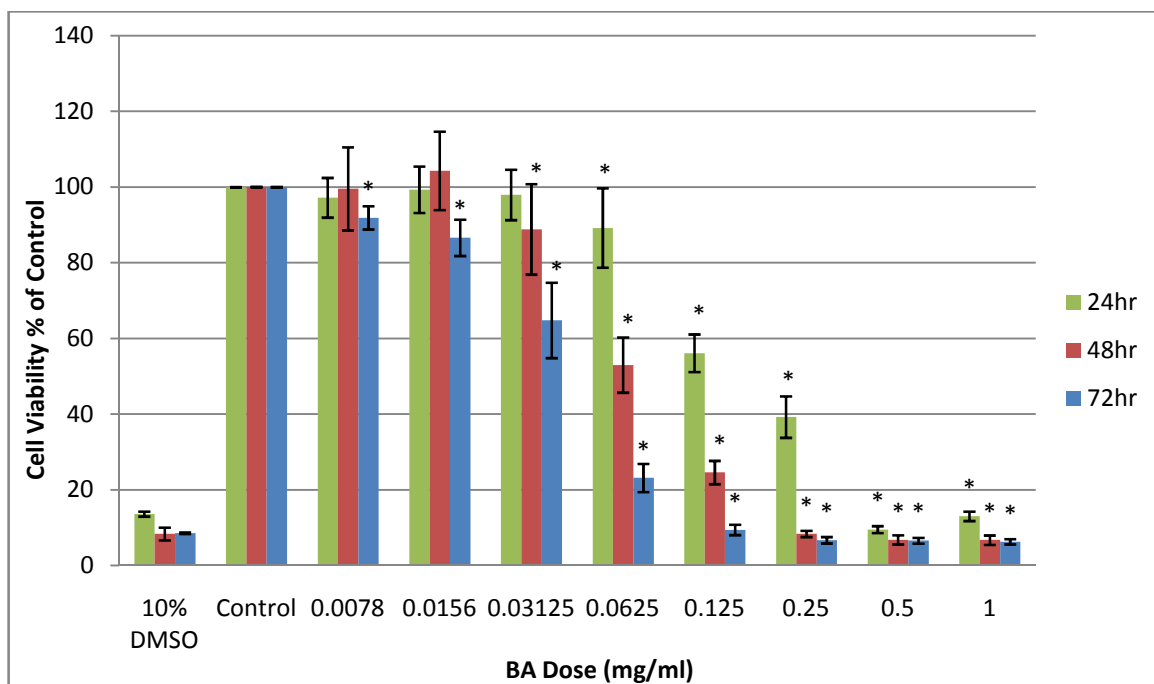
Fig. 8.17. Cellular viability vs. BA monomer dose for the HaCaT cells for 24, 48 and 72 hr exposures.
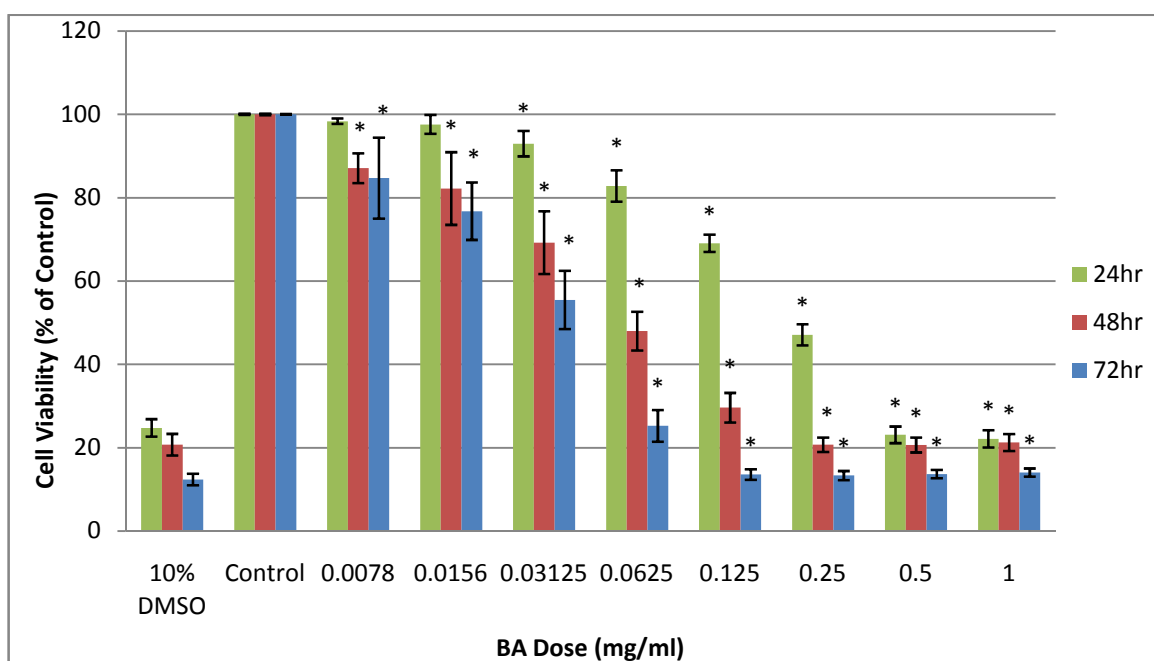
Fig. 8.18. Cellular viability vs. BA monomer dose for the BEAS-2B cells for 24, 48 and 72 hr exposures.

The LD$_{50}$ values for the BA crosslinking monomer are shown in table 8.4. It is clear that the BA monomer demonstrates significant cytotoxicity for the two cell-lines tested here, comparable to the cytotoxicity for the AA monomer as demonstrated in table 8.2. Therefore, it is likely that the BA monomer contributes to the overall cytotoxicity of the DA0, DAG and AA photopolymers. In order to verify this hypothesis, the cytotoxicity of the DA0 and DAG photopolymers without BA was investigated.

Table 8.4 LD$_{50}$ values for the BA monomer		
	LD$_{50}$ 24HR (mg/ml)	LD$_{50}$ 48HR (mg/ml)	LD$_{50}$ 72HR (mg/ml)
HaCaT	0.17	0.07	0.04
BEAS-2B	0.24	0.07	0.03

8.3.2.6 DA0 and DAG photopolymers without BA cellular viability and LD$_{50}$ results

In order to investigate the influence of the crosslinking monomer BA on the cytotoxicity of the DA photopolymer, a study of the cytotoxicity of the DA0 and DAG photopolymer compositions without BA was carried out. The data for cellular viability vs. the dose of photopolymer without BA for the DA0 and DAG compositions is shown in figs. 8.19 and 8.20 respectively. Figs. 8.21 and 8.22 compare the 24 hour exposure data for cellular viability with and without BA for DA0 and DAG respectively. The BEAS-2B cell line was used for these tests. The LD$_{50}$ values for the DA0 and DAG compositions with and without BA are shown in table 8.5 for comparison.
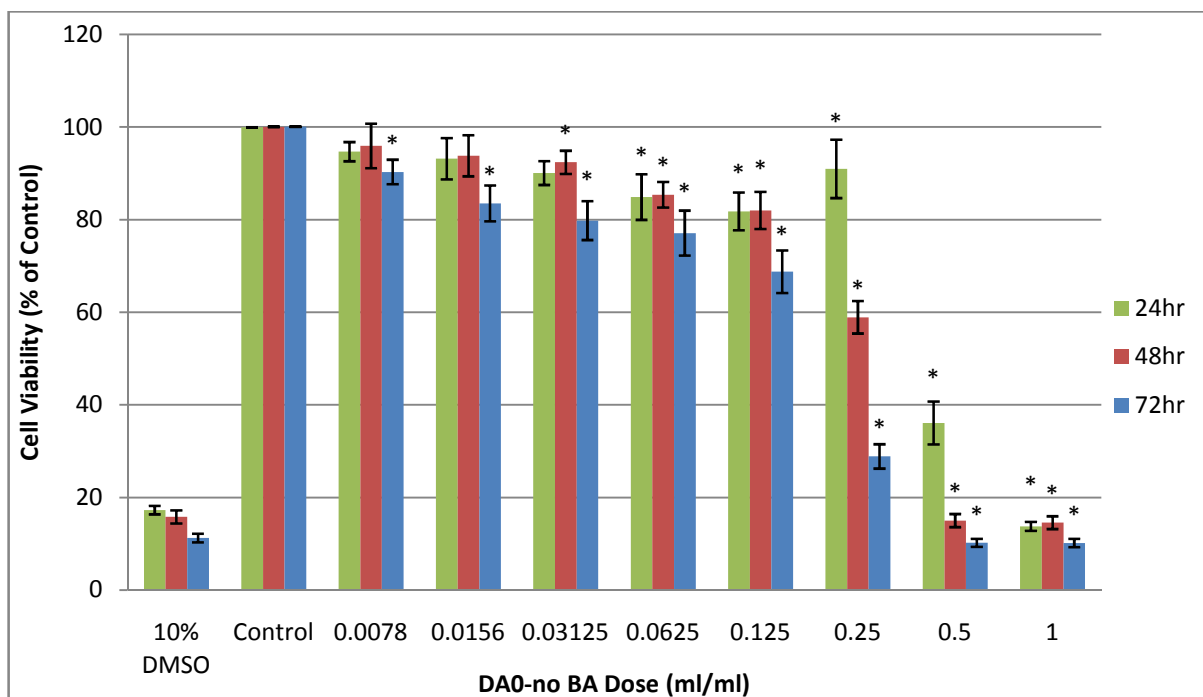
Fig. 8.19. Cellular viability vs. DA0-no BA photopolymer dose for the BEAS-2B cells

for 24, 48 and 72 hr exposures.
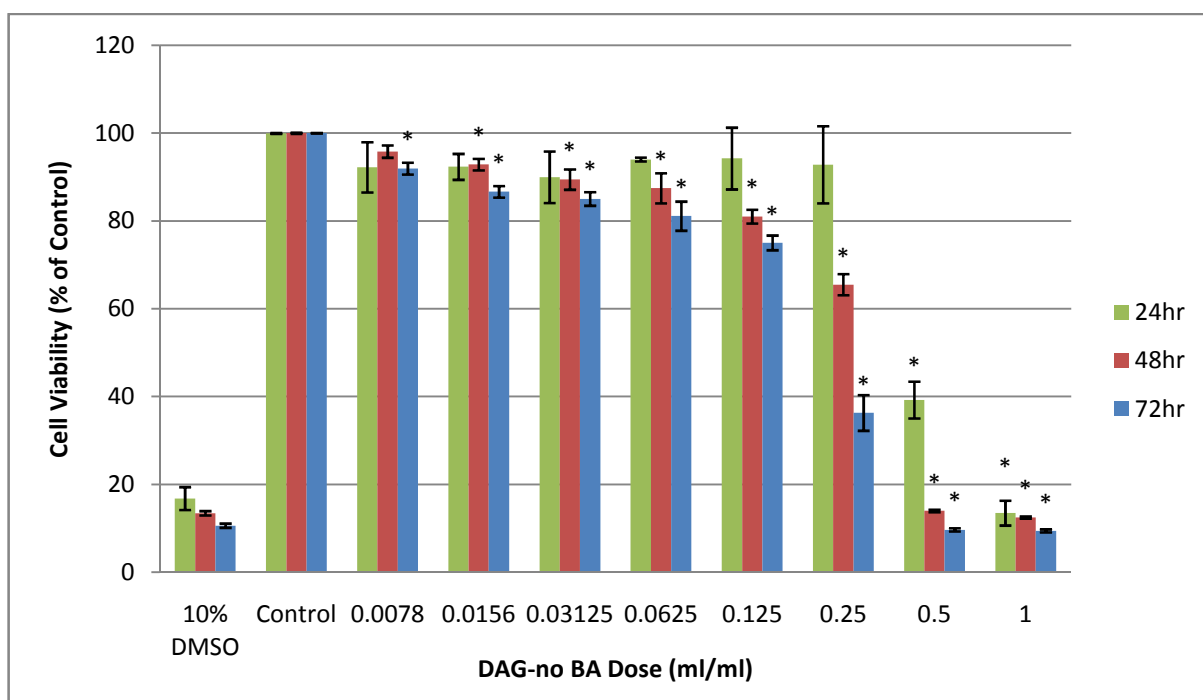
Fig. 8.20. Cellular viability vs. DAG-no BA photopolymer dose for the BEAS-2B cells

for 24, 48 and 72 hr exposures.
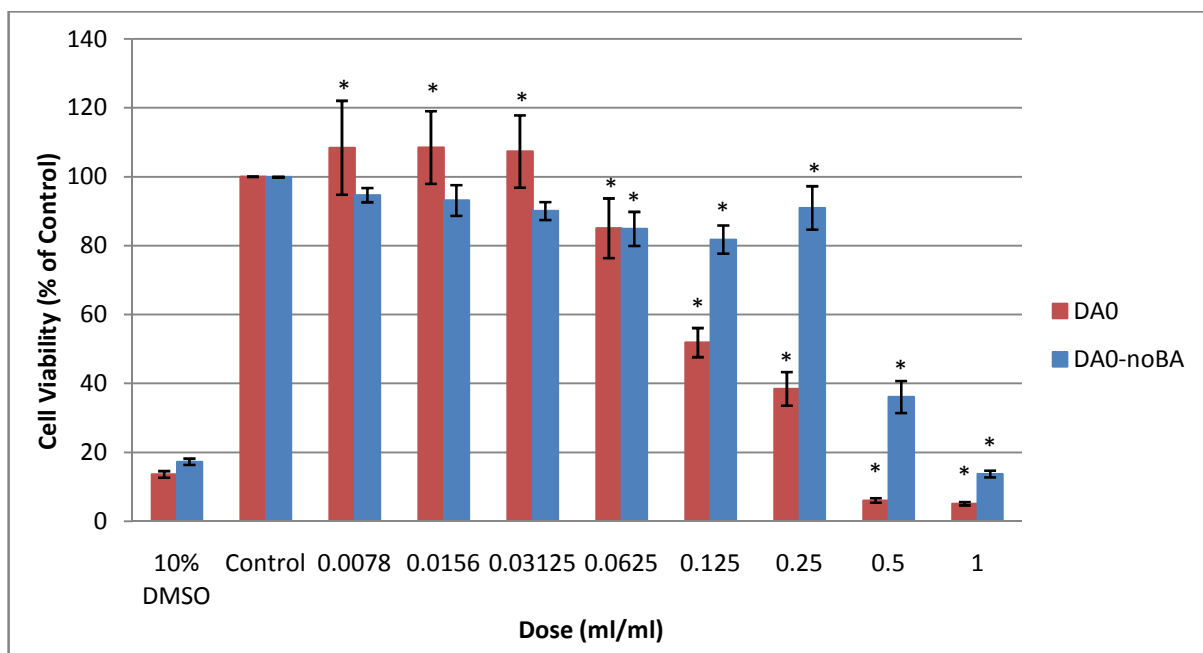
Fig. 8.21. Cellular viability vs. photopolymer dose for the BEAS-2B cells exposed to DA0 and DA0-noBA for a 24 hr exposure.
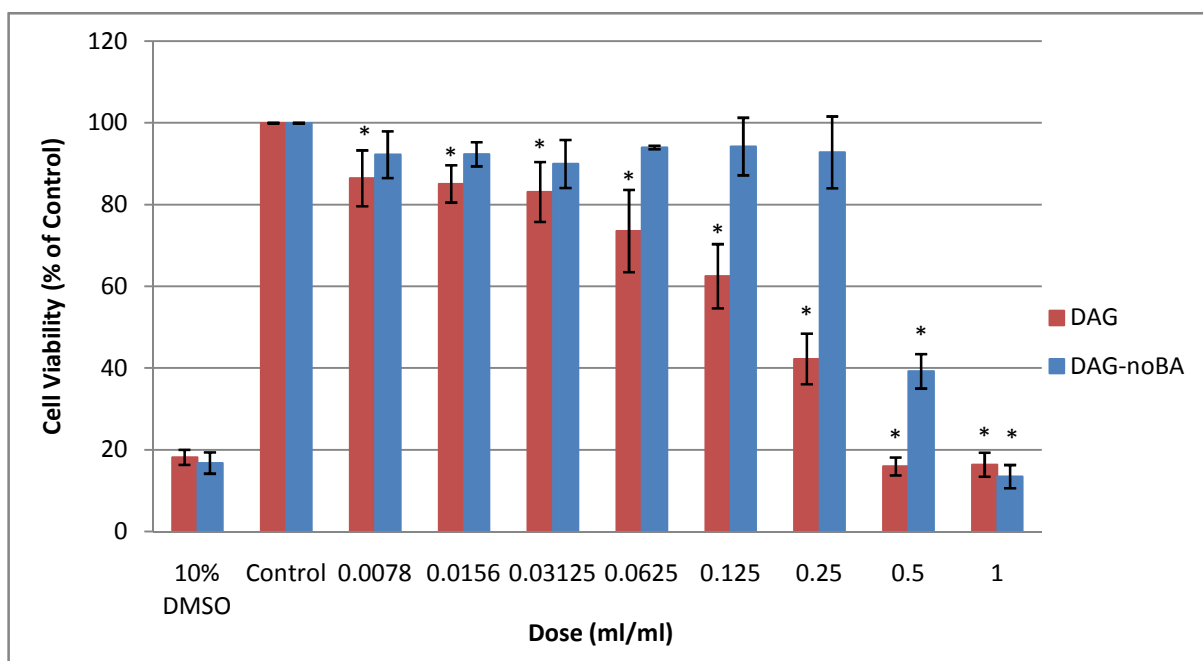
Fig. 8.22. Cellular viability vs. photopolymer dose for the BEAS-2B cells exposed to DAG and DAG-noBA for a 24 hr exposure.

189

Table 8.5 LD$_{50}$ values for DA0 and DAG photopolymers with and without BA for BEAS-2B cell line

	LD$_{50}$ 24HR (ml/ml)	LD$_{50}$ 48HR (ml/ml)	LD$_{50}$ 72HR (ml/ml)
DA0	0.15	0.04	0.05
DA0 – no BA	0.44	0.27	0.14
DAG	0.16	0.05	0.04
DAG – no BA	0.46	0.28	0.18

From table 8.5, it is clear that there the addition of BA to DA0 and DAG photopolymer compositions has a significant effect on the LD$_{50}$ value at all exposure times. In the case of the 24 hour exposure, the LD$_{50}$ value is reduced by 65 % with the addition of BA for both the DA0 and DAG photopolymers. This effect can be clearly seen in figs. 8.21 and 8.22 also. It can therefore be concluded that the inclusion of the crosslinking monomer BA does increase the cytotoxicity profile of the DA photopolymer compositions. The BA monomer's cytotoxicity is comparable to that of the AA monomer; however, it is important to note that unlike AA, BA is not a carcinogen. The concentration of BA in the final photopolymer layer is very small at 3.7 wt. %, and therefore risk of dermal or bronchial exposure to BA after production is very low.

8.3.3 Photopolymer component results

The cytotoxicity of the remaining photopolymer components was investigated, namely polyvinyl alcohol (PVA), triethanolamine (TEA), glycerol and Erythrosin B. The HaCaT cell line was used for these tests.

8.3.3.1 PVA

The data for cell viability vs. PVA dose for the HaCaT cell line is shown in fig. 8.23. For all three exposure times, no decreasing trend in cell viability with increasing concentration was observed for the range of doses tested. This result implies that the PVA solution used in the DA photopolymer compositions has no measurable cytotoxicity for the HaCaT cell line. PVA can therefore be considered highly suitable as a binder in a low-toxicity photopolymer composition. The low-toxicity of this photopolymer component is important, as the binder comprises up to 77 vol. % of the photopolymer in solution, and 37 wt. % of the photopolymer layer in solid form.
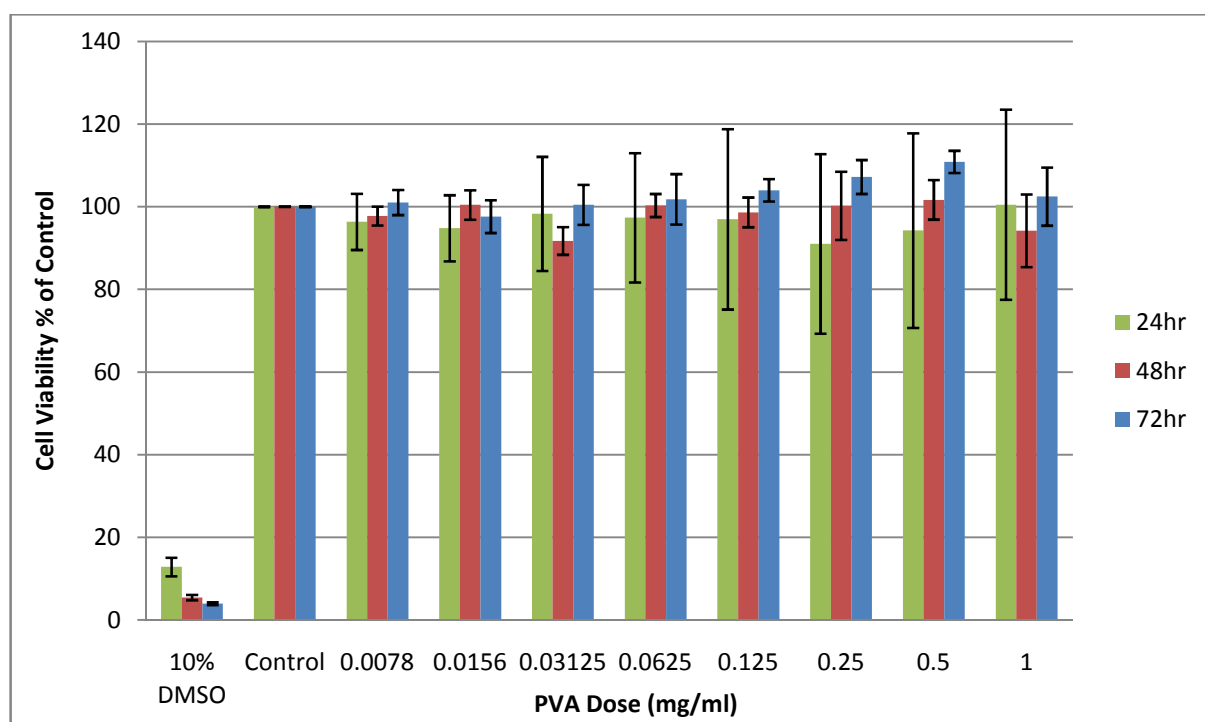
Fig. 8.23. Cellular viability vs. PVA dose for the HaCaT cells for 24, 48 and 72 hr exposures.

8.3.3.2 TEA

The data for cell viability versus TEA dose for the HaCaT cell line is shown in fig. 8.24. A significant decrease of up to 95 % is observed in cell viability as the dose of TEA is increased to 1 mg/ml for all three exposure times. The LD_{50} values for TEA for the 24, 48 and 72 hour exposures were calculated to be 0.03, 0.02, and 0.01 respectively. Surprisingly, these values are even lower than the LD_{50} values for the AA and BA monomers. TEA comprises up to 41 wt. % of the solid photopolymer layer, and therefore is a large component of the overall material. Therefore, its cytotoxicity profile is an important influence on the toxicity of the overall photopolymer material.

Studies carried out by the International Agency for Research on Cancer (IARC) found that skin toxicity after dermal exposure to TEA was observed in rats and mice, and skin irritation of varying degrees was observed in humans [21]. This most likely explains why such significant cell death was observed with TEA for the dermal HaCaT cell line. This is a surprising result, as TEA is widely used as a surfactant in the cosmetics and skincare industry. It is recommended by the Cosmetic Ingredient Review (CIR) Expert Panel that TEA and other ethanolamines are used only for discontinuous, brief use followed by thorough rinsing from the surface of the skin. In products intended for prolonged contact with the skin, the concentration of TEA should not exceed 5 % [22]. The IARC also reports that TEA is classified as a non-carcinogen, and aside from some dermal irritation, its toxicity is classified as low.
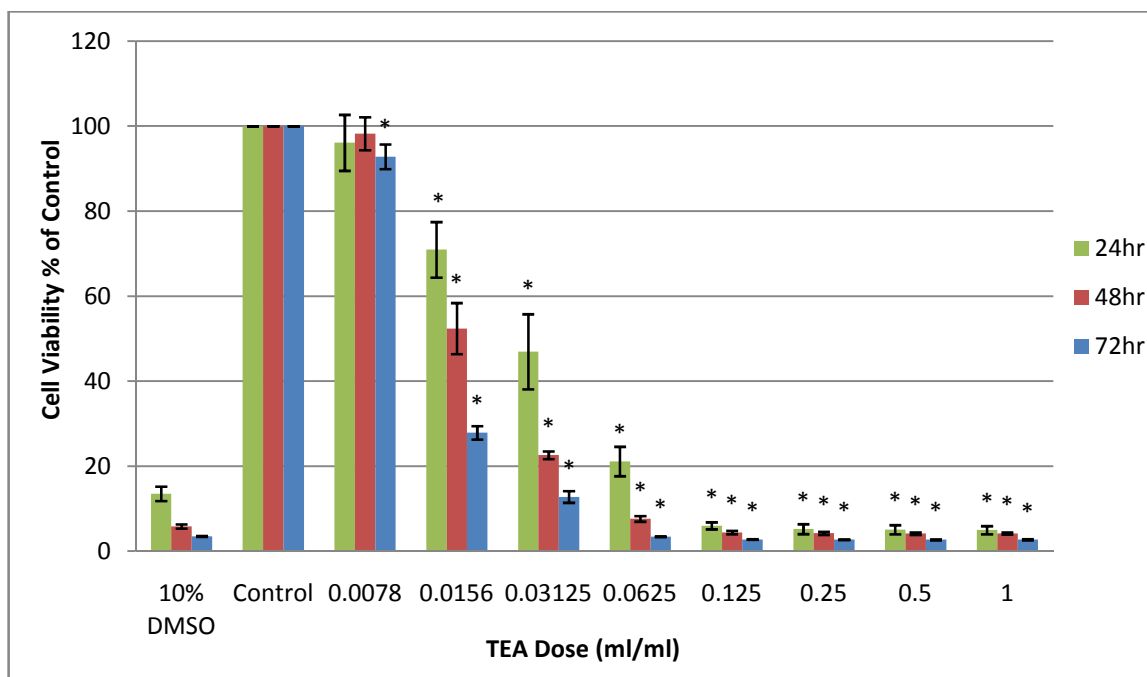
Fig. 8.24. Cellular viability vs. TEA dose for the HaCaT cells for 24, 48 and 72 hr exposures.

8.3.3.3 Glycerol

The data for cell viability versus glycerol dose for the HaCaT cell line is shown in fig. 8.25. The LD_{50} values for glycerol were calculated to be 2.93, 0.58 and 0.50 for the 24, 48 and 72 hour exposures respectively. The concentration of glycerol in the DAG photopolymer solution is 3.7 vol. %. At this concentration, any change in cell viability is within the standard deviation; therefore, it can be concluded that at the concentration of glycerol discussed here, glycerol does not contribute to the toxicity profile of the DA-based photopolymer composition.
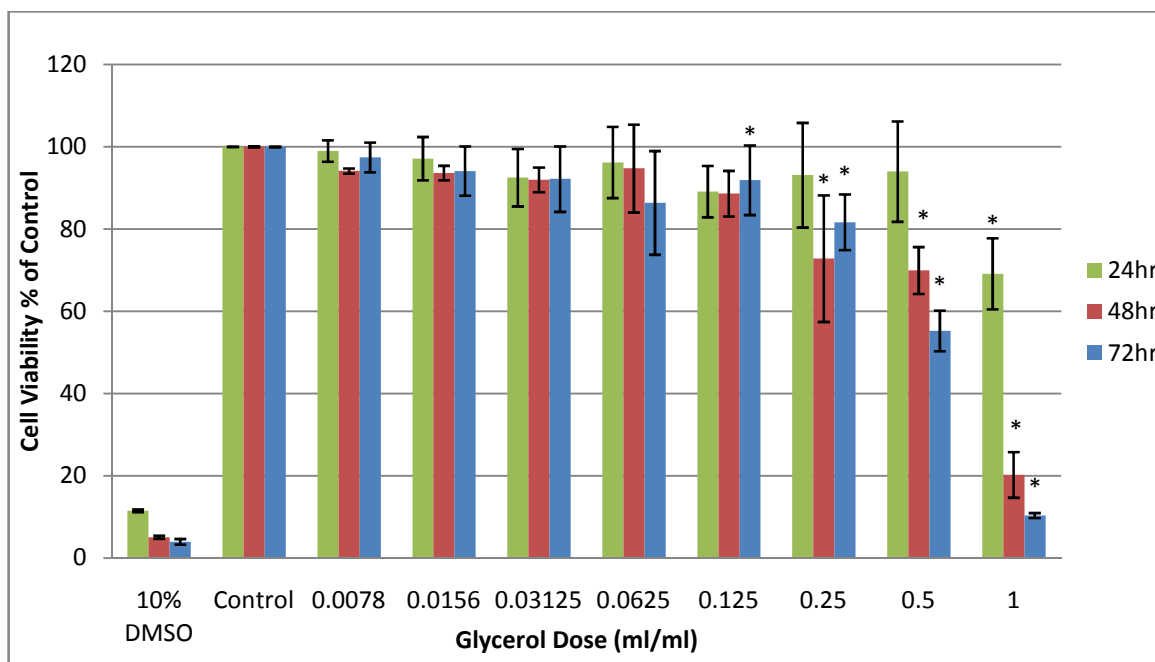
Fig. 8.25. Cellular viability vs. glycerol dose for the HaCaT cells for 24, 48 and 72 hr exposures.

8.3.3.4 Erythrosin B

The data for cell viability versus Erythrosin B dose for the HaCaT cell line is shown in fig. 8.26. The LD_{50} values for the 24, 48 and 72 hour exposures were calculated to be 0.38, 0.24 and 0.19 respectively. Erythrosin B comprises only 0.08 wt. % of the solid DA0 photopolymer layer, and therefore its influence on the toxicity of the final product is very low.
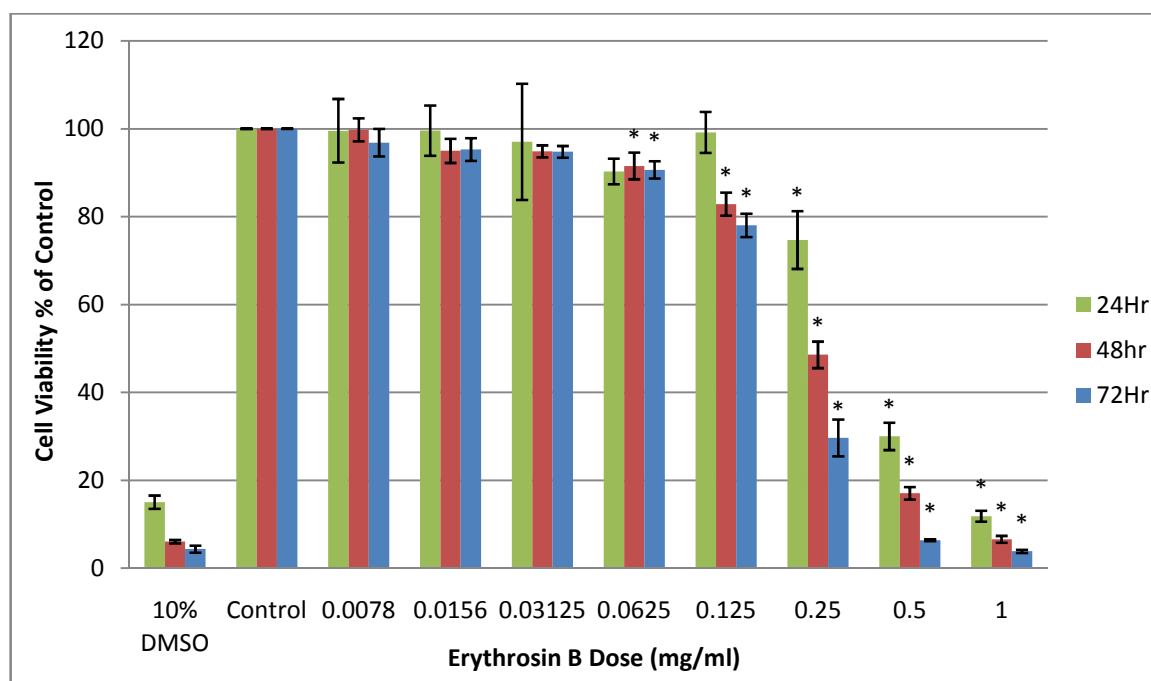
Fig. 8.26. Cellular viability vs. Erythrosin B dose for the HaCaT cells for 24, 48 and 72 hr exposures.

8.4 Conclusions

A comparative cytotoxicity evaluation of the DA and AA monomers was carried out for the first time. It was shown that DA exhibits a significantly lower toxicity profile than AA for both the dermal and bronchial cell lines, with up to two orders of magnitude difference in the LD_{50} concentration doses evaluated. This result makes the new family of DA-based photopolymers very attractive for development for commercial applications because they are environmentally friendly.

A study of the cytotoxicity of the DA0, DAG and AA photopolymers was carried out for the dermal and bronchial cell lines. No significant difference in the LD_{50} values was observed between the DA-based and AA-based photopolymers. This was determined to be due to the presence of the crosslinking monomer BA in all three photopolymers. The

BA monomer demonstrated significantly higher cytotoxicity than predicted. However, the BA monomer is not classified as a carcinogen, unlike the AA monomer. Therefore, although BA is present in both the DA and AA photopolymers, the occupational hazards associated with the large-scale production of a DA-based photopolymer would be much lower than for an AA-based material. Also, the concentration of BA in the DA photopolymer solid layers is low at 3.7 wt. %, implying that the risk of exposure to BA from a DA photopolymer-based product or device is very low.

The cytotoxicity of the remaining photopolymer components was investigated. It was concluded that the components PVA and Glycerol demonstrate no significant cytotoxicity and therefore are compatible with the development of a low-toxicity photopolymer. High cytotoxicity was observed for the electron donor TEA on exposure to the dermal cell line; however, this was concluded to be due to TEA's nature as a skin irritant, and not due to a high toxicity profile. Some cytotoxicity was observed for the photosensitive, xanthene dye Erythrosin B. However, Erythrosin B comprises only 0.08 wt. % of the solid photopolymer layer, and therefore does not contribute significantly to the toxicity profile of the photopolymer composition.

The cytotoxicity evaluation of the DA photopolymer and its components justifies the replacement of AA with DA with the view to reducing occupational hazard risks for large scale holographic device fabrication, as well as the overall toxicity of the photopolymer composition.

References:

[1] D. D. McCollister, F. Oyen, V. K. Rowe, "Toxicology of Acrylamide", Toxicology and Applied Pharmacology 6, 172-181 (1964).

[2] A., G. Lawrence, R. Gentry, T. McDonald, H. Bartow, J. Bounds, N. Macdonald, H. Clewell, B. Allen,C. Van Landingham, "Acrylamide: Review of Toxicity Data and Dose-Response Analyses for Cancer and Noncancer Effects", Critical Reviews in Toxicology 36, 481-608 (2006).

[3] D. J. King, R. R. Noss, "Toxicity of polyacrylamide and acrylamide monomer", Rev. Environ. Health 8, 3-16 (1989).

[4] Health implications of acrylamide in food: report of a joint FAO/WHO consultation, WHO Headquarters, Geneva, Switzerland, 25-27 June, 2002.

[5] L. E. Coleman, J. F. Bork, D. P. Wyman, D. I. Hoke, "Synthesis and polymerization of N[2-(2-methyl-4-oxopentyl)]-acrylamide–A new reactive vinyl monomer", Journal of Polymer Science 3, 1601-1608 (1965).

[6] J. Siemiatycki, L. Richardson, K. Straif, B. Latreille, R. Lakhani, S. Campbell, M Rousseau, P. Boffetta, Environ. Health Perspect. 112, 1447–1459 (2004).

[7] X. X. Ma, G. D. Yao, H. Cheng, Q. L. Zeng, Q. Chen, "Effects of acrylamide on DNA damage in human keratinocytes," Analytical Chemistry 76(5), 1518–1523 (2004).

[8] J. E. Klaunig L. M. Kamendulis, "Mechanisms of acrylamide induced rodent carcinogenesis," Advances in Experimental Medicine and Biology 561, 49–62 (2005).

[9] J. Park, L. M. Kamendulis, M. A. Friedman, J. E. Klaunig, "Acrylamide-induced cellular transformation," Toxicological Sciences 65(2), 177–183 (2001).

[10] H. Tsuda, C. S. Shimizu, M. K. Taketomi, "Acrylamide; induction of DNA damage, chromosomal aberrations and cell transformation without gene mutations," Mutagenesis 8(1), 23–29 (1993).

[11] K. A. Johnson, S. J. Gorzinski, K. M. Bodner, "Chronic toxicity and oncogenicity study on acrylamide incorporated in the drinking water of Fischer 344 rats," Toxicology and Applied Pharmacology 85(2), 154–168 (1986).

[12] T. Takahashi, M. Yoshii, T. Kawano, T. Kosaka, H. Hosoya, "A new approach for the assessment of acrylamide toxicity using a green paramecium," Toxicology in Vitro 19(1), 99–105 (2005).

[13] M. Friedman, "Chemistry, biochemistry, and safety of acrylamide. A review," Journal of Agricultural and Food Chemistry 51(16), 4504–4526 (2003).

[14] D. Cody, A. Casey, I. Naydenova, E. Mihaylova, "A comparative cytotoxic evaluation of acrylamide and diacetone acrylamide to investigate their suitability for holographic photopolymer formulations", Int. J. Polymer Sci. 564319, 1-6 (2013).

[15] T. Mosmann, "Rapid colorimetric assay for cellular growth and survival: application to proliferation and cytotoxicity assays," Journal of Immunological Methods 65(1-2), 55–63 (1983).

[16] D. Hughes, H. Mehmet, Cell Proliferation & Apoptosis, BIOS Scientific, Oxford, UK, 2003.

[17] J. W. Trevan, "Error of determination of toxicity", P. R. Soc. London 101(712), 483-514 (1927).

[18] E. Hodgson, A Textbook of Modern Toxicology, 82, John Wiley & Sons, Hoboken, NJ, USA, 2010.

[19] J. C. Kotz, P. Triechel, and J. R. Townsend, Chemistry and Chemical Reactivity, Cengage Learning, Stamford, Conn, USA, 2009.

[20] N, N' Methylenebisacrylamide MSDS sheet, Sigma Aldrich website, [accessed on 6-2-2014]:

http://www.sigmaaldrich.com/MSDS/MSDS/DisplayMSDSPage.do?country=IE&language=en&productNumber=M7279&brand=SIGMA&PageToGoToURL=http%3A%2F%2Fwww.sigmaaldrich.com%2Fcatalog%2Fproduct%2Fsigma%2Fm7279%3Flang%3Den .

[21] "IARC Monographs on the Evaluation of Carcinogenic Risks to Humans – Some Industrial Chemicals", WHO and IARC, vol. 77, Lyon, France, 2000.

[22] CIR Expert Review Panel, "Final Report on the Safety Assessment of Triethanolamine, Diethanolamine, and Monoethanolamine", International Journal of Toxicology 2(7), 183-235 (1983).

9. INVESTIGATION OF THE EFFECT OF ZEOLITE NANOPARTICLES ON THE DA PHOTOPOLYMER

9.1 Introduction

Large refractive index modulation (Δn) of holograms recorded in photopolymer layers is favourable for holographic applications in order to obtain high diffraction efficiency holograms in thinner layers, or increased data storage density in thicker layers. The idea of incorporating inorganic nanoparticles into holographic photopolymers was first introduced in 1996 by Oliveira et al [1]. By selecting nanoparticles with a refractive index (n) significantly different to that of the host photopolymer material, large Δn values can be achieved due to spatial redistribution of the nanoparticles during holographic recording (see fig. 9.1). Aside from large Δn, other positive effects due to their addition include reduced photopolymerisation-induced shrinkage, increased sensitivity, and improved grating stability. Problems with these nanocomposites can arise due to incompatibility of the nanoparticles with the photopolymer material, as well as increased optical losses due to scattering, if the difference between the refractive index of the nanoparticles and host material is too great [2, 3].

The incorporation of nanoparticles into holographic photopolymers has been extensively researched by many groups for a wide range of inorganic nanoparticles. Oliveira et al observed that the diffusion of ZrO_2 (n = 2.1) nanoparticles within a methacrylate photopolymer resulted in Δn values of up to 1.5×10^{-2} [1]. A description of the generic technique of holographic patterning using nano and mesoparticles was published in 2001 by Vaia et al [4]. The incorporation of TiO_2 nanoparticles (15 nm diameter, n = 2.55) in an acrylate photopolymer formulation by Suzuki et al led to Δn values of 5.1×10^{-3} [5]. Reduced shrinkage was also observed. Sanchez et al improved

on this result by using 4 nm diameter TiO_2 nanoparticles, reaching Δn values of 15.5×10^{-3} [6]. In 2005, Tomita *et al* verified that the significant improvements observed in Δn was due to the mass transport of the nanoparticles during holographic recording, with spatial redistribution of the nanoparticles occurring from bright to dark fringe regions [7]. Other inorganic nanoparticle types with different *n* values such as SiO_2 ($n = 1.46$) [8, 9] have been investigated also, and similar improvements in Δn are reported. In 2008 Tomita *et al* demonstrated that the inclusion of ZrO_2 and SiO_2 nanoparticles in (meth)acrylate photopolymers prevents thermal distortion effects, thus making them suitable for holographic applications over a wider range of environmental conditions [10].
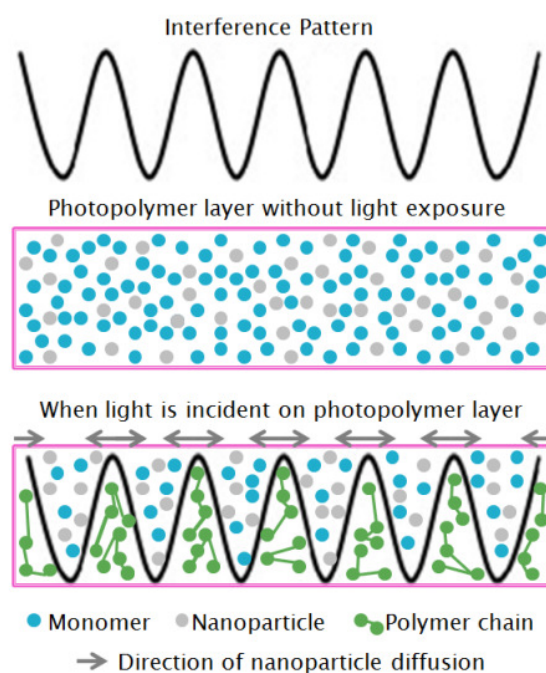
Fig. 9.1. Schematic diagram of grating formation in nanoparticle-doped photopolymer layer on exposure to light.

Other metal nanoparticle types such as Au and Ag have been reported to cause an increase in Δn due to redistribution. Goldenberg *et al* reported Δn values of 7.3×10^{-3}

for a 1.5 wt. % Au-doped acrylate photopolymer [11]. Xue *et al* state that the dispersibility and solubility of Au nanoparticles in acrylate formulations is greatly improved by coating the nanoparticles with citrate ions, due to their electrostatic repulsion action [12]. Research has been carried out into the in-situ fabrication and redistribution of Ag nanoparticles by Balan *et al* in methacrylate-based photopolymer formulations [13-15]. The 5 nm diameter Ag nanoparticles are observed to form due to the reduction of silver cations in the photopolymer solution on exposure to light. Pramitha *et al* observe Δn values of 7.5×10^{-3} for their Ag-doped, water-soluble, acrylate photopolymer using this method [16].

Different quantum dot nanoparticles such as CdSe [17] and ZnO [18] have been incorporated into photopolymer formulations due to their high fluorescence at certain wavelengths. This property is particularly interesting for holographic applications such as sensing and product authentication.

AA-based photopolymer nanocomposites containing three different zeolite nanoparticles with varying miroporosity, namely Silicalite-1 (MFI-structure, diameter of 30 nm), AlPO-18 (AEI-structure, diameter of 180 nm) and Beta (BEA-structure, diameter of 40 nm) have been investigated by Naydenova *et al* [19-22]. It was determined that the hydrophobic nature of the MFI zeolites ensures its pores remain empty when incorporated in the host photopolymer, causing an increase in Δn when redistributed. The inclusion of MFI nanoparticles has also been reported to cause a decrease in shrinkage from 1.32 % to 0.57 % [23, 24], which is just above the commercial limit of shrinkage for data storage applications [25]. No such improvement in Δn was observed for the AEI and BEA type nanoparticles. The AEI type zeolites are hydrophilic in nature, and thus contain water molecules in their pores. In the case of the large-pore BEA zeolites (approximate pore size of 7.6×6.4 Å) which are of interest

here, it was discovered that the AA monomer molecules (approximate size of 5×4 Å) were migrating in to the zeolite pores. In both cases the difference in refractive index between the nanoparticles and the host polymer matrix is not large enough to cause significant increase of the Δn as a result of their redistribution. However, Raman spectroscopy studies by Leite *et al* reported that up to 40 % of the BEA zeolites in the layer are redistributed during holographic recording, indicating that BEA nanoparticles in acrylate photopolymer formulations are highly suitable for holographic applications. It has already been demonstrated that the BEA-doped AA photopolymer can be used as a holographic sensor for toluene, due to changes in the grating optical properties on exposure to the gas [26].

As discussed above, the addition of BEA zeolite nanoparticles to the AA photopolymer material did not result in a large net change in n upon redistribution due to the migration of the AA monomer molecules into the zeolite pores. However, it could be expected that by increasing the size of the monomer molecules in the host photopolymer material, migration of the monomer into the pores of the BEA zeolite would be prevented, thus achieving the maximum Δn possible. As discussed previously, the DA monomer molecule is nearly twice the size of the AA monomer (approximate size of 10×4 Å). Therefore, it was predicted that the DA-based photopolymer will show significantly larger improvement in Δn with the incorporation of the BEA zeolite nanoparticles than the AA-based photopolymer, as migration of the DA monomer molecules into the zeolite pores is restricted by the monomer size.

An experiment was planned and carried out to check the above described expectation. The effect of zeolite nanoparticles with BEA type structure on the optical properties, namely refractive index n, and Δn due to holographic recording, of the DA-based photopolymer formulation was investigated. For this study, two different zeolite

nanoparticles types were used: standard 'empty pore' BEA, and BEA whose pores have been loaded with silver nanoparticles of 1 nm diameter (BEA-Ag). By loading the zeolites with Ag in this way, the refractive index n of the final particle is changed, allowing for comparison of the effect of nanoparticles with different n values on the DA photopolymer, without altering the structure of the nanoparticle itself. The BEA and BEA-Ag nanoparticles were fabricated and characterized by Prof. Svetlana Mintova at the Laboratoire Catalyse & Spectrochimie (LCS) research facility at the University of Caen in Caen, France. The measurements of refractive index were carried out by Dr. Tsvetanka Babeva at the Institute for Optical Materials and Technologies at the Bulgarian Academy of Sciences in Sofia, Bulgaria.

9.2. Experimental

9.2.1 Materials

9.2.1.1 Synthesis of BEA and BEA-Ag zeolite nanoparticles

Zeolite BEA nanocrystals were prepared under hydrothermal conditions from clear precursor suspension with a molar composition: $9TEAOH: 0.25Al_2O_3: 25SiO_2: 295H_2O$. The suspension was prepared by mixing tetraethylammonium hydroxide (TEAOH), aluminium iso-butoxide ($C_9H_{21}O_3Al$), colloidal silica (SiO_2) and water; the mixture was aged for 60 minutes at room temperature and subjected to hydrothermal treatment at 100 °C for 3 days. The crystalline suspension was purified by multistep high-speed centrifugation (20.000 rpm, 60 minutes) and finally redispersed in double distilled water. The ion exchange of BEA nanocrystals was carried out directly in the zeolite suspension using 0.1 M AgNO$_3$ solution under continuously stirring for 3 hours

at room temperature. The obtained suspension was purified twice with water in order to remove the free silver. Then the Ag cations were reduced to Ag metal using reducing agent triethylamine (ratio of BEA suspension to reducing agent of 4 : 0.25) under microwave treatment (60 °C for 5 minutes). Both the BEA and BEA-Ag samples were stabilized in water at pH = 7 with a concentration of solid particles of 4.9 wt/vol %.

9.2.1.2 Nanocomposite layer preparation

The DA0 photopolymer solution was prepared as described in chapter 4. The nanoparticles were dispersed in 4.9 % wt/vol water solution. The solution was then left in an ultrasonic bath for 30 minutes. Different volumes from this dispersion were added to the DA photopolymer solution. Since the addition of the nanoparticle solution resulted in dilution of the original photopolymer solution, the equivalent amount of water was added to the photopolymer solution in order to ensure that all samples prepared from the same stock solution had approximately the same physical layer thickness after drying. After mixing for 15 minutes, 0.3 ml of solution was deposited on to a 75 × 25 mm microscopic glass slide and left to dry for 6 hours. The concentration of nanoparticles in the dry photopolymer nanocomposite layer was 0, 0.25, 0.5, 1, 2 and 5 wt. %, with thickness of 38 ± 3 µm.

9.2.2 Methods

9.2.2.1 Zeolite nanoparticle characterization

X-ray diffraction (XRD) analysis was carried out using a PANalytical X'Pert Pro diffractometer with CuKα monochromatic radiation (λ = 1.5418 Å) in order to

investigate the crystalline structure of the BEA and BEA-Ag zeolites, and to identify any changes due to the addition of the Ag nanoparticles.

UV-Vis spectroscopy measurements of the BEA-Ag zeolite solution were made using a Perkin-Elmer Lambda 900 UV-vis-NIR spectrophotometer. These measurements were carried out in order to identify the presence of any remaining Ag^+ cations and the formation of Ag nanoparticles in the suspensions.

Dynamic light scattering (DLS) measurements of the size distribution of the BEA-Ag and BEA zeolite suspensions were carried out using a Malvern Zetasizer Nano ZS. This measurement also allowed for the identification of Ag nanoparticles existing outside of the zeolite pores, as such clusters would be identified as particles of differing size to the zeolite nanoparticles.

The crystal size and morphology of BEA zeolite containing Ag nanoparticles in suspensions were studied using HREM on 200 kV JEOL 2010 FEG STEM electron microscope (tilt ± 42°). The highly diluted zeolite suspensions containing Ag nanoparticles were sonicated for 15 minutes prior deposition on a holey carbon supported by a nickel grid.

9.2.2.2 Refractive index measurements

Samples were deposited on optical glass plates with a high n (approximately 1.7), ensuring high optical contrast between the layer and substrate. Effective n values of the photopolymer nanocomposites were determined by measuring transmittance, T and reflectances R_f and R_b spectra from front (air) and back (substrate) side of the layers respectively. The measurements were taken using a Cary 5E UV-VIS-NIR

spectrophotometer in the spectral range of 400 - 900 nm with an accuracy of 0.1 and 0.5 % respectively [27]. The simultaneous determination of n, the extinction coefficient k and thickness d of the layers was performed by minimization of the goal function G consisting of discrepancies between measured ("meas") and calculated ("calc") spectra:

$$G = (T_{calc} - T_{meas})^2 + (R_{fcalc} - R_{fmeas})^2 + (R_{bcalc} - R_{bmeas})^2 \qquad (9.1)$$

G was minimized at each wavelength λ in the spectral range from 400 - 900 nm by a Nelder-Mead simplex method [28] using a dense grid of initial values of n, k and d. More details about the calculation procedure and the accuracy of the determination can be found in [27, 29].

9.2.2.3 Recording of holographic transmission gratings and Δn measurements

A two-beam holographic optical setup (fig. 9.2) with an angle of 30.85° between the beams was used to record un-slanted transmission gratings, using a 532 nm vertically-polarised Nd:YVO4 laser. Gratings were recorded in the nanocomposite layers at a spatial frequency of 1000 ± 30 l/mm. The absorption of the photopolymer at 633 nm is negligible, so a 633 nm He-Ne laser was used as the probe beam at the Bragg angle. As the recorded gratings are isotropic in nature, their diffraction efficiency is not dependent on the polarisation of the probe beam. An optical power meter (Newport 1830-C) was used to record the intensity of the diffracted beam, and LabVIEW software was used to plot the data in real-time. In order to measure the diffracted intensity dependence on the incident angle of the probe beam, the grating was placed on a rotational stage (Newport ESP 300). The accuracy of this measurement was 1×10^{-3} deg.
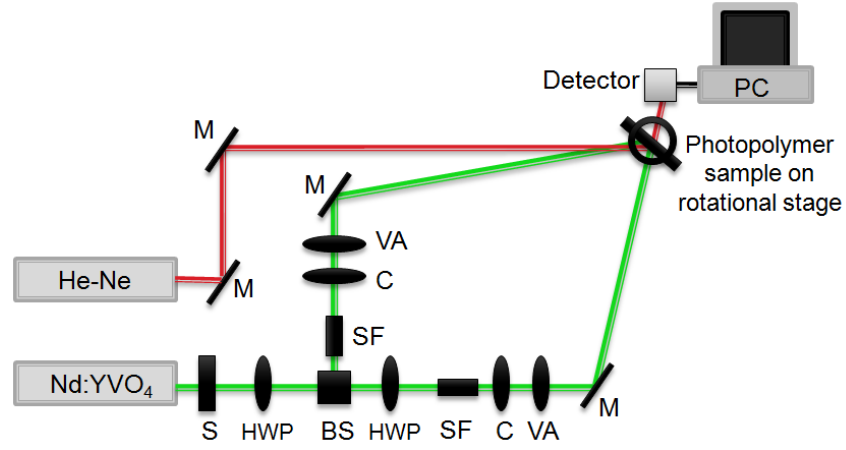
Fig. 9.2. Experimental setup: S: shutter, HWP: half wave plate, BS: polarising beam splitter, SF: spatial filter, C: collimator, VA: variable aperture, M: mirror.

A Q value of 84.68 is obtained for transmission gratings recorded in 38 ± 3 μm thick nanocomposite layers at a spatial frequency of recording of 1000 l/mm. This allows for application of Kogelnik's coupled-wave theory for volume, thick gratings [30], which is used here to determine Δn of the recorded gratings:

$$\Delta n = \frac{\lambda \cos\theta \sin^{-1}(\sqrt{\eta})}{\pi d} \tag{9.2}$$

where θ, λ are the reconstruction beam incident angle and wavelength. η is the diffraction efficiency of the recorded grating at the Bragg angle (defined here as the ratio of the intensity of the first diffraction order and the incident intensity of the probe beam), and d is the thickness of the nanocomposite layer.

9.2.2.4 Determination of nanocomposite layer thickness

The thickness of the nanocomposite layers was determined from the measurement of the angular selectivity of the recorded gratings. The angular selectivity curve was measured at 633 nm by scanning a range of angles of incidence with maximum deviation of ± 3^0

from the Bragg angle. The thickness of the grating, d, was calculated by applying eqn. 9.3 [31]:

$$d = \frac{\left(1 - \frac{\Phi^2}{\pi^2}\right)^{1/2}}{f \cdot \Delta\theta} \times \left(\frac{4n_{av}^{\;2} - \lambda^2 f^2}{4 - \lambda^2 f^2}\right)^{1/2} \tag{9.3}$$

where Φ is the phase difference between the two beams introduced by the diffraction grating, f is the spatial frequency of the grating (normally measured in lines/mm), $\Delta\theta$ is the angle between the central maximum and the first minimum determined from the measured Bragg curve, λ is the probe beam wavelength and n_{ave} is the average refractive index of the nanocomposite layer determined separately for each nanoparticle concentration. The phase difference Φ was calculated from the maximum achieved diffraction efficiency at the Bragg angle, η, for each nanoparticle concentration from eqn. 9.4:

$$\Phi = 2 * \sin^{-1}(\sqrt{\eta}) \tag{9.4}$$

9.3. Results

9.3.1 Characterisation of the BEA and BEA-Ag nanoparticles

The XRD spectra obtained for the BEA and BEA-Ag zeolites are shown in fig. 9.3. It is clear from the spectra that the crystalline structure of the BEA zeolites is preserved after the incorporation of the Ag nanoparticles, as both the position and width of the peaks are similar for the BEA and BEA-Ag samples. The characteristic peak of Ag is observable at 38° for BEA-Ag, verifying the formation of the Ag nanoparticles.
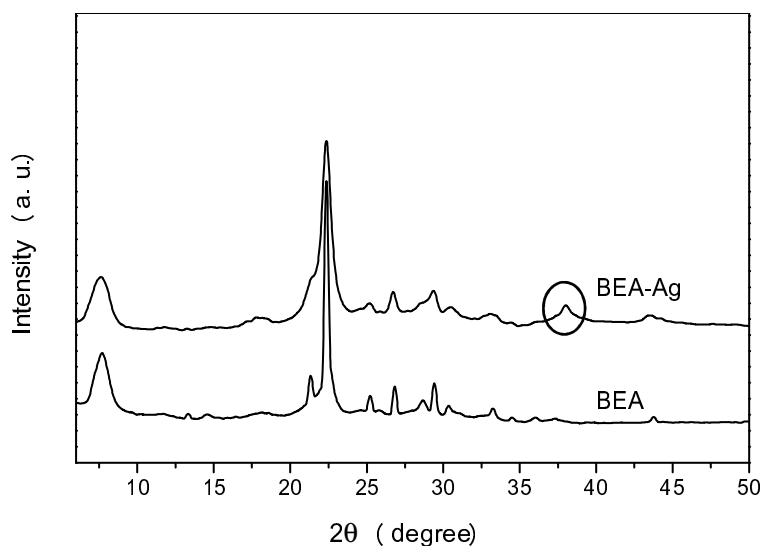
Fig. 9.3. XRD patterns of the BEA and BEA-Ag zeolite samples. The peak highlighted on the BEA-Ag spectrum corresponds to the 38° characteristic peak of the Ag nanoparticles.

The UV-Vis spectra of the BEA-Ag zeolites are shown in fig. 9.4(a). One absorption peak at 410 nm that corresponds to the Ag nanoparticles with nanometer size is present in the spectrum. This confirms that the entire amount of silver cations is reduced to silver metal. The plasmon band keeps a well-defined shape over a period of several weeks, indicating that the silver nanoparticles are stabilized in the BEA zeolite. The Ag^0 in zeolite Beta is found to be stable for more than one microsecond before beginning to aggregate, leading first to Ag_2^+ species in ~1.1 µs. The data suggest that the reduction of extra-framework Ag^+ arises only if the electron donor species are adsorbed on the zeolite particle surface or within the channels [32]. The presence of Ag^0 in the BEA crystals is confirmed by the HRTEM picture shown in fig. 9.4(b). Under high magnification, the zeolite nanoparticles show a high degree of crystallinity and well-

210

aligned crystalline fringes corresponding to the BEA zeolite. The Ag nanoparticles located in the channels of the zeolite crystals can be seen as well.

(a)   **(b)**
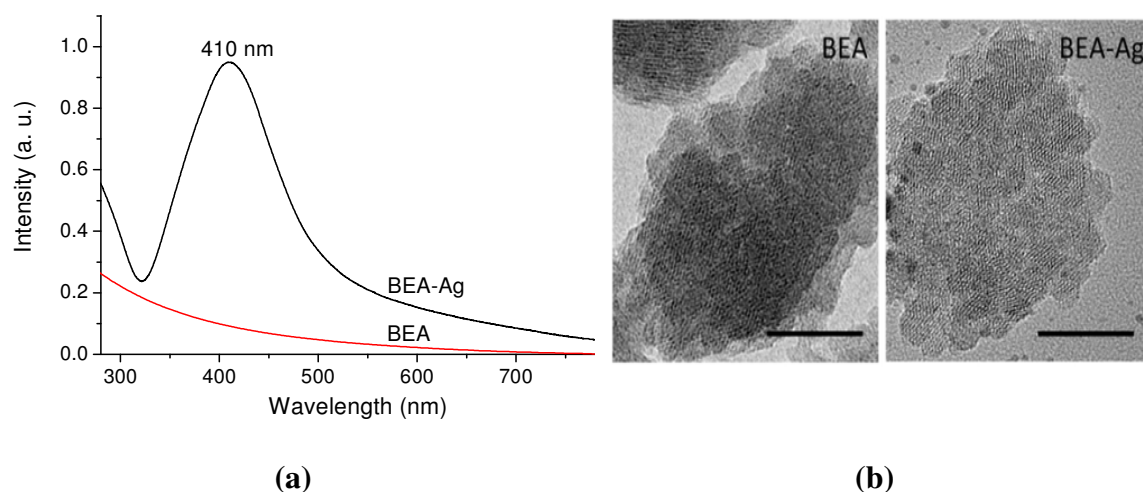
Fig. 9.4. (a) UV-Vis spectra and (b) TEM images of pure BEA and BEA-Ag suspensions. Scale bar of 20 nm.

The average diameter of the pure zeolite BEA and BEA-Ag nanoparticles measured using DLS was approximately 40-100 nm (fig. 9.5). The presence of a single peak confirms that the Ag nanoparticles are introduced in the channels of BEA zeolite, and no additional peak corresponding to pure Ag nanoparticles is measured. The average diameter of the pure BEA and BEA-Ag is very similar and does not change under ion-exchange and reduction treatments.
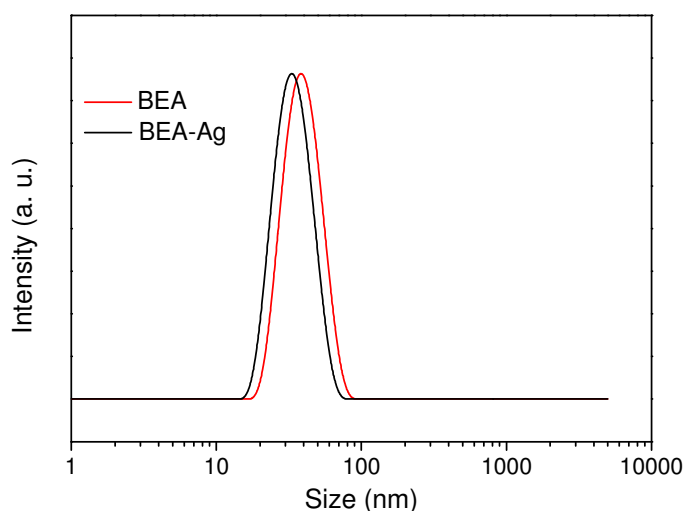
Fig. 9.5. DLS size distribution curve for the BEA and BEA-Ag zeolite nanoparticles in water suspensions.

9.3.2 Refractive index change with addition of nanoparticles

The measured values of *n* at a wavelength of 532 nm for the BEA and BEA-Ag doped DA photopolymer layers are presented in fig. 9.6 as a function of the zeolite concentration. It is seen that in both cases the incorporation of zeolites leads to the decrease of effective *n*, however the effect is significantly more pronounced for the BEA-doped photopolymer. The *n* of the BEA and BEA-Ag nanoparticles was estimated to be 1.299 and 1.443 respectively, compared to 1.500 for the undoped DA photopolymer. It worth noting that the refractive index of the BEA zeolite nanoparticles incorporated in DA photopolymer layers (1.299) is significantly lower than the one estimated for BEA nanoparticles incorporated in AA doped layers (1.456) [33]. This can be explained by the fact that the AA molecule is significantly smaller than the DA molecule and can enter the pores of the BEA zeolite nanoparticle, thus increasing their refractive index. Considering that the *n* of BEA zeolite is lower than that of the DA

212

photopolymer, it is expected that the effective *n* of the doped layers would decrease gradually with increasing concentration of the zeolite. It is seen that the influence of BEA-Ag doping on the effective n is weaker, compared to the BEA case.
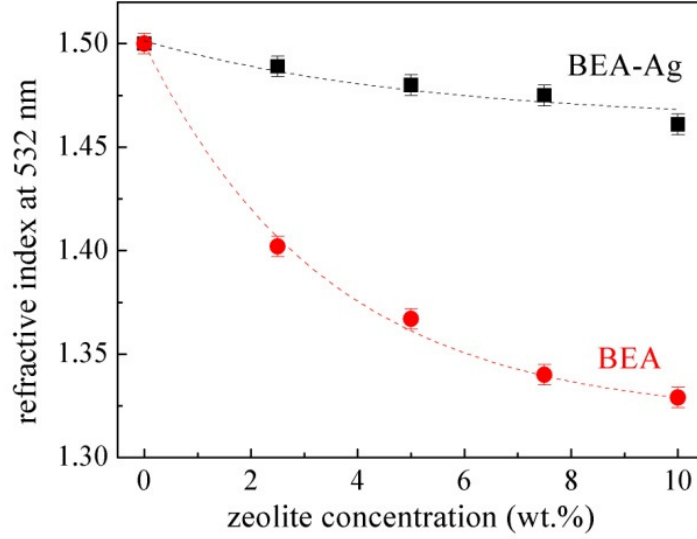
Fig. 9.6. *n* vs. zeolite concentration (wt. %) for the DA photopolymer doped with BEA-Ag (black) and BEA (red) nanoparticles.

9.3.3 Real time measurements of Δn and Bragg selectivity curves

The real time measurement of the Δn of the recorded gratings is shown in fig. 9.7(a) for the DA photopolymer layers doped with BEA nanoparticles. The respective Bragg selectivity curves are shown in fig. 9.7(b). Δn was calculated for each zeolite concentration as described in section 9.2.2.3, and the results of this are shown in fig. 9.7(a). The value of the parameter Δθ for each Bragg curve was determined from the data presented in fig. 9.7(b) and then used with eqn. 9.3 to determine the thickness of the grating.

(a)   **(b)**
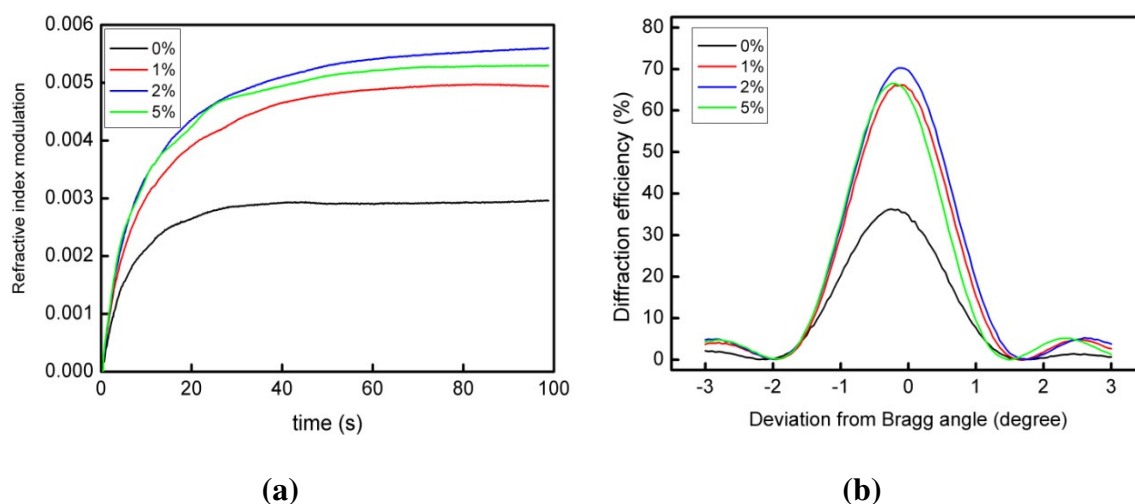
Fig. 9.7. Dependence of the a) real-time Δn and b) angular Bragg selectivity curves on BEA nanoparticle concentration.

9.3.4 Effect of nanoparticle concentration on Δn

Gratings were recorded in the nanocomposite layers as outlined in section 9.2.2.3. The concentration of nanoparticles in the photopolymer layers was increased from 0 - 5 wt. % for BEA, and 0 - 2 wt. % for BEA-Ag. Fig. 9.8 shows the Δn of the recorded gratings as a function of zeolite concentration. The BEA nanoparticles have a significant effect on the Δn of the DA photopolymer, causing an increase of up to 91 % in comparison to the un-doped layers at a concentration of 2 wt. %. For the BEA-Ag nanoparticles, a maximum increase in Δn of 17 % at a concentration of 0.5 wt. % is observed.
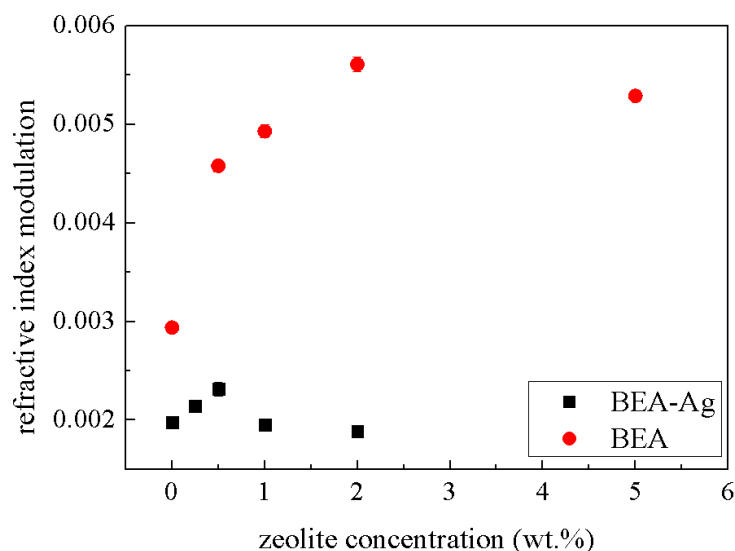
Fig. 9.8. Δn vs. zeolite concentration (wt.%) for the DA photopolymer doped with BEA-Ag (black) and BEA (red) nanoparticles.

9.4 Discussion

9.4.1 Effect of nanoparticles on refractive index

As outlined in section 9.3.2, the effect of increasing the concentration of the BEA nanoparticles on the effective n of the DA photopolymer is much more pronounced than for the BEA-Ag nanoparticles. Due to the Ag metal nanoparticles in the zeolite pores, the BEA-Ag zeolites have a higher n value of 1.443 compared to 1.299 for BEA, thus reflecting the smaller difference between the n values of the undoped photopolymer and the zeolite nanocrystals. In both cases the decrease of the average Δn is largely dependent on zeolite concentration.

The effective n of the DA-based nanocomposite is seen in fig. 9.6 to decrease from 1.50 to 1.33 as the concentration of BEA zeolites is increased from 0 - 10 wt. %. In a previous study the effect of the BEA zeolites on the effective n of the AA-based

photopolymer was investigated. For the AA-based nanocomposites n was seen to decrease from 1.5 to 1.47 only [26]. As discussed above, this could be attributed to the AA monomer molecules entering the zeolite pores and reducing the net change in n between the photopolymer and nanoparticles. In the DA photopolymer nanocomposite, the pores remain empty due to the increased monomer size, hence the larger change in n.

9.4.2 Effect of nanoparticles on Δn

As described in section 9.3.4, the BEA and BEA-Ag nanoparticles are shown to increase the Δn of the DA photopolymer at certain concentrations. The effect is much more significant in the case of the BEA nanoparticles, which are observed to increase the Δn of the nanocomposite layers by up to 91 % compared to the un-doped layers. This large improvement is due to the BEA pores remaining empty within the nanocomposite material, creating a large net change in n between photopolymer and dopant. Therefore, when the nanoparticles are redistributed during holographic recording, the Δn of the DA nanocomposite is significantly increased. For the BEA-Ag nanoparticles, a smaller increase in Δn is observed of 17 % compared to the un-doped layers. The reduced net change in n due to the addition of silver prevents higher Δn values from being achieved.

Using the estimated refractive indices for BEA (1.299) and BEA-Ag (1.443) nanoparticles, the background refractive index of the undoped photopolymer (1.500) and the measured maximum improvement of the Δn for the two compositions, the volume fraction of the redistributed nanoparticles for the optimum concentrations was estimated using eqn. 9.5 [4]:

$$\Delta n = \frac{2f_{nanodopants}}{\pi}\left(n_{nanodopant} - n_{host}\right)\sin(\alpha\pi) \qquad (9.5)$$

where $f_{nanodopants}$ is the volume fraction of nanoparticles in the nanoparticle-rich region, $n_{nanodopant}$ is the refractive index of the nanoparticles (dopants) and n_{host} is the refractive index of the host organic matrix. Assuming the light pattern has a single spatial period, α is the fraction of the period with a rich content of nanoparticles. If it is assumed that the nanoparticle rich region is half of the grating period it can be estimated that the redistributed volume fraction of nanoparticles is 2.3 % in the case of BEA doped layers and 1.1 % in the case of BEA-Ag doped layers. The density of empty BEA nanoparticles (1.45 g/cm^3) [33] can be used to estimate the volume fraction of BEA zeolite nanoparticles in the layer. It was found to be 5.3 % of the total volume of the layer. Thus in the BEA doped layer approximately 43 % of the nanoparticles are redistributed when a maximum improvement of the Δn is achieved. At this stage no estimate of the density of the BEA-Ag nanoparticles is available and therefore it is not possible to give an estimate of the volume fraction of redistributed particles in this case.

An optimum zeolite concentration is observed for both the BEA and BEA-Ag nanoparticles, namely 2 wt. % and 0.5 wt. % respectively. This suggests that at a certain concentration, the proportion of zeolite nanoparticles which are redistributed within the grating during holographic recording is at a maximum. Therefore, at this concentration the effect of the nanoparticles on Δn of the final grating is strongest. As the nanoparticle concentration is increased beyond this, the proportion of the nanoparticles that redistribute is reduced, and therefore the overall effect on Δn is weaker. For the BEA-Ag nanoparticles, a concentration of 0.5 wt. % is shown to be optimum, compared to 2 wt. % for BEA. It is most likely that a lower concentration is optimum for the BEA-Ag than for the BEA nanoparticles due to the incorporation of silver in the zeolite pores.

This added metal will increase the density of the BEA-Ag zeolites, thereby reducing their mobility within the photopolymer layer during recording. Increasing the concentration of the BEA-Ag zeolites will therefore only reduce the proportion of zeolite nanoparticles which are redistributed. Another important reason for the presence of optimum nanoparticle concentration could be related to the fact that the introduction of nanoparticles increases the optical scattering of the nanocomposite material. This leads to increased polymerisation in the dark fringes and a decrease in the achieved Δn. This effect becomes particularly important at higher nanoparticle concentrations.

9.5 Conclusions

The effect of BEA and BEA-Ag zeolite nanoparticles on the optical properties of a DA-based holographic photopolymer has been investigated for the first time. An optimum zeolite concentration is observed for both the BEA and BEA-Ag nanoparticles. It is observed that doping of the DA photopolymer with BEA zeolites results in a significant increase in Δn of up to 91 % at a concentration of 2 wt. % compared to un-doped layers. For the BEA-Ag zeolites, a maximum increase in Δn of up to 17 % at a concentration of 0.5 wt. % is measured. In both cases, the improvement in Δn is largely dependent on zeolite concentration.

The increase in Δn is due to the zeolite redistribution which results in different concentrations of particles in bright and dark fringe regions, therefore resulting in different n values for both areas. As a result, the effect of the BEA nanoparticles on the effective n of the DA photopolymer is much more pronounced than for the BEA-Ag nanoparticles, due to the stronger dependence of n on nanoparticle concentration.

It was demonstrated that the DA photopolymer is compatible as a host material for the porous BEA nanoparticles. This is due to the large size of the DA monomer molecules which restricts monomer migration into the zeolite pores and thus the pores of the BEA nanoparticles remain empty. This suggests that the DA-based nanocomposite material is suitable for application as a holographic gas sensor.

References:

[1] P. W. Oliveira, H. Krug, P. Muller, H.Schmidt, "Fabrication of GRIN-materials by photopolymerisation of diffusion-controlled organic-inorganic nanocomposite materials", MRS Proc. 435, doi:10.1557/PROC-435-553 (1996).

[2] E. Leite, "Photopolymerizable Nanocomposites for Holographic Applications", Doctoral Thesis, Dublin Institute of Technology, 2010 http://arrow.dit.ie/sciendoc/95/ .

[3] N. Suzuki, Y. Tomita, "Holographic scattering in SiO2 nanoparticle-dispersed photopolymer films", Appl. Opt. 46(27), 6809-14 (2007).

[4] R. Vaia, C. Dennis, L. Natarajan, V. Tondiglia, D. Tomlin, T. Bunning, "One-Step, Micrometer-Scale Organization of Nano-and Mesoparticles Using Holographic Photopolymerization: A Generic Technique", Adv. Mat. 13, 1570 (2001).

[5] N. Suzuki, Y. Tomita, T. Kojima, "Holographic recording in TiO2 nanoparticle-dispersed methacrylate photopolymer films", Appl. Phys. Lett. 81, 4121 (2002).

[6] C. Sanchez, M. J. Escuti, C. van Heesch, C. W. M. Bastiaansen, D. J. Broer, J. Loos, R. Nussbaumer, "TiO2 nanoparticle-photopolymer holographic recording", Adv. Func. Mat. 15(10), 1623-1629 (2005).

[7] Y. Tomita, N. Suzuki, K. Chikama, "Holographic manipulation of nanoparticle distribution morphology in nanoparticle-dispersed photopolymers", Optics Letters 30(8), 839-841 (2005).

[8] N. Suzuki, Y. Tomita, "Silica-Nanoparticle-Dispersed Methacrylate Photopolymers with Net Diffraction Efficiency Near 100%", Applied Optics 43(10), 2125-2129 (2004).

[9] Y. Tomita, K. Chikama, Y. Nohara, N. Suzuki, K. Furushima, Y. Endoh, "Two-dimensional imaging of atomic distribution morphology created by holographically induced mass transfer of monomer molecules and nanoparticles in a silica-nanoparticle-dispersed photopolymer film", Optics Letters 31(10), 1402-1404 (2006).

[10] Y. Tomita, T. Nakamura, A. Tago, "Improved thermal stability of volume holograms recorded in nanoparticle–polymer composite films", Opt. Lett. 33(15), 1750-1752 (2008).

[11] L. M. Goldenberg, O. V. Sakhno, T. N. Smirnova, P. Helliwell, V. Chechik, J. Stumpe, "Holographic composites with gold nanoparticles: nanoparticles promote polymer segregation", Chem. Mater. 20(14), 4619–4627 (2008).

[12] X. Xue, F. Hai, L. Gao, F. He, C. Li, Y. Li, M. Huang, "Effect of nanoparticle diameter on the holographic properties of gold nanoparticle dispersed acrylate photopolymer films", Optik - International Journal for Light and Electron Optics, 124(24), 6987–6990 (2013).

[13] L. Balan, R. Schneider, D. J. Lougnot, "A new and convenient route to polyacrylate/silver nanocomposites by light-induced cross-linking polymerization", Progress in Organic Coatings 62(3), 351–357, (2008).

[14] L. Balan, C. Turck, O. Soppera, L. Vidal, D. J. Lougnot, "Holographic recording with polymer nanocomposites containing silver nanoparticles photogenerated in situ by the interference pattern", Chem. Mater. 21(24), 5711–5718 (2009).

[15] L. Balan, J. P. Malval, R. Schneider, D. Le Nouen, D. J. Lougnot, "In-situ fabrication of polyacrylate–silver nanocomposite through photoinduced tandem reactions involving eosin dye", Polymer 51(6), 1363–1369 (2010).

[16] V. Pramitha, K. P. Nimmi, N. V. Subramanyan, R. Joseph, K. Sreekumar, C. S. Kartha, "Silver-doped photopolymer media for holographic recording", Applied Optics 48(12), 2255-2261 (2009).

[17] X. Liu, Y. Tomita, J. Oshima, K. Chikama, K.Matsubara, T. Nakashima, T. Kawai, "Holographic assembly of semiconductor CdSe quantum dots in polymer for volume Bragg grating structures with diffraction efficiency near 100%", Appl. Phys. Lett. 95(26), 2611091-2611093 (2009).

[18] G. G. Goourey, P. de Sainte Claire, L. Balan, Y. Israëli, "Acrylate photopolymer doped with ZnO nanoparticles: an interesting candidate for photo-patterning applications", J. Mat. Chem. C 1(21), 3430-3438 (2013).

[19] I. Naydenova, E. Leite, T. Babeva, N. Pandey, T. Baron, T. Yovcheva, S. Sainov, S. Martin, S. Mintova, V. Toal, "Optical properties of photopolymerizable nanocomposites containing nanosized molecular sieves", J. Opt. 13(4), 1-10 (2011).

[20] A. M. Ostrowski, I. Naydenova, V. Toal, "Light-induced redistribution of Si-MFI zeolite nanoparticles in acrylamide-based photopolymer holographic gratings", J. Opt. A: Pure Appl. Opt. 11, 034004 (2009).

[21] E. Leite, I. Naydenova, S. Mintova, L. Leclercq, V. Toal, "Photopolymerizable nanocomposites for holographic recording and sensor applications", Appl. Opt. 49(19), 3652-3660 (2010).

[22] E. Leite, T. Babeva, E. P. Ng, V. Toal, S. Mintova, I. Naydenova, "Optical properties of photopolymer layers doped with aluminophosphate nanocrystals", J. Phys. Chem. C, 114(39), 16767–16775 (2010).

[23] M. Moothanchery, I. Naydenova, S. Mintova. V. Toal, "Nanozeolite doped photopolymer layers with reduced shrinkage", Opt. Express 19(25), 25786-25791 (2011).

[24] M. Moothanchery, "Studies of shrinkage in photopolymerisable materials for holographic applications", Doctoral Thesis, Dublin Institute of Technology, 2013.

[25] H.J. Coufal, D. Psaltis, G.T. Sincerbox, "Holographic Data Storage", Springer Series in Optical Sciences, Springer-Verlag, Berlin, 2000.

[26] E. Leite, I. Naydenova, N. Pandey, T. Babeva, G. Majano, S. Mintova, V. Toal, "Investigation of the light induced redistribution of zeolite Beta nanoparticles in an acrylamide-based photopolymer", J. Opt. A: Pure Appl. Opt. 11, 024016 (2009).

[27] T. Babeva, S. Kitova, I. Konstantinov, "Photometric methods for determining the optical constants and the thicknesses of thin absorbing films: selection of a combination of photometric quantities on the basis of error analysis", Appl. Opt. 40, 2682-2686 (2001).

[28] W. Press, S. Teukolsky, W. Veterling, 1992 Numerical recipes in C (Cambridge University Press, 1992), Chap. 10, 408-410.

[29] T. Babeva, R. Todorov, S. Mintova, T. Yovcheva, I. Naydenova, V Toal, "Optical properties of silicia-MFI doped acrylamide photopolymer", J. Opt. A: Pure Appl. Opt. 11, 024015 (2009).

[30] H. Kogelnik, "Coupled wave theory for thick hologram gratings", Bell Syst. Tech. J. 48(9), 2909-2947 (1969).

[31] I. Ciapurin, L. Glebov, V. Smirnov, "Modeling of phase volume diffractive gratings, part 1: Transmitting sinusoidal uniform gratings" Opt. Eng. 45, 015802 (2006).

[32] F. Luchez, Z. Tahri, V. De Waele, I. Yordanov, S. Mintova, A. Moissette, M. Mostafavi, O. Poizat, "Photoreduction of Ag+ by Diethylaniline in colloidal zeolite nanocrystal", Micropor. Mesopor. Mater. (2014).

[33] I. Naydenova, E. Leite, T. Babeva, N. Pandey, T. Baron, T. Yovcheva, S. Sainov, S. Martin, S. Mintova, V. Toal, "Optical properties of photopolymerizable nanocomposites containing nanosized molecular sieves", J. Opt. 13 (4), 1-10 (2011).

10. INVESTIGATION OF THE GAS SENSING ABILITY OF ZEOLITE-DOPED DA PHOTOPOLYMER HOLOGRAPHIC GRATINGS

10.1 Introduction

In recent years, the development of chemical and gas sensors has expanded into a huge field, both in terms of financial investment and the volume of researchers [1-7]. This can partly be explained by the increasing legislative demands placed on industry and employers to effectively monitor levels of potentially hazardous or toxic gases in the workplace. The level of toxic fumes from waste products must also be monitored in order to minimise damage to the environment. The global market for gas sensors is expected to reach $2,512.4 million by 2020, according to a market report by Grand View Research Inc., driven largely by new regulatory initiatives [7]. The range of fields that require gas sensing technologies is large and varied, incorporating areas such as the process and petrochemical industries, atmospheric monitoring, and breath diagnostics. A breakdown of the different gases for which sensors are most in demand is shown in fig. 10.1, taken from the report by Grand View Research Inc. [7]. "Other" sensors primarily comprise methane (CH_4), ammonia (NH_3), hydrogen, and hydrocarbon sensors.

An Optical Sensor is a device in which modifications or modulations to some characteristic of light incident on the device which occur due to an external influence can be observed and quantified. Optical sensors have advantages over other sensor types such as semiconductor and electrochemical sensors due to their potential for fast response times and high gas specificity, as well as allowing for label-free, in-situ, real-time measurements [1].
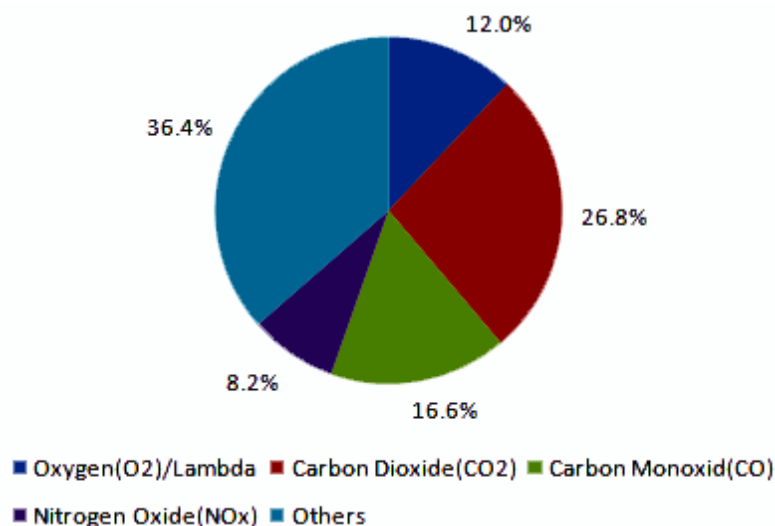
Fig. 10.1. Pie chart representation of the different gases for which sensors are most in demand. Image taken from Grand View Research Inc. Market Research Report entitled "Gas Sensors Market Analysis And Segment Forecasts To 2020" [7].

There are many different technologies under development for optical sensors, most of which are based on the principles of optical absorption, florescence, or chemiluminescence. Refractometric sensors, for which the resonant wavelength depends on changes in the refractive index of the surrounding medium, are another option with a lot of potential for sensing. One such device is the surface plasmon resonance (SPR)-based optical sensor. SPR sensors work on the principle that when excited, the surface plasmons present at a metal-dielectric interface change the refractive index of the dielectric. This in turn alters the propagation constant of the surface plasmons, which changes the resonance condition between the surface plasmons and the interacting optical wave. In this way, the SPR-based devices can be used as a sensor for gas molecules which excite the surface plasmons [8]. This technique has been incorporated

into optical fibres to produce sensors which are suitable for both aqueous and gas phase detection [9].

The use of holographic gratings as refractometric sensing devices for various different analytes has been reported. A holographic glucose sensor has been developed by Lowe *et al* [10]. Absorption of glucose by reflection gratings recorded in an AA-based hydrogel film results in swelling perpendicular to the plane of the polymer layer. The resultant change in periodicity of the reflection grating causes a shift in the reconstructed wavelength. This same principle has been adopted for the development of liquid-phase alcohol [11] and pH [12] sensors. Preliminary studies into the sensing ability of transmission gratings recorded in BEA- and MFI- type zeolite-doped AA photopolymer layers by Leite *et al* have been reported for the analytes Toluene [13] and Isopropanol [14]. Microporous aluminophosphate nanocrystals have also been incorporated into the AA photopolymer to develop an irreversible humidity sensor [15].

In this work, the ability of holographic transmission gratings recorded in the DA-based photopolymer to operate as refractometric gas sensors was studied. Both undoped samples and samples doped with BEA-structure zeolite nanoparticles were investigated. The zeolites provide adsorption sites for the gas molecules, and when redistributed within the grating, it is expected that their presence will increase the sensing ability of the photopolymer material.

For this study, alcohol gases were selected as the main test analyte. An alcohol is defined as an organic compound in which the hydroxyl functional group (-OH) is bound to a carbon atom. Alcohols are one of the most widely used groups of chemicals in research and industry, as they have important application as solvents and play an important role in the production of other chemicals. Alcohols are classified as a volatile

organic compound (VOC), which means they have a low boiling point and are highly reactive. There is evidence that certain alcohols such as methanol are toxic and even fatal to humans, in particular at high concentrations [16]. Therefore, it is easy to understand why the development of sensitive and selective alcohol sensors is of great interest. The detection of alcohol in its gaseous form allows for in-situ, real-time measurements to be carried out. The ability of the DA-based gratings to detect other hydrocarbon gases such as alkanes and CO_2 was also investigated.

10.2 Principle of operation of a holographic gas sensor

A holographic grating may act as a sensor when, under exposure to some analyte, a quantifiable change in the optical or holographic properties of the grating occurs. The use of the AA-based photopolymer as the material for a transmission-mode holographic humidity sensor has been demonstrated by Mikulchyk *et al* [17]. This device works under the principle that when the recorded un-slanted transmission grating is exposed to water vapour at increased relative humidity (up to 60 % RH) the water molecules absorbed by the grating cause the grating to swell. This causes the diffraction efficiency of the grating to increase. However, if the relative humidity is increased above 60 %, irreversible damage to the photopolymer layer is observed due to the large size of the water molecules which become trapped in the permeable polymer material.

A similar principle is in operation for the work reported here. Porous zeolite nanoparticles have been incorporated into the DA photopolymer and redistributed during holographic recording within the grating, as shown in fig. 10.2(a). The difference between the refractive index of the formed polymer chains in the bright fringe regions (n_b) and the refractive index of the nanoparticles in the dark fringe regions (n_d) is what

constitutes Δn. On exposure to a gaseous analyte, it is expected that the gas molecules will adsorb to the zeolite nanoparticles, causing n_d to increase. This will therefore reduce the overall Δn, as shown in fig. 10.2(b). By monitoring changes in Δn during gas exposure, gratings recorded in the zeolite-doped DA photopolymer can therefore be used as a sensing device.

The BEA-structure zeolites are a suitable dopant for gas sensing applications as they are large-pore nanoparticles [18]. As discussed in the chapter 9, the zeolite pores remain empty due to the large size of the DA monomer molecules. It is therefore possible for the gas molecules to be adsorbed inside the BEA zeolite pores (depending on the gas molecule size) as well as to the zeolite surface, potentially maximising the gas molecules' effect on Δn. The hydrophilic nature of the BEA zeolites ensures they are compatible with the water-soluble DA photopolymer also.

(a)   (b)
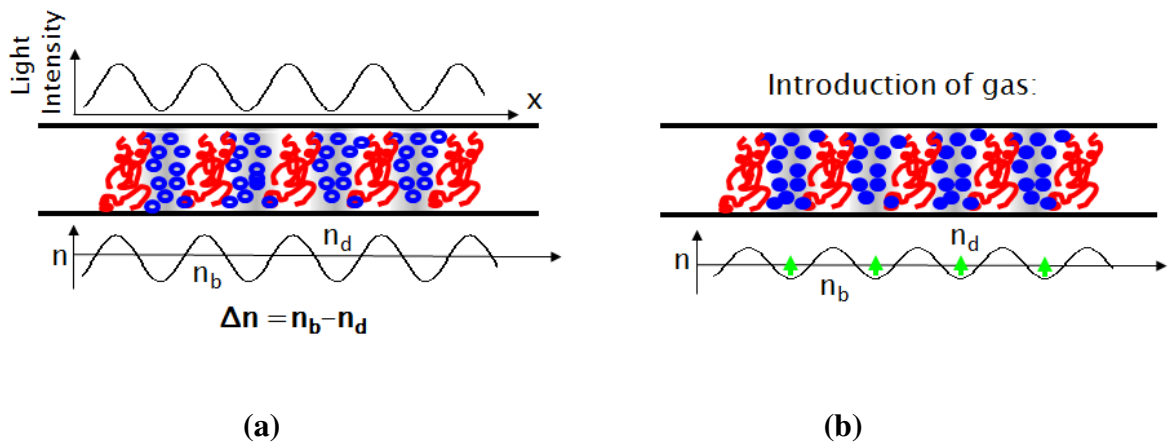
Fig. 10.2. Schematic diagram showing (a) the redistribution of nanoparticles (blue) and polymer chains (red) within the holographic grating and (b) the effect of gas molecules on Δn of the grating.

10.3 Experimental

10.3.1 Materials

38 ± 3 µm thick DA photopolymer layers were prepared containing BEA zeolite concentrations of 0 and 2 wt. % as described in section 9.2.1.2. Transmission gratings were recorded using a 532 nm YAG laser at a spatial frequency of 1000 l/mm as described in section 9.2.1.3. The gratings were then fully bleached after recording using a UV lamp.

10.3.2 Methods

The experimental setup used to investigate the gas sensing ability of the holographic gratings is shown in fig. 10.3. A cylindrical glass tube was used as the gas exposure unit. This exposure unit was connected to both a primary and secondary vacuum, to allow for evacuation of the tube down to pressures of 10^{-6} torr before exposure. In this way it was ensured that as few as possible contaminates or evaporated water molecules were present in the tube or grating before gas exposure which might affect the sensing response data. The holographic grating was placed inside the exposure unit which was then evacuated for 30 minutes before exposure. A 200 µm core UV-Vis optical fibre connected to an Avantes AvaLight-Hal-S white light source was used to illuminate the grating inside the tube. A lens was connected to the fibre to collimate the incident light on to the grating. The spectrum of light diffracted by the grating was then coupled to an Avantes AvaSpec 2048-2 spectrometer using a 400 µm core UV-Vis optical fibre. AvaSoft software v. 7.4 was used to monitor changes to the diffracted spectrum in real-time before, during and after gas exposure. Fig. 10.4 shows an example of the change in

the spectrum of a 2 wt. % zeolite-doped grating exposed to isopropanol gas. The peak

intensity is observed to decrease with increasing exposure time.
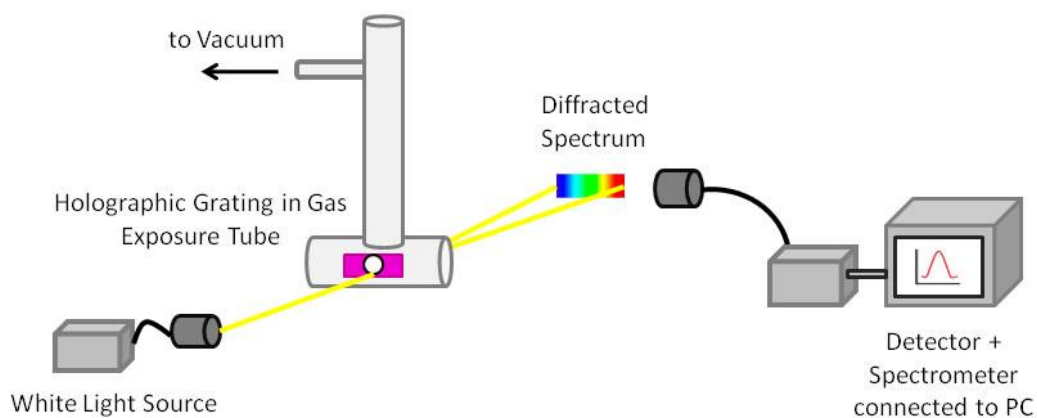
Fig. 10.3. Experimental setup for investigating the gas sensing ability of the DA-based

holographic transmission gratings.

(a)   (b)
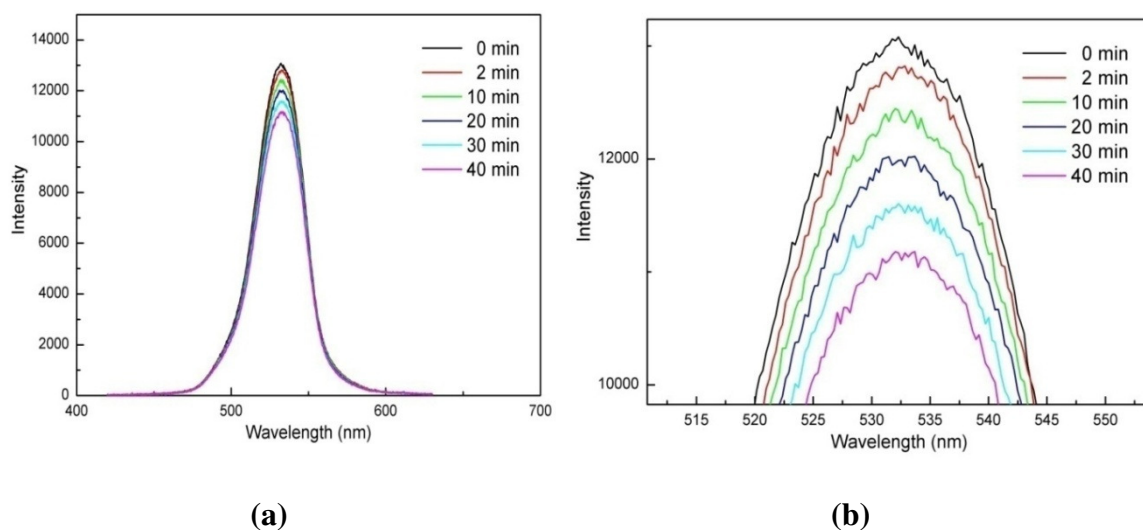
Fig. 10.4. (a) Intensity vs. wavelength (nm) for a 2 wt. % zeolite-doped grating exposed

to isopropanol gas for increasing exposure times, (b) close up of spectra maxima.

10.4 Results and Discussion

For each test analyte, the sensing ability of gratings recorded in the DA photopolymer doped with 0 and 2 wt. % zeolites was investigated. In each case the normalised peak intensity of the diffracted spectrum was plotted against gas exposure time for a gas pressure of 16 torr to allow for comparison of the different gases tested. Depending on the size of the test gas molecule, higher gas pressures were investigated when possible also.

10.4.1 Sensing study for Alcohol gases

The sensing ability of gratings recorded in the DA photopolymer doped with 0 and 2 wt. % zeolites was investigated for three different alcohols, namely Methanol, Isopropanol and 2-Methylpropan-2-ol. These three alcohol molecules were selected due to their differing structural and physical properties, which are outlined in table 10.1. The chemical structures of the test molecules are shown in fig. 10.5. From their comparison it is possible to extract some information about how the adsorption of the gas molecules within the holographic grating depends on the molecular size and structure of the adsorbing molecule.

Table 10.1 Physical properties of Methanol, Isopropanol and 2-Methylpropan-2-ol

	Alcohol Classification	Molecular Weight (g/mol)	Refractive Index	Relative Polarity [19]
Methanol (CH_4O)	1°	32.0	1.329	0.762
Isopropanol (C_3H_8O)	2°	60.1	1.377	0.546
2-Methylpropan-2-ol ($C_4H_{10}O$)	3°	74.1	1.387	0.389

231
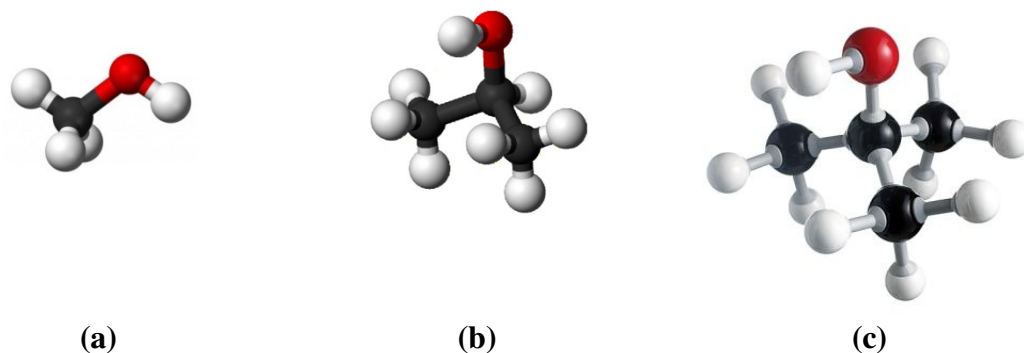
Fig. 10.5. 3D representation of the chemical structures of (a) methanol, (b) isopropanol, and (c) 2-methylpropan-2-ol.

10.4.1.1 Methanol

For methanol, 0 and 2 wt. % doped samples were exposed to gas pressures of 16 and 32 torr. Fig. 10.6 shows the normalised peak intensity of the diffracted spectrum as a function of exposure time for the 16 and 32 torr exposures.

For the 16 torr exposure in fig. 10.6(a), the normalised intensity of the 0 wt. % doped sample is observed to decrease by a small amount, approximately 3 %. In contrast, the 2 wt. % sample initially decreases by 5 %, but the normalised intensity is then seen to increase, with a net increase of 2 % compared to its initial value. As the gas pressure is increased to 32 torr (shown in fig. 10.6(b)), the effect of the gas becomes more pronounced. For both samples the normalised intensity is seen to increase. For the 2 wt. % sample this increase is highest at 8 %, compared to 4 % for the 0 wt. % sample.

Fig. 10.7 shows the effect of gas exposure on a 2 wt. % doped sample for methanol gas pressures of 16, 32, 50 and 70 torr. These gas pressures correspond to concentration values in parts per million (ppm) of 21053, 42105, 65789 and 92105 ppm respectively,

however for convenience the data is expressed in units of torr. For the highest gas pressure of 70 torr, a significant increase is observed in normalised intensity of up to 50 %. For both the 0 and 2 wt. % doped samples, the effect of the methanol gas on the grating was fully reversed on the removal of the gas.

(a)   (b)
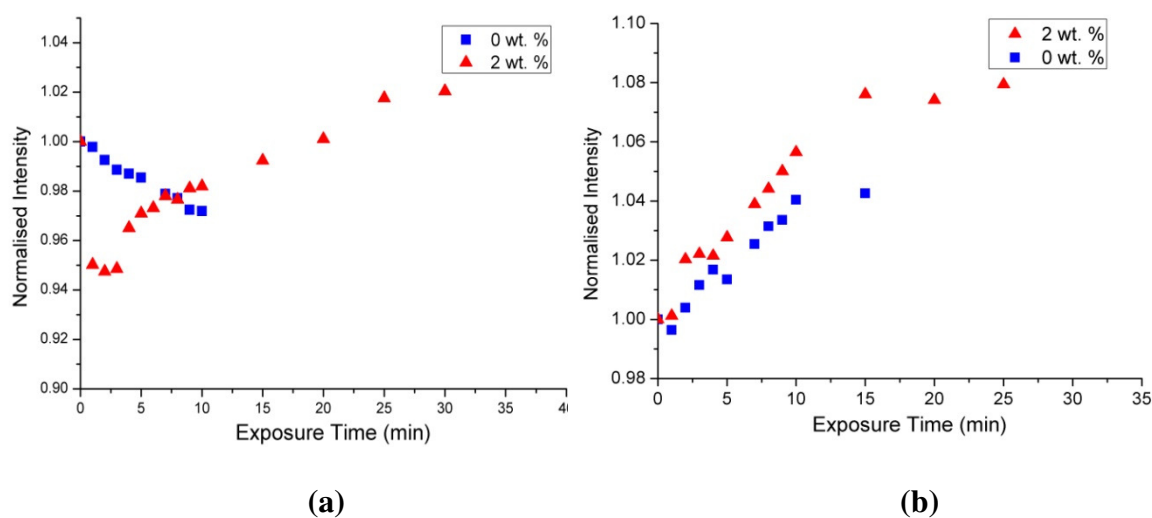
Fig. 10.6. Normalised intensity vs. exposure time (s) for 0 and 2 wt. % zeolite-doped grating exposed to methanol at gas pressure of (a) 16 torr and (b) 32 torr.
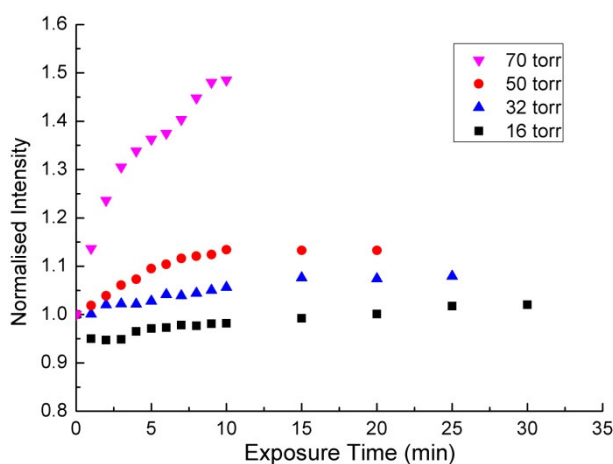
Fig. 10.7. Normalised intensity vs. exposure time (s) for a 2 wt. % zeolite-doped grating exposed to methanol at gas pressures of 16, 32, 50 and 70 torr.

10.4.1.2 Isopropanol

For isopropanol, 0 and 2 wt. % doped samples were exposed to gas pressures of 16 and 32 torr. Fig. 10.8 shows the normalised peak intensity of the diffracted spectrum as a function of exposure time for the 16 and 32 torr exposures. At gas pressures greater than this, irreversible damage to the optical quality of the photopolymer layers was observed, in particular for the zeolite-doped samples due to the increased volume of sites for adsorption.

For the 16 torr exposure to isopropanol, the normalised intensity for the 0 wt. % doped gratings is roughly constant. A decrease of 8 % in normalised intensity is observed however for the 2 wt. % doped sample. As the gas pressure is increased to 32 torr, the effect of isopropanol on the gratings becomes more pronounced. A decrease of 15 % in normalised intensity is observed for the 2 wt. % doped sample. Once again, the normalised intensity for the 0 wt. % doped sample remains approximately constant.

As was observed for methanol, the effect of isopropanol on the normalised intensity was fully reversed on the removal of the gas.
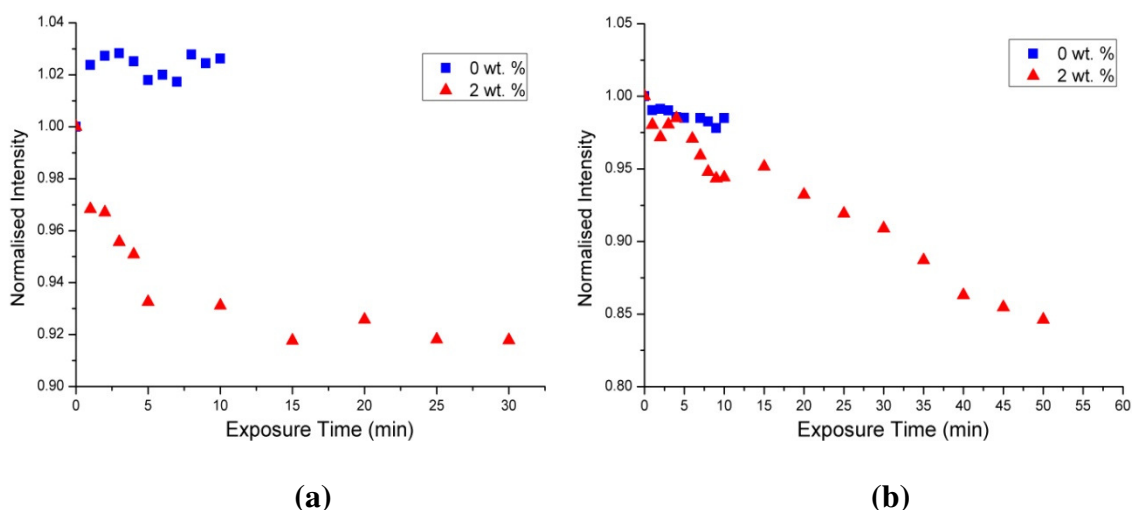
Fig. 10.8. Normalised intensity vs. exposure time (s) for 0 and 2 wt. % zeolite-doped grating exposed to isopropanol at gas pressure of (a) 16 torr and (b) 32 torr.

10.4.1.3 2-Methylpropan-2-ol

For 2-methylpropan-2-ol, 0 and 2 wt. % doped samples were exposed to gas pressures of 16 torr. Fig. 10.9 shows the normalised peak intensity of the diffracted spectrum as a function of exposure time for the 16 torr exposure. At gas pressures greater than 16 torr, irreversible damage to the optical quality of the photopolymer layers was observed.

For both the 0 and 2 wt. % samples, there is an initial drop in normalised intensity of 5 % during the first two minutes, and then a further decrease of 1-2 % over the next 10-15 minutes of exposure.

The effect of the 2-methylpropan-2-ol gas on the grating was reversible upon removal of the gas in the case of both the doped and undoped samples.

Fig. 10.9. Normalised intensity vs. exposure time (s) for 0 and 2 wt. % zeolite-doped grating exposed to 2-methlypropan-2-ol at gas pressure of 16 torr.

10.4.1.4 Discussion

The data for the normalised intensity vs. exposure time is compared for the three gases, methanol, isopropanol and 2-methylpropan-2-ol, for both the 0 and 2 wt. % doped samples exposed to a gas pressure 16 torr. The net change in normalised intensity for both the 0 and 2 wt. % doped samples for all three gases is shown in table 10.2, and the comparison data is also displayed below in fig. 10.10.

Table 10.2. Net change in normalised intensity due to gas exposure at 16 torr			
Zeolite Concentration (wt. %)	Methanol	Isopropanol	2-Methylpropan-2-ol
0	- 2 %	+ 2 %	-5 %
2	+ 2 %	- 5 %	- 8 %

For the 0 wt. % doped gratings, there is only a limited effect at this low gas pressure for all three alcohol gases. For 2-methylpropan-2-ol, the largest change is observed, with the normalised intensity decreasing by 5 %.

For the 2 wt. % doped gratings, there is a more significant change in normalised intensity on exposure to the three gases. For isopropanol and 2-methylpropan-2-ol, decreases in normalised intensity of 5 and 8 % are observed respectively. For methanol, the intensity is initially observed to drop by 5 % after 3 minutes of exposure; however, the intensity then begins to increase, eventually exceeding the initially intensity by 2 %.

The same trend of decreasing normalised intensity with increasing exposure time was observed for both the isopropanol and 2-methylpropan-2-ol gases for the zeolite-doped gratings. For both gases, only a limited effect on the undoped grating was observed. The observed data matches the predicted effect of the gas on the zeolite-doped grating; gas molecules are adsorbed to the porous zeolite nanoparticles which are redistributed within the grating. This adsorption will cause the refractive index of the nanoparticles, and therefore the region of the grating within which they are located (the dark fringe regions), to increase. An increase in the refractive index of the dark fringe regions (n_d) will result in a decrease in the overall Δn of the grating, therefore decreasing the intensity of light diffracted by the grating. When no zeolite nanoparticles are present, as in the case of the undoped sample, the gas can have a limited effect only on the Δn due to the lack of adsorption sites.

In the case of methanol, the smallest gas molecule tested, a surprising result was observed. At 16 torr, the normalised intensity began to increase after 3 minutes of gas exposure for the 2 wt. % doped samples. As the gas pressure was increased above 16 torr, increases in normalised intensity due to methanol exposure were observed for both

the undoped and doped gratings, as shown previously in figs. 10.6 and 10.7. This is the opposite of the trend observed for isopropanol and 2-methylpropan-2-ol. This result implies that the Δn of the holographic grating is increasing during gas exposure. Adsorption of the gas molecules to the zeolites redistributed within the grating will cause their refractive index to increase and have the opposite effect on Δn, therefore some second process must be occurring simultaneously. This second process must also be independent of the zeolite nanoparticles, as an increase of 4 % in normalised intensity was observed for the undoped grating also at the higher gas pressure of 32 torr; however, a larger increase of 6 % was observed for the zeolite-doped sample, implying that the inclusions of zeolites may assist the effect of methanol on the gratings.

One possible explanation is that the small size combined with the high polarity of the methanol molecule allows it to freely enter the pores of the permeable DA polymer which is mainly present in the bright fringe regions, as shown in fig. 10.11. By doing so, the refractive index in the bright fringe regions (n_b) will be increased. If this increase in n_b is larger in relation to the increase in n_d due to adsorption of the methanol molecules to the zeolites when they are present, then the overall Δn will increase, as is the case here. The isopropanol and 2-methylpropan-2-ol molecules have relatively lower polarity which restricts them entering the DA polymer pores in the bright fringe regions, and so no such increase in Δn is observed in their case. Due to the high amount of methanol adsorbed, a swelling of the photopolymer layer doped with zeolite crystals is expected. The more polar molecule such as methanol (0.762) is more reactive in comparison to isopropanol (0.546) and 2-methylpropan-2-ol (0.389), and thus higher swelling of the layer is expected in the presence of methanol.

For all three gases, the effect of the gas molecules on the holographic gratings was fully reversible. This implies that the gas molecules can readily enter and exit the polymer matrix as well as the zeolites.

(a)   (b)
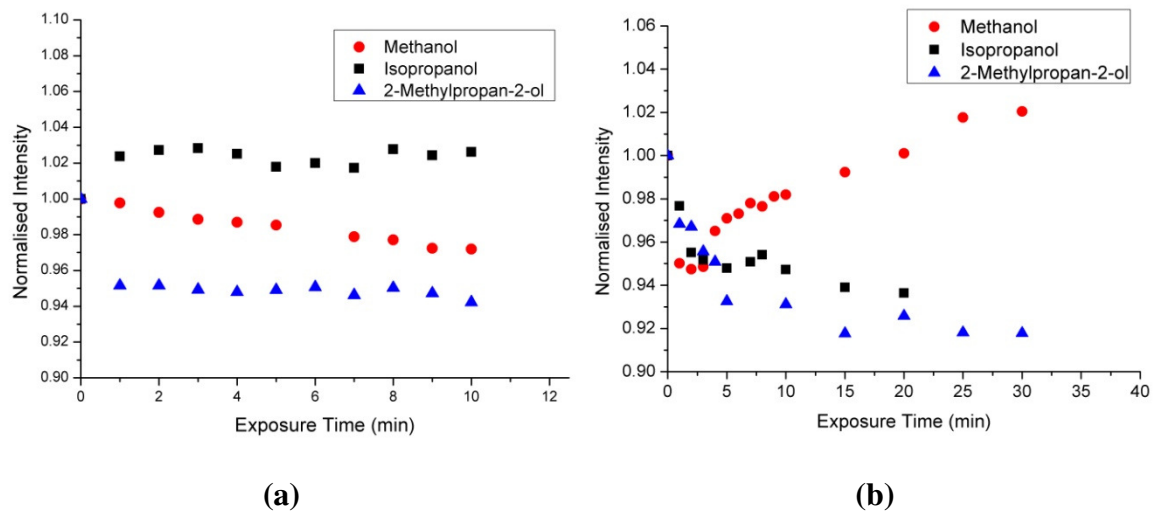
Fig. 10.10. Normalised intensity vs. exposure time (s) for a (a) 0 wt. % and (b) 2 wt. % zeolite-doped grating exposed to methanol, isopropanol and 2-methlypropan-2-ol at a gas pressure of 16 torr.
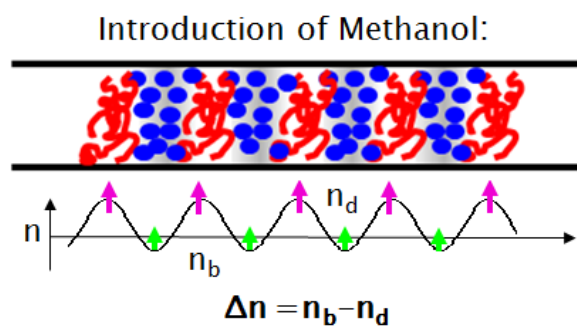
Fig. 10.11. Schematic diagram showing the effect of methanol gas molecules on Δn of the grating.

10.4.2 Sensing study for Alkane gases

The sensing ability of a 2 wt. % zeolite-doped grating recorded in the DA photopolymer was investigated for two different alkanes, Pentane and Cyclohexane. Alkanes are saturated hydrocarbons which unlike alcohols have no -OH group attached to them. As with alcohols, alkanes are widely used as solvents and in the production of other chemicals. The structural and physical properties of the two alkane test molecules are outlined in table 10.3, and the chemical structure of pentane and cyclohexane are shown in fig. 10.12.

Table 10.3 Physical properties of Pentane and Cyclohexane

	Alkane Structure	Molecular Weight (g/mol)	Refractive Index	Relative Polarity [19]
Pentane(C_5H_{12})	unbranched	72.2	1.358	0.009
Cyclohexane (C_6H_{12})	Cyclic (6-vertex ring)	84.2	1.427	0.006

(a)   (b)
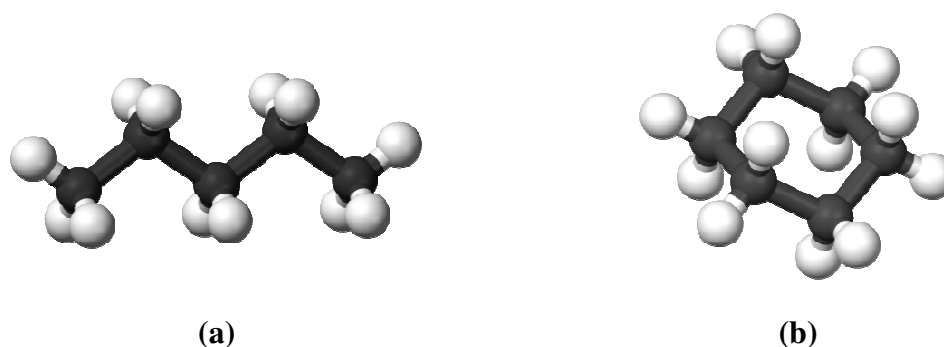
Fig. 10.12. 3D representation of the chemical structures of (a) pentane and (b) cyclohexane.

10.4.2.1 Pentane

A 2 wt. % doped grating was exposed to pentane at gas pressures of 16 and 32 torr, the results of which are shown in fig. 10.13. For the 16 torr exposure, the normalised intensity is approximately constant, showing little to no response of the grating to the pentane gas. For the 32 torr exposure, a decrease in normalised intensity of 6.5 % is observed after 20 minutes of exposure. The effect of pentane on normalised intensity was not reversed upon removal of the gas.
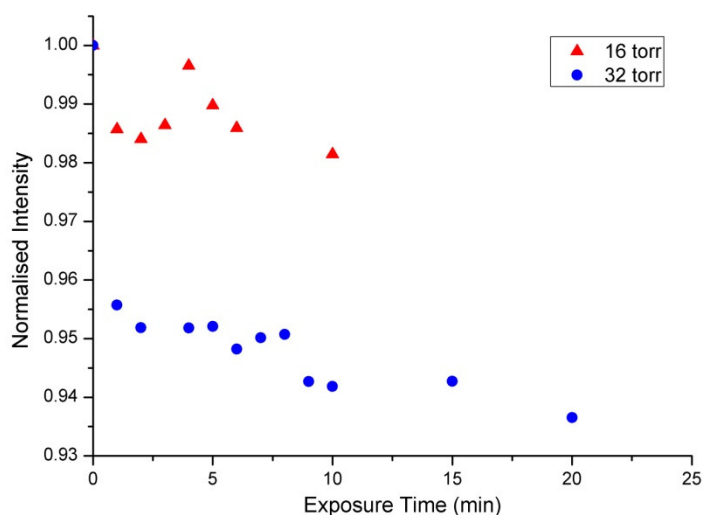
Fig. 10.13. Normalised intensity vs. exposure time (s) for a 2 wt. % zeolite-doped grating exposed to pentane at gas pressures of 16 and 32 torr.

10.4.2.2 Cyclohexane

A 2 wt. % doped grating was exposed to cyclohexane at gas pressures of 16 and 32 torr, the results of which are shown in fig. 10.14. Both exposure pressures show approximately the same rate of decrease in normalised intensity. A decrease of 5 and 7 % was observed for the 16 and 32 torr exposures respectively. The effect of cyclohexane on normalised intensity was not reversed upon removal of the gas.
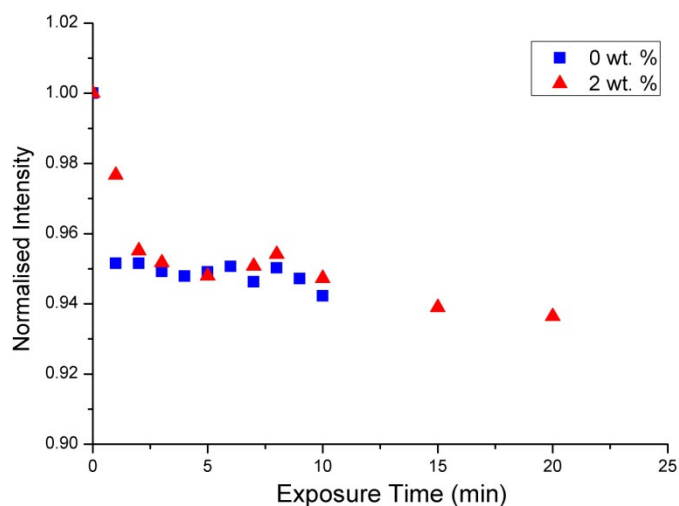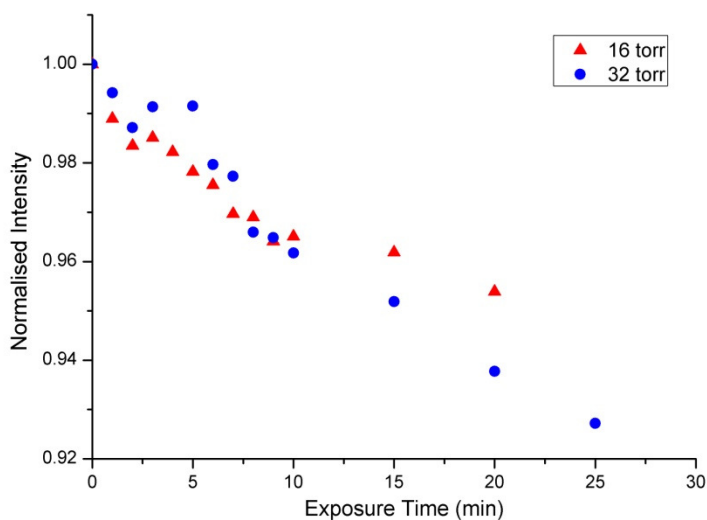
Fig. 10.14. Normalised intensity vs. exposure time (s) for a 2 wt. % zeolite-doped grating exposed to cyclohexane at gas pressures of 16 and 32 torr.

10.4.2.3 Discussion

For both pentane and cyclohexane, a decreasing trend in normalised intensity is observed during gas exposure. This suggests that the adsorption of both gases to the zeolite nanoparticles results in the refractive index contrast between the zeolites and the host photopolymer being reduced, thereby decreasing the overall Δn. The rate of decrease in normalised intensity at 32 torr is much faster for pentane that for cyclohexane (see fig. 10.15(a)). This is most likely due to the larger size and lower polarity of the cyclohexane molecule, and so therefore it is slower to penetrate the polymer structure and adsorb to the zeolites. Cyclohexane also has a stronger effect on the normalised intensity at both gas pressures than pentane, as shown in fig. 10.15. Its high refractive index of 1.427 is significantly closer to the refractive index of the DA polymer (1.500) than any of the previously tested gases; therefore, its reducing effect on Δn will be greater. Unlike for the alcohols, the effect of the alkane gases on the

holographic grating diffraction efficiency is not fully reversible on removal of the gas, which may be due to stronger adsorption to the zeolite surface, and difficulty in being removed due to their low polarity.

(a)   **(b)**
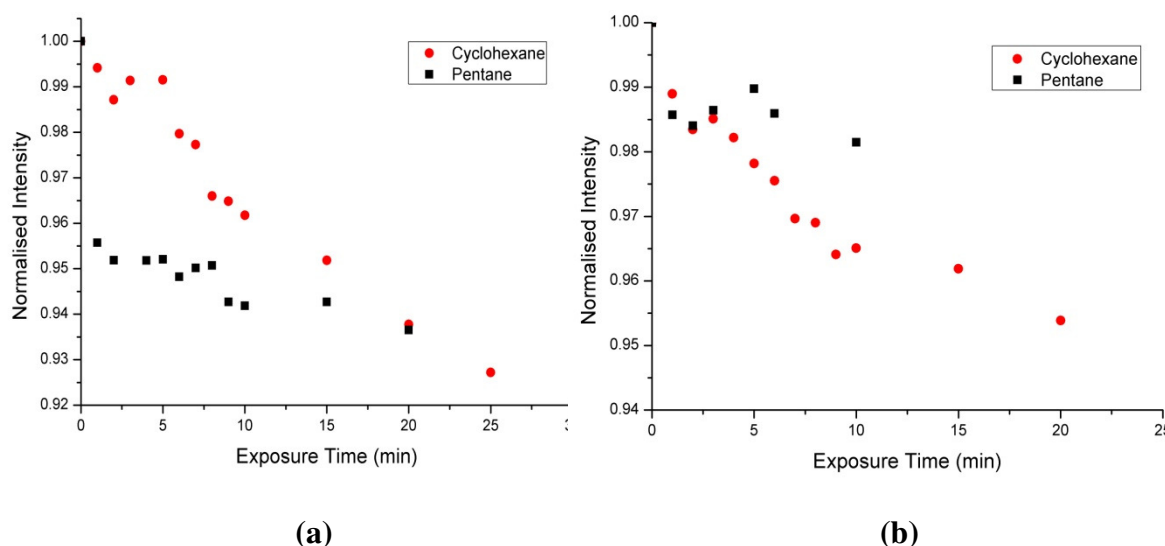
Fig. 10.15. Normalised intensity vs. exposure time (s) for a 2 wt. % zeolite-doped grating exposed to pentane and cyclohexane at a gas pressure of (a) 32 torr and (b) 16 torr.

10.4.2.4 Effect of pore size on Cyclohexane adsorption

A study of the effect of cyclohexane gas on the normalised intensity of a holographic grating recorded in the AA-based photopolymer was previously carried out. For this study, the AA photopolymer was doped with Si-MFI structure zeolite nanoparticles. Si-MFI nanoparticles have a medium pore size (5.5 Å), unlike the large-pore BEA zeolites (7.4 Å). When exposed to cyclohexane gas, no change in the normalised intensity of the AA-based grating doped with Si-MFI was observed. As seen above, in the case of the DA-photopolymer doped with BEA zeolites, a clear decrease in normalised intensity is

observed for two different pressures of cyclohexane gas. This supports the idea that there is a relationship between the size of the gas molecules that can be adsorbed, and the size of the zeolite nanoparticle pores.

10.4.3 Sensing study for CO_2

Carbon Dioxide (CO_2) is a naturally occurring gas, produced as a waste product during photosynthesis. It is present in the Earth's atmosphere at a concentration of 0.039 vol. % However, it is classified as an asphyxiant gas. At concentrations of 7 - 10 vol. % it may cause suffocation, even in the presence of sufficient oxygen. A sensor for CO_2 is one of the most in demand types of sensors [7]. Therefore, it is interesting to test the suitability of the zeolite-doped holographic gratings as a sensor for CO_2. The molecular weight of CO_2 is relatively low at 44.0 g/mol, with a refractive index of 1.112. It is a non polar molecule.

Fig. 10.16. 3D representation of the chemical structure of carbon dioxide.

A holographic grating recorded in a 2 wt. % doped DA photopolymer sample was exposed to gas pressures of 16, 32 and 50 torr, the results of which are shown in fig. 10.17.

For the 16 and 32 torr exposures, no change is observed in the normalised intensity. As the gas pressure is increased to 50 torr, the normalised intensity decreases by a

244

maximum of 2 %. This is a very small decrease for such a high pressure, and suggests that CO_2 is not adsorbing strongly to the zeolite nanoparticles within the grating.
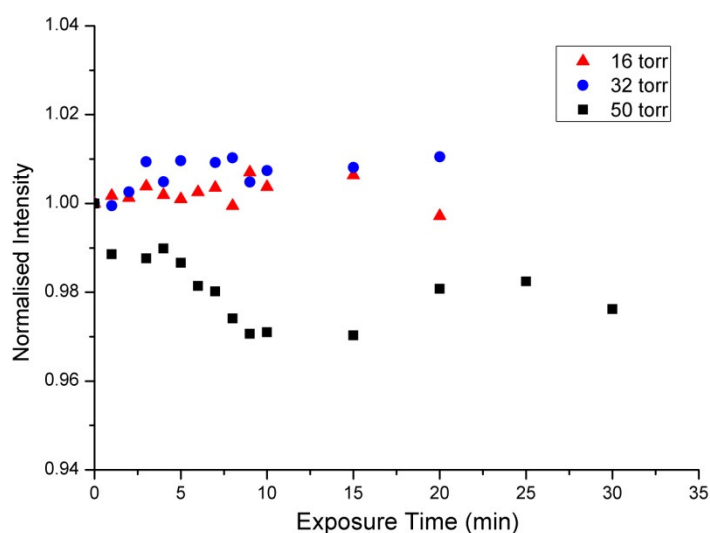
Fig. 10.17. Normalised intensity vs. exposure time (s) for a 2 wt. % zeolite-doped grating exposed to CO_2 at gas pressures of 16, 32 and 50 torr.

10.5 Conclusions

The ability of holographic transmission gratings recorded in a DA photopolymer material to act as a gas sensing device has been investigated for the first time. Three different alcohol type gases were investigated, namely methanol, isopropanol and 2-methylpropan-2-ol. It was found that holographic transmission gratings recorded in undoped DA photopolymer were capable of detecting the presence of these gases by monitoring the change in the intensity of the diffracted spectrum from the grating.

It was observed that the inclusion and redistribution of BEA structure zeolite nanoparticles in the grating enhances its response to the different alcohol gases, in particular at lower gas pressures.

It was observed that exposure to methanol caused the Δn of the holographic grating to increase for a range of gas pressures. One possible explanation for this is adsorption of the small methanol molecules with high polarity to the permeable DA polymer matrix which could lead to a swelling of the layer and thus effectively increase the accumulated phase difference between the two beams propagating in directions along the zero and the first order of diffraction correspondingly. In contrast the isopropanol and 2-methylpropan-2-ol molecules with lower polarity and larger size had the opposite effect on Δn, due to adsorption of the gas molecules to the redistributed zeolite nanoparticles. The effect of the alcohol gases on the holographic grating was observed to be reversible upon removal of the gas, except in instances where damage to the optical quality of the sample was observed due to excessive gas concentrations.

The effect of two different alkane gases, pentane and cyclohexane, on Δn of a 2 wt. % doped grating was investigated. In both cases the Δn of the grating was reduced on exposure to the gas. This reduction was more pronounced for cyclohexane, which is a larger molecule and has a higher refractive index than pentane. Unlike for the alcohols, the effect of the alkane gases on Δn was not observed to be reversible due to their low polarity.

A comparison has been made between the ability of BEA- and Si-MFI-doped photopolymer media for sensing of cyclohexane gas. It has been shown the large pore size of the BEA zeolites facilitates adsorption of the cyclohexane molecules, whereas

the medium pore size of the Si-MFI zeolites prevents adsorption and therefore any measurable change in Δn.

The ability of a 2 wt. % doped holographic grating to be used as a sensor for CO_2 was investigated. No response was observed for gas pressures of 16 and 32 torr, with a small reduction in Δn observed at 50 torr. This low response suggests that the 2 wt. % doped grating is not sensitive enough in its present formulation for use as a CO_2 sensor.

It has been observed that for the alcohol and alkane gases tested, holographic gratings recorded in both the undoped and the zeolite-doped DA photopolymer can successfully be used as a sensing device, as in all cases a response in the form of a change in η of the grating was observed on the introduction of gas, as shown in table 10.4. This fact opens a whole area of applications for the new DA-based photopolymer. Future work should be carried out to investigate in detail the sensitivity of the holographic sensor for different gases, as well as studying the selectivity of the sensor when exposed to mixtures of gases.

Table. 10.4 Response of 2 wt.% BEA-doped sensor to different hydrocarbon gases			
	Response Time (min) for 5 % change in η at 16 torr	Response Time (min) for 5 % change in η at 32 torr	Reversibility
Methanol	1	7	✓
Isopropanol	4	8	✓
2-Methylpropan-2-ol	3	-	✓
Cyclohexane	20	15	X
Pentane	-	2	X

References:

[1] J. Hodgkinson, R. P. Tatam, "Optical gas sensing: a review", Meas. Sci. Technol. 24, 012004 (2013).

[2] H. Bai, G. Shi, "Gas Sensors Based on Conducting Polymers", Sensors 7(3), 267-307 (2007).

[3] A. M. Azad, S. A. Akbar, S. G. Mhaisalkar, L. D. Birkefeld, K. S. Goto, "Solid-State Gas Sensors: A Review", J. Electrochem. Soc. 139(12), 3690-3704 (1992).

[4] G. Eranna, B. C. Joshi, D. P. Runthala, R. P. Gupta, "Oxide Materials for Development of Integrated Gas Sensors—A Comprehensive Review", Critical Reviews in Solid State and Materials Sciences 29(3-4), 111-188 (2004).

[5] Y. Wang, J. T. W. Yeow, "A Review of Carbon Nanotubes-Based Gas Sensors", Journal of Sensors 2009, Article ID 493904, 1-24 (2009).

[6] Transparency Market Research, "Gas Sensors Market - Global Industry Size, Share, Trends, Analysis and Forecast, 2012 - 2018", July 2013. Available online at: http://www.transparencymarketresearch.com/gas-sensors-market.html [Accessed: 19-08-2014].

[7] Grand View Research, "Gas Sensors Market Analysis And Segment Forecasts To 2020", March 2014. Available online at: http://www.grandviewresearch.com/industry-analysis/gas-sensors-market [Accessed: 03-06-2014].

[8] B. Liedberg, C. Nylander, I. Lunström, "Surface plasmon resonance for gas detection and biosensing", Sensors and Actuators 4, 299-304 (1983).

[9] K. Cherif, S. Hleli, A.Abdelghani, N. Jaffrezic-Renault, V. Matejec, "Chemical detection in liquid media with a refractometric sensor based on a multimode optical fibre", Sensors 2, 195-204 (2002).

[10] S. Kabilan, A. J. Marshall, F. K. Sartain, M. C. Lee, A. Hussain, X. Yang, J. Blyth, N. Karangu, K. James, J. Zeng, D. Smith, A. Domschke, C. R. Lowe, "Holographic glucose sensors", Biosensors and Bioelectronics 20(8), 1602–1610 (2005).

[11] A. G. Mayes, J. Blyth, M. Kyröläinen-Reay, R. B. Millington, C. R. Lowe, "A holographic alcohol sensor", Anal. Chem. 71(16), 3390–3396 (1999).

[12] A. J. Marshall, J. Blyth, C. A. B. Davidson, C. R. Lowe, "pH-sensitive holographic sensors", Anal. Chem. 75(17), 4423–4431 (2003).

[13] E. Leite, I. Naydenova, N. Pandey, T. Babeva, G. Majano, S. Mintova, "Investigation of the light induced redistribution of zeolite beta nanoparticles in an acrylamide-based photopolymer", J. Opt. A 11(2) (2009).

[14] M. Zaaeour, B. Dong, I. Naydenova, R. Retoux, S. Mintova, "Progress in Zeolite Synthesis Promotes Advanced Applications", 17th International Zeolite Conference, Moscow, Russia, Microporous and Mesoporous Materials 189(1), 11-21, 2014.

[15] E. Leite, Tz. Babeva, E.-P. Ng, V. Toal, S. Mintova, I. Naydenova ,"Optical Properties of Photopolymer Layers Doped with Aluminophosphate Nanocrystals" Journal of Phys. Chem. C 114(39), 16767–16775 (2010).

[16] M. Akhgari, M. H. Panahianpour, E. Bazmi, A. E. Aleagha, A. Mahdavi, S. H. Nazari, "Fatal methanol poisoning", Toxicol. Ind. Health 29(2) 136-141 (2013).

[17] T. Mikulchyk, S. Martin, I. Naydenova, "Humidity and temperature effect on properties of transmission gratings recorded in PVA/AA-based photopolymer layers", J. Opt. 15, 105301 (2013).

[18] S. Mintova, M. Reinelt, T. H. Metzger, J. Senkera, T. Bein, "Pure silica BETA colloidal zeolite assembled in thin films", Chem. Commun. 3, 326-327 (2003).

[19] C. Reichardt, Solvents and Solvent Effects in Organic Chemistry, Wiley-VCH Publishers, 3rd edition, 2003.

11. CHARACTERISATION OF THE HOLOGRAPHIC RECORDING ABILITY OF THE DA PHOTOPOLYMER IN REFLECTION MODE

11.1 Introduction

As can be seen from previous chapters, a large volume of journal publications on the holographic recording ability of photopolymer media focus on the characterisation of the response of the material in the transmission regime. This is due in part to the lower requirements on the recording material in transmission mode in terms of spatial resolution and recording stability, as well as the relative ease with which high diffraction efficiency (η) holograms can be achieved.

There are many applications for which transmission holograms are suitable, such as transmission-mode HOEs [1, 2], HDS [3, 4] and certain types of sensors [5, 6], as was described in chapter 1. However, there are applications for which transmission holograms are not sufficient. There are restrictions on the spatial resolution that can be achieved in transmission mode. For holographic photopolymers this is limited to approximately 3000 l/mm. Also, transmission holograms must either be reconstructed with the same wavelength of light used to record them, or the angle or reconstruction must be carefully adjusted to match the wavelength used. In order for a hologram to be reconstructed using white light only and to achieve higher spatial resolution, it is necessary to use the reflection regime of recording. The limit of the spatial resolution of holograms recorded in the reflection mode using the IEO's AA photopolymer is nearly double the limit for transmission, at 5700 l/mm for a wavelength of 633 nm [7]. Higher spatial resolution is certainly advantageous for applications such as HDS, as it would allow for larger volumes of information to be stored.

As mentioned above, there is a significantly lower number of journal publications available which detail the development and application of reflection mode holographic photopolymer media in comparison to transmission mode. There are some publications available on the well-known commercial DuPont photopolymer [8-10], however none in recent years. Reflection mode holograms are reported for use as sensors for analytes such as water vapour [11] and acetone [12], as well as several publications on H-PDLC hybrid media for reflection recording [13, 14]. An AA-based photopolymer composition was reported for recording of full colour holograms for the application of display holography [7]. In general however the main volume of published work on reflection holography comes in the form of patents, which demonstrates clearly the general consensus of those in research and industry that reflection holograms are of great interest for commercial applications. The main bulk of these patents protect specific reflection mode holographic photopolymer formulations and hologram recording techniques [15-25]. However, there are some patents focusing on specific applications such as reflection mode HOEs [26, 27] and sensors [28, 29].

Popular reflection mode applications include security and authentication holograms, display holography, reflection mode HOEs and white-light viewable holographic sensors. In particular, the market for holograms for authentication and anti-counterfeiting purposes is large and continuously growing. The market for the sale of counterfeit pharmaceutical drugs online is estimated to be worth between $75 billion and $200 billion each year [30]. A market report by BCC Research expects that the market for authentication technologies will reach $37.7 billion in 2015 [31], reflecting the huge demand for new technologies in this sector.

Security holograms are extremely difficult to forge, recognisable to the public, and are low cost. Reflection holograms on goods such as pharmaceutical products are a

promising solution to the problem of counterfeit goods, as they can provide an impossible-to-replicate authentication solution for packaging. Photopolymer materials have been tipped as "the number one disruptive technology in security printing in the next ten years" by Pira International, a leading Market Research company who specialise in packaging supply chains [32]. In a recent overview at the HoloPack-HoloPrint 2012 conference, Lancaster and Tidmarsh pointed out that the security market is one of the main drivers for growth and innovation in the holography industry, and that the market is changing as customers are demanding more functionality in security technologies [33].

Here, an investigation into the holographic recording ability of the DA photopolymer in the reflection regime is reported. The effect of a Chain Transfer Agent (CTA), namely Citric Acid, on the holographic recording ability of the DA photopolymer in reflection mode has been investigated for recording parameters such as laser intensity, exposure energy and spatial frequency. Comparison has also been made with the recording ability of the DA0 and DAG photopolymer formulations.

11.2 Theory

11.2.1 Mechanism of reflection hologram recording in photopolymers

As discussed in detail in chapter 1, in reflection holograms the recorded fringe-planes are oriented parallel to the surface of the recording medium as shown in fig. 11.1. The reconstructed hologram is observed as a reflection of the reference wave from the surface of the sample. For volume, phase gratings in the reflection regime, the Bragg equation is given by:

$$\lambda = 2n\Lambda \sin \theta \tag{11.1}$$

where λ is the reconstruction wavelength, n is the refractive index of the photopolymer layer, Λ is the grating period and θ is the reconstructing angle. For reflection gratings, the diffraction efficiency η of the recorded grating is given by:

$$\eta = \frac{I_r}{I_o} \times 100 \tag{11.2}$$

where I_r is the intensity of the reconstructed beam and I_o is the intensity of the incident beam. However, in reflection mode, reflectivity losses in the recording intensity from the surface of the sample need to be taken into account, in particular at low spatial frequencies where θ will be large. These losses can be determined using the data for the Fresnel reflection coefficient as a function of the angle to the normal α as shown in fig. 11.2 [34]. For example, using eqn. 1 the angle α is found to be 50° for a spatial frequency of 3050 l/mm and a wavelength of 633 nm. This corresponds to reflectivity losses of approximately 10 % for the s-polarised incident light.
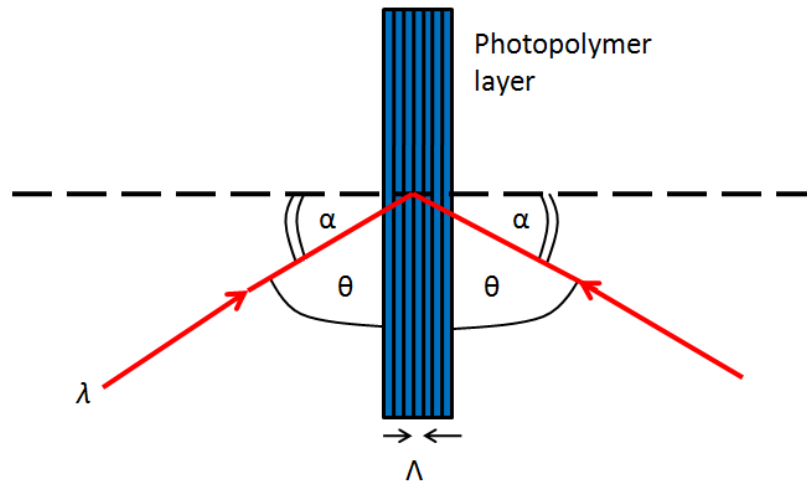
Fig. 11.1. Geometry for recording of reflection gratings.

254
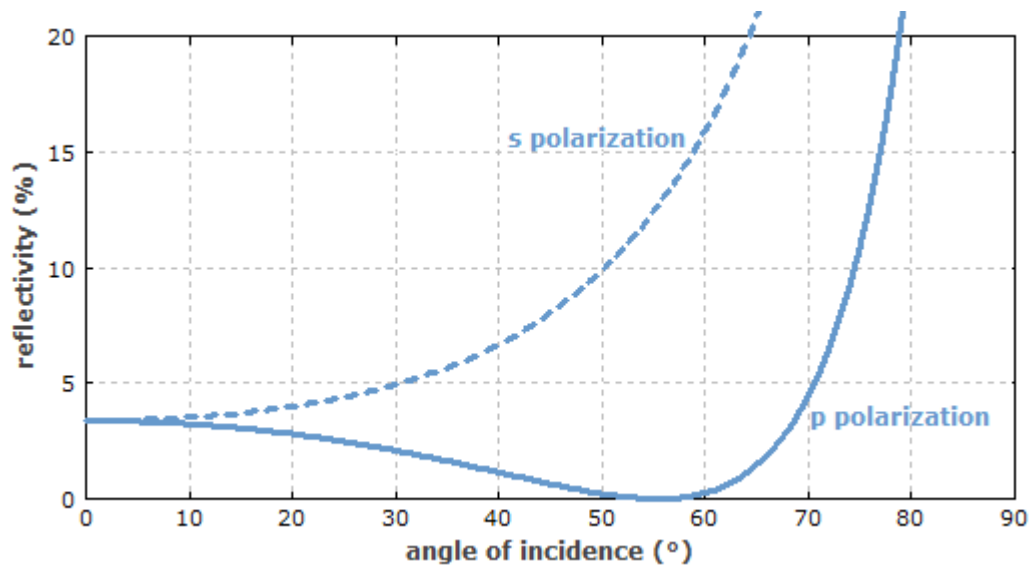
Fig. 11.2. Reflection losses (%) vs. angle of incidence α (°) of p-polarized and s-polarized light at each surface of the plate [34].

11.2.2 Chain transfer agent

The ability of holographic photopolymer media to record high η reflection holograms is limited by several factors. As discussed above, spatial resolution of the material is a big factor. It is important that the recording material is able to achieve high spatial resolution in order to record high quality holograms. For photopolymer media, the formation of large polymer chains during recording growing or extending out of the bright fringe regions and also the diffusion of mobile short polymer chains is problematic. This results in reduced Δn and therefore lower η of the recorded gratings. At lower spatial frequencies such as in transmission mode this is less of an issue, and high η and Δn values are still achievable. However, as the spatial frequency is increased as in the reflection regime, these effects become significantly more pronounced due to reduced fringe spacing. This results in significantly reduced η values for gratings recorded in reflection mode. Meka *et al* report maximum η values of 11.5, 6.0 and 1.6

% at wavelengths of 633, 532 and 473 nm respectively for reflection gratings recorded at spatial frequencies of 4200, 5000 and 5700 l/mm with the IEO's AA-based photopolymer formulation [7]. Fuentes *et al* report a maximum η of 9.1 % at a recording wavelength of 514 nm and a spatial frequency of 5174 l/mm for their AA-based photopolymer composition in reflection mode [35].

The idea of the inclusion of a chain transfer agent (CTA) in the photopolymer formulation was initially proposed by Gleeson *et al* as a potential solution to this problem [36]. A CTA works by prematurely terminating the formation of a growing polymer chain. The freed active radical is then available to intimate the growth of a new polymer chain. In this way the polymer chain length can be restricted, promoting the growth of shorter polymer chains. The reaction may be described as follows:

$$(M)_n \bullet + XA \rightarrow (M)_n{-}X + A \bullet \tag{11.3a}$$

$$A \bullet + M \rightarrow M \bullet \tag{11.3b}$$

Eqn. 11.3a describes the deactivation of a growing polymer chain $(M)_n \bullet$ by the CTA denoted here as XA. A new radical $A \bullet$ is formed as a by-product of this termination reaction, allowing for the initiation and subsequent propagation of a new polymer chain as shown in eqn. 11.3b [37]. This chain may then be terminated by another chain transfer mechanism allowing the whole process to repeat, or by some other termination reaction such as combination or disproportionation [38].

It is worth noting here that the proposed mechanism of improvement of the resolution of the holographic recording material by creation of short polymer chains can only work if the created chains have limited mobility. If the chains are mobile and are capable of diffusing from the bright to the dark fringe areas, this leads to a significant decrease of

the η of the recorded gratings with increasing spatial frequency. There have been a number of publications describing the use of different CTA in AA-based photopolymers which demonstrate an increase of the η typically in order of few percent only. Fernández *et al* report on the use of two different CTA, namely 4,4′-Azobis (4-Cyanopentanoic Acid) (ACPA) [39] and Sodium Formate (HCOONa) [35], for reflection mode recording with an AA-based photopolymer. Although the inclusion of ACPA was shown to reduce the amount of polymerisation-induced shrinkage occurring in the layers, η was only seen to increase from 4 % to 6.2 % at a spatial frequency of 4600 l/mm; no improvement in η was observed with HCOONa. Gleeson *et al* report on the use of HCOONa as a CTA also, reporting an average increase in Δn of 17 % in transmission mode for spatial frequencies in the range of 500 - 2750 l/mm, however no reflection mode experimental results have been reported [36]. Since the DA molecule is significantly larger than the AA molecule, one could expect that the short polymer chains created by the use of a CTA are significantly slower than those created in the AA photopolymer. Thus the use of a CTA is expected to be more successful in improving the performance of the material in reflection mode for the DA-based photopolymer. An alternative approach to a CTA for improving the recording capability of a material in reflection mode is to use exposure conditions which reduce the creation of short mobile polymer chains, and to use a polymer binder with restricted permeability. This second approach has been demonstrated to be particularly successful in AA-based photopolymers [40, 41].

Here, the ability of the chemical Citric Acid to act as a CTA for the DA-based photopolymer has been investigated for the first time. Rodrigues *et al* mention citric acid as one in a list of potential CTA for a cellulose-based, hybrid co-polymer composition [38].

11.3 Experimental

11.3.1 Materials

The different DA-based photopolymer compositions tested were prepared as described in table 11.1. 0.5 ml of the photopolymer solution was deposited on to glass slides (75 × 25 mm) and allowed to dry for 12-24 hours in darkness under normal laboratory conditions (20-25 ℃, 40-60 % RH). Sample thickness was measured using a white-light surface profiler (Micro XAM S/N 8038).

Table 11.1 DA-based compositions for reflection mode tests

	DA0	DAG	DAC1	DAC2	DAC3	DAC4
PVA (10% wt/vol) (ml)	20	20	20	20	20	20
TEA (ml)	2	2	2	2	2	2
DA (g)	1	1	1	1	1	1
BA (g)	0.2	0.2	0.2	0.2	0.2	0.2
Glycerol (ml)	-	1	2	2	2	-
Citric Acid (g)	-	-	0.1	0.2	0.3	0.2
Methylene Blue Dye s. s. (0.11% wt/vol) (ml)	4	4	4	4	4	4

11.3.2 Methods

A 633 nm He-Ne laser was used to record holographic reflection gratings using a standard two-beam optical setup as shown in fig. 11.3. By varying the angle between the two beams, 2θ, the spatial frequency of the recorded grating was varied using eqn. 11.1. An intensity filter was used to control the recording intensity of the two beams. The recording intensity was adjusted to compensate for the reflection losses of the oblique incident angle, determined from fig 11.2. An optical power meter (Newport 1830-C) was used to measure the intensity of the reconstructed reflection beam. η is

defined here as the ratio of the intensity of the reconstructed reflection beam I_r and the incident intensity I_o of the probe beam, as given by eqn. 11.2. η was determined after recording by blocking one of the incident 633 nm beams and then measuring the intensity of the reconstructed beam from the grating. The sample was rotated at a small angle to the normal before recording in order to ensure that during reconstruction, the reconstructed beam could be distinguished from the transmitted beam.
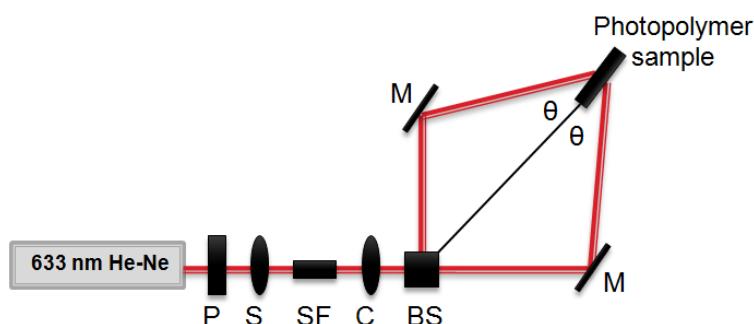
Fig. 11.3. Reflection mode experimental setup: P: polariser, S: shutter, SF: spatial filter, C: collimator, BS: beam splitter, M: mirror.

11.4 Results and Discussion

11.4.1 Comparison of the recording ability of the different DA-based compositions

Reflection gratings were recorded in the different photopolymer compositions described in section 11.3.1 using a total recording intensity of 3.2 mW/cm^2 for 80 seconds, and total exposure energy of 256 mJ/cm^2. The results of η for each of the photopolymer compositions tested are shown in fig. 11.4.

For the standard DA0 and DAG compositions, approximately the same value of η of 10 ± 2 % was achieved. This is comparable to the data obtained with the standard AA-

based photopolymer. Meka *et al* achieved maximum η of 11.5 % for similar recording conditions (total intensity of 3 mW/cm^2, 80 second exposure, 60 ± 5 µm thick samples at 4200 l/mm) using a 633 nm laser. However, the inclusion of the CTA citric acid is shown to significantly increase η, up to threefold in the case of DAC2. For the DAC1, DAC2 and DAC3 compositions, they wt. % of citric acid is 1.24, 2.45 and 3.63 wt. % respectively. From the data it seems that increasing the concentration of citric acid above 2.45 wt. % does not yield any further improvement in η.

An unexpected result was observed for the photopolymer composition DAC4. In this composition, glycerol has been excluded, to see the effect of the CTA on the holographic recording ability of the DA photopolymer in its absence. Surprisingly, only 10 % η gratings could be recorded. These results indicate that both glycerol and citric acid are required in order to achieve high η reflection mode gratings.

It was shown in chapter 7 that the incorporation of glycerol in the DA photopolymer composition resulted in faster polymerisation of the DA photopolymer samples, due to increased polymer chain growth and entanglement, most likely as a result of increased diffusion within the layer. It is possible that the incorporation of glycerol in the DAC composition acts to speed up polymerisation, thereby increasing the solidity of the polymer layer. By doing so, diffusion of short polymer chains is restricted. Therefore, it is proposed that the inclusion of the CTA acts to promote the growth of short polymer chains which is advantageous for high spatial frequencies, while glycerol acts to restrict their movement, resulting in increased η of the recorded gratings.

It is important to consider whether the high η observed for DAC2 in comparison to DA0, DAG and DAC4 is due simply to increased monomer concentration in the samples, and not from the added CTA as expected. In order to verify this, the amount of

the solid monomers DA and BA as a percentage of the total solid weight of the photopolymer sample was calculated for each photopolymer formulation. The results of this are shown in table 11.2. From this it is shown that the wt. % of DA and BA is lowest for the composition DAC2. Thus the increased η cannot be attributed to variation in the monomer concentration and can only be ascribed to the presence of both Citric Acid and Glycerol.
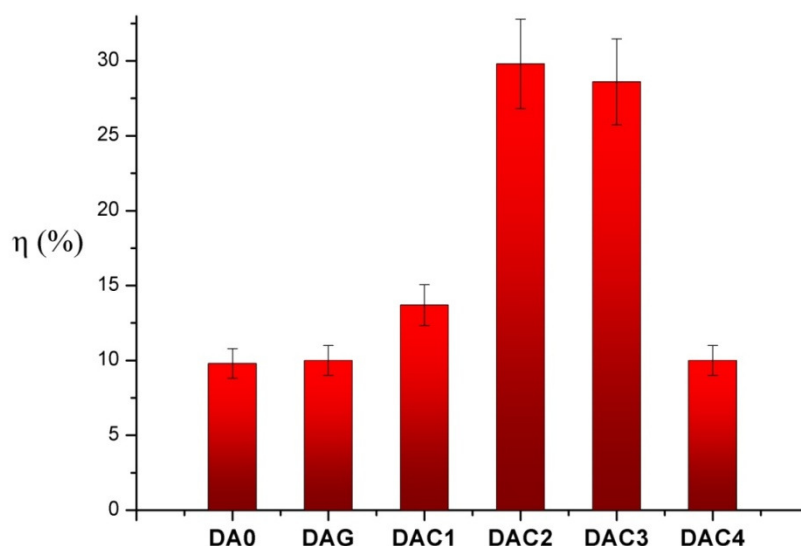
Fig. 11.4. η (%) of recorded reflection gratings for each of the DA-based photopolymer formulations described in table 1.

Table 11.2 % Solid weights of DA and BA monomers in the DA reflection compositions

	DA0	DAG	DAC2	DAC4
DA (wt. %)	18.34	14.9	12.24	17.69
BA (wt. %)	3.67	2.98	2.45	3.54

11.4.2 Reflection mode characterisation of the holographic recording ability of the DAC photopolymer

As discussed in section 11.4.1, the DAC2 photopolymer was observed to achieve the highest η values of all tested compositions containing the CTA citric acid. Therefore, it was chosen as the standard DAC composition for the reflection mode characterisation study. For this study, the dependence of the holographic recording ability of the DAC material on parameters such as recording intensity, exposure energy, sample thickness and spatial frequency was investigated. The use of UV light to "fix" the holographic gratings after recording was also investigated.

11.4.2.1 Intensity and exposure energy dependence for the DAC photopolymer

The dependence of η on recording intensity and recording exposure energy was investigated for the DAC photopolymer at a spatial frequency of 3050 l/mm. A sample thickness of 80 ± 5 µm was used.

For the exposure energy dependence study, reflection gratings were recorded using exposure energies of $90 - 360$ mJ/cm^2, for a recording intensity of 3 mW/cm^2. The results of this study are shown in fig. 11.5. There is clear exposure energy dependence for the DAC photopolymer, with optimum η of 28 % obtained for an exposure energy of 270 mJ/cm^2. As the exposure energy is increased above this, the η of the recorded grating decreases. This is most likely due to excessive formation of polymer chains at higher exposure energies, leading to chain growth and diffusion outside of the illuminated fringe regions which would result in decreased η. It is also possible that stability issues are introduced, in particular for the longer exposure times which exceed

100 seconds. 270 mJ/cm^2 was therefore selected as the optimum exposure energy was all future measurements.
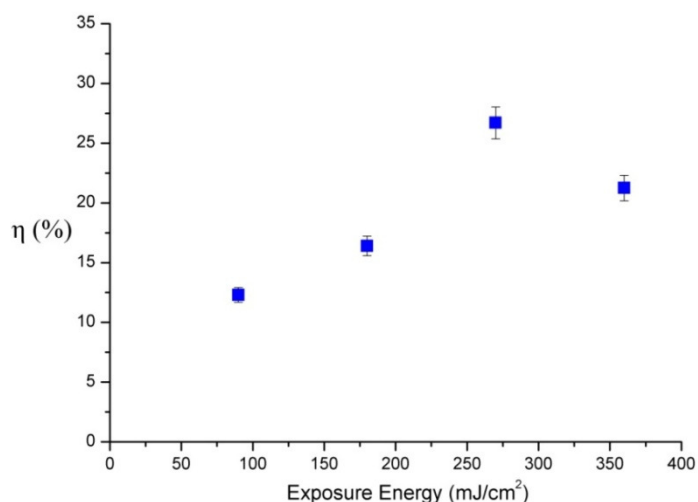
Fig. 11.5. η (%) vs. recording exposure energy (mJ/cm^2) for gratings recorded in the DAC photopolymer at 3050 l/mm for total recording intensity of 3 mW/cm^2.

For the intensity dependence study, the total recording intensity in the two recording beams was varied from 2 – 6 mW/cm^2, while ensuring that the total exposure energy was kept constant at 270 mJ/cm^2. The results of this are shown in fig. 11.6. It is clear from the results that there is limited intensity dependence for the DAC photopolymer for the range of intensities tested. η increases from 25 to 30 % only as the recording intensity is tripled from 2 to 6 mW/cm^2. Limited intensity dependence would be expected with the inclusion of a CTA. In general, the recording intensity governs the length of the polymer chains formed; higher recording intensities result in shorter polymer chain lengths. However, the purpose of a CTA is to restrict chain length, regardless of the recording intensity used. Therefore, it is unlikely that a strong dependence of η on recording intensity will be observed. The intensity of the available

He-Ne lasers was limited to 6 mW/cm^2 so it was not possible to test higher recording intensities.
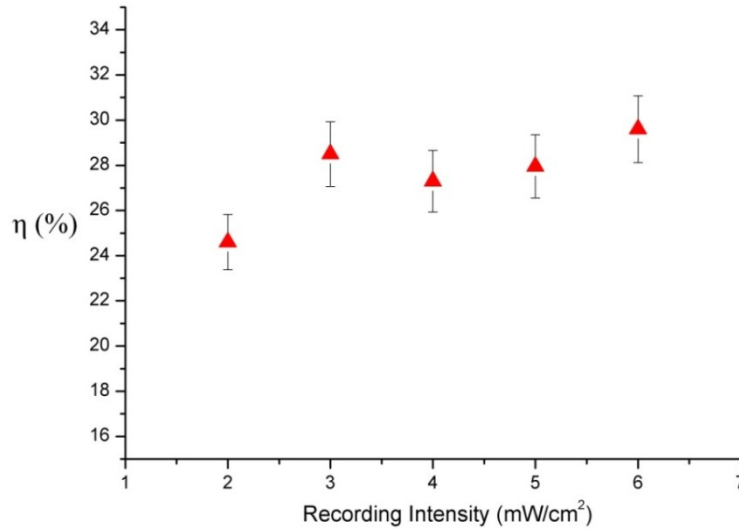
Fig. 11.6. η (%) vs. recording intensity (mW/cm^2) for gratings recorded in the DAC photopolymer at 3050 l/mm for total exposure energy of 270 mJ/cm^2.

11.4.2.2 Sample thickness dependence for the DAC photopolymer

The effect of sample thickness on η for reflection gratings recorded in the DAC photopolymer was investigated. Sample thickness was increased from 40 – 160 µm. Reflection gratings were recorded using a total recording intensity of 3 mW/cm^2, with exposure energy of 270 mJ/cm^2. The results of this study are shown in fig. 11.7. For the sample thicknesses tested, a clear optimum thickness of 80 ± 5 µm was observed. The sample thickness plays a significant role in reflection mode recording. Unlike transmission mode, in reflection the two recording beams are incident from opposite sides of the photopolymer layer. It is important therefore that the recording beams are able to travel through the sample in order to achieve the periodic modulation of the photopolymer via polymerisation that constitutes the reflection grating. Problems can

arise due to excess absorption and scatter of incident light, which limits the materials response in thicker photopolymer layers.
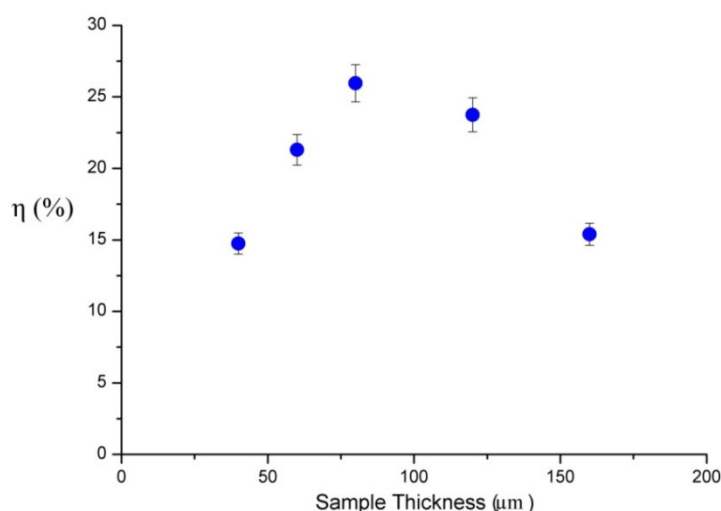
Fig. 11.7. η (%) vs. sample thickness (µm) for gratings recorded in the DAC photopolymer at 3050 l/mm. A total recording intensity of 3 mW/cm^2 was used.

11.4.2.3 Spatial frequency dependence for the DAC photopolymer

A spatial frequency dependence study was carried out for the DAC composition. Reflection gratings were recorded at spatial frequencies from 2500 – 4500 l/mm for recording intensities of 2 – 6 mW/cm^2. The total exposure energy was kept constant at 270 mJ/cm^2. The results of this study are shown in figs. 11.8 and 11.9.

It was observed that as the spatial frequency is increased, the maximum η achievable is decreased from 38 to 15 % for a recording intensity of 6 mW/cm^2, as shown in fig. 11.8. This can be explained by considering that as spatial frequency of recording is increased, the fringe spacing of the gratings is reduced. At higher spatial frequencies, diffusion of short polymer chains from bright to dark regions becomes more problematic, leading to a decrease in η of the recorded gratings. However, even at the highest spatial frequency

tested of 4500 l/mm, gratings with η values of 15 % were obtained. This compares favourably with the 10 % gratings recorded in the DA compositions without the CTA at the lower spatial frequency of 3050 l/mm, which demonstrates the effectiveness of the CTA in the photopolymer composition.

An intensity dependence study was carried out at each spatial frequency tested as shown in fig. 11.9. At 2500 l/mm, clear intensity dependence is observed, with the highest intensities tested of 5 and 6 mW/cm^2 achieving the highest η values. At this relatively low spatial frequency, a faster rate of polymerisation is required in order to produce the volume of polymer chains required for high η gratings. For this spatial frequency which has a relatively large grating spacing, the importance of the inclusion of the CTA may not be as large as at higher spatial frequencies. As the spatial frequency is increased, grating fringe spacing is reduced, and so polymer chain length becomes critical.

As seen in section 11.4.2.1, the inclusion of the CTA appears to limit the intensity dependence of the DAC photopolymer due to the formation of shorter polymer chains, regardless of recording intensity used. As shown in fig. 11.9, for spatial frequencies above 3050 l/mm the trend in intensity dependence appears to become more uniform. This may be partly due to the role of the CTA, which prevents the growth of long polymer chains even at lower recording intensities, and so increases η of the recorded gratings at these intensities.

In general, the optimum recording intensity shifts towards lower values of 3 and 4 mW/cm^2 as spatial frequency is increased. This may be explained by the fact that as the spatial frequency is increased, the fringe spacing is reduced, therefore slower polymerisation is better in order to control the rate of formation of the short polymer

chains and their subsequent diffusion out of the bright fringe regions which would result in reduced η.

The limit of the photopolymers resolution in reflection mode is nearly reached at a spatial frequency of 4500 l/mm. Diffusion of the short polymer chains becomes more problematic and results in the reduction of the Δn between the bright and dark fringe regions.
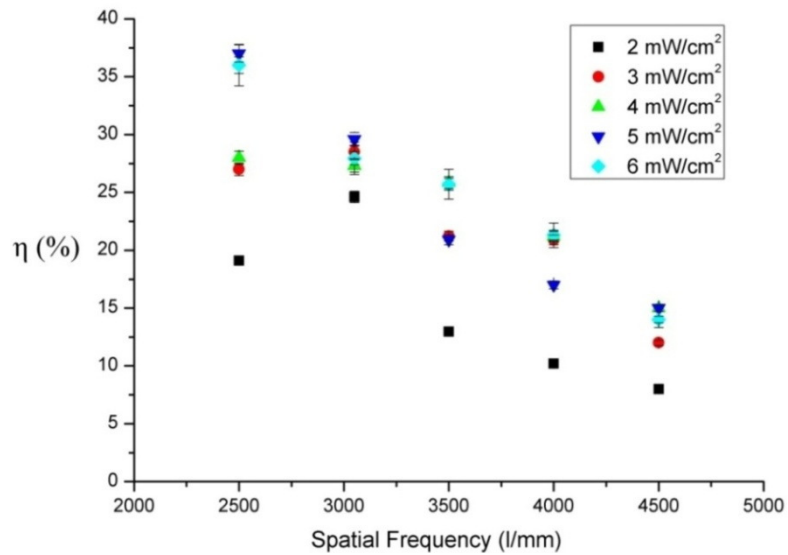
Fig. 11.8. η (%) vs. spatial frequency of recording (l/mm) for gratings recorded in the DAC photopolymer at recording intensities of 2 – 6 mW/cm^2. A total exposure energy of 270 mJ/cm^2 was used.
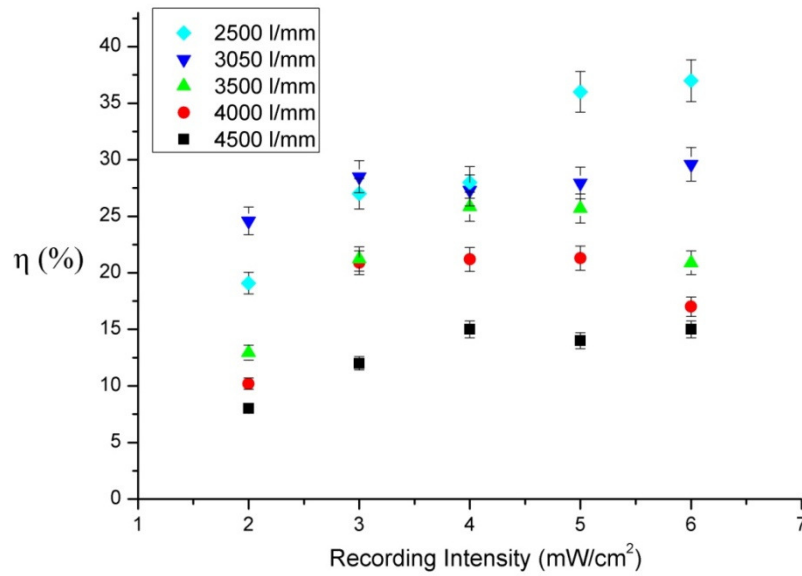
Fig. 11.9. η (%) vs. recording intensity (mW/cm^2) for gratings recorded in the DAC photopolymer at spatial frequencies of 2500 – 4500 l/mm. A total exposure energy of 270 mJ/cm^2 was used.

11.4.2.4 Effect of UV fixing on the DAC photopolymer gratings

It is imperative that the recorded gratings are stable for practically all potential applications. It was observed that the reflection gratings recorded with the DAC composition are not stable, and the η degrades over time. This implies that even if glycerol initially acts to restrict short chain diffusion during recording by speeding up polymerisation, its effect is short-lived. One possible reason for the observed decrease in η was the absorption of water by the photopolymer layers, causing the gratings to swell and degrade. However, this was ruled out as a potential cause by sample lamination, and dehydration of the samples with desiccant after recording. The decrease in η was still observed.

A second possible explanation for this effect is that the short DA polymer chains formed during holographic recording are not completely rigid, and diffuse slowly over time. One technique that has been developed to solve this problem is UV-curing of the gratings recorded in the photopolymer layer after recording [39, 42]. It is proposed by Jenney that this technique reduces the dye to its colourless form so that it can no longer absorb visible light, thus "fixing" the grating by preventing further reactions taking place in the material. However, it is also necessary that diffusion of the short polymer chains and any remaining monomer is restricted within the layer. By absorption of UV light, the double bonds of the remaining unreacted DA and BA monomer molecules are broken, resulting in further polymerisation and crosslinking, and therefore reduced permeability of the photopolymer layer [43, 44]. This in turn will reduce the diffusion of polymer chains which causes the gratings to degrade. The remaining grating is a result of the mass transport of DA monomer from dark to bright fringe regions which occurs during holographic recording [40].

In order to test this hypothesis, a nanosecond pulsed 355 nm UV laser was used to bleach the remaining dye in the photopolymer layers directly after holographic recording, thereby fixing the recorded grating. The maximum repetition rate of the laser, 11 Hz, was observed to be optimum. Layers were bleached for durations of approximately 3 minutes, during which time the samples were completely bleached in the illuminated area. The power per unit area of the laser was approximated to be 150 mW/cm^2.

Fig. 11.10 shows the η of recorded reflection gratings vs. time after recording for three samples, one of which has received no post recording treatment, and two of which have been UV treated. Initially all three gratings have η of approximately 18 %. In the case of the grating which received no treatment, η is observed to decrease quickly with time,

with a 50 % drop observed in the first 5 minutes. For the two gratings which were exposed to UV light after recording, η remains approximately constant over the 20 minute monitoring period.

A shelf life study was carried out for one month after recording to investigate the life-time of the holograms after UV fixing. The results of this study are shown in fig. 11.11. An initial decrease of approximately 4 % in η was observed to occur for all holograms in the first 24 hours after UV-fixing. These holograms were not laminated or protected in any way, and therefore were subject to external influences such as humidity and temperature, which may explain the observed small decrease. This decrease may therefore be prevented by lamination of the holograms. After this initial decrease, no further significant decrease in η was observed over the 28-day period.
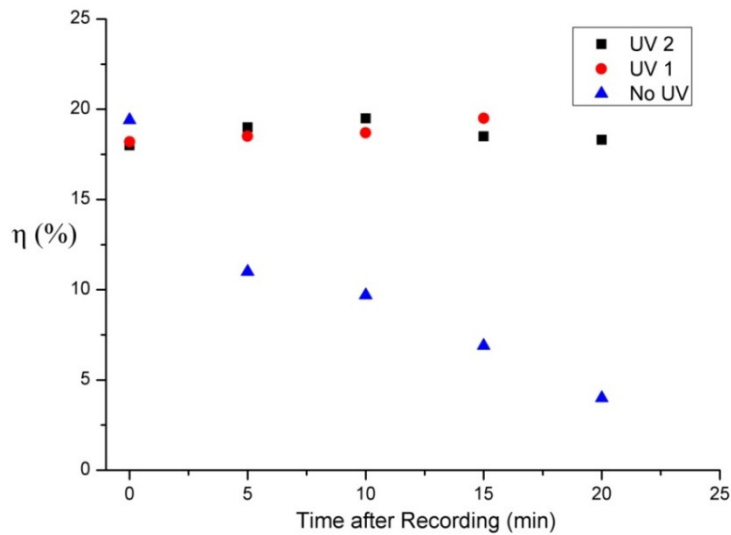
Fig. 11.10. η (%) vs. time after recording (min) for DAC photopolymer samples which have been exposed to UV light after recording, and one sample which received no treatment.
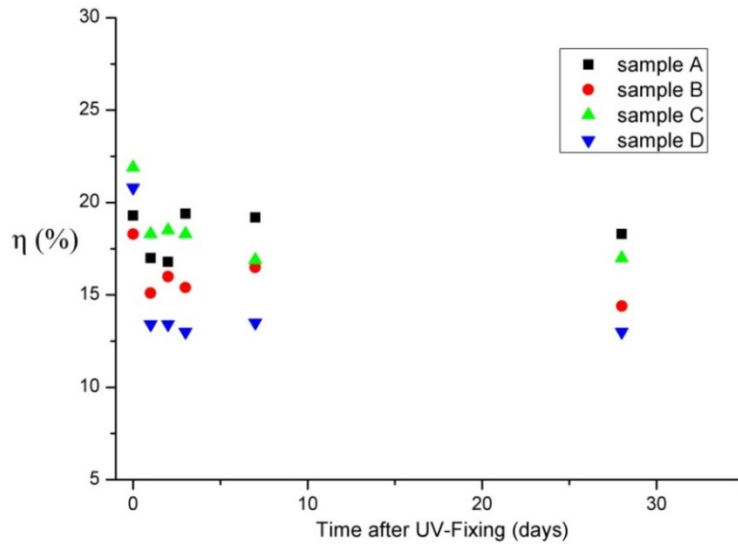
Fig. 11.11. η (%) vs. time after UV-fixing (days) for four reflection gratings recorded in DAC photopolymer samples.

11.5 Conclusions

The holographic recording ability of the DA based photopolymer in the reflection regime has been investigated. The DA0 and DAG photopolymers which do not contain any CTA record reflection gratings at 3050 l/mm with values for η of 10 %. This is comparable to the η achieved with the AA-based photopolymer formulation at a spatial frequency of 4200 l/mm as reported by Meka *et al* [7].

The effect of the incorporation of a CTA, Citric Acid, on the holographic recording ability of the DA photopolymer in reflection mode has been studied. This additive, in combination with glycerol, was observed to cause a three-fold increase in η in comparison to the DA0 and DAG photopolymers for the same recording conditions. At a spatial frequency of 2500 l/mm, η values of up to 38 % were achieved in reflection mode with the DAC photopolymer. To the best of our knowledge a value of η of 38 %

in reflection mode of recording is the highest reported for this spatial frequency in the water-soluble holographic photopolymers.

Extensive characterisation of the response of the DAC photopolymer in reflection mode has been made, including intensity, exposure energy, thickness and spatial frequency dependence. These series of experiments allowed for the optimum recording conditions to be determined. In general the inclusion of the CTA reduces the strength of the intensity dependence in reflection mode recording of the DAC photopolymer. This is due to the fact that the CTA promotes the formation of shorter polymer chains, regardless of the recording intensity used.

It was observed that as the spatial frequency of recording was increased, the η of the recorded reflection gratings was reduced. However, even at the highest spatial frequency tested of 4500 l/mm, η values of 15 % were obtained. This compares favourably with the 10 % gratings recorded in the DA compositions without the CTA at the lower spatial frequency of 3050 l/mm. This demonstrates the effectiveness of citric acid in its role as a CTA and justifies once again its inclusion in the photopolymer composition.

The ability of UV-curing to stabilise the reflection gratings recorded in the DAC photopolymer has been examined. A shelf-life study of the UV-fixed recorded gratings was carried out for one month. It was demonstrated that UV fixing after recording is a very suitable technique for stabilisation of the DAC photopolymer reflection gratings. It was also shown that UV-fixing extends the shelf-life of the recorded reflection holograms.

References:

[1] H. Akbari, I. Naydenova, S. Martin, "Using Acrylamide Based Photopolymers for Fabrication of Holographic Optical Elements in Solar Energy Applications", Appl. Opt. 53(7), 1343-1353 (2014).

[2] W. J. Gambogi, W. A. Gerstadt, S. R. Mackara, A. M. Weber, "Holographic transmission elements using improved photopolymer films", Proc. SPIE 1555, Computer and Optically Generated Holographic Optics; 4th in a Series, 256 (1991).

[3] H. Sherif, I. Naydenova, S. Martin, C. McGinn, V. Toal, "Characterisation of an Acrylamide-based Photopolymer for Data Storage Utilizing Holographic Angular Multiplexing", J. Opt. A: Pure Appl. Opt. 7, 255-260 (2005).

[4] M. Toishi, T. Tanaka, K. Watanabe, K. Betsuyaku, "Analysis of Photopolymer Media of Holographic Data Storage Using Non-local Polymerization Driven Diffusion Model", Jpn. J. Appl. Phys. 46, 3438 (2007).

[5] E. Leite, I. Naydenova, S. Mintova, L. Leclercq, V. Toal, "Photopolymerizable nanocomposites for holographic recording and sensor application", Appl. Opt. 49(19), 3652-3660 (2010).

[6] J. Shi, V. K. S. Hsiao, T. J. Huang, "Nanoporous polymeric transmission gratings for high-speed humidity sensing", Nanotechnology 18 465501 (2007).

[7] C. Meka, R. Jallapuram, I. Naydenova, S. Martin, V. Toal, "Development of a panchromatic acrylamide-based photopolymer for multicolor reflection holography", Appl. Opt. 49(8), 1400-1405 (2010).

[8] W. J. Gambogi, A. M. Weber, J. Trout, "Advances and applications of DuPont holographic photopolymers", Proc. SPIE 2043, Holographic Imaging and Materials, 2 (1994).

[9] W. J. Gambogi, K. W. Steijn, S. R. Mackara, T. Duzick, B. Hamzavy, J. Kelly, "Holographic optical element (HOE) imaging in DuPont holographic photopolymers", Proc. SPIE 2152, Diffractive and Holographic Optics Technology, 282 (1994).

[10] W. J. Gambogi, W. K. Smothers, K. W. Steijn, S. H. Stevenson, A. M. Weber, "Color holography using DuPont holographic recording films", Proc. SPIE 2405, Holographic Materials, 62 (1995).

[11] I. Naydenova, R. Jallapuram, V. Toal, S. Martin, "Characterisation of the humidity and temperature responses of a reflection hologram recorded in acrylamide-based photopolymer", Sensors and Actuators B: Chemical 139(1), 35-38 (2009).

[12] V. K. S. Hsiao, W. D. Kirkey, F. Chen, A. N. Cartwright, P. N. Prasad, T. J. Bunning, "Organic Solvent Vapor Detection Using Holographic Photopolymer Reflection Gratings", Adv. Mater. 17(18), 2211-2214 (2005).

[13] K. Liu, H. Xu, H. Hu, Q. Gan, A. N. Cartwright, "One-Step Fabrication of Graded Rainbow-Colored Holographic Photopolymer Reflection Gratings", Adv. Mater. 24(12), 1604-1609 (2012).

[14] L. V. Natarajan, C. K. Shepherd, D. M. Brandelik, R. L. Sutherland, S. Chandra, V. P. Tondiglia, D. Tomlin, T. J. Bunning, "Switchable Holographic Polymer-Dispersed Liquid Crystal Reflection Gratings Based on Thiol–Ene Photopolymerization", Chem. Mater. 15(12), 2477–2484 (2003).

[15] T. J. Trout, D. M. Chan, B. M. Monroe, "Mixture of fluorinated binder, unsaturated liquid monomer plasticizer, photoinitiator", Patent No. US 4963471 A (1990).

[16] P. J. Martin, R. G. Melega, A. M. Weber, "Photohardened photopolymer layer on support, diffusion layers", US 5725970 A (1998).

[17] B.M. Monroe, W. K. Smothers, "Photopolymerizable compositions and elements for refractive index imaging", US 4942112 A (1990).

[18] W. K. Smothers, "Methine dye, ethylenically unsaturated compound and free radical generators", US 4917977 A (1990).

[19] A. M. Weber, "Speed, acrylic anhydride, polyvinyl acetate binder", US 5013632 A (1991).

[20] J. J. Cowan, "Metallizing and overcoating with dielectric layers", US 4839250 A (1989).

[21] M. J. Neu, J. J. Sullivan, "Method for the manufacture of eye-covering articles bearing decorative reflection holograms", US 6020983 A (2000).

[22] M. L. Armstrong, D. J. Mickish, "Method and system for making a reflection hologram", US 4995685 A (1991).

[23] J. J. Cowan, "Stepped surface relief structures", US 4888260 A (1989).

[24] S. Martin, I. Naydenova, V. Toal, "Method of making a reflection hologram and a reflection hologram", US 8440370 B2 (2013).

[25] D. J. Mickish, S. R. Mackara, T. J. Trout, "Holographic imaging using filters", US 5633100 A (1997).

[26] D. E. Keys, W. K. Smothers, A. F. Harrington, J. Beutel, S. R. Schicker, D. F. Scofield, "Holographic optical elements having a reflection hologram formed in a photopolymer, "US 4942102 A (1990).

[27] H. Ando, S. Namba, "Light-guiding device having a hologram layer", US 5268985 A (1993).

[28] I. Naydenova, H. Sherif, S. Martin, R. Jallapuram, V. Toal, "Holographic sensor", US 8263291 B2 (2012).

[29] J. Blyth, C. R. Lowe, A. G. Mayes, R. B. Millington, "Holographic sensors and their production", US 6689316 B1 (2004).

[30] Deloitte Consulting AG "Pharmaceutics Anti-Counterfeiting – How Secure is Your Supply Chain?" Report (2014).

[31] BCC Research, "Anti-Counterfeiting Packaging Technologies in the Global Pharmaceutical and Food Industries", Market Research Report, FOD042B (2011).

[32] Smithers Pira Market Intelligence, "Ten-Year Forecasts of Disruptive Technologies in Security Printing to 2020", Market Research Report (2010).

[33] I. Lancaster, D. Tidmarsh, "The changing market for security holograms", Presentation at Holo-Pack Holo-Print Holography Conference, Vienna, Austria, 28-30 Oct. 2012.

[34] RP Photonics Encyclopedia, http://www.rp-photonics.com/brewster_plates.html [accessed on: 10/0602104].

[35] R. Fuentes, E. Fernández, C. García, A. Beléndez, I. Pascual, "Study of reflection gratings recorded in polyvinyl alcohol/acrylamide-based photopolymer", Applied Optics 48(34), 6553-6557 (2009).

[36] M. R. Gleeson, D. Sabol, S. Liu, C. E. Close, J. V. Kelly, J. T. Sheridan, "Improvement of the spatial frequency response of photopolymer materials by modifying polymer chain length", JOSA B 25(3), 396-406 (2008).

[37] M. Ortuno, E. Fernandez, R. Fuentes, S. Gallego, I. Pascaual, A. Belendez, "Improving the performance of PVA/AA photopolymers for holographic recording", Optical Materials 35(3), 668-673 (2013).

[38] K. A. Rodrigues, M. M. Vanderhoof, A. M. Carrier, J. Sanders, "Hybrid copolymer compositions", US 20120128608 A1 (2012).

[39] E. Fernández, R. Fuentes, M. Ortuño, A. Beléndez, I. Pascual, "Holographic grating stability: influence of 4,4′-azobis (4-cyanopentanoic acid) on various spatial frequencies", Appl. Opt. 52(25), 6322-6331 (2013).

[40] I. Naydenova, R. Jallapuram, R. Howard, S. Martin, V. Toal, "Investigation of the Diffusion Processes in a Self-Processing Acrylamide-Based Photopolymer System", Appl. Opt. 43(14), 2900-05 (2004).

[41] R. Jallapuram, "Optimization of an acrylamide-based photopolymer for reflection holographic recording", Doctoral Thesis, Dublin Institute of Technology, 2005.

[42] J. A. Jenney, "Holographic recording with photopolymers", JOSA 60(9), 1155-1161 (1970).

[43] Bio-Rad Laboratories Inc., "Acrylamide Polymerization - A Practical Approach", Electrophoresis, Technical Note 1156

[44] Y. C. Jeong, B. Jung, J. Lee, J. K. Park, "Reaction-controlled diffraction grating of photopolymer for use of phase stable holographic optical element", Appl. Phys. Lett. 98, 101103 (2011).

12. INVESTIGATION OF THE PRESSURE SENSING ABILITY OF DA PHOTOPOLYMER REFLECTION GRATINGS

12.1 Introduction

Pressure sensors are widely used for control and monitoring of pressure in thousands of everyday applications. The sectors requiring pressure sensing devices vary greatly, including the petrochemicals, automotive, dental and medical industries; some of the applications of pressure sensors in these fields are outlined in fig. 12.1. The market size of pressure sensors in the year 2011 was \$5.11 billion and is expected to reach \$7.34 billion by 2017, accorded to a market research report published by MarketsandMarkets in 2012 [1]. They predict strong growth of optical sensing technologies for pressure sensing in the future, due to their applications in hazardous environments in particular.

Here, the ability of reflection gratings recorded in the DAC photopolymer composition to act as a pressure sensing device has been investigated. The DAC composition was selected for this study due to its ability to record bright, high diffraction efficiency (η), reflection mode holograms that are visible in white light. The property of reconstructing in white light is an attractive feature for a holographic sensor, as it can provide a visual indication of any change which occurs. The DAC composition enables the recording of reflection holograms which have the ability to produce colour maps of pressure distribution. A hologram which changes colour under pressure is also an attractive option for security and anti-counterfeiting applications. This pressure-sensitive material is low cost and easy to produce.

Automotive	Industrial	Medical/Biomechanics	Occlusion & Dental Analysis
• Nip and pinch rollers • Brakes and friction plates • Tire-tread footprint analysis • Catalytic converters • Wiper-blade design • Airbags • Gaskets and bolted joints • Seating and bedding design • Impact studies • Hose clamps and crimps • Grip and ergonomics • Fasteners • Vibration studies • Door-seal testing • Windshield wiper	• Solar cells • Security devices • Packaging and sealing • Automation • Wafer and lens polishing • Lamination • Printer Ink cartridge • Mold filing • Pressure garments • Robotics • Packaging and sealing • Squeegee balancing • Semiconductor industry • Printed circuit boards • Sports equipment Training devices	• Articulating Gait Analysis • Balance & Posture Assessment • Foot Function and Gait Analysis • Sports Injury & Performance • Pre and Post Surgical Evaluation • Foot wear Research & design • Body mapping • Mattress Design	• General Occlusion • Implant Occlusion • Implant Prosthetics • Abfraction Issues • Abfraction Management • Fixed Prosthetics • Equilibration

Fig. 12.1. Applications requiring a thin film capable of tactile pressure measurements [2].

12.2 Theory

12.2.1 Principle of operation of holographic pressure sensor

When a reflection hologram is illuminated with white light, light of a specific wavelength is reconstructed depending on the recording wavelength used e.g. if a 633 nm laser is used to record the reflection hologram, the reconstructed image will be observed in red, assuming negligible shrinkage of the photopolymer layer due to holographic recording. The reconstructed wavelength corresponds to a particular fringe spacing, Λ, of the hologram, which can be determined using the Bragg equation:

$$\lambda = 2n\Lambda \sin \theta \qquad (12.1)$$

where λ, θ are the reconstruction angle and wavelength, and n is the refractive index of the sample.

The hologram is recorded in an elastic photopolymer material which compresses under pressure, causing the hologram thickness and therefore Λ to be reduced. This reduction in Λ corresponds to a decrease in the wavelength at which the hologram reconstructs, λ. Assuming the hologram has high enough η and is bright, this change will be visible to an observer, as well as quantifiable with a spectrometer. It is expected that the colour of the reconstructed hologram will change progressively from red to yellow to green to blue as the applied pressure increases, corresponding to the reduction in Λ. A schematic diagram of the principle of operation of a holographic pressure sensor is shown in fig. 12.2.
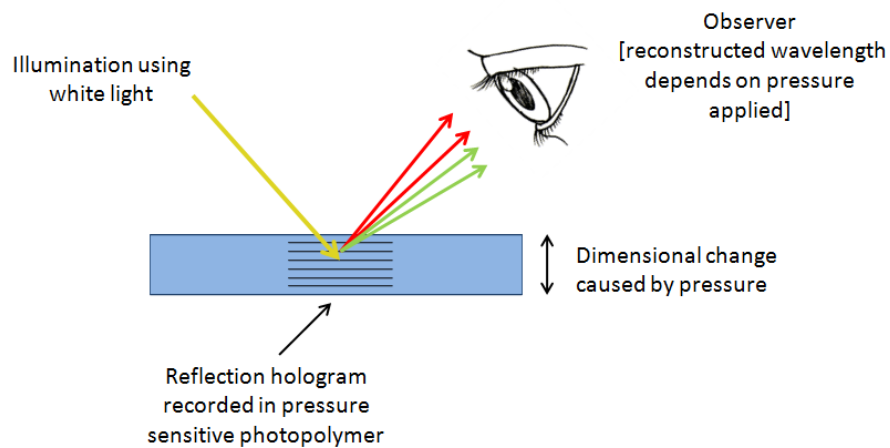
Fig. 12.2. Principle of operation of a holographic pressure sensor.

12.2.2 Photopolymers as media for holographic pressure sensors

Despite developments in the field of holographic recording materials, there remains a need for improved holographic recording compositions for pressure sensing. Photopolymers are an attractive option for this application due to the fact that the material is elastic and can be compressed. Reflection gratings recorded in photopolymer formulations have previously been shown to work as effective relative humidity

sensors, due to their ability to swell and shrink as the humidity of the surrounding environment is changed [3]. It is expected that the similar principle of operation of a holographic pressure sensor will be suitable for applications in photopolymer media.

A photopolymer-based holographic sensor that responded to pressure was described in a patent by Lowe *et al* [4]. In this work, an emulsion consisting of acrylamide:methacrylamide (2:1, v/v) and a crosslinker methylenebisacrylamide (5 mol. %) was deposited on a substrate to create a film, which was then polymerised via a free radical polymerisation reaction. A hologram was recorded while the substrate was soaking in a water bath using a frequency doubled Nd:YAG laser. The resulting hologram was sandwiched using another transparent substrate and pressure was applied onto the holograms using a pair of G-clamps. The pressure of the clamps on the hologram resulted in a contraction in the volume of the hologram, thus causing the λ to blue-shift by a total of 3 nm. While this work demonstrated the principle of operation of a pressure sensitive hologram, a shift of 3 nm in λ is not large enough to produce a change in the colour of the reconstructed hologram visible to the human eye, and implies that the sensitivity of the reported material to pressure is not large enough for pressure sensing applications.

12.3 Experimental

12.3.1 Materials

The DAC photopolymer was prepared as described in chapter 11 by mixing 20 ml of 10 % wt/vol PVA solution, 2 ml of TEA, 1.0 g of DA, 0.2 g of BA, 0.2 g of citric acid, 2 ml of glycerol and 4 ml of 0.11 % wt/vol Methylene Blue dye solution. To prepare the

samples, 0.5 ml of this photopolymer solution was deposited on to a microscope slide (75 × 25 mm) and allowed to dry for 12-24 hours in darkness under normal laboratory conditions (20-25 °C, 40-60 % RH). After holographic recording, the photopolymer layers were laminated with a 50 µm thick Melinex® 401 polyester film in order to protect the recorded gratings when applying pressure.

12.3.2 Methods

12.3.2.1 Reflection grating recording

Reflection gratings were recorded in the DAC photopolymer layers using a 633 nm He-Ne laser as shown in fig. 12.3. The angle between the two beams was set at 80° corresponding to a spatial frequency of the recorded grating of 3050 ± 30 l/mm. The intensity of the recording beams was controlled using a neutral density filter. A total recording intensity of 3 mW/cm^2 was used to record the reflection gratings with total exposure energy of 270 mJ/cm^2.
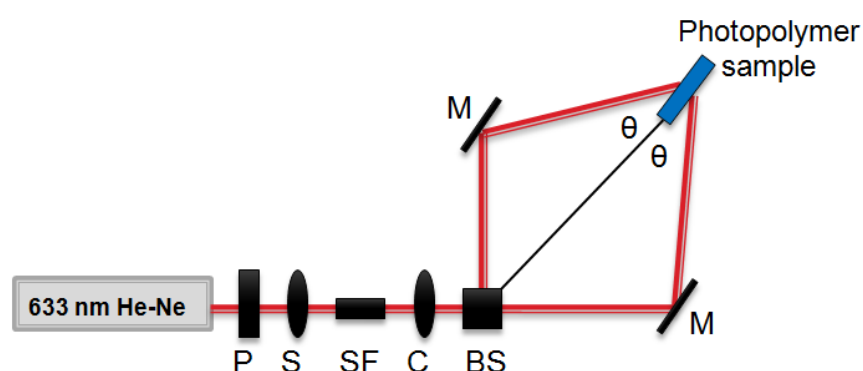
Fig. 12.3. Experimental setup for recording reflection gratings. P: polariser, S: shutter, SF: spatial filter, C: collimator, BS: beam splitter, M: mirror.

12.3.2.2 Pressure application method

Pressure was applied to the reflection gratings using an Instron Series 5569 Tensile Tester. A ball bearing of 3 mm diameter was attached to the tip of the Instron. Initially a flat indenter tip was used, however it proved impossible to apply uniform pressure to the sample using this method. Merlin v. 5.31 software was used to control the downward force applied to the samples.

In this instance, the pressure applied to the photopolymer surface cannot simply be defined as force per unit area, as a spherical surface was used to apply pressure. In order to determine the pressure applied to the samples, it is necessary to use Hertzian Theory of Elastic Deformation [5, 6]. This theory is more generally applied to two spheres in contact (fig. 12.4(a)), however it is also valid for a sphere incident on a flat plane, as a plane can be approximated as a sphere of infinitely large radius (see fig. 12.4(b)).

Consider a sphere of radius r exerting pressure on a flat plane. The radius of the contact area between the sphere and the flat plane is denoted by a. Assuming that the pressure is exerted over a circularly-shaped area and that $a \ll r$, the semi-elliptic Hertzian pressure distribution for a sphere of radius r incident on a flat plane is of the form:

$$P(r) = P_o \left(1 - \frac{r^2}{a^2}\right)^{\frac{1}{2}}$$

(12.2)

where P_o is the maximum contact pressure.

The force exerted by the sphere F can be found by integrating the pressure distribution $P(r)$ around the circumference of the area to which the pressure is applied, in this case a circle:

$$F = \int_0^a P(r) 2\pi r \, dr = \frac{2}{3} \pi P_o a^2$$

(12.3)

Therefore, the maximum contact pressure P_o of a sphere incident on a flat plane is given by:

$$P_o = \frac{3F}{2\pi a^2} \qquad (12.4)$$

An estimate for the radius of the contact area a was determined from images of the photopolymer sample taken after application of pressure using the camera of a Horiba Jobin Yvon confocal Raman spectrometer as shown in fig. 12.5 From these images, a was estimated to be 35 μm.

(a)   **(b)**
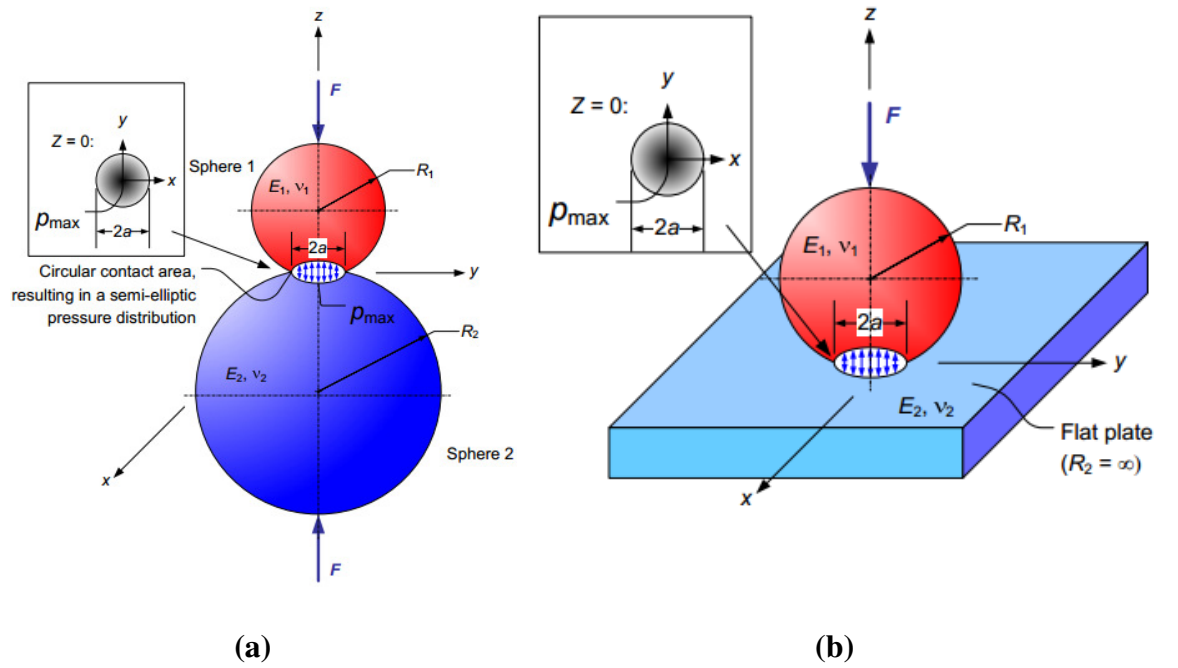
Fig. 12.4 Hertzian description of contact pressure for (a) two incident spheres and (b) a sphere incident on a flat surface or plane [6].
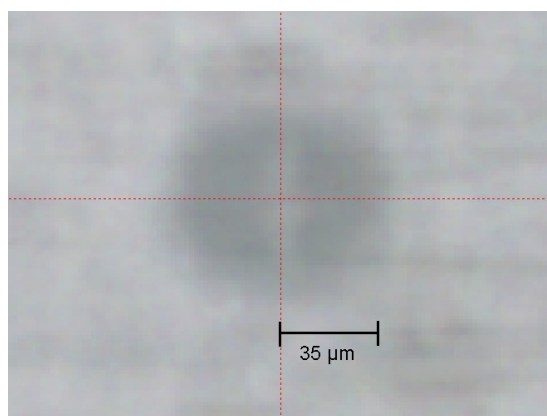
Fig. 12.5. Area of contact of 3 mm diameter ball bearing with the DAC photopolymer layer. Image taken with a Horiba Jobin Yvon confocal Raman spectrometer.

12.3.2.3 White light spectroscopy measurement technique

A measurement technique was needed in order to monitor the shift in the reconstructed wavelength of the reflection gratings after application of pressure. For this purpose, a Horiba Jobin Yvon confocal Raman spectrometer was used. In general, Raman spectrometers operate at defined wavelengths (632 nm, 532 nm etc.) and measure the spectral response of a test sample to that wavelength as a function of wavenumber. However, it is also possible to operate Raman spectrometers using a broad white light source, therefore allowing the collection of a spectrum as a function of wavelength, provided that the signal reflected from the sample is strong enough. The Raman spectrometer was used in this way to measure the position of the reconstructed wavelength from the holographic reflection grating when illuminated with white light.

Raman measurements were performed using a confocal pinhole diameter of 900 µm and a 600 l/mm grating. Due to the strong signal from the reflection gratings, relatively short exposure times of 0.2-0.6 seconds were used for a single accumulation in the

wavelength range of 400-800 nm. Fig. 12.6 shows an example of the reconstructed wavelength peak measured using the Raman method both before and after the application of pressure. Due to some swelling of the DA photopolymer layer after recording, the reconstructed wavelength before pressure is shifted from 633 nm to 665 nm. Such swelling has previously been observed after recording in Methylene Blue-sensitized AA photopolymer samples by Meka *et al* [7]. Both DA and AA photopolymer samples sensitized with Erythrosin B however are observed to shrink after recording, as has been described in chapter 5. It is important to distinguish between the two changes in the reconstructed wavelength occurring; the swelling effect results in an upward shift of the reconstructed wavelength by approximately 30 nm which occurs directly after recording, most likely due to absorption of water vapour by the photopolymer layer. The second change is the decrease in reconstruction wavelength which occurs due to the application of pressure. Downward shifts in wavelength of up to 80 nm can be achieved due to application of pressure.
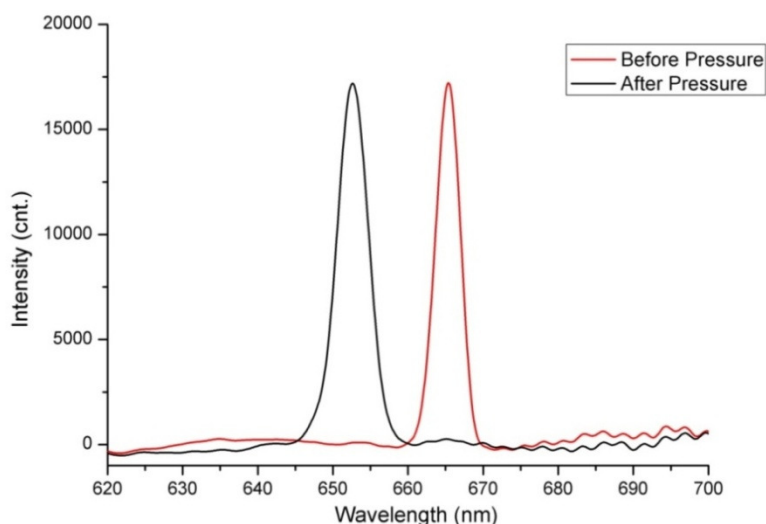
Fig. 12.6. Intensity vs. wavelength (nm) for a reflection grating recorded in the DAC photopolymer before and after application of pressure, measured using the Horiba Jobin Yvon confocal Raman spectrometer.

12.3.2.4 Analysis methods

Using the technique of monitoring the shift in the reconstructed wavelength of the grating, different parameters of interest could be studied. The dependence of the shift in the grating fringe spacing as a function of pressure was measured. By determining the strain of the material as a function of the stress i.e. the pressure applied, an attempt was made to calculate a value for Young's Modulus E of the DAC photopolymer, using the equation:

$$E = \frac{tensile\ stress}{extensional\ strain} = \frac{\sigma}{\varepsilon} = \frac{P_o}{\Delta\Lambda/\Lambda_o} \qquad (12.5)$$

where $\Delta\Lambda$ is the amount by which the grating fringe spacing changes, and Λ_o is the original fringe spacing of the grating [8]. For reflection gratings with spatial frequency of 3050 l/mm, Λ_o has a value of 0.3279 μm. However, due to the swelling observed after recording, Λ_o was shifted to 0.3448 μm corresponding to a lower spatial frequency of 2900 l/mm.

$\Delta\Lambda$ as a function of time after application of pressure was also studied. This allowed for the ability of the photopolymer layer to return to its original Λ_o to be analysed for three different incident pressures. The rate of recovery of the reflection gratings was also calculated.

By taking spectral maps over large areas of the grating, it was possible to analyse the dependence of $\Delta\Lambda$ on the distance from the area of contact of the ball bearing on the sample. This was carried out for different incident pressures.

12.4 Results and Discussion

12.4.1 Dependence of $\Delta\Lambda$ on pressure and calculation of E

The effect of increasing pressure on $\Delta\Lambda$ of the reflection gratings was investigated for pressures ranging from 0.4 to 10 GPa. Fig. 12.7 shows the values for $\Delta\Lambda$ as a percentage of the original fringe spacing ($\Lambda_o = 0.3448$ µm). As pressure is increased, $\Delta\Lambda$ increases from 1 to 12 %. It was not possible to test pressures higher than 10 GPa without cracking the glass substrate.
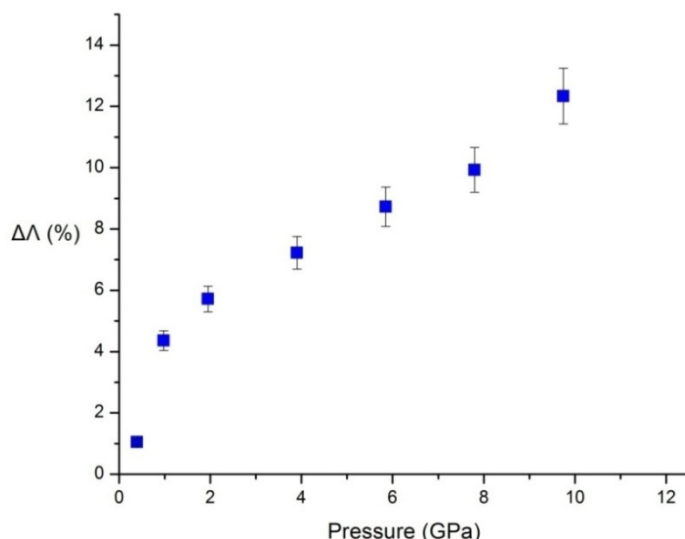
Fig. 12.7. $\Delta\Lambda$ (%) vs. pressure (GPa) for reflection gratings recorded in the DAC photopolymer.

From the data shown in fig. 12.7 it was possible to plot the stress vs. strain curve for the DAC photopolymer. The values for stress and strain are defined above in eqn. 12.5. The stress vs. strain curve for the DAC photopolymer is shown in fig. 12.8(a). The shape of the curve may best be described as an S-shaped curve. S-shaped stress-strain curves are

characteristic of materials with rubber-like elasticity, such as lightly crosslinked polymers [9, 10]. A typical S-shaped curve as defined by Treloar is shown in fig. 12.8(b) [9]. The stiffness of the material increases at high extensions where the polymer chain nears maximum extension.

The S-shaped curve is obviously non-linear. It is not possible therefore to apply Hooke's law and extract a value for E except in the region of very small strains. A linear fit has been applied to the three lowest strain values on the stress-strain curve, and the results of this are shown in fig. 12.9. An R^2 value of 0.939 was obtained for this fit.

The value for E of the laminated DAC photopolymer was determined from the slope of the linear fit of the stress-strain curve for the DAC photopolymer to be 21.23 ± 3.76 GPa. This is significantly higher than the expected E value, as typically for materials with rubber-like elasticity such as polymers exposed to low strain, the value for E is in the range of 0.01-0.1 [11]. A second value for E of the DA photopolymer layer was measured using Atomic Force Microscopy (AFM) techniques, giving a value of 4.9 GPa for the laminated photopolymer layer, and 0.012 GPa for an un-laminated layer.

As mentioned previously, the photopolymer samples are laminated with a 50 µm thick Melinex® 401 polyester film in order to protect the recorded gratings when applying pressure. It is obvious that this laminate greatly influences the stiffness of the photopolymer layer, resulting in an increase in the value for E for the DA photopolymer from 0.012 GPa to 4.9 GPa. This increase in stiffness due to the laminate material may result in reduced sensitivity of the DA reflection gratings to pressure. Optimisation of the laminating material used may therefore be beneficial in order to maximise the response of the laminated grating to pressure.

The value calculated for E of the laminated photopolymer sample from the stress-strain curve is over four times greater than when calculated using the AFM method. Therefore, it is clear that the method of calculating a value for E from the stress-strain curve for the DA photopolymer gratings is not sufficiently accurate. There are several sources of error which may explain the observed discrepancy. A delay time occurred between the application of pressure to the grating and the measurement of the shift in the fringe spacing using the Raman spectrometer. Relaxation of the grating most likely occurred during this time period, which would result in inaccuracies in the value for E. Errors were also most likely introduced by variations in the relative humidity, which would result in discrepancies in the value for Λ_o. Another source of error in the value for E is the lack of data at lower values of strain, due to poor sensitivity of the Instron indenter in the lower force range.

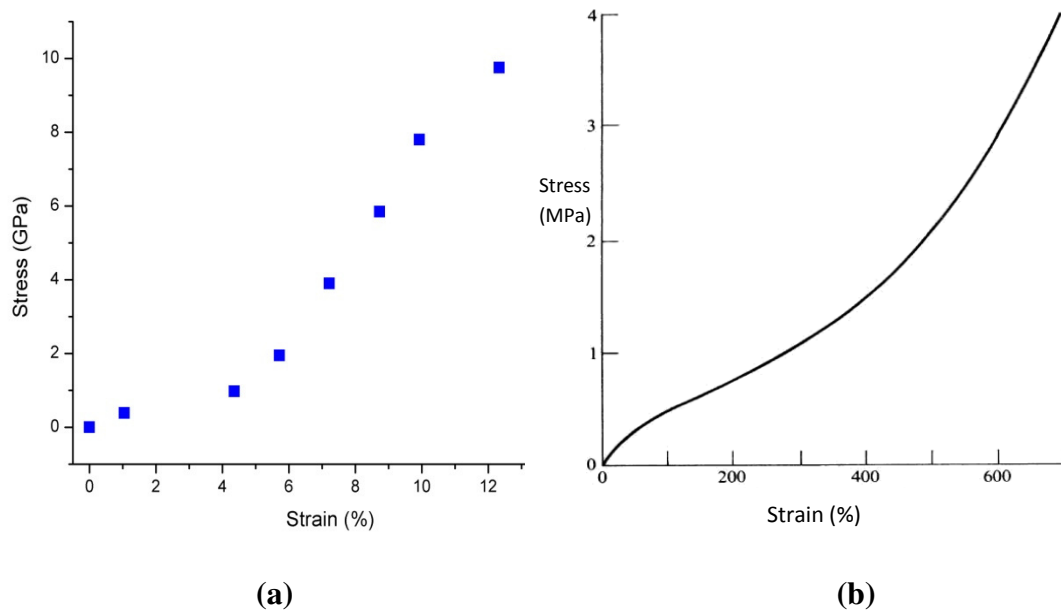(a)   (b)

Fig. 12.8. (a) Stress (GPa) vs. strain (%) for reflection gratings recorded in the DAC photopolymer, compared to (b) a typical s-shaped stress (MPa) vs. strain (%) for vulcanized rubber [9].

$$y = mx + c$$

$$m = 21.23 \pm 3.76 \, GPa$$

$$c = 0.0718 \pm 0.0974$$
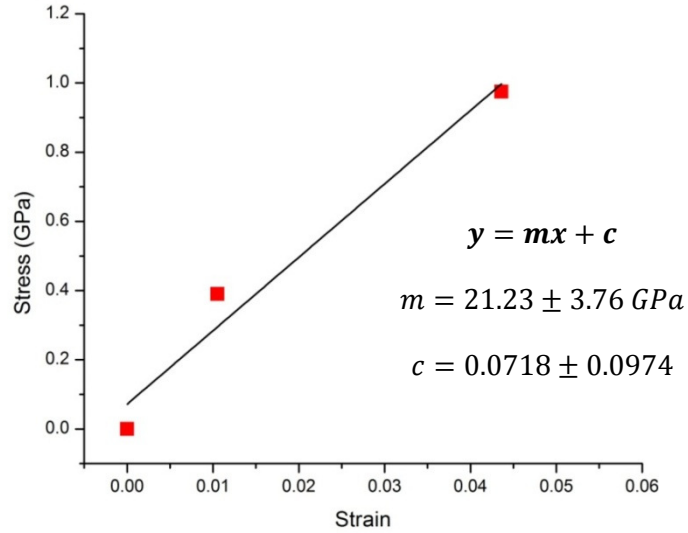
Fig. 12.9. Stress (GPa) vs. strain for low strain values of the reflection gratings recorded in the DAC photopolymer. A linear fit has been applied to the data.

12.4.2 Dependence of $\Delta\Lambda$ on distance from contact area

The change in the fringe spacing $\Delta\Lambda$ as a function of distance from the central point of the contact area was investigated for three different pressures, namely 1, 2 and 6 GPa. This was done in order to investigate the profile of the strain i.e. how strong an effect the application of pressure would have on the fringe spacing of the grating as distance from the contact area was increased. The results of this study are shown in fig. 12.10. From the data it is shown that as expected, the largest value of $\Delta\Lambda$ is obtained at all distances for the highest pressure tested at 6 GPa. The rate of decrease in $\Delta\Lambda$ as a function of distance is also clearly largest for the 6 GPa data. As the pressure decreases, this rate decreases accordingly. Therefore, for lower pressures the surrounding area is less affected by the application of pressure than for higher pressure loads.
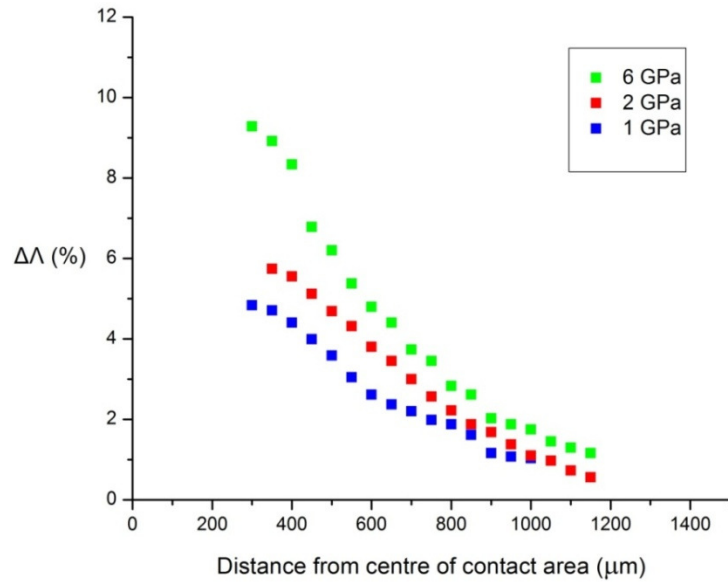
Fig. 12.10. ΔΛ (%) vs. distance (μm) from centre of contact area for reflection gratings in the DAC photopolymer exposed to pressures of 1, 2 and 6 GPa.

12.4.3 Rate of reverse of ΔΛ with time

In order to investigate the reversibility of the change in ΔΛ, ΔΛ was monitored over a period of 48 hours after the application of pressure. This was carried out for three different pressures, 1, 2 and 6 GPa at distances of 300, 400 and 500 μm respectively from the central point of pressure application. This was done in order to have approximately the same initial value of ΔΛ for comparison purposes. The results of this are shown in fig. 12.11. From the data is appears that the recovery of ΔΛ over time follows an exponential decay trend, recovering up to 97 % of the original Λ_o after 48 hours.

Fig. 12.11. ΔΛ (%) vs. time (hr) for reflection gratings recorded in the DAC photopolymer after exposure to pressures of 1, 2 and 6 GPa.

A two-phase exponential decay function was used to fit the ΔΛ vs. time data for the three different pressures 1, 2 and 6 GPa tested, as shown in fig. 12.12. R^2 values of 0.999, 0.998, and 0.989 were obtained for the 1, 2 and 6 GPa data respectively. The two parameter exponential decay function used to fit the data is given by:

$$y = y_o + A_1 e^{\left(-\frac{x}{t_1}\right)} + A_2 e^{\left(-\frac{x}{t_2}\right)} \tag{12.6}$$

where y_o is the final value of ΔΛ, A_1, A_2 and t_1, t_2 are the amplitudes and time constants of the first and second decay reactions respectively. The values for these variables for each fit are shown in table 12.1.

Table 12.1 Two-phase exponential decay fit data for intensity vs. time

Pressure (GPa)	y_o	A_1	t_1 (s)	A_2	t_2 (s)
1	2.98±0.03	1.65±0.03	12.96±0.69	2.27±0.04	0.50±0.03
2	3.19±0.04	2.24±0.04	10.98±0.59	1.78±0.06	0.38±0.06
6	3.55±0.08	2.42±0.14	7.40±0.91	0.87±0.17	0.01±0.02

From the data in Table 12.1 it is clear that for both the first and second decay processes in the two-phase exponential decay, the rate of recovery of the fringe spacing of the reflection grating increases with increasing pressure. This may be explained by the fact that for higher stress loads, the sample has a relatively larger amount of fringe spacing to recover, and therefore will the recovery rate will be faster for higher pressures.

The percentage recovery of the fringe spacing for the different pressures tested is shown in fig 12.13. It is observed that the fringe spacing is recovered to the largest extent for the lowest applied pressure of 1 GPa. This is logical as by exerting less pressure, the elastic limit of the material may not be exceeded, thereby allowing the photopolymer layer to better return to its original fringe spacing. By increasing the pressure, it becomes more difficult for the material to return to the original value as the elastic limit may be reached or exceeded.
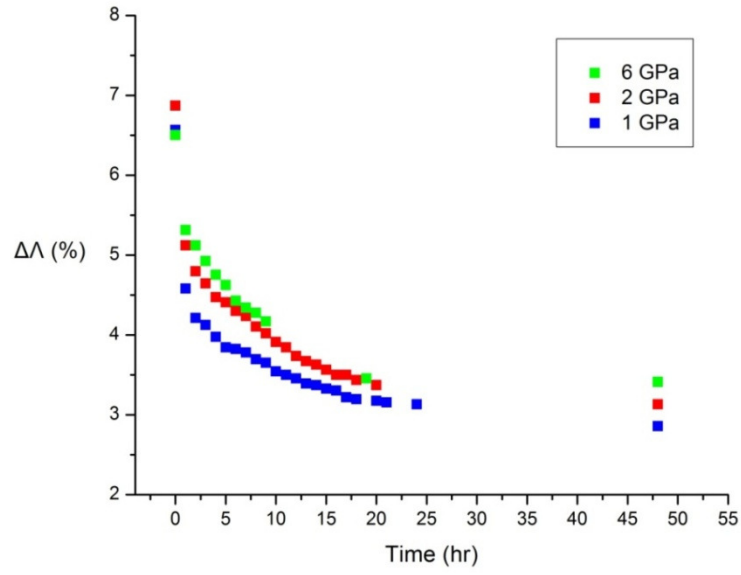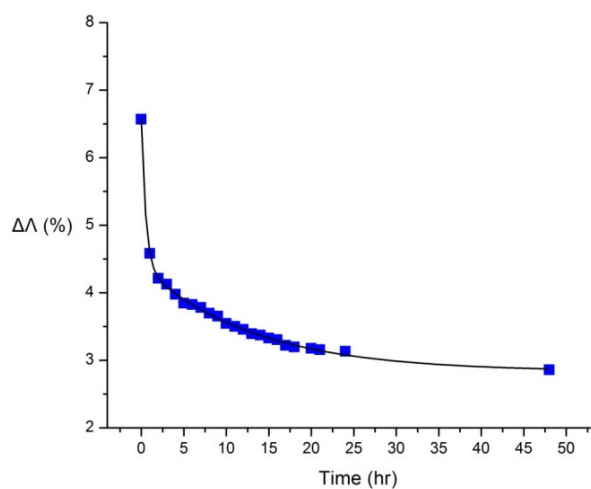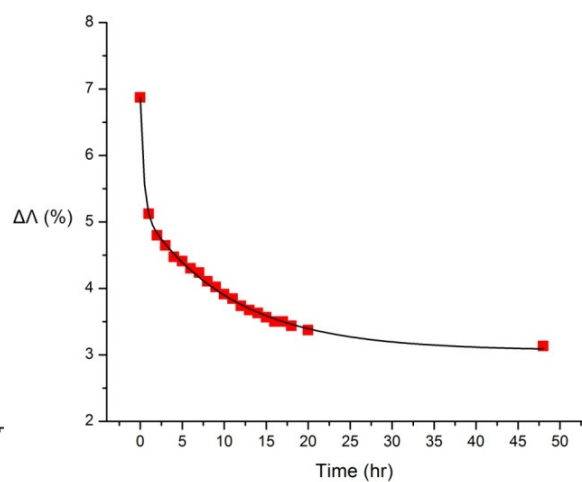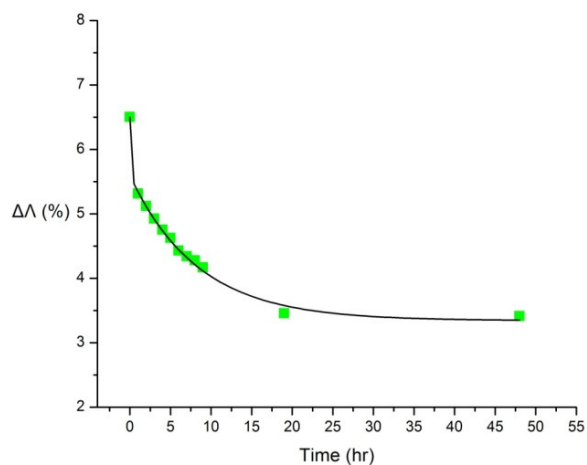
Fig. 12.12. ΔΛ (%) vs. time (hr) for reflection gratings recorded in the DAC photopolymer after exposure to a pressure of (a) 1 GPa, (b) 2 GPa, and (c) 6 GPa. Data has been fitted with a two parameter exponential decay function.
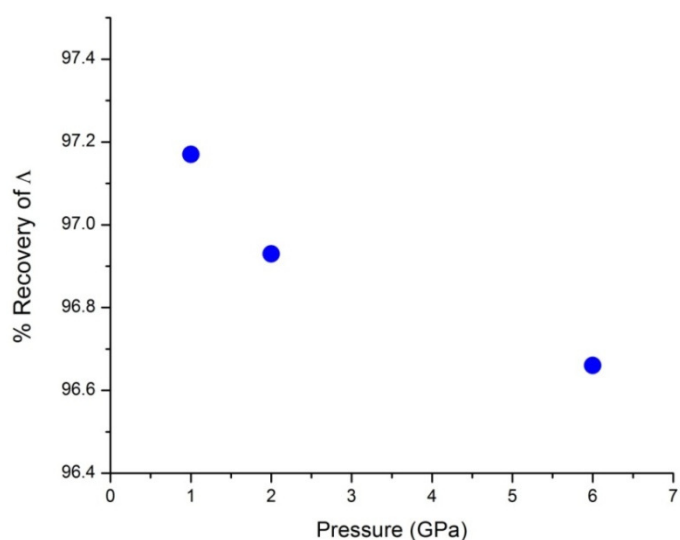
Fig. 12.13. % recovery of Λ_o vs. pressure (GPa) for reflection gratings recorded in the DAC photopolymer after 48 hours.

12.4.4 Examples of pressure sensitive reflection holograms

The pressure sensitivity of Denisyuk-type reflection gratings recorded in the DAC photopolymer is visually demonstrated in fig. 12.14. The Denisyuk-type gratings were recorded as described in section 1.3.1.2 of chapter 1, using a mirror as the object. In this figure, pressure has been applied to the reflection gratings using several different shapes as shown in (a) to (d). In the regions where pressure has been applied, a clear change in colour of the reconstructed grating is visible from the red colour of the original recorded grating to orange, yellow, green and blue, with increasing pressure. A stylus was used to write the letters X and Y on the grating surface as shown in (e). This technique was also proven to cause a change in colour of the reconstructed grating. Finally, a Denisyuk-type hologram was recorded of a 10c coin, as shown in (f). The application of pressure to this hologram resulted in a visible change in colour, without any damage to the reconstructed image.
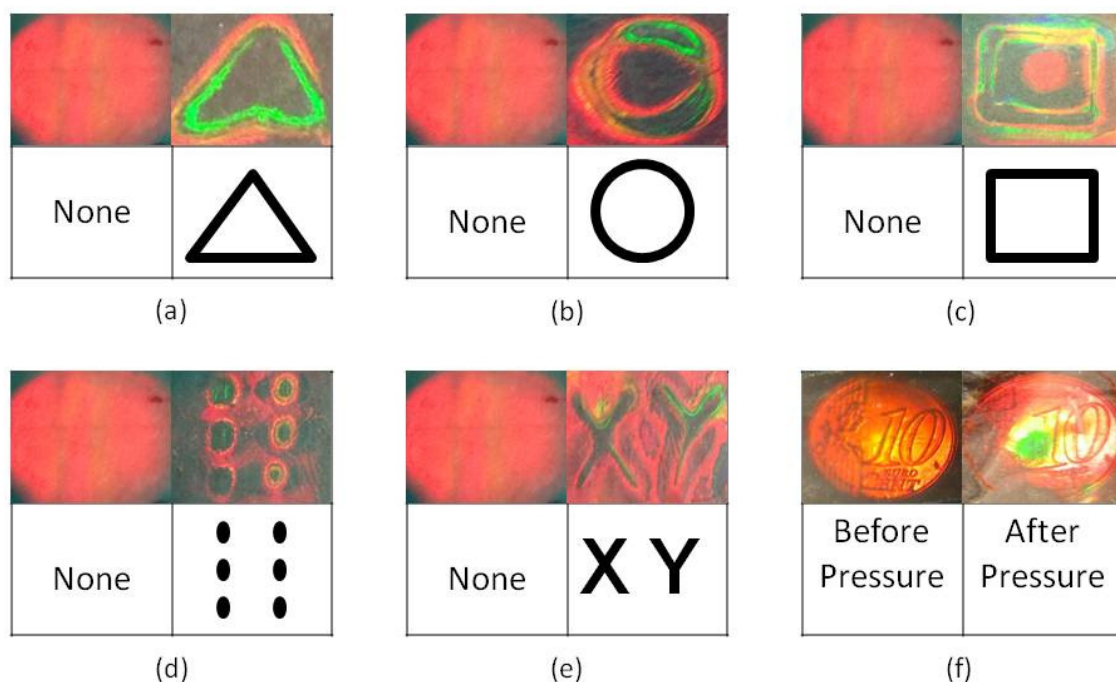
Fig. 12.14. Reflection grating before and after application of pressure using (a) a triangular-shaped stamp, (b) a circular-shaped stamp, (c) a square-shaped stamp, (d) a six-pronged stamp and (e) a stylus to write the letters X and Y. Shown in (f) is a reflection hologram of a 10c coin before and after application of pressure.

12.5 Conclusions

The ability of reflection gratings recorded in the DAC photopolymer to operate as a holographic pressure sensor has been investigated. The application of pressure to a holographic grating resulted in a quantifiable change in the fringe spacing of the grating. The fringe spacing of the reflection gratings was observed to blue-shift by up to 12 % compared to unpressurised samples, for pressures of between 0.5 - 10 GPa. Up to 97 %

of the original fringe spacing value was recovered after a recovery time of 48 hours for pressures of 1, 2 and 6 GPa.

It has been demonstrated that the application of pressure to both reflection gratings and Denisyuk-type holograms of objects results in a progressive colour change of the reconstructed hologram from red to yellow to green to blue with increasing pressure. This colour change is easily visible in white light.

The ability of the reflection gratings recorded in the photopolymer layer to respond to pressure in a visible and quantifiable way lends itself to the development of holographic pressure sensors. This is of particular interest for the DAC photopolymer composition as it is capable of recording high diffraction efficiency holograms, easily viewable by an observer. A patent on the development of a holographic pressure sensor using the DAC photopolymer composition has been filed.

Future work will include the further optimization of the DAC composition for specific pressure sensing applications. It may be desirable that the effect on the hologram due to pressure be fully reversible or irreversible, depending on the application. One possible method which could be implemented to modify reversibility could be to increase the mechanical stiffness of the PVA-based photopolymer layers using a series of freeze-thaw cycles, as has been described by King *et al* [12]. Optimisation of the laminating material applied to protect the gratings should also be carried out, in order to maximise the response of the laminated grating to pressure.

References:

[1] MarketsandMarkets, "Pressure Sensor Market (2012 – 2017) - Global Forecast, Trend & Analysis – Segmentation by technology [Piezoresistive, Capacitive, Electromagnetic (Reluctance), Resonant Solid State, Optical], Applications [process and non process] and Geography", Market Research Report (2012).

[2] E. Mihaylova, D. Cody, I. Naydenova, S. Martin, V. Toal, " Research on Holographic Sensors and Novel Photopolymers at the Centre for Industrial and Engineering Optics", published in Holography - Basic Principles and Contemporary Applications, edited by Dr. Emilia Mihaylova, InTech, DOI: 10.5772/56061 (2013).

[3] I. Naydenova, R. Jallapuram, V. Toal, S. Martin, "Characterisation of the Humidity and Temperature Responses of a Reflection Hologram Recorded in Acrylamide-Based Photopolymer", Sensors and Actuators B: Chemical 139(1), 35-38 (2009).

[4] C. R. Lowe, J. Blyth, A. P. James, "Interrogation of a sensor", US 20080094635 A1 (2008).

[5] K. L. Johnson, Contact Mechanics, Cambridge University Press, Cambridge, 1985.

[6] Presentation on "Contact Stresses and Deformation", available online at: http://www.mech.utah.edu/~me7960/lectures/Topic7-ContactStressesAndDeformations.pdf [accessed on 10/07/14].

[7] C. Meka, "Development of Acrylamide Based Photopolymer for Full Colour Display Holography", Doctoral Thesis, Dublin Institute of Technology, 2010.

[8] N. Giordano, College Physics: Reasoning and Relationships, Cengage Learning, 2009.

[9] L. R. G. Treloar, The Physics of Rubber Elasticity, Oxford University Press, 1975.

[10] A. Ciesielski, An Introduction to Rubber Technology, iSmithers Rapra Publishing, 1999.

[11] P. B. Lindley, Engineering Design with Natural Rubber, Edn. 4, Malaysian Rubber Producers' Research Association, 1974.

[12] D. M. King, C. M. Moran, J. D. McNamara, A. J. Fagan, J. E. Browne, "Development of a Vessel-Mimicking Material for use in Anatomically Realistic Doppler Flow Phantoms", Ultrasound in Medicine and Biology 37(5), 813-826 (2011).

13. SUMMARY

13.1 Main conclusions from the PhD research

In this thesis, the development and characterisation of a novel, reduced-toxicity photopolymer material for holographic applications has been described. The main conclusions from this research are as follows:

- The DA monomer is suitable as a replacement of AA in the standard photopolymer composition. It is expected that the DA monomer operates within the photopolymer composition in the same manner as the AA monomer, forming polymer chains due to the presence of the initiating species, which are then crosslinked in the presence of the crosslinking monomer. The formation of holographic gratings in the DA photopolymer is governed by the same processes of diffusion and polymerisation, as is the case for the AA-based photopolymer.

- The reduced toxicity of the DA monomer in comparison to AA has been conclusively shown via an independent cytotoxicity evaluation. The replacement of AA with DA in the photopolymer composition therefore reduces occupational hazards involved in its production, in addition to the removal of the only carcinogenic component of the photopolymer material.

- It was shown that the DA-based photopolymer is capable of recording gratings in transmission mode with diffraction efficiencies of greater than 80 % in 60 μm thick layers and achieving Δn values of up to 3.5×10^{-3} over a wide range of spatial frequencies, from 100 to 3000 l/mm. This is comparable to the recording ability of the AA-based photopolymer in transmission mode, and suggests that the DA photopolymer is suitable for a wide range of transmission mode holographic applications, such as HOEs, sensors and security features.

- The polymerisation-induced shrinkage of the DA photopolymer layer has been measured via real-time holographic interferometric techniques. The dependence of the shrinkage on parameters such as recording intensity and sample thickness has been characterised. It was observed that the DA photopolymer on average demonstrates approximately 10-15 % less shrinkage as a percent of sample thickness than the AA photopolymer.

- It has been shown that the incorporation of glycerol in the photopolymer composition allows for the preparation of DA photopolymer layers with improved uniformity and optical quality. The experimental results suggest that glycerol acts in several capacities within the photopolymer layer. It has been shown that glycerol's nature as a plasticiser results in increased diffusion of the different photopolymer components within the layer during holographic recording. This corresponds to an increase in the rate of polymerisation of the photopolymer layer, as well as promoting DA polymer chain growth and chain entanglement. Glycerol also reduces the rate of photobleaching of the DA photopolymer layer on exposure to light.

- It has been demonstrated that the DA photopolymer is suitable for the incorporation of BEA-type zeolite nanoparticles. Improvements in Δn of up to 91 % in photopolymer layers doped with 2 wt. % BEA zeolite have been observed in comparison to undoped layers. It was observed that the inclusion and redistribution of zeolites in the grating enhances its response to act as a sensor for different alcohol gases.

- The DA-based photopolymer is suitable for reflection mode holographic recording and applications, recording gratings with diffraction efficiency values of 10 % in both the DA0 and DAG formulations.

- The incorporation of the chain transfer agent Citric Acid in the DAG photopolymer results in nearly a four-fold increase in diffraction efficiency of up to 38 % at a spatial frequency of 2500 l/mm. As the spatial frequency is increased to 4000 l/mm, diffraction efficiency values of over 20 % are still achievable. The effectiveness of UV light to stabilise the reflection gratings after recording has been demonstrated. To the best of the author's knowledge, this is the first time diffraction efficiency values of this magnitude have been reported in the reflection regime of recording.

- Reflection gratings recorded in the DA photopolymer composition can successfully be used as pressure sensing devices. The application of pressure to a holographic grating results in a quantifiable change in the fringe spacing of the grating. The fringe spacing of the DA-based reflection gratings was observed to blue-shift by up to 12 % compared to unpressurised samples for an applied pressure of 10 GPa.

- It was demonstrated that a pressure-induced change in the reconstructed wavelength of the reflection holograms is easily visible in white light. To the best of the author's knowledge, this is the first report of a pressure sensitive holographic photopolymer in which the application of pressure induced thickness changes, leading to a change in the colour of the reconstructed hologram which can be observed by the human eye.

13.2 Future work

From the research that has been carried out to date, it is clear that there are many areas in which further work would be beneficial.

- Characterisation of the holographic recording ability of the DA0, DAG and DAC photopolymers at different recording wavelengths should be carried out in order to have a more comprehensive picture of the new photopolymer media, e.g. 633 and 473 nm testing in transmission mode, 532 and 473 nm testing in reflection mode. An investigation of the ability of the DA-photopolymer to record holographic gratings using UV light may also be interesting for certain applications.

- A theoretical model entitled the Two-Way Diffusion Model has previously been developed by Babeva *et al* to describe both monomer and polymer diffusion effects observed experimentally in the AA photopolymer, and to quantify diffusion coefficients [1]. Application of this model to the DA photopolymer would be interesting for further investigation of how the increased size of the DA monomer molecule affects the diffusion of monomer and polymer chains, and would allow for further comparison of the holographic recording mechanisms of the two different photopolymer compositions.

- It has previously been shown by Moothancherry *et al* that the inclusion of different zeolite nanoparticles can significantly reduce the shrinkage of the AA photopolymer [2]. An investigation of the effect of the incorporation of nanoparticles in the DA photopolymer on the amount of polymerisation-induced shrinkage that occurs during holographic recording should be carried out.

- The effect of BEA-structure zeolite nanoparticles on the ability of gratings recorded in the DA photopolymer to act as gas sensors has been investigated. The samples showed a strong response to some alcohol type hydrocarbon gases (e.g. Methanol, Isopropanol), however for larger gas molecules a weaker effect was observed (e.g. 2-Methylpropan-2-ol, Pentane). It would be interesting to investigate the effect of other zeolite nanoparticle types with different pore sizes (e.g. Silica-MFI, AlPO) as well as non-zeolite type nanoparticles for sensing applications.

- The pressure sensing ability of the DAC photopolymer should be further investigated, to allow for the development of pressure sensors for specific applications. For example, it would be beneficial if the extent of reversibility of the effect of pressure on the reflection gratings could be controlled.

13.3 Dissemination of the PhD research

13.3.1 Journal publications

- D. Cody, I. Naydenova, E. Mihaylova, "New non-toxic holographic photopolymer", Journal of Optics 14(1), DOI:10.1088/2040-8978/14/1/015601 (2011).
  [Selected as a "Featured Article" for its quality and significance within the optics community by Journal of Optics].

- D. Cody, I. Naydenova, E. Mihaylova, "Effect of glycerol on a diacetone acrylamide-based holographic photopolymer material", Applied Optics 52(3), 489-494 (2012).

- D. Cody, A. Casey, I. Naydenova, E. Mihaylova, "A Comparative Cytotoxic Evaluation of Acrylamide and Diacetone Acrylamide to Investigate Their Suitability for Holographic Photopolymer Formulations", International Journal of Polymer Science, DOI:10.1155/2013/564319 (2013).

- D. Cody, E. Mihaylova, L. O'Neill, T. Babeva, H. Awala, R. Retoux, S. Mintova, I. Naydenova, "Effect of zeolite nanoparticles on the optical properties of diacetone acrylamide-based photopolymer", Optical Materials, DOI:10.1016/j.optmat.2014.05.021 (2014).

13.3.2 Patent application

- Patent application no. 1411640.4 filed in Great Britain on 30th June 2014, "A holographic recording composition", to protect the use of the DA-based composition for holographic pressure sensor devices.

13.3.3 Book chapter

- E. Mihaylova, D. Cody, I. Naydenova, S. Martin, V. Toal, " Research on Holographic Sensors and Novel Photopolymers at the Centre for Industrial and Engineering Optics", published in Holography - Basic Principles and Contemporary Applications, edited by Dr. Emilia Mihaylova, InTech, DOI: 10.5772/56061 (2013).

13.3.4 Conference proceedings

- D. Cody, I. Naydenova and E. Mihaylova, "Diacetone acrylamide-based non-toxic holographic photopolymer", SPIE Photonics Europe 2012, Optical Modelling and Design II, 84291B DOI:10.1117/12.923116, Brussels, Belgium (2012).

13.3.5 Oral and Poster presentations

13.3.5.1 Oral presentations

- D. Cody, E. Mihaylova, T. Babeva, H. Awala, R. Retoux, S. Mintova, I. Naydenova, "Diacetone Acrylamide-based Holographic Nanocomposite for Sensing Applications", II International Conference on Applications in Optics and Photonics, Aveiro, Portugal, 26-30th May 2014.

- D. Cody, E. Mihaylova, T. Babeva, S. Mintova, I. Naydenova, "Effect of BEA Zeolite Nanoparticles on the Optical Properties of Diacetone Acrylamide-Based Photopolymer", 5th International Symposium: Advanced Micro- & Mesoporous Materials, Varna, Bulgaria, 5-8th September 2013.

- D. Cody, I. Naydenova, E. Mihaylova, "Development of a Diacetone Acrylamide-based Holographic Photopolymer" 3rd Annual Postgraduate Research Symposium, Dublin Institute of Technology, 6th November 2012.

- D. Cody, I. Naydenova, E. Mihaylova, "Diacetone Acrylamide-based Non-Toxic Holographic Photopolymer" SPIE Photonics Europe 2012, Square Meeting Centre, Brussels, 16-19th April 2012.

13.3.5.2 Poster presentations

- D. Cody, E. Mihaylova, M. Moothanchery, V. Toal, I. Naydenova, "Measurement of the Polymerisation-Induced Shrinkage in a Diacetone Acrylamide Photopolymer using Real-Time Holographic Interferometry Technique", COST Action Meeting, DIT, Dublin, 24-25th April 2014.

- D. Cody, E. Mihaylova, T. Babeva, S. Mintova, I. Naydenova, "Effect of BEA Zeolite Nanoparticles on the Optical Properties of Diacetone Acrylamide-Based Photopolymer", 5th International Symposium: Advanced Micro- & Mesoporous Materials , Varna, Bulgaria, 5-8th September 2013.

- D. Cody, I. Naydenova, E. Mihaylova, "Novel Low-Toxicity Photopolymer for recording and inscription of Microstructures by Holographic Patterning", 7th International Summer School: New Frontiers in Optical Technologies, Tampere, Finland, 5-9th August 2013.

- D. Cody, I. Naydenova, E. Mihaylova, "Novel Periodic Microstructures recorded in a Low-Toxicity Photopolymer", 13th European Conference on Organised Films, Tyndall National Institute, Cork, Ireland, 8-12th July 2013.

- D. Cody, E. Mihaylova, I. Naydenova, V. Toal, "Characterisation of a New Non-toxic Holographic Photopolymer for Transmission Mode Recording", IOP Rosse Medal Competition, RCSI, Dublin, 30th March 2012.

- D. Cody, E. Mihaylova, I. Naydenova, V. Toal, "Silver Doping for Modifying the Properties of Non-Toxic Holographic Photopolymers", 4th International Symposium: Advanced Micro- and Mesoporous Materials, Varna, Bulgaria, 6 – 9th September 2011.

- D. Cody, E. Mihaylova, I. Naydenova, V. Toal, "Development of New Non-Toxic Photopolymers for Holographic Applications", Photonics Ireland, Malahide, Dublin, 7-9th September 2011.

- D. Cody, E. Mihaylova, I. Naydenova, V. Toal, "Development of Environmentally Friendly Photopolymers for Holographic Applications", IOP Ireland Spring Weekend, Louth, Ireland, 15-17th April 2011.

References:

[1] T. Babeva, I. Naydenova, D. Mackey, S. Martin, V. Toal, "Two-way diffusion model for short-exposure holographic grating formation in acrylamide-based photopolymer," J. Opt. Soc. Am. B 27, 197-203 (2010).

[2] M. Moothanchery, I. Naydenova, S. Mintova, V. Toal, "Nanozeolite doped photopolymer layers with reduced shrinkage", Opt. Express 19, 25786-91 (2011).